



Année académique 2003-2004

Université de Liège  
Faculté des Sciences  
Département de Physique  
Physique Théorique Fondamentale

# Deep Inelastic Scattering at small $x$

## Perturbative QCD and $S$ -matrix theory

G. Soyez

Thèse présentée en vue  
de l'obtention du grade de  
Docteur en Sciences Physiques



*Each small candle  
lights a corner of the dark*  
Roger Waters - Each Small Candle



*Hey you! out there on the road  
Always doing what you're told  
Can you help me  
Hey you! out there beyond the wall  
Breaking bottles in the hall  
Can you help me  
Hey you! don't tell me there's no hope at all  
Together we stand, divided we fall  
Pink Floyd - Hey you*

## Acknowledgements

First of all, I would like to thank Jean-René Cudell who guided me throughout this Ph.D.. It was a great pleasure to discuss with him about physics or anything else. I also thank the Belgian FNRS for financial support as well as the University of Liège for hosting me during 4 years. I also would like to thank E. Martynov: it was a great pleasure to work with him on  $t$ -channel unitarity. I'm also very grateful to U.K. Yang, who gave me important information concerning the CCFR measurements, and to J. Stirling and R. Thorne for interesting discussions about PDF and global fits.

Moreover, I really would like to thank all my close relations: parents and friends, for all the courage and happiness they gave me at every moment. And finally, I want to give a special thank to my father who taught me an innumerable number of things. Without his everyday presence during the last 25 years, this thesis would probably never have existed.



# Contents

<b>1</b>	<b>Introduction</b>	<b>1</b>
<b>2</b>	<b>Deep Inelastic Scattering</b>	<b>7</b>
2.1	Basics . . . . .	7
2.2	Parton model . . . . .	9
2.3	Frames in DIS . . . . .	11
2.3.1	Björken frame . . . . .	11
2.3.2	Breit frame . . . . .	11
2.3.3	Dipole frame . . . . .	12
<b>I</b>	<b>The DGLAP Evolution equation</b>	<b>13</b>
<b>3</b>	<b>Factorisation theorem and DGLAP evolution</b>	<b>15</b>
3.1	Factorising the $\gamma^*q$ amplitude: the non-singlet case . . . . .	15
3.2	Renormalisation group techniques . . . . .	19
3.3	The full $\gamma^*p$ amplitude and the DGLAP equation . . . . .	21
3.4	Extension to the singlet case . . . . .	22
3.5	The full DGLAP evolution equation . . . . .	23
<b>4</b>	<b>The leading-order DGLAP evolution equation</b>	<b>27</b>
4.1	Splittings from the factorisation theorem . . . . .	27
4.2	LO DGLAP and gluon ladders . . . . .	30
<b>II</b>	<b>Analytic <math>S</math>-matrix theory</b>	<b>33</b>
<b>5</b>	<b>Regge Theory</b>	<b>35</b>
5.1	$S$ -matrix theory . . . . .	35
5.1.1	Definition . . . . .	35
5.1.2	Postulates . . . . .	36
5.1.3	Useful $2 \rightarrow 2$ kinematics . . . . .	39
5.2	Regge theory . . . . .	40
5.2.1	Complex angular momenta and Sommerfeld-Watson transform . . . . .	40
5.2.2	Regge poles and Regge cuts . . . . .	41

5.2.3	Domain of applicability . . . . .	42
5.2.4	Mellin transform in DIS . . . . .	42
5.2.5	The Froissart-Martin bound . . . . .	43
<b>6</b>	<b>Testing Regge theory in DIS</b>	<b>47</b>
6.1	The simplest models . . . . .	47
6.1.1	The pomeron term . . . . .	47
6.1.2	The reggeon terms . . . . .	48
6.2	Direct comparison with the data . . . . .	49
6.3	Form factors and the full dataset . . . . .	49
6.4	Conclusion . . . . .	52
<b>7</b>	<b><math>t</math>-channel-unitarity rules</b>	<b>57</b>
7.1	$t$ -channel unitarity in the hadronic case . . . . .	58
7.1.1	Elastic unitarity . . . . .	58
7.1.2	Further elastic thresholds . . . . .	61
7.1.3	Inelastic thresholds . . . . .	63
7.1.4	Remarks . . . . .	64
7.2	General proof of $t$ CU relations: hadronic case . . . . .	64
7.3	The photon case . . . . .	67
7.4	General properties of $t$ CU relations: photon case . . . . .	68
7.5	Specific examples . . . . .	70
7.6	Colliding poles and $t$ CU relations . . . . .	71
<b>8</b>	<b>Test of the <math>t</math>CU relations</b>	<b>73</b>
8.1	Regge models . . . . .	73
8.2	Regge region . . . . .	75
8.3	Factorising $t$ CU relations . . . . .	75
8.4	Dataset . . . . .	76
8.5	Parametrisations . . . . .	76
8.5.1	Previous parametrisations . . . . .	76
8.5.2	New parametrisation: triple pole . . . . .	76
8.5.3	New parametrisation: double pole . . . . .	77
8.6	Box diagram . . . . .	79
8.7	Results . . . . .	79
8.7.1	Total $\gamma p$ and $\gamma\gamma$ cross sections . . . . .	81
8.7.2	Fits to $F_2^p$ . . . . .	81
8.7.3	Fits to $F_2^\gamma$ . . . . .	82
8.8	Conclusion . . . . .	82
<b>III</b>	<b>Linking DGLAP evolution with Regge theory</b>	<b>89</b>
<b>9</b>	<b>Constraints on initial distributions</b>	<b>91</b>
9.1	Initial distributions . . . . .	92

9.1.1	The large- $x$ problem . . . . .	93
9.1.2	The triple-pole case . . . . .	95
9.1.3	The generalised double-pole case . . . . .	95
9.1.4	Remark: influence of the GRV parametrisation . . . . .	96
9.2	Fit . . . . .	96
9.3	Results . . . . .	97
9.4	Conclusion . . . . .	99
<b>10</b>	<b>DGLAP evolution of residues</b>	<b>107</b>
10.1	Regge theory at large $Q^2$ and the DGLAP essential singularity . . . . .	107
10.2	Mixing DGLAP evolution with Regge theory . . . . .	108
10.3	Initial distributions . . . . .	108
10.4	Fitting the form factors . . . . .	109
10.4.1	Scheme 1 . . . . .	109
10.4.2	Scheme 2 . . . . .	110
10.5	Results . . . . .	111
10.5.1	Form factors . . . . .	111
10.5.2	Parton Distributions . . . . .	113
10.5.3	Analytic form factors . . . . .	116
10.5.4	$F_2^c$ and $F_L$ . . . . .	118
10.6	Extension to $Q^2 = 0$ . . . . .	120
10.7	$F_2^\gamma$ predictions . . . . .	122
10.8	Conclusion . . . . .	126
<b>11</b>	<b>Global QCD fit</b>	<b>133</b>
11.1	Fitted and evolved quantities . . . . .	133
11.2	Initial parametrisation . . . . .	136
11.3	Fitted experiments . . . . .	138
11.4	Results . . . . .	141
11.5	Conclusions and perspectives . . . . .	142
<b>12</b>	<b>Conclusions</b>	<b>161</b>
<b>A</b>	<b>Feynman rules in QCD</b>	<b>167</b>
<b>B</b>	<b>Useful Mellin transforms</b>	<b>169</b>
<b>C</b>	<b>The box diagram</b>	<b>171</b>
<b>D</b>	<b>Momentum sum rule and gluon distribution</b>	<b>173</b>



*You tell me that silence is nearer to peace than poems  
But if for my gift I brought you silence (for I know silence)  
You would say: "This is not silence, this is another poem"  
And you would hand it back to me.  
Leonard Cohen - Gift*

# Chapter 1

## Introduction

Understanding the structure of hadrons is a longstanding problem. From the point of view of quantum field theory, strong interactions are described [1–4] by Quantum Chromodynamics (QCD), which introduces quarks and gluons as the fundamental constituents of hadrons. Unfortunately, unlike in the case of the Quantum Electrodynamics (QED), the QCD coupling constant  $\alpha_s$  is of order 1. This means that we cannot perform a perturbative analysis. However, QCD has the very important property, known as *asymptotic freedom*, that the running coupling constant  $\alpha_s(Q^2)$  goes to zero when  $Q^2$  grows, or, equivalently, when we go to small distances [3]. As a consequence of this property, we often try to study processes insensitive to the infrared region<sup>1</sup> in order to apply perturbative QCD (pQCD).

Deep Inelastic Scattering (DIS), where we collide protons with highly-virtual photons, is one possibility to satisfy this requirement. In this case, the proton is probed by a photon of small size ( $\sim 1/Q$ ) and we can study it in the perturbative domain. In the large- $Q^2$  limit, the proton is made of partons (quarks and gluons) and the photon interacts with free partons [5]. In this limit, neglecting QCD corrections, the proton structure functions are independent of  $Q^2$  and are proportional to the probability of finding individual partons inside the proton. This is known as *Björken scaling* and the probability densities are called *parton distribution functions* (PDF). If we now take into account QCD corrections, the parton densities start to depend on  $Q^2$  and their evolution in  $Q^2$  is given by the Dokshitzer-Gribov-Lipatov-Altarelli-Parisi (DGLAP) evolution equations [6]. We must point out that these equations, based on perturbative QCD, are only valid in the high- $Q^2$  limit. Moreover, they only give the evolution of the PDF with  $Q^2$  and we still need to fix them at an initial scale  $Q_0^2$ . This is similar to renormalisation where we can, *e.g.*, obtain the behaviour of the running coupling  $\alpha_s(Q^2)$ , but we cannot predict  $\Lambda_{QCD}$  from first principles.

From experimental measurements, it appears that the proton structure function  $F_2(x, Q^2)$  rises quite fast at small  $x$ . In the small- $x$  limit, the DGLAP equation predicts a rise of  $F_2$  corresponding to an essential singularity in the complex- $j$  plane, which is in disagreement with Regge theory. From the pQCD point of view, large- $s$  (small- $x$ ) corrections, which need to be resummed, appear besides the large- $Q^2$  corrections. These high-energy corrections have been computed [7] by Balitsky, Fadin, Kuraev and Lipatov<sup>2</sup> and predict a power behaviour

---

<sup>1</sup>These processes are called *infrared safe*.

<sup>2</sup>Their result is referred to as the BFKL equation.

for  $F_2$  at small  $x$ . Unfortunately, the calculations go into the non-perturbative region and are not stable against next-to-leading order corrections [8]. The NLO BFKL equation is still an active field of research and obtaining a consistent explanation of the rise of  $F_2$  using QCD still remains a challenge.

Another approach to DIS is  $S$ -matrix theory [9], which describes hadronic interactions starting with basic principles such as unitarity or analyticity. In this framework, Regge has introduced [10, 11] a theory of complex orbital momenta  $j$  which allows to constrain the energy dependence of high-energy interactions. Contrarily to perturbative techniques, Regge theory can be used when  $Q^2$  is small. The most famous application is probably the Donnachie-Landshoff two-pomerons model [12–14] where the rise of  $F_2$  is described by two powers of  $1/x$ :  $F_2(x, Q^2) = A_h(Q^2)x^{-\varepsilon_h} + A_s(Q^2)x^{-\varepsilon_s}$ , corresponding to two simple poles at  $j = 1 + \varepsilon_h \approx 1.4$  and  $j = 1 + \varepsilon_s \approx 1.1$  in the complex angular-momentum space. The Regge approach nevertheless has two drawbacks. First of all, although the  $s$  behaviour of the amplitudes is constrained, it is not univoquely determined; besides the Donnachie-Landshoff model, it is also possible to describe  $F_2$  using, for example, multiple-pole pomerons [15–18]. Furthermore, Regge theory tells us nothing about form-factors which are unknown functions of  $Q^2$ .

In this thesis, I shall show how it is possible to obtain a description of DIS combining Regge theory and pQCD. To begin with, I shall explain the theoretical basis of large- $Q^2$  corrections. I shall give a proof of the factorisation theorem [19], showing that in the large- $Q^2$  limit, introducing a factorisation scale  $\mu_F$ , the  $\gamma^*p$  amplitude can be expressed as the product of a short-distance, perturbative factor multiplying a long-distance contribution. With this crucial result at hand,  $\mu_F$ -independence of the amplitude directly leads to the DGLAP evolution equation. I shall also compute the leading-order (LO) splitting functions from the factorisation theorem and show that, from the point of view of Feynman diagrams, the LO DGLAP equation resums diagrams proportional to  $\alpha_s^n \log^n(Q^2/\mu_F^2)$ . I shall conclude by the solution and the basic properties of the DGLAP evolution equations. Since analysis of the experimental data directly based only on the resolution of the DGLAP equations are numerous [20–24], I shall explain their technique without performing such a global fit. We shall see further that we can constraint these fits using Regge theory.

In the second part of this thesis, I shall study the Regge-theory approach to DIS. As a first step, I shall explain the postulates of  $S$ -matrix theory and their first consequences such as the Cutkosky rules [25] or the dispersion relations. If we want to study high-energy scattering in the formalism of  $S$ -matrix theory, it is very useful to introduce Regge theory. The idea of this theory is to perform a Sommerfeld-Watson transform on the partial-wave expansion of the amplitudes in order to introduce complex angular momenta. The study of the analytic properties of the amplitudes in this complex plane constrains their behaviour at high energy. In this introduction to Regge theory, I shall also give its domain of applicability, which will be widely used when we shall compare models with experimental data. Moreover, in DIS we often use the Mellin transform, for example to obtain the DGLAP equation. Thus, I shall show how the Sommerfeld-Watson transform becomes a Mellin transforms in low- $x$  DIS. Another interesting property arising from the unitarity of  $S$ -matrix theory is the fact that total cross-sections for on-shell particles cannot grow faster than  $\log^2(s)$  at high energy [26, 27]. Since throughout this thesis, we shall be interested by multiple-

pole pomerons, corresponding to a logarithmic rise of  $F_2$ , as an alternative to simple-pole pomerons, I shall conclude this introductory chapter on  $S$ -matrix theory by giving a proof of this limit known as the *Froissart-Martin bound* [26, 27].

The first question one may ask about Regge theory is “how can we apply it to DIS?”. The easiest method is the following. Start with a given singularity structure in the complex- $j$  plane which corresponds to an energy dependence of the amplitude. In order to reproduce the rise of the cross-sections and of the structure functions, the leading singularity must be a simple pole at  $j = 1 + \varepsilon > 1$ , corresponding to a  $x^{-\varepsilon}$  rise, or a multiple pole at  $j = 1 + \varepsilon \geq 1$ , corresponding to a  $\log^n(1/x)x^{-\varepsilon}$  rise. Since Regge theory does not say anything about the residues of the singularities, these shall be parametric functions of  $Q^2$  and we adjust the parameters in order to reproduce the experimental data for  $F_2$  and for the total cross-section in the high-energy region. As said before, the most famous model using this approach is the two-pomeron Donnachie-Landshoff model, using two simple poles at  $j \approx 1.4$  and  $j \approx 1.1$ . However, this model suffers from several unnatural features: first of all, it violates the Froissart bound for total cross-sections, secondly, the hard pomeron is not present in all interactions while, as we shall see later, all hadronic interactions are expected to have the same singularity structure, thirdly and most importantly, one needs to modify by hand the DGLAP evolution equation and apply it only to the part of the cross-section corresponding to the hard pomeron. For these reasons, it is interesting to consider multiple-pole models. In this thesis, I shall therefore concentrate on multiple-pole pomerons at  $j = 1$ , corresponding to a logarithmic behaviour<sup>3</sup> of the cross-sections at high energy. As a first step, I shall simply use the standard approach and adjust some analytical functions of  $Q^2$  in order to reproduce the proton structure function  $F_2^p$  and the total  $\gamma p$  cross-section. The double-pole model has been studied in [15, 16, 18], so I shall only apply this approach to the triple-pole-pomeron case. We shall see that it is possible to fit the  $F_2^p$  data, together with the total  $\gamma p$  cross-section, up to  $Q^2 = 3000 \text{ GeV}^2$  and with the energy cut<sup>4</sup>  $\sqrt{s} > 10 \text{ GeV}$ . Besides this fit, the COMPETE collaboration [28] has shown that all hadronic cross-sections and  $\rho$  factors can be described at high energy by a triple-pole pomeron. To summarise this first application of Regge theory to DIS, we can say that the triple-pole pomeron can be used to describe both hard data in DIS and soft data in hadronic interactions.

Another interesting aspect of  $S$ -matrix theory is the factorisation theorem. In Regge theory, amplitudes can be calculated considering exchanges of objects corresponding to a given high-energy behaviour, such as, for example, the  $a_2/f$  reggeon. In such a case, the amplitudes vary from process to process only because of the coupling of these objects to the interacting particles. Note that this coupling is directly related to the residues of the poles in complex- $j$  plane. They depend, for example, on  $Q^2$  and  $t$  and can vanish if the exchanged object does not have compatible quantum numbers. In this framework, the coupling for a particle  $a$  interacting with a particle  $b$  is proportional to the product  $C_a C_b$  where  $C_a$  and  $C_b$  are the couplings of the exchanged objects with particles  $a$  and  $b$  respectively. This property from Gribov and Pomeranchuk [29] was proven for simple-pole exchanges and considering only the two-particles threshold, *i.e.* for values of  $t$  such that we do not have more than two

---

<sup>3</sup>A double pole at  $j = 1$  corresponds to a logarithmic rise and a triple-pole to a squared-logarithm behaviour.

<sup>4</sup>More precisely, we shall see in chapter 5 that Regge theory requires a cut on  $\cos(\theta_t)$ .

particles in the intermediate states. We shall show in this thesis that, using unitarity in the  $t$  channel<sup>5</sup>, the original argument can be extended to more (elastic or inelastic) thresholds and to the case of multiple-pole pomerons. An important consequence of factorisation is that all hadronic interactions must have the same singularity structure. In our derivation, we shall obtain  $t$ -channel-unitarity ( $t$ CU) rules giving the residues of a pole of any order in the  $bb$  amplitude as functions of the residues in the  $ab$  and  $aa$  amplitudes. I shall first give a proof of this result using the usual method of continuing amplitudes around the  $t$ -channel discontinuities for elastic and inelastic thresholds and, then, give a complete proof relying on  $t$ -channel unitarity which only requires that the adjoint of the  $S$  matrix be defined. In the same chapter, we shall consider the extension of the factorisation theorem to the case of photons. Due to the fact that they are massless, the final state can contain any number of infinitely many soft photons, leading to a finite result when we resum all these in both the final and the intermediate state, and giving a zero probability to emit a definite number of photons [30]. This problem, known as the infrared catastrophe, makes the definition of a  $S$ -matrix for QED problematic. Furthermore, as only part of the cross section is considered (as the final state must contain hadrons), it is not possible to consider an  $S$  matrix. I shall show what parts of the factorisation theorem can be kept in the case of photons, and what structure singularities can have.

Once we have proven the extended version of the factorisation theorem, the natural use of it is to check whether the  $t$ CU rules can be applied to predict the  $\gamma\gamma$  cross-section and the  $F_2^\gamma$  measurements in the Regge domain from the  $pp$  and  $\gamma p$  cross-sections and the  $F_2^p$  structure function. Unfortunately, we shall see that the double-pole pomeron model produces negative cross-sections in  $\gamma\gamma$  when  $Q_1^2 = Q_2^2 \neq 0$  and that we meet the same problem with the parametrisation of the triple-pole introduced previously. Since in this analysis, we have only introduced the box-diagram as an additional singularity in  $F_2^\gamma$ , this failure does not necessarily mean that the double- and triple-pole pomeron models are definitively ruled out. This can be explained either by a bad choice for the  $Q^2$  dependence of the residues, or by the fact that we must add more singularities such as, for example, a BFKL pomeron. For the double-pole pomeron case, we have not been able to obtain good predictions for the  $\gamma\gamma$  data by simply modifying the  $Q^2$  dependence of the couplings, but we shall show that, adding a series of sub-leading simple poles to the leading double pole at  $j = 1$ , we obtain a generalised version of the double-pole pomeron which behaves like a double pole at small  $x$ , which can be seen as a unitarisation of the BFKL pomeron and which reproduces the  $F_2^\gamma$  measurements with the box diagram as the only additional singularity. Concerning the triple-pole pomeron model, we shall show that a modification of the  $Q^2$  dependence of the residues allows to keep a very good description of the  $F_2^p$  data and to obtain good results<sup>6</sup> for  $F_2^\gamma$ .

---

<sup>5</sup>This means that we apply unitarity constraints on the amplitudes analytically continued to the region of the corresponding  $t$ -channel processes, using crossing symmetry.

<sup>6</sup>In order to test the factorisation theorem without entering too much into the details of the form factors  $Q^2$  dependence, we have limited this study to  $Q^2 = 150 \text{ GeV}^2$ . Since our previous fit involving only the  $\gamma p$  experiments extends up to  $3000 \text{ GeV}^2$ , we have chosen to show it in this thesis. Although it is not sufficient to reproduce all  $\gamma^*\gamma^*$  data, it teaches us that  $F_2^p$  may behave like a triple-pole at small  $x$ , and, again, there is room for additional singularities in the  $\gamma^*\gamma^*$  interactions at non-zero  $Q^2$ .

Up to now, I have talked about models that use either perturbative QCD, or Regge theory. One must of course ask if it is possible to have a description of DIS at soft and hard scales compatible with both approaches. I shall answer this question in the third part of this thesis. A lot of physicists working in the QCD framework are trying to find an equation for small- $x$  phenomenology solving the problems of the BFKL equation. Most of them base their work on the concept of saturation, which comes from the idea that, when  $x$  becomes smaller and smaller, more and more gluons are produced and, at some level, must lead to non-linear effects due to gluon recombinations. I shall adopt another approach here: we shall assume that Regge theory gives the energy dependence and check if the DGLAP evolution equation can tell us something about the  $Q^2$  evolution. To motivate this approach, let us consider the following argument: the initial distributions used in the global DGLAP fits behave like a power of  $x$  at small  $x$ , but this power does not correspond to the singularities present in hadronic cross sections. Since it is possible to describe all hadronic phenomena using the same singularity structure, one may ask if one can also use this behaviour in initial parton distributions used in DGLAP fits. In such a case, we can fix the quark distribution at an initial scale  $Q_0^2$  using the Regge fit obtained before for the generalised double-pole or for the triple-pole pomeron model, and parametrise the gluon distribution using the same high-energy behaviour. Solving the DGLAP evolution equation, we can describe  $F_2^p$  at larger  $Q^2$ . In this model, we assume that Regge theory can give the small- $Q^2$  behaviour of the  $\gamma^*p$  interactions and the DGLAP equation reproduces the high- $Q^2$  data. Note that since the Regge models introduced previously do not extend up to  $x = 1$ , I shall describe the large- $x$  initial distributions using a standard PDF set, e.g. the GRV98 [21] parton densities. I shall argue that this is perfectly adequate for our high-energy analysis and that the choice of the PDF set at large  $x$  does not influence the small- $x$  results. This proves that we can use Regge theory to constrain the initial distributions for a DGLAP fit. Moreover, this technique allows to split the proton structure function in flavour-singlet and flavour-non-singlet components, as they evolve differently with DGLAP<sup>7</sup>, and to obtain information which is not contained in usual Regge theory. Then, in order to perform the evolution, we also introduce a gluon distribution which is neither provided by Regge theory.

Once we know that we can combine Regge theory and DGLAP evolution, the next step is to use DGLAP evolution to obtain some information about the residues unpredicted by Regge theory. To achieve this program, I shall assume that we can apply Regge theory not only for soft scales but also at large values of  $Q^2$ . If this is the case, the residues of the triple-pole pomeron must be compatible with the DGLAP evolution equation. The problem here is that the DGLAP evolution generates an essential singularity at  $j = 1$ , due to the  $1/x$  behaviour of the gluon splitting function. This problem comes from the fact that the DGLAP equation does not resum properly the high-energy contributions as does BFKL, and there must exist a mechanism through which this essential singularity is removed. In our case, the essential singularity generated by the DGLAP evolution interferes with the triple-pole at  $j = 1$ . There is however a possibility to solve that problem in such a way that the DGLAP evolution keeps a triple-pole at  $j = 1$  at all  $Q^2$ . The idea is to consider that, although the DGLAP evolution generates an analytically nasty essential singularity, one may see it as an

---

<sup>7</sup>The flavour-singlet quark distribution is coupled to the gluon density.

approximation to a well-behaved result. To get the residues of the triple-pole pomeron at  $Q^2 = Q_0^2$ , we can use it as an initial condition for a DGLAP evolution, without worrying about the presence of an essential singularity for  $Q^2 \neq Q_0^2$ . We shall see that this allows to find the residues of our Regge model at high  $Q^2$ . In order to find the residues at small  $Q^2$ , we can use an analytical expression, matching the high- $Q^2$  results and compatible with the  $F_2^p$  measurements at small  $Q^2$ . Note that this technique which uses DGLAP evolution does not only give a fit to  $F_2^p$ , but also allows to split the latter into quark components and to predict a gluon density. All these parton distributions are described with the same singularity structure in the complex- $j$  plane. Furthermore, I shall show that the obtained gluons give good predictions for the charm structure function  $F_2^c$  and for the longitudinal structure function  $F_L$ . To end this analysis of the residues using the DGLAP equation, I shall discuss the compatibility of these results with the factorisation theorem and the  $F_2^\gamma$  measurements at high virtualities.

Finally, I shall study the possibility of removing the dependence on a standard PDF set at large  $x$  in the Regge-constrained DGLAP fit. This means that we shall extend our analytic parametrisation of the initial distributions up to  $x = 1$ . I shall therefore perform a global QCD fit using a triple-pole pomeron model a small  $x$  and inserting powers of  $1 - x$  to reproduce the distributions at high  $x$ . However, if we want to fix properly the high- $x$  behaviour of the PDF, we may not restrict our analysis to  $F_2^p$  only: we must include other experiments such as those measuring  $F_2^d$  or neutrino data, which in turn require to split the flavour-non-singlet quark distribution into valence and sea quark distributions. This introduces a lot of additional parameters compared to the situation where we use a standard set at large  $x$ . Nevertheless, I shall show that using the triple-pole pomeron in the initial parton distributions gives a global QCD fit at least as good as the previous ones (CTEQ, MRST, GRV, ...).

To conclude this thesis, I shall summarise and compare the results obtained using different approaches. I shall also discuss their possible extensions.

# Chapter 2

## Deep Inelastic Scattering

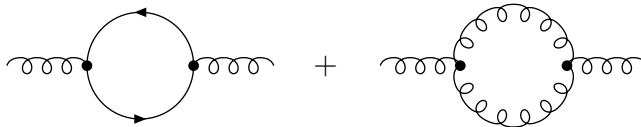
### 2.1 Basics

Since the main subject of this thesis is Deep Inelastic Scattering (DIS), we shall start by explaining what this consists of and how it is related to the study of strong interactions. We shall introduce the basic concepts of DIS in this chapter and leave more powerful techniques for the next ones.

In the mid sixties, Zweig [31] and Gell-Mann [32] classified the hadrons (mesons and baryons) in groups corresponding to representations of the  $SU_f(3)$  group<sup>1</sup>. This describes the hadrons as being extended objects constituted of *quarks*. Following the idea of Quantum Electrodynamics (QED), physicists introduced a lagrangian description for these new particles which is known as *Quantum Chromodynamics* (QCD)[1–4]. In the latter case, the lagrangian is invariant under the  $SU_c(3)$  transformations. Gauge invariance of the lagrangian under transformations from this non-abelian group introduces a vector boson coupled to the quark field *and to itself*: the *gluon*. With this lagrangian description of strong interactions, one can write Feynman rules (see Appendix A) for QCD and compute perturbative amplitudes. Unfortunately, the situation is not as simple as in the QED case due to the fact that the QCD coupling constant is large:

$$\alpha_s = \frac{g^2}{4\pi} \sim 1$$

and a perturbative treatment of QCD may not be valid. However, if we consider one-loop corrections to the gluon propagator, one has to sum two Feynman diagrams



---

<sup>1</sup>The subscript  $f$  here means that the symmetry acts in flavour space. In the  $SU_f(3)$  case, we have three quark flavours:  $u$ ,  $d$  and  $s$ . This subscript is introduced in order to distinguish the effective flavour symmetry with the colour  $SU_c(3)$  symmetry of the QCD lagrangian.

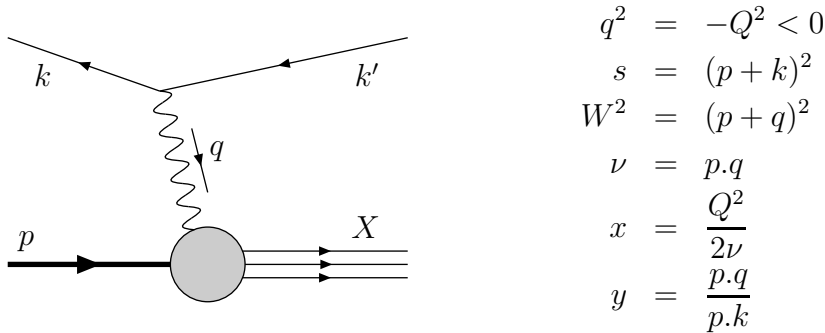
which leads to the following running coupling constant

$$\alpha_s(Q^2) = \frac{12\pi}{(33 - 2n_f) \log(Q^2/\Lambda_{QCD}^2)}$$

where  $\Lambda_{QCD} \approx 200$  MeV is the Landau pole and  $n_f$  is the number of active flavours. The important point here is that gluon self-interaction gives a running coupling constant which decreases with  $Q^2$ . This property is known as *asymptotic freedom* and means that at small distances,  $\alpha_s$  goes to 0 and quarks are free. Thus, if we can observe the small-distance structure of a hadron, we expect to see free partons (quarks or gluons).

Moreover, due to confinement, quarks and gluons are not directly observable and we only see hadrons. Due to the high value of the coupling constant, perturbative QCD (pQCD) is unable to predict the wavefunctions of the hadrons in terms of quarks and gluons, which remains an open question. Since experimentally, we have hadrons in initial and final states, which are non-perturbative objects, we cannot predict hadronic cross-sections only from pQCD. However, we may ask whether it is possible to get some information on the hadron structure from pQCD. In other words, are there QCD processes which are insensitive to the non-perturbative region *i.e.* which are computable at the parton level and do not depend on hadronisation? As we shall see, we can find such processes. Due to the fact that they do not depend on the large-distance behaviour of the strong interactions, we call them *infrared safe* processes.

Throughout this thesis, we shall concentrate more precisely on one of them: *Deep Inelastic Scattering* (DIS). The idea of DIS is to probe the small-distance structure of the proton using a virtual photon as shown below:



We therefore study the inclusive process  $ep \rightarrow eX$ . Let us show that when the virtuality  $Q^2$  of the proton is large, this process is infrared safe and gives information about the small-distance structure of the target. The starting point is to split this interaction into a leptonic tensor  $L_{\mu\nu}$  describing the photon emission and a hadronic tensor containing information about the proton

$$|\mathcal{M}|^2 = L^{\mu\nu} W_{\mu\nu}.$$

The leptonic part is easily calculable from Feynman rules

$$L_{\mu\nu} = e^2 \text{tr}(\not{k} \gamma_\mu \not{k}' \gamma_\nu) = 4e^2 (k_\mu k'_\nu + k_\nu k'_\mu - g_{\mu\nu} k \cdot k').$$

The hadronic part is given by the hadronic electromagnetic current  $j_\mu$

$$\begin{aligned} W_{\mu\nu} &= \frac{1}{4\pi} \sum_X \langle P | j_\nu^\dagger(0) | X \rangle \langle X | j_\mu(0) | P \rangle (2\pi)^4 \delta^4(p + q - p_X) \\ &= \frac{1}{4\pi} \int d^4z e^{iq \cdot z} \langle P | j_\nu^\dagger(z) j_\mu(0) | P \rangle \\ &= \frac{1}{4\pi} \int d^4z e^{iq \cdot z} \langle P | [j_\nu^\dagger(z), j_\mu(0)] | P \rangle. \end{aligned}$$

The important point in this expression is that for  $Q \gg \Lambda_{QCD}$  we have  $z \sim 1/Q \ll 1/\Lambda_{QCD}$ , thus the long distance effects are suppressed at high  $Q^2$  and DIS is infrared safe.

Fortunately, the tensor  $W_{\mu\nu}$  can be simplified using gauge invariance  $q^\mu W_{\mu\nu} = q^\nu W_{\mu\nu} = 0$ . One easily checks that the general form of such a tensor is<sup>2</sup>

$$W^{\mu\nu} = \left( g^{\mu\nu} - \frac{q^\mu q^\nu}{q^2} \right) W_1(x, Q^2) + \left( p^\mu + \frac{1}{2x} q^\mu \right) \left( p^\nu + \frac{1}{2x} q^\nu \right) W_2(x, Q^2)$$

where there only remain two unknown functions  $W_1$  and  $W_2$ , or equivalently  $F_1$  and  $F_2$ :

$$\begin{aligned} F_1(x, Q^2) &= W_1(x, Q^2), \\ F_2(x, Q^2) &= \nu W_1(x, Q^2), \\ F_L(x, Q^2) &= F_2(x, Q^2) - 2x F_1(x, Q^2). \end{aligned}$$

$F_1$ ,  $F_2$  and  $F_L$  are called the *proton structure functions*.

## 2.2 Parton model

It is convenient to work in the frame where the proton is moving very fast. Its 4-momentum is then light-like and we can introduce a second light-like vector with  $n \cdot p = 1$

$$\begin{aligned} p^\mu &\equiv (P, 0, 0, P), \\ n^\mu &\equiv \left( \frac{1}{2P}, 0, 0, -\frac{1}{2P} \right). \end{aligned}$$

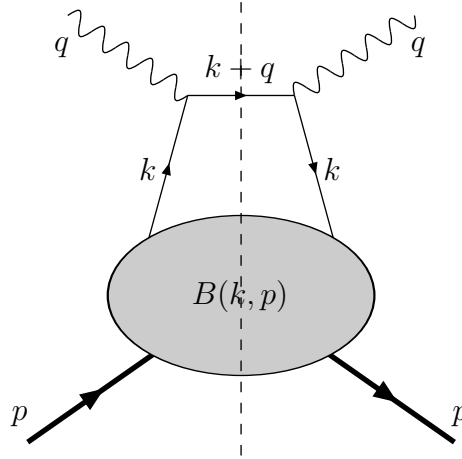
With these definitions, we can project the structure functions out of the hadronic tensor

$$\begin{aligned} F_2 &= \nu n^\mu n^\nu W_{\mu\nu}, \\ F_L &= \frac{4x^2}{\nu} p^\mu p^\nu W_{\mu\nu}. \end{aligned}$$

We then consider that the proton is constituted of *partons* and that the virtual photon scatters on one of them.

---

<sup>2</sup>Assuming parity is conserved.



If  $e_q$  is the charge of the struck parton, the hadronic tensor is then given by

$$W^{\mu\nu} = e_q^2 \int \frac{d^4k}{(2\pi)^4} \text{tr} [\gamma^\mu (\not{k} + \not{q}) \gamma^\nu B(k, p)] \delta((k+q)^2).$$

To perform  $k$ -integration we shall use the light-cone expression for  $k$

$$k^\mu = \xi p^\mu + \frac{k^2 + k_\perp^2}{2\xi} n^\mu + k_\perp^\mu.$$

Considering the high- $Q^2$  limit (called *Björken limit*), we neglect the other scales in the on-shell condition which becomes

$$\delta((k+q)^2) \approx \frac{1}{2\nu} \delta(\xi - x).$$

If we introduce the quark distribution

$$q(x) = \int \frac{d^4k}{(2\pi)^4} \text{tr} [\not{n} B(k, p)] \delta(\xi - x),$$

the  $F_2$  structure function becomes

$$\begin{aligned} F_2 &= \frac{1}{2} e_q^2 \int \frac{d^4k}{(2\pi)^4} \text{tr} [\not{n} (\not{k} + \not{q}) \not{n} B(k, p)] \delta(\xi - x) \\ &= e_q^2 x q(x). \end{aligned} \tag{2.1}$$

Moreover, in the parton model<sup>3</sup>  $F_L = \mathcal{O}(\frac{1}{\nu})$ , which means that in our limit,  $F_2 = 2xF_1$ . Equation (2.2) is a very well-known property called *Björken scaling* [5]. This property tells us that  $F_2$  scales *i.e.* is  $Q^2$ -independent. Physically, the virtual photon strikes a parton with a fraction  $x$  of the proton momentum and  $q(x)$  is the probability to find such a parton inside the proton. Taking into account all possible flavours, we finally have

$$F_2(x)|_{\text{Björken scaling}} = x \sum_{\text{flavours}} e_q^2 [q(x) + \bar{q}(x)]. \tag{2.2}$$

<sup>3</sup>If we take into account QCD corrections, the first logarithmic corrections to  $F_L$  have the form  $\alpha_s^n \log^{n-1}(Q^2)$  *i.e.* are only present starting at NLO.

## 2.3 Frames in DIS

In QCD, the interpretation of physical phenomena depends on the reference frame. This is simply due to the fact that, under a Lorentz transformation, the fields are modified. Therefore, depending on the effect we want to highlight, it is important to choose carefully the reference frame in which we work. We shall briefly introduce the most important frames used in DIS.

### 2.3.1 Björken frame

This frame has already been introduced to obtain Björken scaling. If we introduce the light-cone variables

$$p^\pm = \frac{E \pm p_x}{\sqrt{2}},$$

it is the frame where the proton moves very fast:

$$p^+ \gg m, \quad p^- \ll m \quad \text{and} \quad \vec{p}_\perp = \vec{0}_\perp.$$

The partons have a momentum  $\xi p$  which means that they also move along the “+” direction. If  $n$  is the 4-vector introduced above, the photon has a momentum

$$q^\mu = \nu n^\mu + q_\perp^\mu,$$

with  $Q^2 = \vec{q}_\perp^2$ .

As we have seen, this frame is perfectly suited to introduce Björken scaling. It is the frame where we can properly define parton distributions, even if we take into account QCD corrections<sup>4</sup>.

### 2.3.2 Breit frame

The Breit frame is the frame where the photon has a vanishing energy and the proton is moving close to the light-cone. In this case,

$$\begin{aligned} p &\equiv \left( \sqrt{\frac{Q^2}{4x^2} + m^2}, \frac{Q}{2x}, \vec{0}_\perp \right) \approx \left( \frac{Q}{2x} + \frac{xm^2}{Q}, \frac{Q}{2x}, \vec{0}_\perp \right) \\ q &\equiv \left( 0, -Q, \vec{0}_\perp \right). \end{aligned}$$

Since, in the rest frame, the proton has a space-time extension

$$\Delta x^+ \sim \Delta x^- \sim \frac{1}{m},$$

---

<sup>4</sup>We shall see in the next chapter that, in addition, we must work in the light-cone gauge, where QCD corrections take the form of ladders.

its extension in the moving frame is

$$\Delta x^+ \sim \frac{Q}{m^2}, \quad \Delta x^- \sim \frac{1}{Q}.$$

Since the photon has  $\Delta x^+ \sim 1/Q$ , we have, for  $Q^2 \gg m^2$ ,

$$(\Delta x^+)_{\text{photon}} \ll (\Delta x^+)_{\text{proton}}.$$

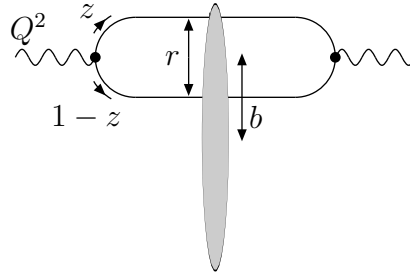
This shows that the photon can resolve partons.

### 2.3.3 Dipole frame

The idea of the dipole frame is to have a picture of DIS where the photon splits into a  $q\bar{q}$  dipole and that dipole interacts with the proton. If the lifetime of the dipole is much larger than the interaction time, we can factorise the  $\gamma^*p$  cross-section as follows

$$\sigma^{\gamma^*p}(x, Q^2) = \int d^2b d^2r \int_0^1 dz \left| \Psi(Q^2; \vec{b}, \vec{r}, z) \right|^2 \sigma_{\text{dipole}}(x; \vec{b}, \vec{r}, z),$$

where  $\Psi$  is the photon wavefunction. This picture can be represented in this way:



In this frame, both the proton and the photon are near the light-cone and move along the  $z$  axis in opposite directions :

$$p \equiv \left( P + \frac{M^2}{2P}, P, \vec{0}_\perp \right),$$

$$q \equiv \left( \sqrt{q_0^2 - Q^2}, -q_0, \vec{0}_\perp \right),$$

with  $q_0 \gg Q$ . With these definitions, we must have  $\nu = p \cdot q \approx 2Pq_0$ . On the other hand, if we want both the proton and the photon near the light-cone, we must have  $P$  and  $q_0 \gg Q$ . Thus  $\nu \gg Q^2$  and  $x \ll 1$ . This means that the dipole frame is suited to study DIS at small  $x$ , or in the double leading approximation ( $x \ll 1$  and  $Q^2 \gg m_p^2$ ). Due to the fact that we have  $p^+$  very large and  $q^+$  very small, the photon lifetime is much bigger than the interaction time.

Finally, note that, in this frame, the partonic structure of the proton is no longer valid and the photon does not probe the proton structure. Instead of describing the  $\gamma^*p$  interaction as a parton taken out of the proton following by the interaction between this parton and the virtual photon, in the dipole frame, we shall have a dipole interacting with the gluonic field inside the proton<sup>5</sup>. This interaction does not involve one single parton.

<sup>5</sup>This interaction can be expressed in terms of Wilson lines.

# Part I

## The DGLAP Evolution equation



*A kite is a victim you are sure of you love it because it pulls  
Gentle enough to call you master, strong enough to call you fool;  
Because it lives like a trailed falcon in the high sweet air,  
And you can always haul it down to tame it in your drawer.*  
Leonard Cohen - A kite is a victim

## Chapter 3

# Factorisation theorem and DGLAP evolution

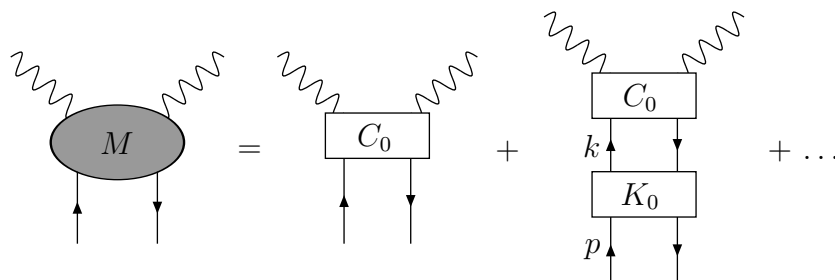
Since the DGLAP equation is based on the QCD factorisation theorem, which is by itself a powerful result, I will first explain how to prove that theorem. I will then explain how to obtain the DGLAP equation itself and study its properties and tests. The factorisation theorem tells us that we can write the  $\gamma^*q$  cross section at large  $Q^2$  as the product of a short-distance part and a long-distance interaction containing all collinear singularities.

Complete proofs of the factorisation theorem being rare, we shall explain it in detail for the non-singlet case, following [19]. We shall then explain shortly how to extend the results for the flavour-singlet case.

### 3.1 Factorising the $\gamma^*q$ amplitude: the non-singlet case

Our task is to extract the collinear singularities out of the  $\gamma^*p$  interaction. These correspond to logarithmic divergences of the form  $\log(Q^2/p^2)$ , where  $p$  is the momentum of the proton. Thus, the large- $Q^2$  limit corresponds to the small- $p^2$  one, and divergences are also called mass singularities<sup>1</sup>.

First of all, let us consider the squared matrix element for  $\gamma^*q$  interactions, denoted by  $M$ . We want to extract mass singularities of  $M$  in the light-cone gauge<sup>2</sup>.  $M$  can be expanded in terms of the 2-particle-irreducible (2PI) kernels  $K_0$  and  $C_0$  as follow [37, 38]



<sup>1</sup>The infrared divergences cancel between real emission and virtual corrections as required by the KLN theorem [33]. They are responsible for the presence of the '+' distribution in the splitting functions.

<sup>2</sup>Using the light-cone gauge  $n \cdot A = 0$ ,  $n^2 = 0$  allows to keep the probabilistic interpretation when going from leading order to next-to-leading order, to simplify calculations and to compare results with the Operator Product Expansion techniques [34–36].

In this expansion, the kernel  $K_0$  contains the propagators of its upper lines. One can show [39] that, as long as we keep external legs unintegrated, these 2PI kernels are finite in the axial gauge.

In order to simplify expressions, we shall omit all the 4-momentum indices, e.g. we shall write  $C_0$  instead of  $C_{0\alpha\beta}^{\mu\nu}$ , and, the product of two kernels containing indices summation and phase-space integration will be denoted by  $\otimes$

$$(A \otimes B)(p, q) = \int \frac{d^d k}{(2\pi)^d} A^{\mu\nu}(p, k) B^{\rho\sigma}(k, q),$$

with  $d = 4 + \varepsilon$  (we shall use dimensional regularisation to extract the collinear divergences). Note that, using the parametrisation introduced previously

$$k^\mu = \xi p^\mu + \frac{k^2 + k_\perp^2}{2\xi} n^\mu + k_\perp^\mu,$$

with  $p^2 = n^2 = 0$  and  $p \cdot n = 1$ , the phase space integration can be rewritten under the form

$$d^d k = \frac{d\xi}{2\xi} d^{d-2} k_\perp dk^2.$$

Finally, for contractions of spin or indices between 4-momenta and kernels we shall use the following notation

$$\begin{aligned} [\not{k} A] &\equiv (\not{k})_{\mu\nu} A^{\mu\nu}_{\alpha\beta}, \\ \not{k} A] &\equiv A^{\mu\nu}_{\alpha\beta} (\not{k})^{\alpha\beta}. \end{aligned}$$

With these simplifications, the ladder expansion gives

$$M = C_0 \otimes (\mathbb{1} + K_0 + K_0 \otimes K_0 + \dots) = C_0 \otimes \frac{1}{\mathbb{1} - K_0} = C_0 \otimes \Gamma_0. \quad (3.1)$$

We now want to split this amplitude into some part containing all divergences and some short-distance kernel free of collinear singularities. This can be performed by introducing a projector  $\mathbb{P} = \mathbb{P}_\varepsilon \times \mathbb{P}_n$  where

1.  $\mathbb{P}_n$  decouples  $C_0$  and  $\Gamma_0$  in spinor indices (they both behave like scalars when  $\mathbb{P}_n$  is applied),
2.  $\mathbb{P}_\varepsilon$  extract the collinear singularities out of the phase space integrations. These singularities behave like  $1/\varepsilon$  and arise from the  $dk^2/k^2$  integration in  $4 + \varepsilon$  dimensions.

The explicit form of  $\mathbb{P}_n$  can be found from the decomposition of  $K_0$

$$K_0 \not{p}] = A \not{k}_\parallel + B \not{k}_\perp + C \not{\eta} k^2 + D \not{\eta} \not{k}_\perp \not{k}_\parallel, \quad (3.2)$$

where  $A$ ,  $B$ ,  $C$  and  $D$  are dimensionless quantities. Since the only other scale present in  $K_0$  is  $\mu$ , the unit of mass in the dimensional regularisation,  $A$ ,  $B$ ,  $C$  and  $D$  depend on  $\frac{k^2}{\mu^2}$ ,  $\xi$  and  $\varepsilon$ , and the divergent part of the  $k$  integration will have the following form

$$\int_0^{-Q^2} \frac{dk^2}{k^4} \int_0^{-(1-x)k^2} dk_{\perp}^2 \left( \frac{k_{\perp}^2}{\mu^2} \right)^{\varepsilon} (K_0 \not{p})$$

In this integration,  $k^2$  has to be smaller than the hard scale of the process and the limits on  $k_{\perp}$  come from the condition  $(p-k)^2 > 0$ . Since we are only interested in the divergent contribution, we have  $k_{\perp}^2 \approx -k^2$  and all terms proportional to  $k_{\perp}$  or  $k^2$  in (3.2) will not contribute. Therefore,

$$K_0 \not{p} = \not{k} \left[ \frac{\not{p}}{4\xi} K_0 \not{p} \right] + \text{finite part.}$$

The projector  $\mathbb{P}_n$  will thus be defined through

$$A \mathbb{P}_n B = A \not{k} \left[ \frac{\not{p}}{4\xi} B \right]. \quad (3.3)$$

On the other hand, the projector  $\mathbb{P}_{\varepsilon}$  will keep the collinear pole in the  $k^2$  integration in the  $\left[ \frac{\not{p}}{4\xi} B \right]$  part and set  $k^2 = 0$  in the  $A \not{k}$  part.

We must use this projector to carry mass singularities out of the ladder expansion (3.1). The first step is to write

$$\begin{aligned} M &= C_0 + C_0 \sum_{n=1}^{\infty} K_0^{n-1} (\mathbb{1} - \mathbb{P}) K_0 + C_0 \sum_{n=1}^{\infty} K_0^{n-1} \mathbb{P} K_0 \\ &= C_0 \left[ \mathbb{1} + \sum_{n=0}^{\infty} K_0^n (\mathbb{1} - \mathbb{P}) K_0 \right] + M \mathbb{P} K_0. \end{aligned}$$

Putting the last term in the left-hand side, we can repeat the same trick for the remaining sum,

$$\begin{aligned} M(\mathbb{1} - \mathbb{P} K_0) &= C_0 \left[ \mathbb{1} + \sum_{n=0}^{\infty} K_0^n (\mathbb{1} - \mathbb{P}) K_0 \right] \\ &= C_0 \left\{ \mathbb{1} + (\mathbb{1} - \mathbb{P}) K_0 + \sum_{n=0}^{\infty} K_0^n (\mathbb{1} - \mathbb{P}) [K_0 (\mathbb{1} - \mathbb{P}) K_0] \right\} \\ &\quad + M \mathbb{P} [K_0 (\mathbb{1} - \mathbb{P}) K_0], \end{aligned}$$

and we can again put the last term in the LHS

$$M \{ \mathbb{1} - \mathbb{P} K_0 - \mathbb{P} [K_0 (\mathbb{1} - \mathbb{P}) K_0] \} = C_0 \left\{ \mathbb{1} + (\mathbb{1} - \mathbb{P}) K_0 + \sum_{n=0}^{\infty} K_0^n (\mathbb{1} - \mathbb{P}) [K_0 (\mathbb{1} - \mathbb{P}) K_0] \right\}.$$

By repeating these steps, we build a series on both sides and end up with

$$M = \left( C_0 \frac{1}{\mathbb{1} - (\mathbb{1} - \mathbb{P}) K_0} \right) \left( \frac{1}{\mathbb{1} - \mathbb{P} K} \right) \quad (3.4)$$

where

$$K = K_0 \left( \frac{1}{\mathbb{1} - (\mathbb{1} - \mathbb{P})K_0} \right) \quad (3.5)$$

$$\frac{1}{\mathbb{1} - \mathbb{P}K} = \mathbb{1} + \mathbb{P}K + (\mathbb{P}K)(\mathbb{P}K) + \dots \quad (3.6)$$

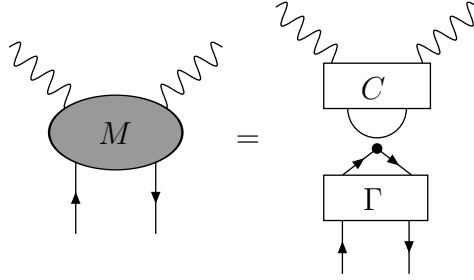
Note that, from the construction above, the projectors  $\mathbb{1} - \mathbb{P}$  in the series expansion act on the full expression on the right. This is obviously not the case for the expansion of  $(\mathbb{1} - \mathbb{P}K)^{-1}$ . This makes important differences since, e.g.  $(\mathbb{P}K)(\mathbb{P}K)$  contains double poles in  $\varepsilon$  while  $\mathbb{P}(K\mathbb{P}K)$  only contains simple poles.

Finally, we must multiply  $M$  by  $Z_F(\alpha_s)$ , the residue of the pole of the full quark propagator. One can show that it has the form

$$Z_F(\alpha_s) = 1 + \frac{1}{\varepsilon}Z_1(\alpha_s) + \frac{1}{\varepsilon^2}Z_2(\alpha_s) + \dots$$

The factor  $Z_F$  will take into account virtual corrections needed to cancel the infrared singularities in the real emissions<sup>3</sup>.

We thus have rewritten  $M$



where  $C = C_0 \frac{1}{\mathbb{1} - (\mathbb{1} - \mathbb{P})K_0}$  is free of mass singularity and  $\Gamma = \frac{1}{\mathbb{1} - \mathbb{P}K}$  contains all collinear singularities as well as the residue of the pole of the full quark propagator.

The explicit expression of this result can be written

$$\begin{aligned} M &= \frac{1}{2} [M \not{p}] \\ &= \frac{1}{2} Z_F \left[ C \frac{1}{\mathbb{1} - \mathbb{P}K} \not{p} \right] \\ &= \frac{1}{2} Z_F [C \not{k}]_{k^2=0} \left( \frac{1}{\xi} \mathbb{1} + \mathbb{P}_\varepsilon \left[ \frac{\not{k}}{4\xi} \mathbb{P}K \frac{1}{\mathbb{1} - \mathbb{P}K} \not{p} \right] \right). \end{aligned}$$

To obtain the last equality, we have used the fact that when  $k^2 = 0$ ,  $k_\perp = 0$  and thus  $k = \xi p$ . For the same reason, the first factor will only depend on  $\xi$  and, developing the remaining  $\mathbb{P}_\varepsilon$  projector, we can write the result as a convolution

$$M \left( \frac{Q^2}{\mu^2}, x, \alpha_s, \frac{1}{\varepsilon} \right) = \int_x^1 \frac{d\xi}{\xi} C \left( \frac{Q^2}{\mu^2}, \frac{x}{\xi}, \alpha_s \right) \Gamma \left( \frac{Q^2}{\mu^2}, \xi, \alpha_s, \frac{1}{\varepsilon} \right),$$

<sup>3</sup>This is a consequence of the KLN theorem.

with

$$\begin{aligned} C\left(\frac{Q^2}{\mu^2}, \frac{x}{\xi}, \alpha_s\right) &= \frac{1}{2} \left[ C_0 \frac{1}{\mathbb{1} - (\mathbb{1} - \mathbb{P})K_0} \not{k} \right]_{k^2=0}, \\ \Gamma\left(\frac{Q^2}{\mu^2}, x, \alpha_s, \frac{1}{\varepsilon}\right) &= Z_F(\alpha_s) \left\{ \delta(1-x) + \text{pp} \int \frac{d^d k}{(2\pi)^d} \delta(x-\xi) \xi \left[ \frac{\not{\eta}}{4\xi} K \frac{1}{\mathbb{1} - \mathbb{P}K} \not{k} \right] \right\}, \end{aligned} \quad (3.7)$$

the prefix pp meaning that the principal value of the integral has to be computed.

Physically,  $\Gamma(Q^2/\mu^2, x, \alpha_s, 1/\varepsilon)$  can be seen as a parton density in the parent quark, while  $C(Q^2/\mu^2, x, \alpha_s)$  appears as a short-distance cross-section and is called the *coefficient function*. Depending on the quantity you want to calculate ( $F_2^\nu$ ,  $F_2$  or  $F_L$ ), only  $C_0$  will be different. This means that, provided we probe the proton with a highly-virtual object, only the coefficient function will be process-dependent, while  $\Gamma$  is some fixed QCD object.

Before going into the consequences of this result, it is interesting to note that, in Mellin space<sup>4</sup>, factorisation is written as a simple product instead of the convolution in momentum space

$$M(Q^2, j, \alpha_s, 1/\varepsilon) = C(Q^2/\mu^2, j, \alpha_s) \Gamma(Q^2, j, \alpha_s, 1/\varepsilon). \quad (3.8)$$

Finally, the density  $\Gamma$  is normalised to the  $\gamma^*q$  cross-section ( $C = \delta(1-x)$ ): if  $\frac{d\sigma_0}{dQ^2}$  is the elastic photon-parton differential cross-section,

$$\frac{d\sigma}{dx dQ^2} = \frac{d\sigma_0}{dQ^2} \Gamma(Q^2, x, \alpha_s, 1/\varepsilon).$$

## 3.2 Renormalisation group techniques

Eq. (3.4) can also be written  $M(\mathbb{1} - \mathbb{P}K) = C$ , which looks like a mass renormalisation  $M_{\text{bare}}Z = M_r$ . The main difference in our case is that  $\Gamma$ , and thus  $\mathbb{1} - \mathbb{P}K$ , seems to depend on  $Q^2/\mu^2$ , but one of the important result of the factorisation theorem is that  $\Gamma$  is actually independent of  $Q^2/\mu^2$ . To see this, start from the fact that one can show that the 2PI kernel is finite. Since the projector  $\mathbb{P}$  extracts the  $1/\varepsilon$  divergences,  $K_0$  and  $K_0 [(\mathbb{1} - \mathbb{P})K_0]^n$  are finite when  $\varepsilon \rightarrow 0$  before the last  $dk^2/k^2$  integration. Thus, we can write

$$\Gamma(Q^2/\mu^2, x, 1/\varepsilon) = \delta(1-x) + \text{pp} \int_{-Q^2}^0 \frac{dk^2}{k^2} \Phi(k^2/\mu^2, x, \varepsilon),$$

where  $\Phi$  is finite when  $\varepsilon \rightarrow 0$ . On the other hand, we have

$$\Gamma(Q^2/\mu^2, x, 1/\varepsilon) = \delta(1-x) + \sum_{i=1}^{\infty} \frac{1}{\varepsilon^i} \Gamma_i(Q^2/\mu^2, x)$$

---

<sup>4</sup>Mellin space corresponds to  $x$  moments.

$$f(j) = \int_0^1 dx x^{j-1} f(x), \quad \text{and} \quad f(x) = \frac{1}{2i\pi} \int_{c-i\infty}^{c+i\infty} dj x^{-j} f(j),$$

where the integration contour stands at the right of all  $f$  singularities (see Appendix B).

Differentiating these two expressions with respect to  $Q^2$  and comparing coefficients gives  $\partial_{Q^2}\Gamma_i = 0$  for all  $i$ , and thus

$$\partial_{Q^2}\Gamma = 0.$$

as stated.

This proves that we can apply the well-known renormalisation group techniques to our problem. Let  $\mathcal{D}$  denote the total derivative with respect to  $\mu^2$

$$\mathcal{D} = \mu\partial_\mu + \left[ \beta(g) + \frac{1}{2}g\varepsilon \right] \partial_g.$$

Being a physical quantity,  $M$  must be  $\mu$ -independent. So, working in Mellin space, we have from (3.8)

$$\mathcal{D} \log(M) = \mathcal{D} \log(C) + \mathcal{D} \log(\Gamma) = 0.$$

If we introduce

$$\gamma(j, \alpha_s, \varepsilon) = \frac{1}{2}\mathcal{D} \log(\Gamma) = \frac{1}{2} \left[ \beta(g) + \frac{1}{2}g\varepsilon \right] \partial_g \log(\Gamma(j, \alpha_s, 1/\varepsilon)), \quad (3.9)$$

we have the following ‘‘renormalisation group equation’’

$$[\mathcal{D} + 2\gamma(j, \alpha_s)] C(Q^2/\mu^2, j, \alpha_s, \varepsilon) = 0. \quad (3.10)$$

The key point of this expression is the fact that, since both  $\mathcal{D}$  and  $C$  do not contain poles in  $\varepsilon$ ,  $\gamma$  is itself free of poles in  $\varepsilon$ . Expanding  $\Gamma(j) = 1 + \sum_i \Gamma_k \varepsilon^{-k}$ , we get

$$\gamma = \frac{1}{2}\alpha_s \partial_{\alpha_s} \Gamma_1 \quad (3.11)$$

which is useful to calculate  $\gamma$ .

Finally, if we integrate (3.9), we have

$$\Gamma(j, \alpha_s, 1/\varepsilon) = \exp \left[ \int_0^{\alpha_s} \frac{d\lambda}{\lambda} \frac{\gamma(j, \lambda)}{\bar{\beta}(\lambda) + \varepsilon/2} \right], \quad (3.12)$$

with

$$\bar{\beta}(\alpha_s) = \frac{1}{g}\beta(g) = - \left[ \frac{\alpha_s}{4\pi}\beta_0 + \left( \frac{\alpha_s}{4\pi} \right)^2 \beta_1 + \dots \right].$$

Using the  $\mu$  independence of  $M$ , we can write

$$M(Q^2, j, \alpha_s, 1/\varepsilon) = C(1, j, \alpha_s(Q^2)) \exp \left[ \int_0^{\alpha_s(Q^2)} \frac{d\lambda}{\lambda} \frac{\gamma(j, \lambda)}{\bar{\beta}(\lambda) + \varepsilon/2} \right], \quad (3.13)$$

where all divergences are contained in the second factor.

The function  $\gamma(j, \alpha_s)$  introduced here is often called the *anomalous dimension*. It can be calculated perturbatively to any order in  $\alpha_s$  by computing  $\Gamma$  from (3.7) and using (3.11).

### 3.3 The full $\gamma^*p$ amplitude and the DGLAP equation

The last step in order to recover the full DIS properties is to consider an incoming proton instead of a single quark. The total  $\gamma^*p$  squared amplitude will be the  $\gamma^*q$  squared amplitude we just calculated convoluted with the quark *bare* density inside the proton.

Let us call  $H$  the 2PI  $p \rightarrow q$  kernel. We can define the *bare parton density* as

$$q_{\text{bare}} = x \int \frac{d^d k}{(2\pi)^d} \delta(x - \xi) \left[ \frac{\not{n}}{4k \cdot n} H \not{p} \right].$$

If we assume that  $H$  verifies<sup>5</sup>

$$H(k^2, x) = \frac{1}{k^2} \int \frac{d^{d-2} k_{\perp}}{2(2\pi)^d} \left[ \frac{\not{n}}{4k \cdot n} H \not{p} \right] \leq C |k^2|^\eta$$

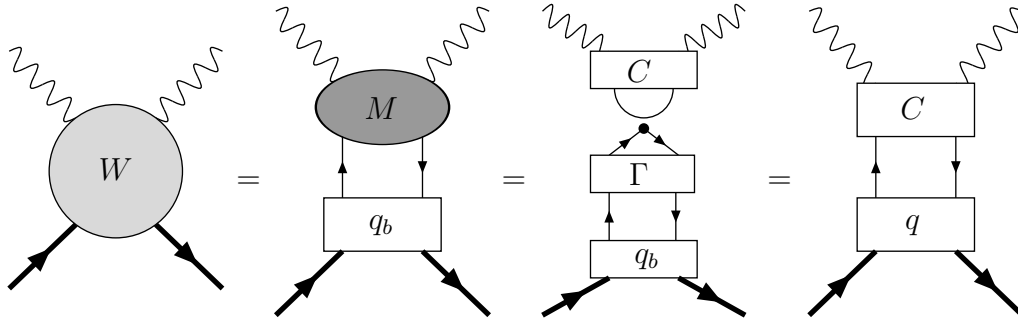
when  $|k^2| \rightarrow \infty$  for some  $C$  and  $\eta > 0$ , the bare parton density becomes<sup>6</sup>

$$q_{\text{bare}}(x, \alpha, 1/\varepsilon) = \int_{-Q^2}^0 \frac{dp^2}{p^2} H(p^2, x) = \int^{-\infty} \frac{dp^2}{p^2} H(p^2, x) + \mathcal{O} \left[ \left( \frac{\mu^2}{Q^2} \right)^\eta \right]. \quad (3.14)$$

The lower limit in this integral will generate the mass divergences which, due to the KLN theorem [33], must cancel the ones from the  $\gamma^*q$  interaction. Using (3.13), this allows us to define the *dressed* density through

$$q(j, Q^2) = \exp \left[ - \int_0^{\alpha(Q^2)} \frac{d\lambda}{\lambda} \frac{\gamma(j, \lambda)}{\beta(\lambda) + \varepsilon/2} \right] q_{\text{bare}}(j, Q^2). \quad (3.15)$$

Diagrammatically, the process of factorisation for  $\gamma^*p$  interaction can be summarised as follows



The dressed partonic density is a very important quantity. For example, from (3.13) and (3.15), we see that the  $F_2$  structure function is given by

$$F_2(x, Q^2) = x e_q^2 \int_x^1 \frac{d\xi}{\xi} C_2 \left( 1, \frac{x}{\xi}, \alpha_s(Q^2) \right) q(\xi, Q^2).$$

<sup>5</sup>We say that  $H(k^2, x)$  is tempered.

<sup>6</sup>Contributions from the last term, going to 0 like a power of  $Q^2$ , are called a **higher twists** and are neglected here.

At leading order in  $\alpha_s$ , the coefficient function is  $\delta(1-x)$  and

$$F_2(x, Q^2) = x e_q^2 q(\xi, Q^2).$$

Since, obviously,  $q(\xi, Q^2)$  depends on  $Q^2$ , we have a **violation of the Bjorken scaling** which is one of the most powerful results of QCD. Similarly to the case of renormalisation, the theory is unable to predict the parton densities for all values of  $x$  and  $Q^2$ , but gives the dependence on the scale. Actually, by differentiating (3.15) with respect to  $Q^2$ , we find

$$Q^2 \partial_{Q^2} q(j, Q^2) = \gamma(j, \alpha(Q^2)) q(j, Q^2), \quad (3.16)$$

or in  $x$ -space,

$$\boxed{Q^2 \partial_{Q^2} q(x, Q^2) = \int_x^1 \frac{d\xi}{\xi} P\left(\frac{x}{\xi}, \alpha(Q^2)\right) q(\xi, Q^2)}. \quad (3.17)$$

This is the *DGLAP evolution equation* and  $P(x)$  is called the *splitting function*.

### 3.4 Extension to the singlet case

If we allow for flavour-singlet exchanges, we now may have gluons in the vertical propagators. This means that, in addition to the quark projector  $\mathbb{P}$  introduced in (3.3), we now need a gluon projector. Again, we need a projector that decouples Lorentz indices and extracts the collinear singularities. Using the same kind of argument than for the quark case, we easily find

$$A \mathbb{P}_g B = [A_{\mu\nu} d^{\mu\nu}(k)]_{k^2=0} \mathbb{P}_\varepsilon \left[ \frac{-g^{\alpha\beta}}{2+\varepsilon} B_{\alpha\beta} \right], \quad (3.18)$$

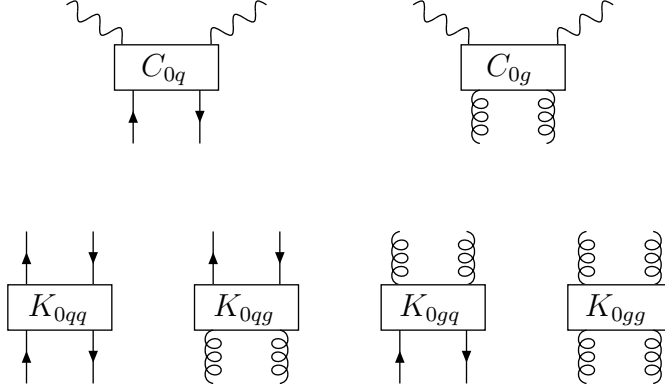
where  $\frac{1}{2+\varepsilon}$  is the average over gluon helicities and  $d^{\mu\nu}(k)$  is the numerator of the gluon propagator in the axial gauge

$$d^{\mu\nu}(k) = -g^{\mu\nu} + \frac{k^\mu n^\nu + n^\mu k^\nu}{k \cdot n}. \quad (3.19)$$

If we call  $\mathbb{P}_q$  the projector in the non-singlet case, we can introduce

$$\mathbb{P} = \begin{pmatrix} \mathbb{P}_q & \cdot \\ \cdot & \mathbb{P}_g \end{pmatrix}, \quad K_0 = \begin{pmatrix} K_{0qq} & K_{0qg} \\ K_{0gq} & K_{0gg} \end{pmatrix} \quad \text{and} \quad C_0 = \begin{pmatrix} C_{0q} \\ C_{0g} \end{pmatrix},$$

where the kernels  $C_{0a}$  and  $K_{0ab}$  can be represented as follows



In addition to the  $\gamma^*q$  amplitude, we must now also consider the  $\gamma^*g$  amplitude. With the notations introduced before and the gluon projector (3.18), all the results obtained in the previous section are still valid if we consider that all quantities carry indices identifying quarks and gluons, e.g.

$$M = \begin{pmatrix} M_{\gamma^*q} \\ M_{\gamma^*g} \end{pmatrix}.$$

As a consequence, equations (3.7), (3.8) and (3.11) hold with  $M$  and  $C$  considered as vectors and  $\Gamma$  and  $\gamma$  as  $2 \times 2$  matrices. The DGLAP evolution equation then becomes

$$\partial_{Q^2} \begin{pmatrix} q(j, Q^2) \\ g(j, Q^2) \end{pmatrix} = \begin{pmatrix} \gamma_{qq}(j, \alpha_s(Q^2)) & \gamma_{qg}(j, \alpha_s(Q^2)) \\ \gamma_{gq}(j, \alpha_s(Q^2)) & \gamma_{gg}(j, \alpha_s(Q^2)) \end{pmatrix} \begin{pmatrix} q(j, Q^2) \\ g(j, Q^2) \end{pmatrix}. \quad (3.20)$$

### 3.5 The full DGLAP evolution equation

To be complete, we now need to consider all quark flavours and gluons. This means that the full DGLAP equation can be written

$$\partial_{Q^2} \begin{pmatrix} q_a(j, Q^2) \\ \bar{q}_b(j, Q^2) \\ g(j, Q^2) \end{pmatrix} = \begin{pmatrix} \gamma_{q_a q_c} & \gamma_{q_a \bar{q}_d} & \gamma_{q_a g} \\ \gamma_{\bar{q}_b q_c} & \gamma_{\bar{q}_b \bar{q}_d} & \gamma_{\bar{q}_b g} \\ \gamma_{g q_c} & \gamma_{g \bar{q}_d} & \gamma_{g g} \end{pmatrix} \Big|_{j, \alpha_s(Q^2)} \begin{pmatrix} q_c(j, Q^2) \\ \bar{q}_d(j, Q^2) \\ g(j, Q^2) \end{pmatrix}, \quad (3.21)$$

or, in  $x$ -space,

$$\partial_{Q^2} \begin{pmatrix} q_a(x, Q^2) \\ \bar{q}_b(x, Q^2) \\ g(x, Q^2) \end{pmatrix} = \int_x^1 \frac{d\xi}{\xi} \begin{pmatrix} P_{q_a q_c} & P_{q_a \bar{q}_d} & P_{q_a g} \\ P_{\bar{q}_b q_c} & P_{\bar{q}_b \bar{q}_d} & P_{\bar{q}_b g} \\ P_{g q_c} & P_{g \bar{q}_d} & P_{g g} \end{pmatrix} \Big|_{\frac{x}{\xi}, \alpha_s(Q^2)} \begin{pmatrix} q_c(\xi, Q^2) \\ \bar{q}_d(\xi, Q^2) \\ g(\xi, Q^2) \end{pmatrix}, \quad (3.22)$$

where  $a, b, c$  and  $d$  run over quark flavours. This complicated set of 13 coupled equations can be simplified. We can reorganise the quark distributions into 11 flavour-non-singlet

distributions

$$\begin{aligned}
V_a &= q_a^-, \\
T_3 &= u^+ - d^+, \\
T_8 &= u^+ + d^+ - 2s^+, \\
T_{15} &= u^+ + d^+ + s^+ - 3c^+, \\
T_{24} &= u^+ + d^+ + s^+ + c^+ - 4b^+, \\
T_{35} &= u^+ + d^+ + s^+ + c^+ + b^+ - 5t^+,
\end{aligned}$$

where  $q^\pm = q \pm \bar{q}$ , and one singlet distribution

$$\Sigma = \sum_a q_a^+. \quad (3.23)$$

Using flavour symmetry, one can write the splitting functions as the sum of a non-singlet and a singlet contribution<sup>7</sup>

$$\begin{aligned}
P_{q_a q_b} &= P_{qq}^V \delta_{ab} + P_{qq}^S, \\
P_{q_a \bar{q}_b} &= P_{q\bar{q}}^V \delta_{ab} + P_{q\bar{q}}^S.
\end{aligned}$$

In these conditions, each of the densities  $V_a$  (resp.  $T_i$ ) evolves alone with  $P^- = P_{qq}^V - P_{q\bar{q}}^V$  (resp.  $P^+ = P_{qq}^V + P_{q\bar{q}}^V$ ) as splitting and the quark singlet distribution evolves coupled with the gluon distribution, through the following equation

$$\partial_{Q^2} \begin{pmatrix} \Sigma(x, Q^2) \\ g(x, Q^2) \end{pmatrix} = \int_x^1 \frac{d\xi}{\xi} \begin{pmatrix} P_{qq} & 2n_f P_{qg} \\ P_{gq} & P_{gg} \end{pmatrix} \Big|_{\frac{x}{\xi}, \alpha_s(Q^2)} \begin{pmatrix} \Sigma(\xi, Q^2) \\ g(\xi, Q^2) \end{pmatrix} \quad (3.24)$$

with  $P_{qq} = P^+ + 2n_f P_{qq}^S$ .

Finally, one can obtain some interesting conditions on the splitting functions considering conserved quantities. From quark number conservation, we must have

$$\begin{aligned}
0 &= \partial_{Q^2} \int_0^1 dx q^-(x, Q^2) \\
&= \int_0^1 dx \int_x^1 \frac{d\xi}{\xi} P^- \left( \frac{x}{\xi} \right) q^-(\xi, Q^2) \\
&= \int_0^1 d\xi q^-(\xi, Q^2) \int_0^1 dx P^-(x)
\end{aligned}$$

Thus,

$$\int_0^1 dx P^-(x) = 0. \quad (3.25)$$

Similarly, from momentum conservation

$$\int_0^1 dx x [\Sigma(x) + g(x)] = 1, \quad (3.26)$$

---

<sup>7</sup>Note that the singlet contribution is the same for the  $qq$  and the  $q\bar{q}$  splittings.

we get

$$\begin{aligned}\int_0^1 dx x [P_{qq}(x) + P_{gq}(x)] &= 0, \\ \int_0^1 dx x [2n_f P_{qg}(x) + P_{gg}(x)] &= 0.\end{aligned}\tag{3.27}$$

These three relations are called *sum rules* and are very useful to find the virtual corrections to the splitting functions at  $x = 1$ .



# Chapter 4

## The leading-order DGLAP evolution equation

### 4.1 Splittings from the factorisation theorem

We have seen in the previous chapter that the anomalous dimensions can be calculated using relation (3.11). In perturbation theory, we can expand the splitting functions in series of the strong coupling constant

$$P_{ab}(x) = \left(\frac{\alpha_s}{2\pi}\right) P_{ab}^{(0)}(x) + \left(\frac{\alpha_s}{2\pi}\right)^2 P_{ab}^{(1)}(x) + \dots$$

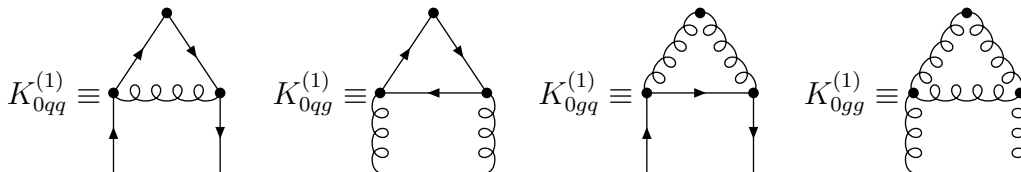
The first (resp. second, ...) term of the series is usually called the *leading-order (LO) splitting functions* (resp. *next-to-leading-order (NLO)*, ...). In this section, we shall calculate the leading-order splitting functions from the relations obtained in the factorisation theorem. If we develop the 2PI kernel  $K_0$  in series of the coupling constant

$$K_0 = \sum_{k=1}^{\infty} \alpha_s^k K_0^{(k)},$$

we can easily see that

$$\Gamma = \alpha_s \mathbb{P} K_0^{(1)} + \mathcal{O}(\alpha_s^2).$$

From this expression, we see that the four splittings  $P_{qq}$ ,  $P_{qg}$ ,  $P_{gq}$  and  $P_{gg}$  are related to the 2PI kernels  $K_{0ab}$  at first order in  $\alpha_s$ :



Let us first compute the quark-quark splitting. Using the full expression of the projector, we have

$$\Gamma_{qq} \left( x, \frac{1}{\varepsilon} \right) = Z_F x \text{pp} \int \frac{d^d k}{(2\pi)^d} \delta(x - \xi) \left[ \frac{\not{\eta}}{4\xi} \alpha_s K_{0qq}^{(1)} \not{p} \right],$$

with

$$\begin{aligned} \left[ \frac{\not{p}}{4\xi} \alpha_s K_{0qq}^{(1)} \not{p} \right] &= \frac{g^2}{\mu^\varepsilon} \text{tr} \left( \frac{\not{p}}{4\xi} \not{k} \gamma_\mu \not{p} \gamma_\nu \not{k} \right) d^{\mu\nu}(p-k) \frac{1}{k^4} (2\pi) \delta^+((p-k)^2) \frac{1}{N_c} \text{tr}(\tau_a \tau^a) \\ &= \frac{g^2 - 2k^2}{\mu^\varepsilon} \frac{1 + \xi^2}{\xi} \frac{2\pi}{k^4} \delta^+(k^2 - 2p \cdot k), \end{aligned}$$

where  $d_{\mu\nu}$  is the gluon propagator given by eq (3.19). In this last expression, we can replace  $\xi$  by  $x$  and put most of the factors in front of the integration which becomes successively

$$\begin{aligned} \Gamma_{qq} \left( x, \frac{1}{\varepsilon} \right) &= Z_F x C_F \frac{1+x^2}{1-x} \text{pp} \int \frac{dx}{2x} dk^2 d^2 k_\perp (-k^2)^\varepsilon \frac{8}{(2\pi)^{3+\varepsilon}} \frac{g^2}{\mu^\varepsilon} \frac{1}{k^2} \frac{1}{4x} \delta^+ \left( k^2 - \frac{k^2 + k_\perp^2}{\xi} \right) \\ &= Z_F C_F \frac{1+x^2}{1-x} \text{pp} \int \frac{d(-k^2)}{(-k^2)} \frac{g^2}{8\pi^2} \left( \frac{-k^2}{4\pi^2 \mu^2} \right)^{\varepsilon/2} \\ &= Z_F C_F \frac{1+x^2}{1-x} \frac{2}{\varepsilon} \frac{\alpha_s}{2\pi}. \end{aligned}$$

From (3.11), we can extract the quark-quark splitting function (we shall come back on virtual corrections later)

$$P_{qq}(x) = C_F \frac{1+x^2}{1-x}. \quad (4.1)$$

Before moving to the other splittings, we can point out that most of the details of this calculation do not depend on the process under consideration. Actually, if we remove all the kinematics and the extraction of the  $1/\varepsilon$  pole, we see that

$$P_{qq}(x) = \frac{-x}{2k^2} \text{tr} \left( \frac{\not{p}}{4\xi} \not{k} \gamma_\mu \not{p} \gamma_\nu \not{k} \right) d^{\mu\nu}(p-k) \frac{1}{N_c} \text{tr}(\tau_a \tau^a),$$

provided that we impose  $\xi = x$  and  $2p \cdot k = k^2$ . This means that for the other splittings, we only need to compute the trace of the fermion loops, the denominator of the gluon propagators and the colour factor, inserting the projectors and the factor  $\frac{-x}{2k^2}$ . Using this trick and writing  $V_{\alpha\beta\gamma}(p, q, r)$  the 3-gluons vertex, we obtain easily

$$\begin{aligned} P_{qq}(x) &= \frac{-x}{2k^2} \text{tr} \left( \frac{\not{p}}{4\xi} \not{k} \gamma_\mu (\not{p} - \not{k}) \gamma_\nu \not{k} \right) d^{\mu\nu}(p) \frac{1}{N_c^2 - 1} \text{tr}(\tau_a \tau^a) \\ &= T_R [(1-x)^2 + x^2], \end{aligned} \quad (4.2)$$

$$\begin{aligned} P_{gq}(x) &= \frac{-x}{2k^2} (-g_{\mu\nu}) d^{\mu\rho}(k) d^{\nu\sigma}(k) \text{tr}(\gamma_\sigma (\not{p} - \not{k}) \gamma_\rho \not{p}) \frac{1}{2} \frac{1}{N_c} \text{tr}(\tau_a \tau^a) \\ &= C_F \frac{1 + (1-x)^2}{x}, \end{aligned} \quad (4.3)$$

$$\begin{aligned} P_{gg}(x) &= \frac{-x}{2k^2} (-g_{\mu\nu}) d^{\mu\rho}(k) d^{\nu\sigma}(k) d^{\alpha\beta}(p) d^{\kappa\lambda}(p-k) V_{\alpha\rho\kappa}(p, -k, k-p) V_{\beta\sigma\lambda}(p, -k, k-p) \\ &\quad \frac{1}{2} \frac{1}{N_c^2 - 1} f_{abc} f^{abc} \\ &= 2C_A \left( \frac{x}{1-x} + \frac{1}{x} - 1 + x - x^2 \right). \end{aligned} \quad (4.4)$$

Besides all these results, we still need to compute the virtual corrections  $Z_F$  (resp.  $Z_G$ ) which contributes to the quark-quark (resp. gluon-gluon) splitting functions. These corrections are infrared singularities which cancel the infrared divergences in  $P_{qq}(x)$  and  $P_{gg}(x)$  when  $x \rightarrow 1$ . We can of course calculate the one-loop corrections to the quark and gluon propagators and extract the pole in  $p^2 \rightarrow 0$ , but there is a much more straightforward method<sup>1</sup>. From quark number and momentum conservation, we have seen that splitting functions have to satisfy the sum rules (3.25) and (3.27). Since all virtual correction appear at  $x = 1$ , they must have the form  $K\delta(1-x)$ . Using the sum rule (3.25), we have

$$\begin{aligned} K &= -C_F \int_0^1 dx \frac{1+x^2}{1-x} \\ &= C_F \left[ \frac{3}{2} - \int_0^1 dx \frac{2}{1-x} \right]. \end{aligned}$$

If we introduce the *plus* distribution defined through

$$\begin{aligned} \frac{1}{(1-x)_+} &= \frac{1}{1-x} \quad \text{for } 0 \leq x < 1, \\ \int_0^1 dx \frac{f(x)}{(1-x)_+} &= \int_0^1 dx \frac{f(x) - f(1)}{1-x}, \end{aligned}$$

we obtain the complete quark-quark splitting function

$$P_{qq}(x) = C_F \left[ \frac{1+x^2}{(1-x)_+} + \frac{3}{2}\delta(1-x) \right]. \quad (4.5)$$

Moreover, with these virtual corrections included, we see that equations (4.5) and (4.3) satisfy

$$\int_0^1 dx x [P_{qq}(x) + P_{gq}(x)] = 0.$$

Similarly, the virtual corrections to the gluon splitting function can be directly calculated using the last sum rule and we get

$$\begin{aligned} K &= -2n_f T_R \int_0^1 dx x [x^2 + (1-x)^2] - 2C_A \int_0^1 dx x \left( \frac{x}{1-x} + \frac{1}{x} - 1 + x - x^2 \right) \\ &= -2C_A \int_0^1 dx \frac{1}{1-x} + \frac{11C_A - 4n_f T_R}{6}, \end{aligned}$$

which gives the final gluon-gluon splitting function

$$P_{gg}(x) = 2C_A \left( \frac{x}{(1-x)_+} + \frac{1}{x} - 1 + x - x^2 \right) + \frac{11C_A - 4n_f T_R}{6} \delta(1-x). \quad (4.6)$$

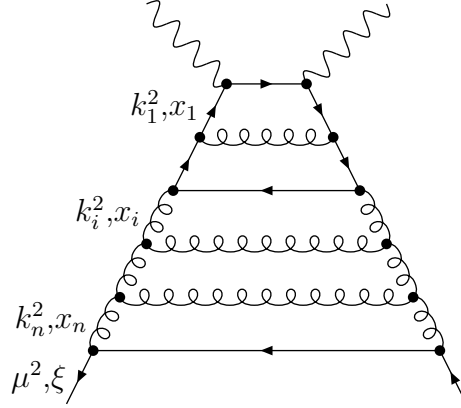
---

<sup>1</sup>The reader who wants a explicit calculation of the infrared corrections from Feynman graphs can read [19].

## 4.2 LO DGLAP and gluon ladders

Instead of using the whole machinery from the factorisation theorem, it may be more interesting to look directly at which Feynman diagrams correspond to the DGLAP limit, order by order in  $\alpha_s$ .

One can easily show that, at leading order, only ladder diagrams contribute in the DGLAP limit, in the light-cone gauge  $A^+ = 0$



In the large  $Q^2$ -limit, these ladders are  $k^2$ -ordered

$$Q^2 \equiv k_0^2 \gg k_1^2 \gg \dots \gg k_n^2 \gg \mu^2.$$

If we do not take into account the final convolution with  $q(\xi)$ , the contribution from the ladder is (one can show that  $x_1 = x$ )

$$\int_{\mu^2 < k_n^2 < \dots < k_1^2 < Q^2} dk_1^2 \dots dk_n^2 \prod_{i=2}^n \int_{x_{i-1}}^1 \frac{dx_i}{x_i} |\mathcal{M}|^2.$$

The computation of the squared-amplitude  $|\mathcal{M}|^2$  is done by removing rungs one by one, starting at the bottom. Performing this operation, we shall build the splitting functions in the same way as in the previous section. Note that, after the reduction of the emission  $k_{i+1} \rightarrow k_i$ , we must replace  $k_i$  by  $x_i p$ , because only the component of  $k$  parallel to  $p$  will lead to collinear divergences. Including the propagators, we end up with ( $x_{n+1} \equiv \xi$ )

$$F_2^{(n)} = \left(\frac{\alpha_s}{2\pi}\right)^n \int_{\mu^2 < k_n^2 < \dots < k_1^2 < Q^2} \frac{dk_1^2}{k_1^2} \dots \frac{dk_n^2}{k_n^2} \prod_{i=2}^n \int_{x_{i-1}}^1 \frac{dx_i}{x_i} \int_{x_n}^1 \frac{d\xi}{\xi} \prod_{i=1}^n P_i \left(\frac{x_i}{x_{i+1}}\right) q(\xi),$$

which, after integration on the virtualities, becomes

$$F_2^{(n)} = \frac{1}{n!} \left[ \frac{\alpha_s}{2\pi} \log \left( \frac{Q^2}{\mu^2} \right) \right]^n \bigotimes_{i=1}^n P_i \left( \frac{x_i}{x_{i+1}} \right) \otimes q(\xi).$$

From all these calculations, we can see that at leading order, the splitting functions have a simple physical interpretation:  $P_{ab}(x)$  is the probability to find a parton of type  $a$  in a parton of type  $b$ , the final parton carrying a momentum fraction  $x$  of the parent parton<sup>2</sup>.

The DGLAP equation is easily solvable in Mellin space. Actually, at leading order, we have<sup>3</sup>

$$\partial_{Q^2} q(j, Q^2) = \frac{\alpha_s(Q^2)}{2\pi} \gamma(j) q(j, Q^2).$$

The solution of this equation can be checked to be

$$\frac{q(j, Q^2)}{q(j, Q_0^2)} = \left[ \frac{\alpha(Q_0^2)}{\alpha(Q^2)} \right]^{\frac{6}{33-2n_f} \gamma(j)}. \quad (4.7)$$

We can now look at the small- $x$  behaviour of the solution. In that limit, the splitting functions become

$$P_{qq} \approx C_F, \quad P_{qg} \approx T_R, \quad P_{gq} \approx \frac{2C_F}{x}, \quad P_{gg} \approx \frac{2C_A}{x}.$$

In the limit  $x \rightarrow 0$ , the splitting functions are thus dominated by  $1/x$  terms, which correspond to a single pole at  $j = 1$ . This simple pole in the splitting functions leads to an **essential singularity** in the gluon and singlet distributions. Note that a more careful study [40] shows that, starting with  $g(x, Q_0^2) = 1/x$ , we find

$$g(x, Q^2) = \frac{1}{x} \exp \left\{ \sqrt{\frac{48n_f}{33-2n_f} \log \left[ \frac{\log(Q^2/\Lambda^2)}{\log(Q_0^2/\Lambda^2)} \right]} \log \left( \frac{1}{x} \right) \right\}.$$

We see that the essential singularity is dominated by all powers of  $1/x$  greater than 1.

However, the presence of this essential singularity is very annoying from the point of view of Regge theory<sup>4</sup> and, although everybody seems to agree that it is not a physical one, nobody knows exactly how to remove it. This is also the main obstacle when trying to compare Regge theory with DGLAP evolution.

The usual way to use this equation is to choose a set of initial distributions  $q_i(x, Q_0^2, \vec{a})$  to compute  $q_i(x, Q^2, \vec{a})$  using (3.22) and to adjust the parameters  $\vec{a}$  in order to reproduce the experimental data. This approach has already been successfully applied many times [20–24] and is often considered a very good test of pQCD. Nevertheless, these studies do not care about the singularity structure of the initial distributions, ending up with results that disagree with Regge theory, and thus with QCD. We shall show in chapter 11 that it is possible to solve this problem.

<sup>2</sup>This is true if we do not include the virtual corrections which give a negative contribution in  $x = 1$  and ensure the validity of sum-rules.

<sup>3</sup>We only consider one equation. The extension to coupled equations is straightforward.

<sup>4</sup>One can check that an essential singularity at  $j = 1$  is not sufficient to reproduce the large- $s$  behaviour of the total cross-sections.



## Part II

# Analytic $S$ -matrix theory



*The shortest path between two truths  
in the real domain passes through  
the complex domain*  
-Jacques Hadamard

# Chapter 5

## Regge Theory

Since we shall often use  $S$ -matrix theory (often called Regge theory) in the following chapters, we shall summarise in a few pages its basic concepts and the properties we shall use later.

Note that this is just a short introduction explaining the basic concepts. The reader who wants a more complete description can have a look at recent books [9].

### 5.1 $S$ -matrix theory

#### 5.1.1 Definition

The element  $if$  of the  $S$  matrix represents the overlap of two states  $|i\rangle$  and  $|f\rangle$ , where the initial state is made of free particles at  $t \rightarrow -\infty$  and the final state of free particles at  $t \rightarrow +\infty$ .

$$S_{if} = \langle f|i\rangle.$$

Instead of considering the  $S$  matrix in itself, we often remove the part where no interaction occurs

$$S_{if} = \delta_{if} + iT_{if},$$

and work with the  $T$  matrix. The  $T$  matrix is related to the scattering amplitude  $\mathcal{A}_{if}$  through the relation

$$T_{if} = (2\pi)^4 \delta^4 \left( \sum_i p_i - \sum_f p_f \right) \mathcal{A}_{if}, \quad (5.1)$$

where we have explicitly taken into account momentum conservation.

### 5.1.2 Postulates

1. The  $S$  matrix is Lorentz-invariant.
2. The  $S$  matrix is unitary.
3. The  $S$  matrix is analytic in momentum variables.

#### Lorentz invariance

Let us consider, for example, a  $2 \rightarrow 2$  process  $a + b \rightarrow a' + b'$ . Lorentz invariance means that the amplitude for that process must be a function of the 10 invariants  $p_i^2$  and  $p_i \cdot p_j$ . Since incoming and outgoing particles are on-shell,  $p_i^2 = m_i^2$  and, within the scalar products, 4 are constrained by energy-momentum conservation. We are thus left with only 2 independent parameters.

We usually introduce the variables  $s$ ,  $t$  and  $u$ , called *Mandelstam variables* and defined through

$$\begin{aligned} s &= (p_a + p_b)^2 = (p'_a + p'_b)^2, \\ t &= (p_a - p'_a)^2 = (p_b - p'_b)^2, \\ u &= (p_a - p'_b)^2 = (p_b - p'_a)^2. \end{aligned}$$

Out of these 3 variables, only 2 are independent and one may check that they are related by

$$s + t + u = m_a^2 + m_b^2 + m_a'^2 + m_b'^2.$$

#### Unitarity

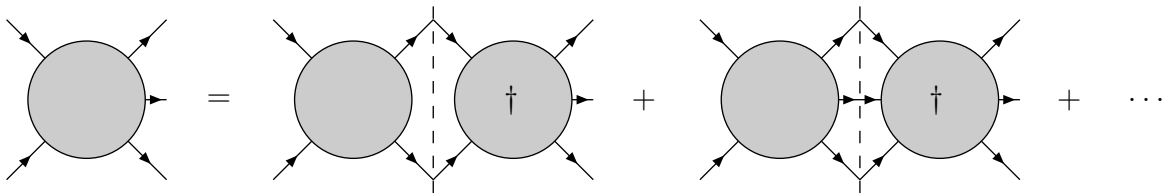


Figure 5.1: Illustration of the Cutkosky rules allowing to compute the imaginary part of a process with the sum over all possible intermediate states. The dashed line means that the cut lines must be considered on-shell

Conservation of probability imposes that, starting with a fixed initial state  $|i\rangle$ , the probability to finish in an unspecified final state must be 1. Thus

$$SS^\dagger = \mathbb{1},$$

which can be written in terms of the  $T$  matrix

$$TT^\dagger = i(T^\dagger - T).$$

If we use equation (5.1) and the fact that  $\Im m z = \frac{z-z^*}{2}$ , the unitarity condition becomes

$$2 \Im m \mathcal{A}_{if} = (2\pi)^4 \delta^4 \left( \sum_i p_i - \sum_f p_f \right) \sum_n \mathcal{A}_{in} \mathcal{A}_{nf}^\dagger \quad (5.2)$$

This is illustrated in Fig. 5.1 and is often called the *Cutkosky rules*. It allows to compute the imaginary part of one process by considering all possible intermediate states.

If we take  $i = f$  in (5.2), we obtain

$$\sigma_{tot}(s) = \frac{1}{16\pi s} \Im m \mathcal{A}(s, 0), \quad (5.3)$$

which is often referred to as the *optical theorem*.

Note that the Cutkosky rules can be applied to any number of particle in the initial and final states. This also means that the optical theorem gives the total inclusive cross-section for a process with any number of particles in the initial state.

### Analyticity

Analyticity of the  $S$  matrix would be a consequence of causality if it were not for the uncertainty principle (see [41]). It means that, if we allow for Mandelstam variables to be complex, the  $S$  matrix is an analytical function of them, with singularities requested by unitarity<sup>1</sup>.

Analyticity of the  $S$  matrix has many important consequences. Combined with unitarity, it allows, for example, to find the  $s$ -plane singularities arising from  $n$ -particle production. Actually, the imaginary part of the amplitude is, considering  $s$  complex<sup>2</sup>

$$\Im m \mathcal{A}(s, t) = \frac{\mathcal{A}(s, t) - \mathcal{A}^*(s, t)}{2i} = \frac{\mathcal{A}(s, t) - \mathcal{A}(s^*, t)}{2i}.$$

This means that, above the  $n$ -particle threshold, we must have a discontinuity

$$\Im m \mathcal{A}(s, t) = \frac{1}{2i} \lim_{\varepsilon \rightarrow 0} [\mathcal{A}(s + i\varepsilon, t) - \mathcal{A}(s - i\varepsilon, t)], \quad (5.4)$$

which corresponds to a cut on the real- $s$  axis with a branchpoint at the  $n$ -particle threshold.

Another property arising from unitarity is *crossing symmetry*. This tells us that, if we consider the process  $a + b \rightarrow c + d$  and its amplitude  $\mathcal{A}_{a+b \rightarrow c+d}(s, t, u)$ , the Mandelstam variables verify  $s > 0$ ,  $t, u < 0$ . If we analytically continue this amplitude to the region where  $t > 0$ ,  $s, u < 0$ , we shall have

$$\mathcal{A}_{a+b \rightarrow c+d}(s, t, u) = \mathcal{A}_{a+\bar{c} \rightarrow \bar{b}+d}(t, s, u),$$

<sup>1</sup>Perturbative field theory gives an example.

<sup>2</sup>We have used the Schwarz reflexion principle which states that if a function is real on some part of the real axis, then  $f^*(z) = f(z^*)$ . Physically, this means that we analytically continue  $\mathcal{A}(s, t)$  around the cut.

where the last process has all its Mandelstam variables in the physical domain. Similarly, we have

$$\mathcal{A}_{a+b \rightarrow c+d}(s, t, u) = \mathcal{A}_{a+\bar{d} \rightarrow \bar{b}+c}(u, t, s).$$

Since  $u = \sum_i m_i^2 - s - t$ , the  $s$ -channel discontinuities in the process  $a + \bar{d} \rightarrow \bar{b} + c$ , will become cuts on the negative parts of the  $s$ -axis for the process  $a + b \rightarrow c + d$ .

A third consequence of unitarity is the *dispersion relations*, allowing to reconstruct the full amplitude given only its imaginary part. The Cauchy theorem states that, for  $s_0$  complex and any contour  $\mathcal{C}$  enclosing  $s_0$  such that  $\mathcal{A}(s, t)$  has no singularity inside the contour,

$$\mathcal{A}(s_0, t) = \frac{1}{2i\pi} \oint_{\mathcal{C}} \frac{\mathcal{A}(s, t)}{s - s_0} ds.$$

We may vary the contour in such a way that it goes around the positive and negative cuts on the  $s$ -axis. Assuming that the integration on the circle goes to zero when its radius goes to infinity, we are only left with the integration around cuts

$$\begin{aligned} 2i\pi \mathcal{A}(s_0, t) &= \int_{\infty}^{s_{th}^+} \frac{\mathcal{A}(s - i\varepsilon, t)}{s - s_0} ds + \int_{s_{th}^+}^{\infty} \frac{\mathcal{A}(s + i\varepsilon, t)}{s - s_0} ds \\ &+ \int_{-\infty}^{s_{th}^-} \frac{\mathcal{A}(s - i\varepsilon, t)}{s - s_0} ds + \int_{s_{th}^-}^{-\infty} \frac{\mathcal{A}(s + i\varepsilon, t)}{s - s_0} ds, \end{aligned}$$

which, using relation (5.4) and replacing  $s$  by  $u$  in the negative discontinuity becomes

$$\mathcal{A}(s_0, t) = \frac{1}{\pi} \int_{s_{th}^+}^{\infty} \frac{\Im m \mathcal{A}(s, t)}{s - s_0} ds + \frac{1}{\pi} \int_{u_{th}^+}^{\infty} \frac{\Im m \mathcal{A}(s(u, t), t)}{u - u_0} du.$$

Note finally that, if the integration over the circle does not vanish at infinity, we may use the following method called *subtraction*: choose one point  $s_1$  and write the previous relation for  $\mathcal{A}(s_0, t) - \mathcal{A}(s_1, t)$ . This gives

$$\mathcal{A}(s_0, t) = \mathcal{A}(s_1, t) + \frac{s_0 - s_1}{\pi} \int_{s_{th}^+}^{\infty} \frac{\Im m \mathcal{A}(s, t)}{(s - s_0)(s - s_1)} ds + \frac{s_0 - s_1}{\pi} \int_{u_{th}^+}^{\infty} \frac{\Im m \mathcal{A}(s, t)}{(u - u_0)(u - u_1)} du. \quad (5.5)$$

If this is not sufficient, we can perform multiple subtractions. For example, we can rewrite (5.5) as

$$\frac{\mathcal{A}(s_0, t) - \mathcal{A}(s_1, t)}{s_0 - s_1} = \frac{1}{\pi} \int_{s_{th}^+}^{\infty} \frac{\Im m \mathcal{A}(s, t)}{(s - s_0)(s - s_1)} ds + u \text{ term.}$$

We can then take another arbitrary point  $s_2$  and subtract from this expression its value for  $s_0 = s_2$ . This leads to

$$\begin{aligned} \mathcal{A}(s_0, t) &= \frac{s_0 - s_2}{s_1 - s_2} \mathcal{A}(s_1, t) + \frac{s_0 - s_1}{s_2 - s_1} \mathcal{A}(s_2, t) \\ &+ \frac{(s_0 - s_1)(s_0 - s_2)}{\pi} \int_{s_{th}^+}^{\infty} \frac{\Im m \mathcal{A}(s, t)}{(s - s_0)(s - s_1)(s - s_2)} ds + u \text{ term.} \end{aligned}$$

For more than two subtractions, one easily shows by induction that

$$\sum_{i=0}^n \frac{\mathcal{A}(s_i, t)}{\prod_{j \neq i} (s_i - s_j)} = \frac{1}{\pi} \int_{s_{th}^+}^{\infty} \frac{\Im m \mathcal{A}(s, t)}{\prod_{j=0}^n (s - s_j)} ds + u \text{ term.} \quad (5.6)$$

### 5.1.3 Useful $2 \rightarrow 2$ kinematics

If we consider the process  $a + \bar{a} \rightarrow b + \bar{b}$  in the centre-of-mass frame, we have

$$\begin{aligned} p_a &\equiv \left( \sqrt{p_i^2 + m_a^2}, 0, 0, p_i \right), \\ p_b &\equiv \left( \sqrt{p_i^2 + m_a^2}, 0, 0, -p_i \right), \\ p_c &\equiv \left( \sqrt{p_f^2 + m_b^2}, p_f \sin(\theta), 0, p_f \cos(\theta) \right), \\ p_d &\equiv \left( \sqrt{p_f^2 + m_b^2}, -p_f \sin(\theta), 0, -p_f \cos(\theta) \right). \end{aligned}$$

Using the definition of  $s$  and  $t$ , we find after a little bit of algebra

$$\begin{aligned} p_i^2 &= \frac{s}{4} - m_a^2, \\ p_i^2 &= \frac{s}{4} - m_a^2, \\ \cos(\theta) &= \frac{s + 2(t - m_a^2 - m_b^2)}{\sqrt{(s - 4m_a^2)(s - 4m_b^2)}}. \end{aligned} \quad (5.7)$$

For further purposes, it is interesting to continue analytically  $\cos(\theta)$  to the region  $s < 0$ ,  $t > 0$  ( $\cos(\theta) > 1$ ). This gives

$$\cos(\theta_t) = \frac{t + 2(s - m_a^2 - m_b^2)}{\sqrt{(t - 4m_a^2)(t - 4m_b^2)}} \stackrel{t=0}{=} \frac{s - m_a^2 - m_b^2}{2m_a m_b},$$

where  $s$  and  $t$  now refer to the  $t$ -channel process  $a + b \rightarrow a + b$ . For the case of protons and virtual photons, this gives, at high energy

$$\begin{aligned} \cos(\theta_t^{(pp)}) &= \frac{s}{2m_p^2}, \\ \cos(\theta_t^{(\gamma^*p)}) &= \frac{\sqrt{Q^2}}{2xm_p}, \\ \cos(\theta_t^{(\gamma^*\gamma^*)}) &= \frac{s + Q_1^2 + Q_2^2}{2Q_1 Q_2}. \end{aligned} \quad (5.8)$$

As we shall see further, these relations will be useful to estimate the domain of applicability of Regge theory.

## 5.2 Regge theory

Regge theory is the study of the analytic properties of the  $S$  matrix at high energy  $s \gg |t|, m_i^2$ . In this section, we shall start by introducing complex angular momenta and then explain the most important consequences of analytical properties.

### 5.2.1 Complex angular momenta and Sommerfeld-Watson transform

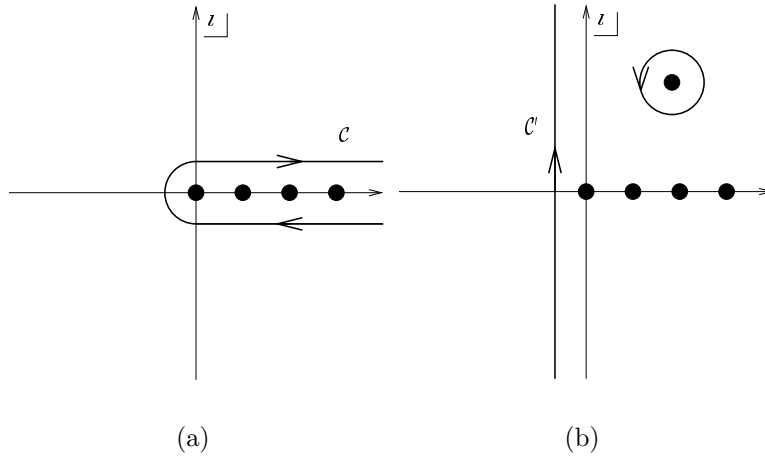


Figure 5.2: Integration contours for the Sommerfeld-Watson transform.

Let us consider the process  $a + \bar{c} \rightarrow \bar{b} + d$ . We can make a partial-wave expansion of its amplitude

$$\mathcal{A}(s, t) = \sum_{l=0}^{\infty} (2l+1) A_l(s) P_l(\cos(\theta)),$$

where  $P_l(x)$  is the  $l$ -th Legendre polynomial and, according to eq. (5.7) where we have neglected the masses,

$$\cos(\theta) = 1 + \frac{2t}{s}.$$

The quantities  $A_l(s)$  are called *partial-waves amplitudes*. We can now use crossing symmetry and obtain the amplitude for the process  $a + b \rightarrow c + d$

$$\mathcal{A}(s, t) = \sum_{l=0}^{\infty} (2l+1) A_l(t) P_l\left(1 + \frac{2s}{t}\right).$$

The trick is then to use the Sommerfeld-Watson transform in order to rewrite the sum as an

integral in the complex angular momentum space<sup>3</sup>

$$\mathcal{A}(s, t) = \frac{1}{2i} \int_{\mathcal{C}} \frac{2l+1}{\sin(l\pi)} A(l, t) P_l \left( 1 + \frac{2s}{t} \right) dl,$$

where the contour  $\mathcal{C}$  is represented in Fig. 5.2.1(a). Note that the continuation  $A(l, t)$  of  $A_l(t)$  is not unique. It can be shown that we need to consider two functions  $A^{(+)}(l, t)$  and  $A^{(-)}(l, t)$ , which are respectively the continuation of the even and odd partial wave amplitudes. This leads to the following expression for the amplitude

$$\mathcal{A}(s, t) = \frac{1}{2i} \sum_{\eta=\pm 1} \int_{\mathcal{C}} \frac{e^{-i\pi l} + \eta}{2} \frac{2l+1}{\sin(l\pi)} A^{(\eta)}(l, t) P_l \left( 1 + \frac{2s}{t} \right) dl. \quad (5.9)$$

The parameter  $\eta$  is called *signature*.

### 5.2.2 Regge poles and Regge cuts

The next step is to modify the contour  $\mathcal{C}$  as shown in Fig. 5.2.1(b). We are then left with one integration on an axis parallel to the imaginary axis and a set of residues of poles to the right

$$\begin{aligned} \mathcal{A}(s, t) &= \frac{1}{2i} \sum_{\eta=\pm 1} \int_{\frac{1}{2}-i\infty}^{\frac{1}{2}+i\infty} \frac{e^{-i\pi l} + \eta}{2} \frac{2l+1}{\sin(l\pi)} A_l(t) P_l \left( 1 + \frac{2s}{t} \right) dl \\ &+ \sum_{\eta=\pm 1} \sum_{i_\eta} \frac{e^{-i\pi\alpha_{i_\eta}(t)} + \eta}{2} \frac{\beta_{i_\eta}(t)}{\sin(\alpha_{i_\eta}(t)\pi)} P_{\alpha_{i_\eta}(t)} \left( 1 + \frac{2s}{t} \right) \end{aligned}$$

where  $\alpha_{i_\eta}(t)$  is the position of the poles, which are complex functions of  $t$ , and  $\beta_{i_\eta}(t)$  the residues of the poles multiplied by  $\pi(2\alpha_{i_\eta}(t) + 1)$ . The poles  $\alpha_{i_\eta}(t)$  are called *Regge poles*. Note that in the previous expression, we must also have contributions from cuts which will be called *Regge cuts*.

If we now take the high-energy limit  $s \gg |t|$ , the Legendre polynomials become

$$P_l \left( 1 + \frac{2s}{t} \right) \xrightarrow{s \gg |t|} \frac{\Gamma(2l+1)}{\Gamma(l+1)} \left( \frac{s}{2t} \right)^l. \quad (5.10)$$

In such a case, the integration on the axis  $-\frac{1}{2} + il$  behaving like a negative power of  $s$  becomes negligible and, reabsorbing constant terms into  $\beta$ , we are left with only Regge poles and cuts

$$\mathcal{A}(s, t) \xrightarrow{s \gg |t|} \sum_{\eta=\pm 1} \sum_{i_\eta} \frac{e^{-i\pi\alpha_{i_\eta}(t)} + \eta}{2} \beta_{i_\eta}(t) \left( \frac{s}{2t} \right)^{\alpha_{i_\eta}(t)} + \text{cuts}. \quad (5.11)$$

This expression will be dominated by the rightmost Regge pole. Its most important consequence is the fact that a pole at  $l = \alpha$  corresponds to an amplitude proportional to  $s^\alpha$  and the position of the pole can only depend on  $t$ .

---

<sup>3</sup>The extension of the Legendre polynomials  $P_l(x)$  to complex values of  $l$  are hypergeometrical functions.

### 5.2.3 Domain of applicability

In order to keep only the first few terms of (5.11), we need to work at sufficiently large values of  $\cos(\theta_t)$ .

We shall also use a cut on the natural Regge variable  $2\nu$ . Therefore we shall use the data in the region

$$\begin{aligned}\cos(\theta_t) &\geq \frac{n^2}{2m_p^2} \text{ GeV}^2, \\ \sqrt{2\nu} &\geq n \text{ GeV},\end{aligned}\tag{5.12}$$

where the expression for  $\cos(\theta_t)$  is given by eq. (5.8). For the  $\gamma\gamma$  and the  $\gamma p$  total cross sections, as well as for the photon structure function where  $P^2 \rightarrow 0$ ,  $\cos(\theta_t) \rightarrow \infty$ , and only the cut on  $2\nu$  constrains the Regge region. More precisely, the limit on  $2\nu$  translates into the following limits on  $s$

$$\begin{cases} \sqrt{s - 2m_p^2} \geq n \text{ GeV} & \text{for } pp \text{ cross-section} \\ \sqrt{s - m_p^2} \geq n \text{ GeV} & \text{for } \gamma p \text{ cross-section} \\ \sqrt{s} \geq n \text{ GeV} & \text{for } \gamma\gamma \text{ cross-section} \end{cases}.$$

Furthermore, in the case of one virtual photon, experimentalists measure the  $ep$  or the  $ee$  cross sections. From these, one can extract a cross section for  $\gamma^*p$  or  $\gamma^*\gamma^*$  scattering, provided one factors out a flux factor. As is well known, the latter is univoquely defined only for on-shell particles:

$$\sigma_{tot} = \lim_{Q^2 \rightarrow 0} \frac{4\pi^2\alpha}{Q^2} F_2.\tag{5.13}$$

The flux factor can then be modified arbitrarily, provided that the modifications vanish as  $Q^2 \rightarrow 0$ . This means, for example, that we can always multiply the left-hand side of (5.13) by an arbitrary power of  $(1-x)$ . Hence one should in principle limit oneself to small values of  $x$  only and require

$$x \leq x_{\max}.\tag{5.14}$$

Note that in the case of two off-shell photons, experimentalists measure  $\sigma_{TT} + \sigma_{TL} + \sigma_{LT} + \sigma_{LL}$ , so that no flux factor is necessary.

We must also point out that, although Regge theory can be applied without fear to the study of total-cross sections, where incoming and outgoing particles are on-shell, we do not know if it can be applied to DIS, as new singularities can appear as  $Q^2$  grows.

### 5.2.4 Mellin transform in DIS

In the DIS case, we have shown that at high energy,

$$\cos(\theta_t) = \frac{\sqrt{Q^2}}{2xm_p}.$$

In such a case, we can simplify the Legendre polynomial in the partial wave expansion

$$P_l(\cos(\theta_t)) \approx \frac{\Gamma(2l+1)}{\Gamma^2(l+1)} [\cos(\theta_t)]^l \approx \frac{\Gamma(2l+1)}{\Gamma^2(l+1)} \left( \frac{\sqrt{Q^2}}{2xm_p} \right)^l.$$

Therefore, in the integration over  $l$ , we can replace  $s$  by  $x$ , which gives<sup>4</sup>

$$f(x, Q^2) = \frac{1}{2i\pi} \int_{c-i\infty}^{c+i\infty} dl x^{-l} \tilde{f}(l, Q^2),$$

where  $c$  is such that the integration contour is at the right of all the singularities in the complex- $l$  plane.

This expression can easily be inverted:

$$\tilde{f}(l, Q^2) = \int_0^1 dx x^{l-1} f(x, Q^2).$$

$\tilde{f}$  is called the *Mellin transform* of  $f$ , and we often use the notation  $j$  (or  $\omega$ ) instead of  $l$ .

### 5.2.5 The Froissart-Martin bound

To conclude this introduction to analytic  $S$ -matrix theory, we shall show that the total cross-section cannot grow faster than  $\log^2(s)$  at high energy. This result is known as the *Froissart bound* [26, 27].

The first step is to impose unitarity conditions on the partial-wave amplitudes. We shall therefore start with the partial-wave expansion:

$$\mathcal{A}(s, \theta) = \sum_{l=0}^{\infty} (2l+1) A_l(s) P_l(\cos(\theta)).$$

Since the total cross-section is larger than the elastic cross-section, unitarity of the  $S$  matrix requires that

$$\int \frac{d\Omega_1}{4\pi} \frac{d\Omega_2}{4\pi} f^*(\Omega_1) \Im m \mathcal{A}(s, \theta_{12}) f(\Omega_2) \geq \int \frac{d\Omega_1}{4\pi} \frac{d\Omega_2}{4\pi} \frac{d\Omega_3}{4\pi} f^*(\Omega_1) \mathcal{A}^*(s, \theta_{13}) \mathcal{A}(s, \theta_{32}) f(\Omega_2),$$

where  $\Omega_i = (\theta_i, \phi_i)$  are solid angles,  $\theta_{ij}$  is the angle between  $\Omega_i$  and  $\Omega_j$ , and  $f(\omega)$  is an arbitrary function integrable on the unit sphere. In this relation, the equality holds when there are no inelastic contribution to the cross-section *i.e.* when  $s$  is below the first inelastic threshold. Using the partial-wave expansion, this becomes

$$\begin{aligned} & \sum_{l=0}^{\infty} (2l+1) \Im m A_l(s) \int \frac{d\Omega_1}{4\pi} \frac{d\Omega_2}{4\pi} f^*(\Omega_1) P_l(\cos(\theta_{12})) f(\Omega_2) \\ & \geq \sum_{j,l=0}^{\infty} (2l+1)(2j+1) A_j^*(s) A_l(s) \int \frac{d\Omega_1}{4\pi} \frac{d\Omega_2}{4\pi} \frac{d\Omega_3}{4\pi} f^*(\Omega_1) P_j(\cos(\theta_{13})) P_l(\cos(\theta_{32})) f(\Omega_2). \end{aligned}$$

---

<sup>4</sup>Since DIS is fully inclusive, we compute  $|\mathcal{A}_{\gamma p \rightarrow X}|^2$  and we are thus working at  $t = 0$ .

To perform the  $\Omega_3$  integration in the right-hand-side of the inequality, note that we can freely choose the origin for  $\theta_3$ . If we use,  $\theta_3 = \theta_{13}$ , we have

$$\begin{aligned} \int_0^{2\pi} d\phi_3 P_j(\cos(\theta_{13}))P_l(\cos(\theta_{32})) &= P_j(\cos(\theta_{13})) \int_0^{2\pi} d\phi_3 P_l(\cos(\theta_{32})) \\ &= 2\pi P_j(\cos(\theta_{13}))P_l(\cos(\theta_{13}))P_l(\cos(\theta_{12})). \end{aligned}$$

Using the orthogonality condition for the Legendre polynomials

$$\int_{-1}^1 d\cos(\theta) P_j(\cos(\theta))P_l(\cos(\theta)) = \frac{2}{2l+1}\delta_{jl},$$

the unitarity condition becomes

$$\sum_{l=0}^{\infty} (2l+1) [\Im m A_l(s) - |A_l(s)|^2] \int \frac{d\Omega_1}{4\pi} \frac{d\Omega_2}{4\pi} f^*(\Omega_1)P_l(\cos(\theta_{12}))f(\Omega_2) \geq 0.$$

This relation is in particular true for  $f(\Omega) = P_j(\cos(\theta))$ . In this case, we have

$$\begin{aligned} \int \frac{d\Omega_2}{4\pi} P_l(\cos(\theta_{12}))P_j(\cos(\theta_2)) &= \frac{1}{2} \int_{-1}^1 d\cos(\theta_2) P_l(\cos(\theta_1))P_l(\cos(\theta_2))P_j(\cos(\theta_2)) \\ &= \frac{1}{2l+1}P_l(\cos(\theta_1))\delta_{jl}. \end{aligned}$$

Using once again the orthogonality condition to remove the  $\Omega_1$  integration, we finally obtain

$$\Im m A_l(s) - |A_l(s)|^2 \geq 0.$$

This relation implies that the partial wave stay within the circle of radius  $\frac{1}{2}$  centred at  $\frac{i}{2}$ , as shown in figure 5.3.

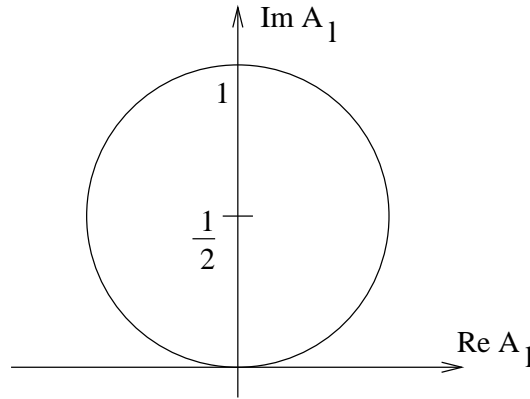


Figure 5.3: Unitarity constraint for the partial-wave amplitudes.

Moreover, this constraint implies that  $|A_l(s)| \leq 1$ , so the unitarity of the  $S$  matrix teaches us that

$$\boxed{|A_l(s)|^2 \leq \Im m A_l(s) \leq 1}. \quad (5.15)$$

With that result, we can now start the derivation of the Froissart bound. As a first step, we shall assume that the amplitudes are tempered:

$$\exists s_m, \delta, C_0 \mid \forall s > s_m, \forall t : |A(s, t)| < C_0 s^\delta.$$

In terms of the partial-wave amplitudes, since from (5.15) each term of the sum is positive, this means that

$$\left| (2l+1) \Im m A_l(s) P_l \left( 1 + \frac{2t}{s-4m^2} \right) \right| < C_0 s^\delta,$$

Since for large values of  $l$  and for  $x > 1$ , the Legendre polynomials verify

$$P_l(x) > \frac{C}{\sqrt{2l+1}} (1 + \sqrt{2x-2})^l,$$

where  $C$  is some positive constant, this turns into a boundary on  $\Im m A_l$

$$\begin{aligned} \Im m A_l &< \frac{C_0 s^\delta}{C \sqrt{2l+1}} \left( 1 + \sqrt{\frac{2t}{s-4m^2}} \right)^{-l} \\ &< C' \exp \left[ \delta \log(s) - 2l \sqrt{\frac{t_0}{s}} \right], \end{aligned}$$

where  $C'$  is another positive constant. Thus,  $A_l$  decreases exponentially with  $l$  and becomes negligible when

$$l > L = K \sqrt{s} \log(s).$$

So, we have for the amplitude

$$\mathcal{A}(s, t) = \sum_{l=0}^L (2l+1) A_l(s) P_l(\cos(\theta)) + R_L(s, t),$$

with  $|R_L(s, t)| < s^{-N}$ , where  $N$  can be made as large as we want by choosing  $K$ . Therefore, as  $s \rightarrow \infty$ ,

$$\Im m \mathcal{A}(s, 0) < \sum_{l=0}^L (2l+1) \sim L^2 = K^2 s \log^2(s).$$

Using the optical theorem, this finally gives

$$\boxed{\sigma_{\text{tot}} < C \log^2 \left( \frac{s}{s_0} \right)}, \quad (5.16)$$

which is the Froissart-Martin bound.

In addition to these considerations, Martin and Lukaszuk [42] have shown that, for hadronic cross sections, we have

$$\sigma \leq \frac{\pi}{m_\pi^2} \log^2 \left( \frac{s}{s_0} \right),$$

with  $\frac{\pi}{m_\pi^2} \approx 67$  mb. Therefore, if we take the  $pp$  total cross section from the Donnachie-Landshoff model [43]

$$\sigma_{pp}(s) = 21.7s^{0.08} + 56.1s^{-0.45} \text{ mb}$$

and if we assume  $s_0 \approx 1 \text{ GeV}^2$ , we obtain a violation of the Froissart-Martin bound for  $\sqrt{s} \approx 10^{30} \text{ GeV}$ . This means that even if, strictly speaking, the DL model violates the Froissart-Martin bound, this violation occurs at such a high energy that we do not need to worry about it in the energy region of the actual experiments.

# Chapter 6

## Testing Regge theory in DIS

The aim of this chapter is to see how Regge theory can be used to describe the proton structure function  $F_2^p$ . Many models based on Regge theory are able to reproduce hadronic cross sections [44]. In this chapter, we consider the extension of these models to the  $\gamma^*p$  amplitudes. In our analysis, we shall also include the  $\sigma_{\gamma p}$  data in order to have the correct behaviour when  $Q^2$  goes to 0. In DIS, Regge theory constrains the  $s$  behaviour but does not say anything about the  $Q^2$  dependence. The Regge couplings are therefore functions of  $Q^2$ .

### 6.1 The simplest models

As the hadronic cross sections,  $F_2$  will be dominated by 2 contributions: a pomeron, reproducing the rise of  $F_2$  at small  $x$ , and reggeons associated with the meson trajectories. Note that when  $Q^2$  goes to 0, we can find the total  $\gamma p$  cross-section using the relation

$$\sigma_{\gamma p} = \left[ \frac{4\pi^2\alpha_e}{Q^2} F_2 \right]_{Q^2=0}. \quad (6.1)$$

#### 6.1.1 The pomeron term

For the pomeron contribution to  $F_2$ , we shall consider 4 different possibilities:

1. A power behaviour:

$$F_2(x, Q^2) = a(Q^2)x^{-\varepsilon}.$$

From the total-cross-section analysis, we know that with a unique term, we are only able to reproduce the proton-proton cross-section. This term, with  $\varepsilon \approx 0.09$ , is called the *soft pomeron* but is unable to describe the steeper rise of  $\gamma^*p$  amplitudes. The solution is to add another contribution, called the *hard pomeron*, which leads to

$$F_2(x, Q^2) = a_s(Q^2)x^{-\varepsilon_s} + a_h(Q^2)x^{-\varepsilon_h} \quad (6.2)$$

The hard pomeron has  $\varepsilon \approx 0.4$ . In the complex- $j$  plane, this corresponds to 2 simple poles at  $j = 1 + \varepsilon_s$  and  $j = 1 + \varepsilon_h$ :

$$F_2(j, Q^2) = \frac{a_s(Q^2)}{j - 1 - \varepsilon_s} + \frac{a_h(Q^2)}{j - 1 - \varepsilon_h}$$

This is the Donnachie-Landshoff (DL) two pomerons model [12, 13].

2. A logarithmic behaviour<sup>1</sup>:

$$F_2(\nu, Q^2) = A(Q^2) \log(2\nu) + B(Q^2). \quad (6.3)$$

In the complex- $j$  plane, this expression become

$$F_2(j, Q^2) = \frac{A(Q^2)}{(j-1)^2} + \frac{B(Q^2)}{j-1}.$$

and this behaviour is often called the *double-pole pomeron* [15, 16, 18].

3. A squared-logarithmic behaviour:

$$F_2(\nu, Q^2) = A(Q^2) \log^2(2\nu) + B(Q^2) \log(2\nu) + C(Q^2), \quad (6.4)$$

$$= A(Q^2) \log^2 \left[ \frac{2\nu}{2\nu_0(Q^2)} \right] + C(Q^2). \quad (6.5)$$

In the complex- $j$  plane, this expression become

$$F_2(j, Q^2) = \frac{2A(Q^2)}{(j-1)^3} + \frac{B(Q^2)}{(j-1)^2} + \frac{C(Q^2)}{j-1}.$$

and this behaviour is often called the *triple pole pomeron* [17, 18].

Note that, in order to extend these parametrisations to  $x = 1$ , we must include powers of  $(1-x)$ , which will act as daughter trajectories. For example, Donnachie and Landshoff introduced an overall factor of  $(1-x^2)^3$  in their expressions. It is important to point out that, at small  $x$ , when we use the double and triple-pole models, we do not need to add a new singularity to reproduce the  $\gamma^*p$  amplitudes on top of the ones present in soft  $pp$  cross sections, which is not the case of the simple-pole model.

### 6.1.2 The reggeon terms

The reggeon terms correspond to the exchange of mesons trajectories. We usually consider 4 trajectories: the  $a_2$ ,  $f_0$ ,  $\rho$  and  $\omega$  trajectories. However, the  $\rho$  and  $\omega$  trajectories do not appear in  $\gamma^*p$  interactions and the  $a_2$  and  $f_0$  trajectories are often considered as degenerate. Since we shall always work at  $t = 0$ , we only need the trajectory intercept  $\alpha_{a_2, f_0}(0) \approx 0.4$  and the reggeon contribution is

$$r(Q^2) \nu^{-\alpha(0)}.$$

which corresponds, in complex- $j$  plane, to a simple pole at  $j = 1 - \alpha(0)$ .

---

<sup>1</sup>We used the DIS Regge variable  $\nu$  instead of  $x$ .

Model	$\chi^2/pts$	Remarks
DL	0.931	
double	0.827	
triple	0.694	
	0.831	$c > 0$

Table 6.1: Result of the fit at specific values of  $Q^2$  for different models. The fit include 817 points split in 42 bins.

## 6.2 Direct comparison with the data

As explained previously (see section 5.2.3), we shall only consider data in the correct region. In practice, we shall choose  $n = 10$ , which means  $\sqrt{s} \geq 10$  GeV for cross-sections and  $\frac{\sqrt{Q^2}}{xm_p} > \frac{100}{2m_p^2}$  GeV<sup>2</sup> for  $F_2$ . Before searching the expressions of the  $Q^2$ -dependent residues, we shall analyse the different models for some specific values of  $Q^2$ . Within the data we look at the most populated  $Q^2$  bins (containing at least 10 points) and try to find the residues for the Donnachie-Landshoff model and for the double and triple-pole pomeron models<sup>2</sup>:

$$\begin{aligned}
 F_2^{(DL)}(x, Q_i^2) &= \frac{Q_i^2}{4\pi^2\alpha_e} (1-x^2)^3 [a(Q_i^2)(2\nu)^{0.4} + b(Q_i^2)(2\nu)^{0.08} + c(Q_i^2)(2\nu)^{-0.45}] \\
 F_2^{(2)}(x, Q_i^2) &= \frac{Q_i^2}{4\pi^2\alpha_e} [a(Q_i^2) \log(2\nu) + b(Q_i^2) + c(Q_i^2)(2\nu)^{-0.35}] \\
 F_2^{(3)}(x, Q_i^2) &= \frac{Q_i^2}{4\pi^2\alpha_e} \left\{ a(Q_i^2) [\log(2\nu) - b(Q_i^2)]^2 + c(Q_i^2) + d(Q_i^2)(2\nu)^{-0.45} \right\}
 \end{aligned}$$

Using this technique, we can directly extract the form factors without needing their analytic dependence in  $Q^2$ . We can see from Table 6.1 that each of these models can be successfully used to reproduce the data. Since the DL model [12–14] is extensively described in their papers and the double-pole pomeron model is presented in papers [15, 16, 18], we shall focus our analysis on the triple-pole pomeron case.

For the triple pole, we impose positivity of the pomeron term by requiring  $a$  and  $c$  to be positive. Adjusting the previous expression to each  $Q^2$  bin gives the form-factors presented in Fig. 6.1

## 6.3 Form factors and the full dataset

We shall now analyse the full dataset instead of specific  $Q^2$  values. If we want to reproduce  $F_2$  at any  $Q^2$  value, we need to fix the  $Q^2$  dependence of the form-factors. Apart from the fact that gauge invariance requires that they linearly vanish when  $Q^2 \rightarrow 0$ , they are

<sup>2</sup>Note that the intercept of the reggeon term is not the same from one model to the other, in agreement with the total hadronic cross-section analysis.

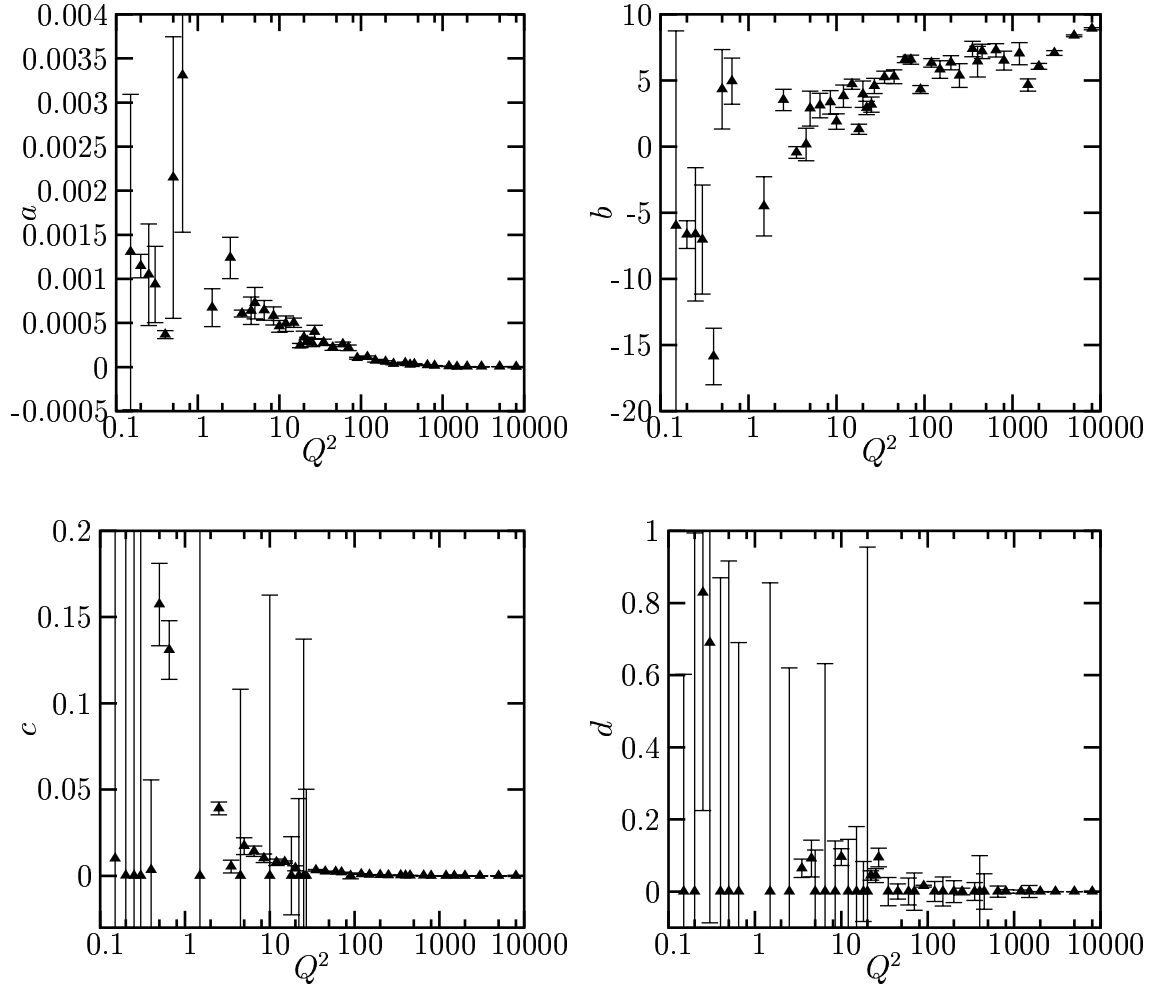


Figure 6.1: Form factors extracted from the data for individual  $Q^2$  bins.

completely undetermined. We shall see that, as soon as we do not extend the fit to very large values of  $Q^2$ , we can take

$$\phi(Q^2) = A_\phi Q^2 \left( \frac{Q_\phi^2}{Q^2 + Q_\phi^2} \right)^{\varepsilon_\phi} \quad (6.6)$$

$$b(Q^2) = b_0 + b_1 \left( \frac{Q^2}{Q^2 + Q_b^2} \right)^{\varepsilon_b} \quad (6.7)$$

where  $\phi = a, c, d$ . If we want to go to very high values of  $Q^2$ , the  $b$  form factor must be replaced by

$$b(Q^2) = b_0 + b'_1 \left[ \log \left( 1 + \frac{Q^2}{Q_b^2} \right) \right]^{\varepsilon_b} \quad (6.8)$$

As a starting point, we shall only consider the latest HERA data on  $F_2$ . These data, which go up to  $Q^2 = 135 \text{ GeV}^2$ , have a very good level of precision and allow for good

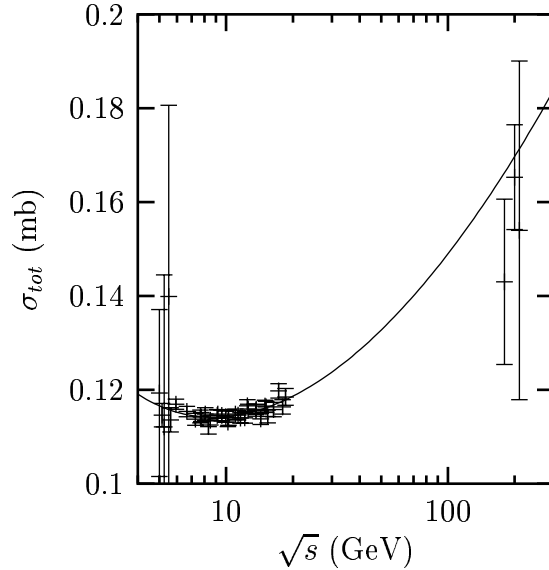


Figure 6.2: Fit to the total cross section data for  $\sqrt{s} \geq 5$  GeV.

theoretical tests as they are almost entirely in the Regge region. Again, we have cut the Regge domain with  $n = 10$  and we have included the  $\gamma p$  total cross-section for<sup>3</sup>  $\sqrt{s} \geq 5$  GeV. The resulting values of the parameters are given in Table 6.2. We imposed that the fit smoothly reproduces the value of  $\nu_0(0) = \exp\left[\frac{b(0)}{2}\right]$  which results from a global fit to all hadronic cross sections [44]. The fit gives a  $\chi^2$  of 185.2 for 241 points (including 38 points for the total cross section), which is somewhat better than those of [13, 18]. We show in Figs. 6.2 and 6.3 the curves corresponding to these results.

It is interesting to note that such simple forms for the residues as (6.6, 6.7), which achieve a remarkably low  $\chi^2$  up to 135 GeV<sup>2</sup>, do not extend well beyond 500 GeV<sup>2</sup>. Although it is not clear that Regge theory does not require new singularities at large  $Q^2$  values, we shall try to extend the triple-pole pomeron fit to all experiments and to the whole  $Q^2$  range. Replacing the parametrisation (6.7) with (6.8) allows us to extend the fit to the full Regge region, and produces a reasonable  $\chi^2/dof$ : we obtain 1411 for 1166 points (including 21 points for the total cross section above  $\sqrt{s} = 10$  GeV)<sup>4</sup>, but the  $\chi^2$  for the new HERA points [72, 73, 81] gets degraded to 311. This is largely due to the tiny size of the errors on the new data, and to some inconsistencies in the full dataset. A fine-tuning of the form factors [18] could presumably lead to a better  $\chi^2$ , but what we would learn from such an exercise is unclear. We show in Figs. 6.4, 6.5 and 6.6 the results of this global fit, and, as we can see, the full Regge region is well accounted for. Note that although all the data are fitted to, we show only the data from HERA, as the number of values of  $Q^2$  would otherwise be too large to be represented in this manner.

<sup>3</sup>Due to their large error bars, the points between 5 and 10 GeV do not contribute much.

<sup>4</sup>Note that the fit of [13] give a  $\chi^2$  of 3941 on those points.

$Q^2 \leq 135 \text{ GeV}^2$			$Q^2 \leq 3000 \text{ GeV}^2$		
parameter	value	error	parameter	value	error
$A_a$	0.0098	0.0031	$A_a$	0.00994	0.00017
$Q_a$	0.99	0.13	$Q_a$	1.885	0.075
$\epsilon_a$	0.721	0.026	$\epsilon_a$	0.900	0.011
$A_c$	0.945	0.008	$A_c$	0.9573	0.0039
$Q_c$	0.696	0.035	$Q_c$	0.624	0.016
$\epsilon_c$	1.340	0.040	$\epsilon_c$	1.390	0.023
$A_d$	0.430	0.066	$A_d$	0.274	0.027
$Q_d$	0.26	0.37	$Q_d$	32.0	5.6
$\epsilon_d$	0.45	0.10	$\epsilon_d$	1.69	0.15
$b_0$	3.00	0.64	$b'_0$	3.0000	0.0092
$b_1$	3.31	0.27	$b'_1$	0.138	0.054
$Q_b$	18.2	8.9	$Q'_b$	4.6	1.7
$\epsilon_b$	3.2	1.3	$\epsilon'_b$	1.86	0.15

Table 6.2: The values of the parameters corresponding to Eqs. (6.6, 6.7) for the low-to-intermediate  $Q^2$  fit, and those of the global fit to the whole Regge region, corresponding to Eqs. (6.6,6.8).

## 6.4 Conclusion

In conclusion, we see that several scenarios compatible with Regge theory are possible to describe structure functions. All of them share the characteristic that one needs several components to describe DIS and soft scattering at the same time. We believe that the present parametrisation shows that no unexpected behaviour is needed to reproduce DIS, and that the pomeron may well be a single object, connecting all regions of  $Q^2$  smoothly, and exhibiting the same singularities in DIS and in soft scattering. How to obtain such a simple form in the region of overlap between perturbative QCD and Regge theory remains an open question, and we shall come back later on how to link Regge theory and perturbative QCD.

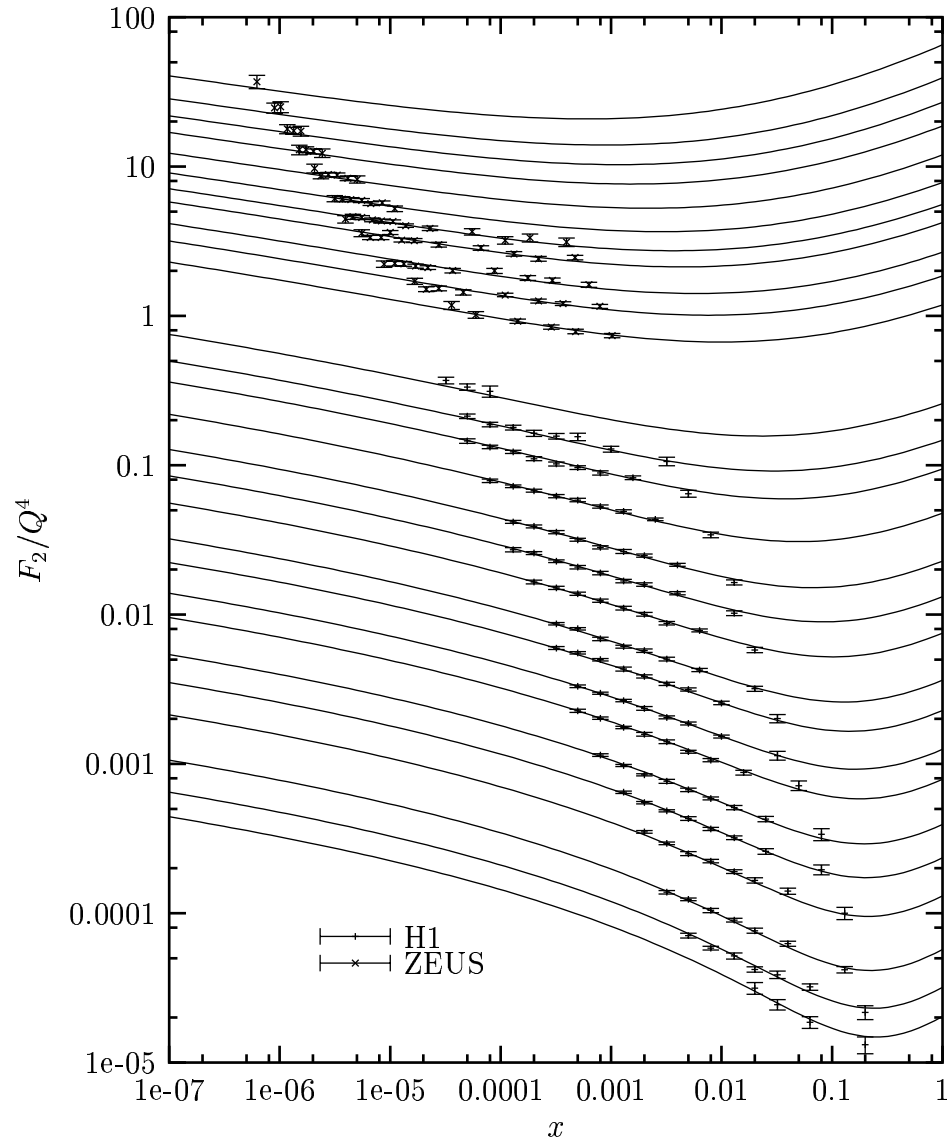


Figure 6.3: Fit to the new HERA data [73, 81] for  $Q^2 \leq 135 \text{ GeV}^2$ .

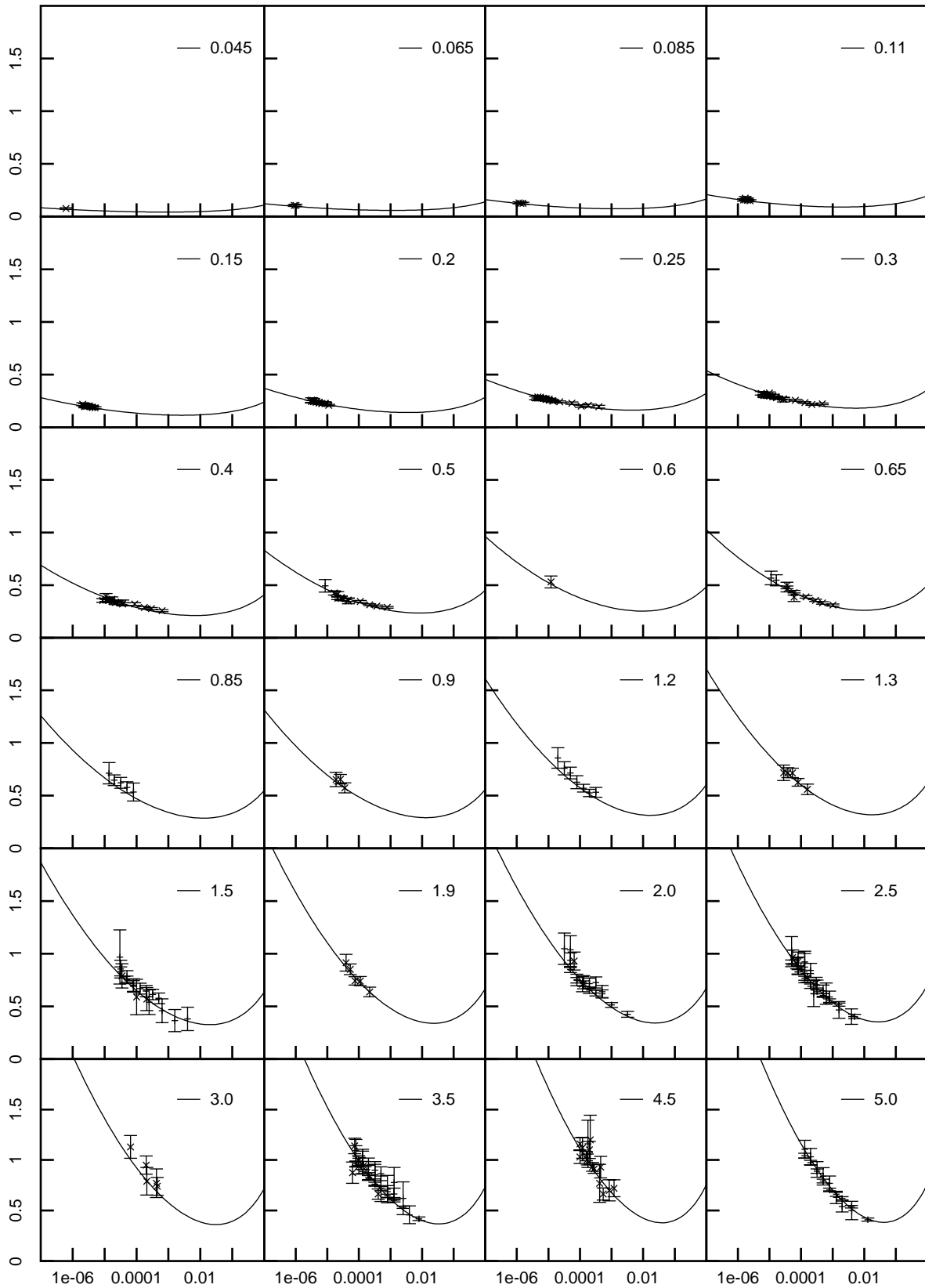


Figure 6.4: Result of a global fit to all the data in the Regge region, for  $0.045 \leq Q^2 \leq 5 \text{ GeV}^2$ .  $F_2(x, Q^2)$  is shown as a function of  $x$ , for each  $Q^2$  value indicated (in  $\text{GeV}^2$ ). Only data from HERA are shown.

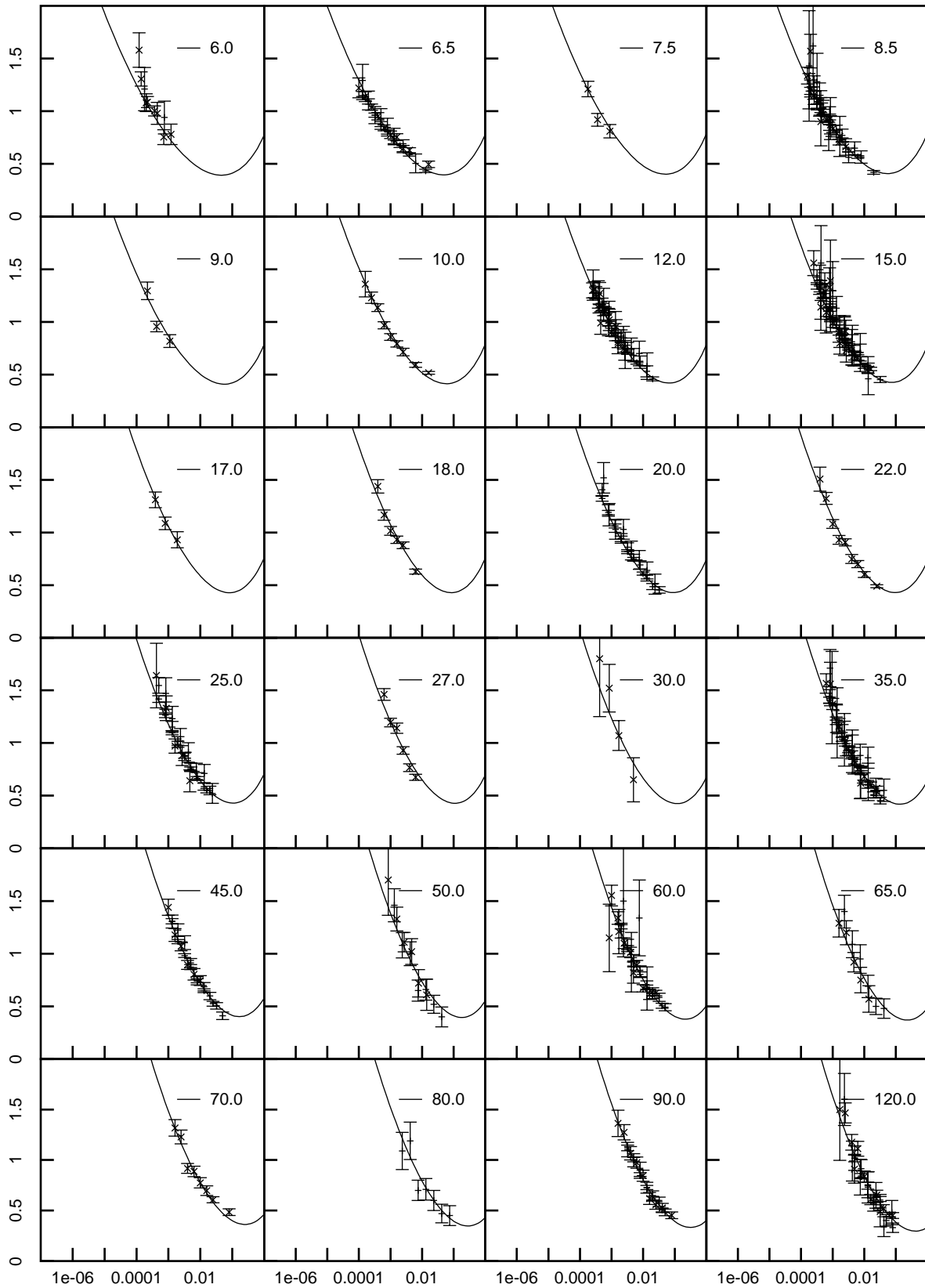


Figure 6.5: Result of a global fit to all the data in the Regge region, for  $6 \leq Q^2 \leq 120 \text{ GeV}^2$ .  $F_2(x, Q^2)$  is shown as a function of  $x$ , for each  $Q^2$  value indicated (in  $\text{GeV}^2$ ). Only data from HERA are shown.

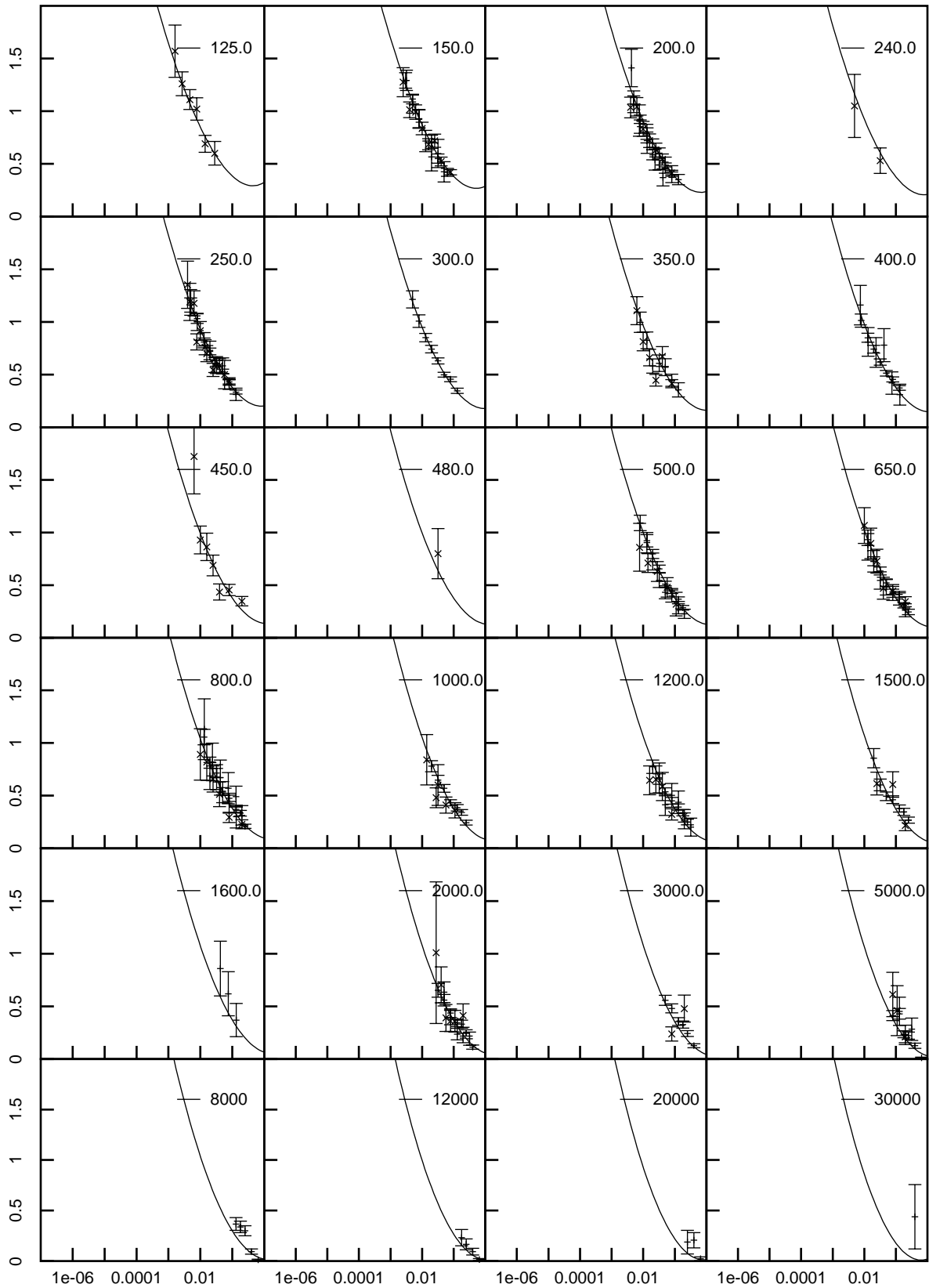


Figure 6.6: Result of a global fit to all the data in the Regge region, for  $Q^2 \geq 125 \text{ GeV}^2$ .  $F_2(x, Q^2)$  is shown as a function of  $x$ , for each  $Q^2$  value indicated (in  $\text{GeV}^2$ ). Only data from HERA are shown.

# Chapter 7

## $t$ -channel-unitarity rules

We have seen in chapter 6 that no new singularity is needed to reproduce the DIS data [17,18], provided that one assumes a logarithmic behaviour of cross sections as functions of  $\nu$ . Double or triple poles at  $j = 1$  provide such a behaviour, and enable one to reproduce all soft and hard  $\gamma p$  data within the Regge region.

How to bridge the gap between those models and QCD remains a challenge, as the description of the proton, being non-perturbative, remains at best tentative. However, LEP has now provided us with a variety of measurements of the  $\gamma\gamma$  total cross sections, for on-shell photons, and of  $F_2^\gamma$  for off-shell ones [88,89]. One may hope that this will be a good testing ground for perturbative QCD [45], and that these measurements will provide guidance for the QCD understanding of existing models. Hence it is important to build a unified description of all photon processes, and to explore where perturbative effects may manifest themselves. The natural framework for such a goal is the “factorisation theorem” of the analytic  $S$  matrix, which relates  $\gamma\gamma$ ,  $\gamma p$  and  $pp$  amplitudes. This theorem is based on  $t$ -channel unitarity, *i.e.* unitarity in the crossed channel. As proved by Gribov and Pomeranchuk [29] for the case of simple poles, one obtains the factorisation of the residues at each pole. For more general analytic structures, one obtains more complicated relations, which we shall spell out in this chapter.

Furthermore, a relation between  $\gamma\gamma$  and  $\gamma p$  processes may be of practical use as some of the measurements have big systematic uncertainties. As it is now well known [46], the LEP measurements are sensitive to the theoretical Monte Carlo used to unfold the data, leading to rather different conclusions concerning the energy dependence of the data. This problem is manifest in the case of total cross sections, where the unfolding constitutes the main uncertainty. In the case of HERA data, the measurement of the total cross section also seems to be affected by large uncertainties. Again, a joint study of both processes could help constrain the possible behaviours of these cross sections.

To decide whether new singularities can appear in  $\gamma p$  and  $\gamma\gamma$  scattering, one must first recall why singularities are supposed to be universal in hadronic cross sections. The original argument [29,47] made use of analytic continuation of amplitudes in the complex- $j$  plane from one side of a 2-particle threshold to the other, which lead to universal simple poles and factorisation of their residues. One might wonder whether these relations are broken by the presence of inelastic thresholds. Moreover, for massless particles the complex- $j$  plane gets

split in two regions, as the  $s$  and  $u$  thresholds join, which invalidates the analytic continuation used in the original proof.

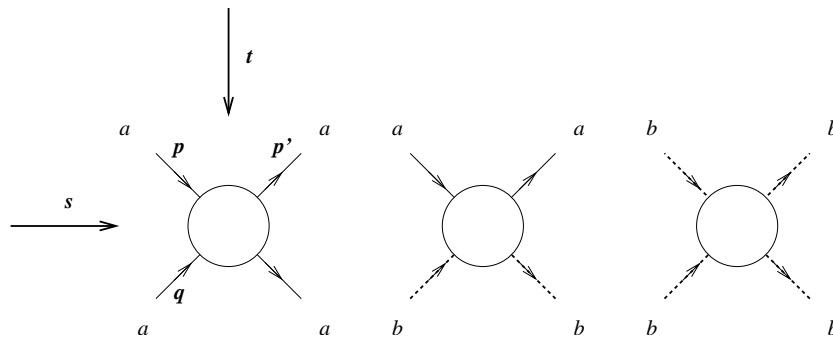
We show<sup>1</sup> that it is in fact possible to reproduce these results without analytic continuation to the second sheet, and that one can obtain a general formula for complex- $j$  plane amplitudes, which is valid no matter what the singularity is, and which leads to consequences similar to factorisation. We want to stress here that our goal is not to decide theoretically between these possibilities by solving the unitarity equations, but only to provide a relation between various amplitudes. One must also point out that double and triple poles at  $t = 0$  may result from colliding simple poles.

We shall also argue in the third section that such a formula may be applicable to photon cross sections at  $Q^2 = 0$ , and give its generalisation to off-shell photons.

## 7.1 $t$ -channel unitarity in the hadronic case

### 7.1.1 Elastic unitarity

We start by considering the amplitudes for three related processes:



We shall refer to the momenta of the incoming particles as  $p$  and  $q$ , and we use the Mandelstam variables  $s = (p + q)^2$  and  $t = (p - p')^2$ . In the  $s$  channel, these diagrams describe the processes  $aa \rightarrow aa$ ,  $ab \rightarrow ab$ , and  $bb \rightarrow bb$ . The continuation of these amplitudes to the  $t$  channel describes the processes  $a\bar{a} \rightarrow a\bar{a}$ ,  $a\bar{a} \rightarrow b\bar{b}$ ,  $b\bar{b} \rightarrow b\bar{b}$ .

We shall write  $A^{ab}(l, t, m_a, m_b)$  for the  $t$ -channel partial-wave elastic amplitude for the process  $a + b \rightarrow a + b$ , and denote by the superscript (1) the physical-sheet amplitude, and by the superscript (2) its analytic continuation round a  $cc$  threshold branch point and back to the same value of  $t$  (see Fig. 7.1).

Unitarity and analyticity of the amplitude then impose the following relation on the discontinuity through the threshold, which we shall prove later on

$$A_{ab}^{(1)} - A_{ab}^{(2)} = \rho_c(t) A_{ac}^{(1)} A_{cb}^{(2)} = \rho_c(t) A_{ac}^{(2)} A_{cb}^{(1)} \quad (7.1)$$

with  $\rho_c(t) = \sqrt{\frac{t-4m_c^2}{t}}$ .

<sup>1</sup>The model presented here and in the following chapter is based on [48].

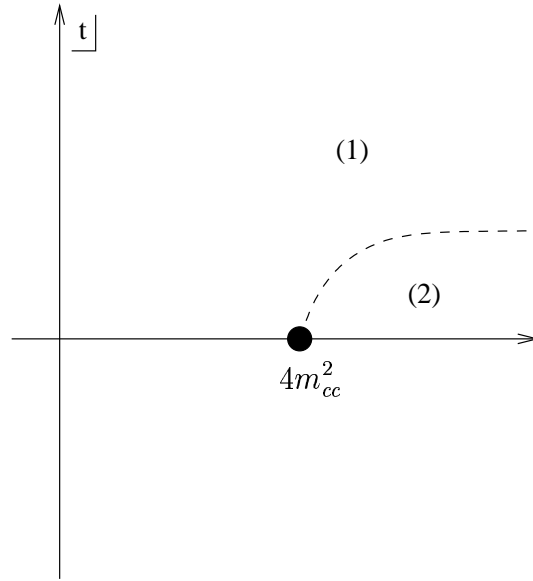


Figure 7.1: the amplitude and its continuation around a  $cc$  threshold.

In the case of hadrons, one can consider the equation through some threshold, and the equations that the amplitudes of the intermediate particles will themselves obey through the same threshold. For instance, we can consider three coupled equations for protons and pions, across the  $\pi\pi$  threshold (see Fig. 7.2):

$$\begin{aligned} A_{pp}^{(1)} - A_{pp}^{(2)} &= \rho_\pi(t) A_{p\pi}^{(1)} A_{\pi p}^{(2)}, \\ A_{p\pi}^{(1)} - A_{p\pi}^{(2)} &= \rho_\pi(t) A_{p\pi}^{(2)} A_{\pi\pi}^{(1)}, \\ A_{\pi\pi}^{(1)} - A_{\pi\pi}^{(2)} &= \rho_\pi(t) A_{\pi\pi}^{(1)} A_{\pi\pi}^{(2)}. \end{aligned} \quad (7.2)$$

From (7.2), we can write

$$A_{\pi\pi}^{(1)} = \frac{A_{\pi\pi}^{(2)}}{1 - \rho_\pi(t) A_{\pi\pi}^{(2)}} \quad (7.3)$$

We see that if  $A_{\pi\pi}^{(1)}$  has a singularity at  $j = \alpha(t)$ , then  $A_{\pi\pi}^{(2)}$  cannot have that singularity, which must be shifted at some other value when one goes around the cut. For instance, near a simple pole at  $j = \alpha$ , one has  $A^{(1)} \approx \frac{K}{j-\alpha}$ , and  $A^{(2)} \approx \frac{K}{j-\alpha+\rho_\pi K}$ .

Equation (7.2) can be conveniently written in matrix form:

$$T_0^{(1)} - T_0^{(2)} = T_0^{(1)} R_\pi T_0^{(2)} \quad (7.4)$$

with

$$T_0 = \begin{pmatrix} A_{\pi\pi} & A_{\pi p} \\ A_{p\pi} & A_{pp} \end{pmatrix}$$

and the threshold matrix

$$R_\pi = \begin{pmatrix} \rho_\pi & 0 \\ 0 & 0 \end{pmatrix}.$$

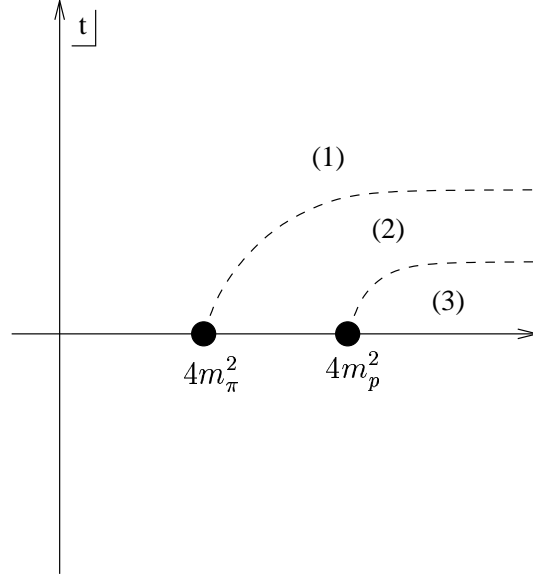


Figure 7.2: the amplitude and its continuation at the  $\pi\pi$  and  $pp$  branch-points.

To obtain the most constraining set of equations, one then writes the discontinuities of  $A^{(2)}$  across the  $pp$  threshold (the amplitudes across this threshold are denoted by a superscript (3)). This gives, using the same notation as before:

$$T_0^{(2)} - T_0^{(3)} = T_0^{(2)} R_p T_0^{(3)} \quad (7.5)$$

with

$$R_p = \begin{pmatrix} 0 & 0 \\ 0 & \rho_p \end{pmatrix}.$$

Putting Eqs. (7.4, 7.5) together, one then gets:

$$\begin{aligned} T_0^{(1)} - T_0^{(3)} &= T_0^{(1)} R_\pi T_0^{(2)} + T_0^{(2)} R_p T_0^{(3)} \\ &= T_0^{(1)} (R_\pi + R_p) T_0^{(3)} + T_0^{(1)} R_\pi (T_0^{(2)} - T_0^{(3)}) \\ &\quad + (T_0^{(2)} - T_0^{(1)}) R_p T_0^{(3)} \\ &= T_0^{(1)} R T_0^{(3)} \end{aligned} \quad (7.6)$$

with  $R = R_\pi + R_p$ . Note that in this case  $T_0^{(3)} = T_0^{(1)\dagger}$ .

One can then solve the equation for  $T_0^{(1)}$  to obtain

$$T_0^{(1)} [1 - R T_0^{(3)}] = T_0^{(3)} \quad (7.7)$$

This situation generalises that of Eq. (7.3):  $T_0^{(1)}$  is a function of  $T_0^{(3)}$  and its singularities cannot come from singularities in the right-hand side of Eq. (7.7), because they are exactly matched by corresponding factors in the left-hand side. Note that this is why we needed to

consider both thresholds, as otherwise some amplitudes would not be present in the r.h.s. of (7.6).

Hence *the amplitudes*  $A_{\pi\pi}$ ,  $A_{pp}$  *and*  $A_{\pi p}$  *have common singularities* which can only come from zeroes  $z_m$  of the determinant of the matrix in brackets in the right-hand side of (7.7):

$$\Delta = \det \left( 1 - RT_0^{(3)} \right) = 0 \text{ for } j = z_m. \quad (7.8)$$

Near each zero  $z_m$ , we can write,

$$A_{ij}^{(1)} = \frac{a_{ij}}{\Delta}. \quad (7.9)$$

This is the basis of the complex- $j$ -plane factorisation of the amplitudes contained in  $T_0$ . Indeed, we can write

$$A_{pp}^{(1)} A_{\pi\pi}^{(1)} - \left( A_{\pi p}^{(1)} \right)^2 = \det(T_0) = \frac{\det(D)}{\Delta}. \quad (7.10)$$

We see that near the zeroes we obtain

$$\lim_{j \rightarrow z_m} \left[ A_{pp}^{(1)}(j) - \frac{\left( A_{\pi p}^{(1)}(j) \right)^2}{A_{\pi\pi}^{(1)}(j)} \right] = \text{finite terms}. \quad (7.11)$$

Having in mind the extension to the photon case, one should now address the following questions:

1. The factorisation relations hold for  $t$  above the  $4m_p^2$  threshold. Can they be continued down to negative  $t$ , and in particular what is the role of other elastic thresholds and of the inelastic thresholds ?
2. For on-shell photons, the inelastic cut goes down to  $t = 0$  and thus splits the complex- $t$  plane in two. Can one still derive factorisation, without using the concept of continuation around a cut ?

### 7.1.2 Further elastic thresholds

Imagine now that we introduce yet another elastic threshold, e.g. for  $K$  production (see Fig. 7.3). We can now go through the above argument, and obtain

$$T_0^{(1)} - T_0^{(4)} = T_0^{(1)} R T_0^{(4)} \quad (7.12)$$

where all matrices are now  $3 \times 3$ :

$$T_0 = \begin{pmatrix} A_{\pi\pi} & A_{\pi K} & A_{\pi p} \\ A_{K\pi} & A_{KK} & A_{Kp} \\ A_{p\pi} & A_{pK} & A_{pp} \end{pmatrix}$$

and

$$R = \begin{pmatrix} \rho_\pi & 0 & 0 \\ 0 & \rho_K & 0 \\ 0 & 0 & \rho_p \end{pmatrix}.$$

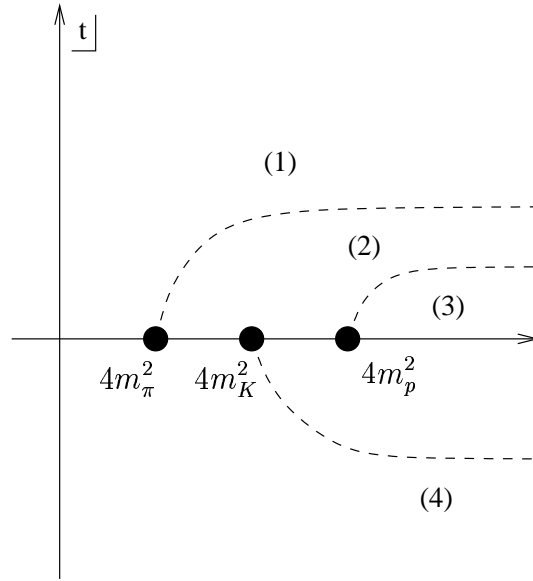


Figure 7.3: the amplitude and its continuation at the  $\pi\pi$ ,  $KK$  and  $pp$  branch-points.

This time,  $T_0^{(4)} = T_0^{(1)\dagger}$ .

One again obtains a relation similar to (7.9):

$$A_{ij}^{(1)} = \frac{a'_{ij}}{\Delta'}, \quad (7.13)$$

but now  $a'$  and  $\Delta'$  include contributions from the  $K$  threshold.

However, one can see that by orienting the cuts as in Fig. (7.3): the previous relation (7.7) between  $T^{(1)}$  and  $T^{(3)}$  still holds. The new relations involving  $A^{(4)}$  can be obtained in a way similar to (7.6), if one solves the equation expressing  $T_0^{(3)}$  as a function of  $T_0^{(4)}$ .

Hence, although the expression of the amplitude looks different when a different number of threshold is considered, it is in fact guaranteed to lead to the same function  $A^{(1)}$ , which presumably has the same singularities above and below threshold.

We have pointed out that the form of the relation obtained remains identical if one considers the discontinuity of the amplitude across all cuts, i.e. the amplitude and its hermitian conjugate (if one assumes as usual that the amplitudes are real analytic functions and symmetric  $a_{ij} = a_{ji}$ ):

$$T_0^{(1)} = \frac{\left(T_0^{(1)}\right)^\dagger}{\mathbb{1} - R \left(T_0^{(1)}\right)^\dagger} \quad (7.14)$$

This relation holds for an arbitrary number  $N$  of elastic channels ( $T_0$  and  $R$  are then  $N \times N$  matrices), and will be proved later in this chapter. As one goes down in  $t$ , one loses the  $N^{\text{th}}$  threshold, and the element  $R_N$  becomes 0. Effectively, the problem then reduces to an  $(N-1) \times (N-1)$  system, and the  $N^{\text{th}}$  equation becomes trivial.

### 7.1.3 Inelastic thresholds

In the same way as for the  $K$  threshold, we can introduce inelastic thresholds. Imagine that we go through an  $n$ -pion threshold. We can then write, in the  $\pi\pi$  case:

$$T^{(1)} - T^{(5)} = C(T^{(1)}, T^{(5)}) \quad (7.15)$$

with  $T^{(5)}$  the continuation of the amplitudes across the  $\pi\pi$  and the  $n\pi$  cuts. The matrix  $T$  is now:

$$T = \begin{pmatrix} A_{\pi\pi} & A_{\pi\pi \rightarrow n\pi} \\ A_{n\pi \rightarrow \pi\pi} & A_{n\pi \rightarrow n\pi} \end{pmatrix}$$

The only difference with the previous case is that for inelastic amplitudes the matrix  $R$  gets replaced by an operator  $C$ , which involves integration over the  $n$ -particle intermediate state and the transformation to the complex- $j$  plane.

Explicitly, one gets:

$$A_{\pi\pi}^{(1)} - A_{\pi\pi}^{(5)} = A_{\pi\pi}^{(1)} \rho_\pi A_{\pi\pi}^{(5)} + C(A_{\pi\pi \rightarrow n\pi}^{(1)}, A_{n\pi \rightarrow \pi\pi}^{(5)}) \quad (7.16)$$

$$A_{\pi\pi \rightarrow n\pi}^{(1)} - A_{\pi\pi \rightarrow n\pi}^{(5)} = A_{\pi\pi}^{(1)} \rho_\pi A_{\pi\pi \rightarrow n\pi}^{(5)} + C(A_{\pi\pi \rightarrow n\pi}^{(1)}, A_{n\pi \rightarrow n\pi}^{(5)}) \quad (7.17)$$

To solve this system, note that the  $2 \rightarrow n$  process can go either through the 2-pion threshold first or not, yielding from (7.17):

$$A_{\pi\pi \rightarrow n\pi}^{(1)} = M + A_{\pi\pi}^{(1)} \rho_\pi M \quad (7.18)$$

with

$$\begin{aligned} M &= A_{\pi\pi \rightarrow n\pi}^{(5)} + C(A_{\pi\pi \rightarrow n\pi}^{(5)}, A_{n\pi \rightarrow n\pi}^{(5)}) \\ &+ C(C(A_{\pi\pi \rightarrow n\pi}^{(5)}, A_{n\pi \rightarrow n\pi}^{(5)}), A_{n\pi \rightarrow n\pi}^{(5)}) + \dots \end{aligned} \quad (7.19)$$

The first equation then becomes:

$$A_{\pi\pi}^{(1)} \{1 - \rho_\pi [A_{\pi\pi}^{(5)} - C(M, A_{n\pi \rightarrow \pi\pi}^{(5)})]\} = [A_{\pi\pi}^{(5)} - C(M, A_{n\pi \rightarrow \pi\pi}^{(5)})] \quad (7.20)$$

We see that the elastic amplitude  $A_{\pi\pi}^{(5)}$  gets the same corrections on both sides of the equation, so that the inclusion of inelastic thresholds does not change our conclusions (7.11) about singularities. We show further in this chapter that this relation remains the same in the case of an arbitrary number of elastic and inelastic thresholds:

$$T_0(\mathbb{I} - RD) = D \quad (7.21)$$

where  $T_0$  is the matrix containing all elastic amplitudes, and  $D$  is an unknown matrix containing the effects of inelastic thresholds and the contribution of elastic amplitudes across the cuts. Again, the singularities of  $T_0$  must come from the zeroes  $z_m$  of

$$\Delta = \det(\mathbb{I} - RD) \quad (7.22)$$

and one obtains again (7.10) and (7.11).

### 7.1.4 Remarks

1. The factorisation relations are in general broken when one considers  $n$ -trajectory exchanges. However, the conclusion is that, after all the ( $s$ -channel) unitarising exchanges are taken into account, one must end up again with an amplitude factorising at each singularity, even if the latter is not a simple pole.
2. The matrix  $D$  is sensitive to the existence of thresholds associated with bound states, and does not know directly about quarks and gluons which do not enter the unitarity equations. Hence *the zeroes  $z_m$  are not calculable perturbatively.*
3. One could have a spurious cancellation of the singularity if  $D_{pq}$  has a zero at  $j = z_m$ . However, as both quantities are  $t$ -dependent, it is unlikely for this cancellation to occur for all  $t$  or for all processes. It is however possible to “hide” a singularity, *e.g.* at  $t = 0$  for  $pp$  and  $\bar{p}p$  scattering. This might provide an explanation for the absence of an odderon pole in forward scattering data.
4. *Each singularity factorises separately.* Hence it does not make sense to consider globally factorising cross sections or amplitudes in the  $s, t$  representation, unless of course the amplitude can be reproduced by only one leading singularity.
5. The relations (7.11) lead to a definite prediction for the residues (or couplings) of the singularities above threshold  $t > 4m_a^2$ . As no singularity occurs when  $t$  is continued to the physical region for the  $s$  channel processes, these relations still remain true there.
6. We have mentioned that one always obtains a relation between the amplitude and its complex conjugate. This in fact is obtained in the next section as a consequence of the unitarity of the  $S$  matrix. The relations between amplitudes across a cut are really derived from the relation between the amplitude and its complex conjugate. Hence for massless particles, provided the  $S$  matrix exists, the relations should still hold as they do not require explicit continuation.

## 7.2 General proof of $t$ CU relations: hadronic case

Assuming that  $m_b$  is the lowest hadronic mass, we know that  $aa \rightarrow aa$ ,  $ab \rightarrow ab$  and  $bb \rightarrow bb$  have thresholds for  $t > 4m_a^2 > 4m_b^2$ . In general, if  $t$  is large enough, there are many possible intermediate states for each process under consideration, which we must take into account to write the unitarity relations. These states can be grouped into subsets which have the same quantum numbers, and for which one can derive factorisation.

Starting with the unitarity of the  $S$  matrix:

$$S^\dagger S = SS^\dagger = \mathbb{1} \tag{7.23}$$

and setting  $S = \mathbb{1} + iT$ , we obtain

$$T - T^\dagger = iT^\dagger T = iTT^\dagger. \tag{7.24}$$

One can define the invariant amplitude  $\mathcal{A}_{if}$  by the matrix elements

$$\langle f|T|i \rangle = (2\pi)^4 \delta^4(p_f - p_i) \mathcal{A}_{if}. \quad (7.25)$$

Eq. (7.24) then becomes the following at the amplitude level:

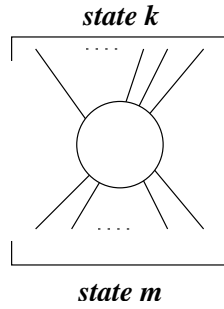
$$\mathcal{A}_{if} - \mathcal{A}_{if}^\dagger = C_s^{if}(\mathcal{A}, \mathcal{A}^\dagger). \quad (7.26)$$

We define the  $C_s$  operator as the following convolution:

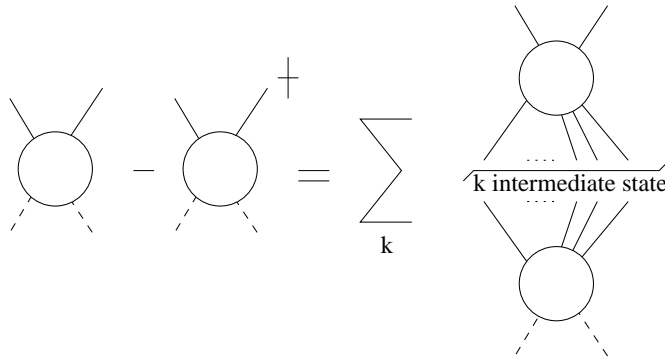
$$C_s^{if}(\mathcal{A}^\dagger, \mathcal{A}) = C_s^{if}(\mathcal{A}, \mathcal{A}^\dagger) = 2i \sum_k \int dPS \mathcal{A}_{ik} \mathcal{A}_{kf}^\dagger \quad (7.27)$$

where  $k$  labels the possible intermediate on-shell  $n$ -particle states in the  $t$  channel, which can differ by the number and nature of produced particles, and  $dPS$  represents the differential  $n$ -particle Lorentz-invariant phase space associated with these states.

If the particles are massive, we can enumerate these open channels and assume that  $k$  runs from 1 to  $N + 2$ , the number of open channels depending on the value of  $t$ , *i.e.* of the energy in that channel. In particular, we shall find in this set of states the  $a\bar{a}$  and  $b\bar{b}$  intermediate states to which we respectively assign the labels  $k = 1, 2$ . Note that in general the label  $k$  does not refer to the number of particles in the intermediate state, and that  $k$  can stand for particles different from  $a$  and  $b$ . So in general the amplitude  $\mathcal{A}_{km}$  represents the following process:



Eq. (7.26) can be represented by:



We can now imagine that we split the amplitude into charge-parity +1 and charge-parity -1 parts, and perform a Watson-Sommerfeld transform (see (5.9))

$$\mathcal{A}_{ab}^{\pm}(\nu, t) = \frac{1}{2i} \int dj P_j(\cos(\theta_t)) \frac{2j+1}{\sin(\pi j)} A_{ab}^{\pm}(j, t) \frac{e^{-i\pi j} \pm 1}{2}, \quad (7.28)$$

with<sup>2</sup>  $\nu = p.q$ . As previously, we shall consider the matrix  $T$  build with the amplitudes in complex- $j$  space

$$T = \begin{pmatrix} A_{\pi\pi} & A_{\pi p} & \dots & A_{\pi f} & \dots \\ A_{p\pi} & A_{pp} & \dots & A_{pf} & \dots \\ \vdots & \vdots & \ddots & \vdots & \vdots \\ A_{i\pi} & A_{ip} & \dots & A_{if} & \dots \\ \vdots & \vdots & \dots & \vdots & \ddots \end{pmatrix}.$$

After continuing the relation (7.27) to complex  $l \equiv j$ , we deform the contour of integration so that only the singularities of  $T(j, t)$  will contribute. All amplitudes become functions of  $j$ , and the operator  $C_s$  changes to  $C$ , which has the following properties:

- It is associative and distributive

$$C(\alpha A_1 + \beta A_2, B) = \alpha C(A_1, B) + \beta C(A_2, B). \quad (7.29)$$

- In the case of 2-particle intermediate states  $k$ , the form of  $C$  is particularly simple:

$$C_2^{if}(T^\dagger, T) = \rho_k A_{ik} A_{kf}^\dagger = (TRT^\dagger)_{if} \quad (7.30)$$

with  $\rho_k = 2i\sqrt{\frac{t-4m_k^2}{t}}$ , and  $R_{km} = \rho_k \delta_{km}$ .

To proceed further, we shall represent the  $T$  matrix in the following form, for  $k \leq N+2$ :

$$T = \left( \begin{array}{c|c} T_0(2 \times 2) & T_u(2 \times N) \\ \hline T_l(N \times 2) & T_r(N \times N) \end{array} \right), \quad (7.31)$$

where we have indicated the dimensions of the sub-matrices in parenthesis.  $T_0$  contains the elastic amplitudes ( $i, f=1, 2$ ), the upper matrix  $T_u$  contains the inelastic amplitudes  $i = 1, 2 \rightarrow k > 2$ , and the lower matrix  $T_l$  the inelastic amplitudes  $k > 2 \rightarrow i = 1, 2$ .  $T_r$  stands for the rest of the amplitudes  $k \rightarrow m$ , with  $k$  and  $m > 2$ .

The system (7.26) can then be written:

$$T_0 - T_0^\dagger = T_0 R T_0^\dagger + C(T_u, T_u^\dagger), \quad (7.32)$$

$$T_u - T_l^\dagger = T_0 R T_l^\dagger + C(T_u, T_r^\dagger), \quad (7.33)$$

$$T_l - T_u^\dagger = T_l R T_0^\dagger + C(T_r, T_u^\dagger), \quad (7.34)$$

$$T_r - T_r^\dagger = C(T_l, T_l^\dagger) + C(T_r, T_r^\dagger). \quad (7.35)$$

---

<sup>2</sup>In the following, we shall only consider the charge-parity +1 part of the amplitudes without carrying the superscript +.

To derive factorisation, it is enough to consider the first two relations (7.32, 7.33). We assume that the second equation can be solved by a series expansion, yielding

$$T_u = M + T_0 R M \quad (7.36)$$

with  $M$  the solution of  $M = T_l^\dagger + C(M, T_r^\dagger)$ :

$$M = T_l^\dagger + C(T_l^\dagger, T_r^\dagger) + C(C(T_l^\dagger, T_r^\dagger), T_r^\dagger) + \dots \quad (7.37)$$

We can put this form into Eq. (7.32), which then gives

$$T_0(\mathbb{I} - R D) = D \quad (7.38)$$

with

$$D = \left[ T_0^\dagger + C(M, T_u^\dagger) \right]. \quad (7.39)$$

### 7.3 The photon case

The basic problem here concerns the fact that photons are massless. Because of this, one has perturbatively an infrared singularity in all amplitudes containing a fixed number of photons. These singularities are cancelled by virtual corrections in inclusive cross sections, and the standard strategy to solve the problem is to perform a resummation of soft photons *à la* Bloch-Nordsieck [49]. One then only considers inclusive quantities which include an infinite resummation of soft photons. The outcome of this resummation is that the exclusive amplitudes connecting states with a finite number of photons are identically zero. This means that the  $S$  matrix is not defined, and that asymptotic states with a fixed number of particles cannot be used to build the theory. The formalism that we have developed then breaks down (or becomes trivial: Eq. (7.10) gives  $0 = 0$ ), and one can only use  $S$ -matrix theory to treat hadronic interactions.

One can salvage part of the  $t$ CU relations if one keeps only the hadronic part of the photon wave function, and neglects electromagnetic interactions altogether. Assuming that an  $S$  matrix still describes the interactions of this part of the wave function, one then keeps a subset of the equations (7.10), effectively removing photon thresholds from the unitarity equations, and treating photons as external states only. In practice, the equations (7.10, 7.21) remain the same, provided that we write the threshold matrix  $R$  as

$$R = \begin{pmatrix} \rho_p & 0 \\ 0 & 0 \end{pmatrix}. \quad (7.40)$$

This means that  $\Delta = 1 - \rho_p D_{pp}$  only involve  $D_{pp}$ , hence singularities can now come from other elements of  $D$ , and  $\det(D)$  can contain singularities not present in  $\Delta$ , hence breaking the factorisation relation (7.11). Namely, we obtain

$$\begin{aligned} A_{pp} &= \frac{D_{pp}}{\Delta}, \\ A_{\gamma p} &= \frac{D_{\gamma p}}{\Delta}, \\ A_{\gamma\gamma} &= \frac{\rho_p D_{\gamma p}^2}{\Delta} + D_{\gamma\gamma}. \end{aligned} \quad (7.41)$$

Extra singularities can come from  $D_{\gamma p}$  or  $D_{\gamma\gamma}$ . In the first case, the nature of the singularity is different in  $\gamma p$  and in  $\gamma\gamma$ , and the coupling of the singularity, which contains  $\Delta$ , must be of non-perturbative origin. On the other hand, singularities in  $D_{\gamma\gamma}$  can be purely perturbative.

In the DIS case, as off-shell photons do not enter the intermediate states, one still has the above equations (7.41) and the possibility of extra singularities. Details and general formulae are given in the next section, where one obtains an equation similar to (7.41), with a matrix  $D$  depending on the off-shellnesses of photons:

$$T_0(Q_{in}, Q_{out}) = D(Q_{in}, Q_{out}) + \frac{D(Q_{in}, 0)RD(0, Q_{out})}{\mathbb{1} - RD(0, 0)}. \quad (7.42)$$

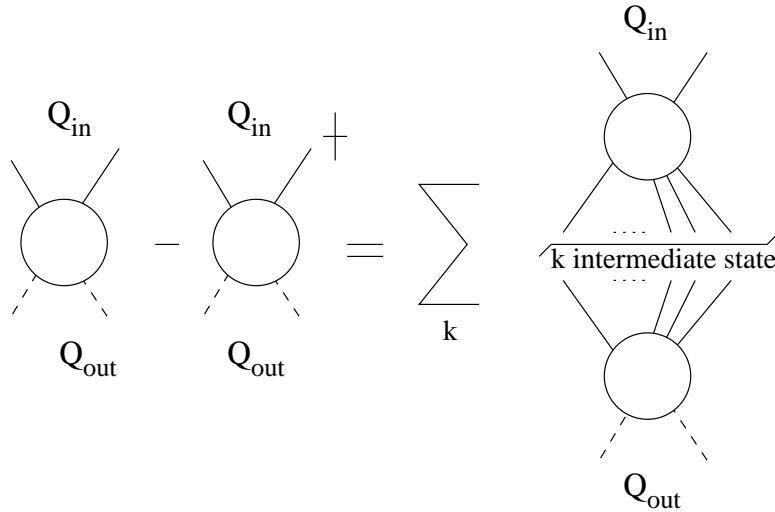
where  $Q_{in}$  stands for the two virtualities  $(Q_1^2, Q_2^2)$  of the initial states in the  $t$  channel, and  $Q_{out}$  for the two virtualities  $(Q_3^2, Q_4^2)$  of the final states.

We want to point out that the position of the possible new singularities can depend on  $Q^2$ , and as the photon states do not enter unitarity equations, these singularities can be fixed in  $t$ .

## 7.4 General properties of $t$ CU relations: photon case

The virtual photons must not be included in the intermediate states of Eq. (7.26). One can still define an  $S$  matrix in this case, at least in the one-photon approximation, as the electron contributions can be factored and cancelled on each side of the unitarity equations.

In this case, we want to indicate explicitly whether the external legs of the  $2 \rightarrow 2$ ,  $2 \rightarrow n$  and  $n \rightarrow 2$  amplitudes are off-shell or not. We introduce the notations  $T_0(Q_{in}, Q_{out})$ ,  $T_u(Q_{in})$  and  $T_l(Q_{out})$ , where  $Q_{in}$  stands for the two virtualities  $(Q_1^2, Q_2^2)$  of the initial states in the  $t$  channel, and  $Q_{out}$  for the two virtualities  $(Q_3^2, Q_4^2)$  of the final states, and we write  $Q_{in} = 0$  or  $Q_{out} = 0$  in the case of on-shell states, and the relations (7.26) can be visualised as follows:



The system of equations (7.32-7.35) then becomes:

$$\begin{aligned} T_0(Q_{in}, Q_{out}) - T_0^\dagger(Q_{in}, Q_{out}) &= T_0(Q_{in}, 0)RT_0^\dagger(0, Q_{out}) \\ &\quad + C(T_u(Q_{in}), T_u^\dagger(Q_{out})), \end{aligned} \quad (7.43)$$

$$T_u(Q_{in}) - T_l^\dagger(Q_{in}) = T_0(Q_{in}, 0)RT_l^\dagger(0) + C(T_u(Q_{in}), T_r^\dagger), \quad (7.44)$$

$$T_l(Q_{out}) - T_u^\dagger(Q_{out}) = T_l(Q_{out})RT_0^\dagger(0, 0) + C(T_r, T_u^\dagger), \quad (7.45)$$

$$T_r - T_r^\dagger = C(T_l(0), T_l^\dagger(0)) + C(T_r, T_r^\dagger). \quad (7.46)$$

The resolution of the system proceeds as before with the elimination of  $T_u(Q_{in})$ :

$$T_u(Q_{in}) = M(Q_{in}) + T_0(Q_{in}, 0)RM(0) \quad (7.47)$$

with  $M$  the solution of  $M(Q) = T_l^\dagger(Q) + C(M(Q), T_r^\dagger)$ :

$$M(Q_{in}) = T_l^\dagger(Q_{in}) + C(T_l^\dagger(Q_{in}), T_r^\dagger) + C(T_l^\dagger(Q_{in}), T_r^\dagger), T_r^\dagger) + \dots \quad (7.48)$$

The first equation however now gives

$$T_0(Q_{in}, Q_{out}) = D(Q_{in}, Q_{out}) + T_0(Q_{in}, 0)RD(0, Q_{out}) \quad (7.49)$$

with

$$D(Q_{in}, Q_{out}) = T_0^\dagger(Q_{in}, Q_{out}) + C(M(Q_{in}), T_u^\dagger(Q_{out})). \quad (7.50)$$

For DIS, we consider<sup>3</sup>  $Q_{out} = 0$  and  $Q_1^2 = Q_2^2 = Q^2 \equiv -q^2$ . This gives us

$$T_0(Q_{in}, 0)(\mathbb{1} - RD(0, 0)) = D(Q_{in}, 0). \quad (7.51)$$

Hence we see that all the on-shell singularities must be present in the off-shell case, due to the factor  $(\mathbb{1} - RD(0, 0))$ , but we can have new ones coming from the singularities  $D(Q_{in}, 0)$ . These singularities can be of perturbative origin (*e.g.* the singularities generated by the DGLAP evolution) but their coupling will depend on the threshold matrix  $R$ , and hence they must know about hadronic masses, or in other words they are not directly accessible by perturbation theory.

In the case of  $\gamma^*\gamma^*$  scattering, we take  $Q_{in} = Q^2$  and  $Q_{out} = P^2 = -p^2$ , and Eq. (7.49) gives

$$T_0(Q_{in}, Q_{out}) = D(Q_{in}, Q_{out}) + \frac{D(Q_{in}, 0)RD(0, Q_{out})}{\mathbb{1} - RD(0, 0)}. \quad (7.52)$$

This shows that the DIS singularities will again be present, either through  $\Delta$ , or through extra singularities present in DIS (in which case their order will be different in  $\gamma\gamma$  scattering, at least for  $Q_{in} = Q_{out}$ ).

It is also possible to have extra singularities purely from  $D(Q_{in}, Q_{out})$ . *A priori* these could be independent from the threshold matrix  $R$ , and hence be of purely perturbative origin (*e.g.*  $\gamma^*\gamma^* \rightarrow \bar{q}q$  or the BFKL pomeron coupled to photons through a perturbative impact factor).

---

<sup>3</sup>Note that the same kind of relations and conclusions would hold for off-forward parton distribution functions.

## 7.5 Specific examples

Eq. (7.11) is usually not mentioned, and only its consequences for the residues of simple poles are considered. However, we have shown that it is true in general, and that it leads to specific predictions for any singularity structure of  $T_{pq}(j)$ , *e.g.* for a given order of the zeroes of  $z_m$ . We shall give here the formulae that correspond to simple, double or triple poles, which seem to be three possibilities emerging from fits to hadronic amplitudes at  $t = 0$  [44]. We shall refer to these relations as the *t*-Channel Unitarity (*t*CU) relations. The case of cuts will not be explicitly considered here, although Eq. (7.11) holds also for them.

For isolated simple poles

$$A_{pq} = \sum_m \frac{R_{pq}^m}{j - z_m}, \quad (7.53)$$

one obtains the usual relations for the residues [29]

$$R_{22}^m = \frac{(R_{12}^m)^2}{R_{11}^m}. \quad (7.54)$$

If  $A_{pq}$  has coinciding simple and double poles

$$A_{pq} = \frac{S_{pq}}{j - z} + \frac{D_{pq}}{(j - z)^2}, \quad (7.55)$$

one obtains the new relations

$$\begin{aligned} D_{11}D_{22} &= (D_{12})^2, \\ D_{11}S_{22} + S_{11}D_{22} &= 2D_{12}S_{12}. \end{aligned} \quad (7.56)$$

In the case of triple poles

$$A_{pq} = \frac{S_{pq}}{j - z} + \frac{D_{pq}}{(j - z)^2} + \frac{F_{pq}}{(j - z)^3}, \quad (7.57)$$

the relations become

$$\begin{aligned} F_{11}F_{22} &= (F_{12})^2, \\ F_{11}D_{22} + D_{11}F_{22} &= 2F_{12}D_{12}, \\ D_{11}D_{22} + S_{11}F_{22} + S_{22}F_{11} &= 2S_{12}F_{12} + D_{12}^2. \end{aligned} \quad (7.58)$$

It is worth pointing out that the double pole relations are not the limit of the triple pole relations for a vanishing triple pole residue. Similarly, the simple-pole relations cannot be obtained from the double-pole ones. The reason for this is that the relations (7.10) relate the poles of order  $2n$  to  $n + 1$ ,  $n$  being the maximal order of the pole. Hence the first double-pole relation is contained in the triple-pole ones, but not the second one, and the simple-pole relation is entirely separate.

## 7.6 Colliding poles and $t$ CU relations

To conclude this chapter, we shall show that if we consider two colliding simple poles leading to a double pole at  $t = 0$ , we can obtain the double-pole  $t$ CU relations by taking the limit  $t \rightarrow 0$  in the simple poles relations. Let us consider the following amplitude ( $p, q = \pi, p$ )

$$A_{pq} = \frac{a_{pq} + b_{pq}(j - \alpha_0)}{(j - \alpha_0)^2 - (\alpha't)^2}.$$

For  $t \neq 0$ , this corresponds to two simple poles at  $j = \alpha_0 \pm \alpha't$

$$A_{pq} = \frac{a_{pq} + b_{pq}\alpha't}{2\alpha't} \frac{1}{j - \alpha_0 - \alpha't} - \frac{a_{pq} - b_{pq}\alpha't}{2\alpha't} \frac{1}{j - \alpha_0 + \alpha't},$$

while, when  $t \rightarrow 0$ , it becomes a double pole

$$A_{pq} = \frac{a_{pq}}{(j - \alpha_0)^2} + \frac{b_{pq}}{j - \alpha_0}.$$

Since we have only simple poles when  $t \neq 0$ , one may apply the usual factorisation relation

$$\left( \frac{a_{11} \pm b_{11}\alpha't}{2\alpha't} \right) \left( \frac{a_{22} \pm b_{22}\alpha't}{2\alpha't} \right) = \left( \frac{a_{12} \pm b_{12}\alpha't}{2\alpha't} \right)^2,$$

which can be rewritten

$$\begin{aligned} (a_{11}a_{22} - a_{12}^2) + (b_{11}b_{22} - b_{12}^2)(\alpha't)^2 &= 0, \\ a_{11}b_{22} + b_{11}a_{22} &= 2a_{12}b_{12}. \end{aligned}$$

And we clearly see that these relations become (7.56) when  $t \rightarrow 0$ .

Similarly, one can obtain the triple-pole relations (7.58) by considering the collision of 3 simple poles. Note that in both the double- and the triple-pole cases at least one of the colliding poles must have a negative residue.



# Chapter 8

## Test of the $t$ CU relations

If we assume as in [18] and chapter 6 that no other singularity is present in DIS, stringent constraints come from the positivity requirement for  $\gamma\gamma$  total cross sections and  $F_2$ . We show that it is possible to obtain a good fit to all photon data for  $Q^2 < 150 \text{ GeV}^2$  by using either double- or triple-pole parametrisations. For total cross sections, no extra singularity seems to be needed, whereas for high  $Q^2$  data, we must introduce the box diagram. We conclude this study by outlining its consequences on the evolution of parton distributions and on the possibility of observing the BFKL pomeron.

### 8.1 Regge models

In order to test the previous equations, and to evaluate the need for new singularities, we shall use models that reproduce  $pp$ ,  $\gamma p$  and  $\gamma\gamma$  cross sections. Previous studies [44] have shown that there are at least three broad classes of models that can reproduce all forward hadron and photon data.

The general form of these parametrisations is given, for total cross sections of  $a$  on  $b$ , by the generic formula<sup>1</sup>

$$\sigma_{ab}^{tot} = (R_{ab} + H_{ab})/s, \quad (8.1)$$

where  $R_{ab}$  is the contribution of the highest meson trajectories ( $\rho$ ,  $\omega$ ,  $a$  and  $f$ ) and the rising term  $H_{ab}$  stands for the pomeron. The first term is parametrised via Regge theory, and we allow the lower trajectories to be partially non-degenerate, *i.e.* we allow one intercept for the charge-even trajectories, and another one for the charge-odd ones [50]. Hence we use

$$R_{ab} = Y_{ab}^+ (\tilde{s})^{\alpha_+} \pm Y_{ab}^- (\tilde{s})^{\alpha_-}, \quad (8.2)$$

with  $\tilde{s} = 2\nu/(1 \text{ GeV}^2)$ ,  $\nu = p \cdot q$ .

---

<sup>1</sup>The real part of the amplitudes, when needed to fit the  $\rho$  parameter, which is the ratio between the real part and the imaginary part of the amplitude, is obtained from  $s \leftrightarrow u$  crossing symmetry.

As for the pomeron term, we consider the following possibilities:

$$H_{ab} = X_{ab} [\tilde{s}]^{\alpha_\varphi}, \quad (8.3)$$

$$H_{ab} = \tilde{s} D_{ab} [\log \tilde{s} + \log C_{ab}], \quad (8.4)$$

$$H_{ab} = \tilde{s} t_{ab} \left[ \log^2 \left( \frac{\tilde{s}}{d_{ab}} \right) + \log(c_{ab}) \right]. \quad (8.5)$$

These forms come from simple, double or triple poles in the Watson-Sommerfeld transform of the amplitude (see Eq. (7.28) in the previous chapter), in the limit of  $\cos(\theta_t)$  large, so that the contribution from the integration contour vanishes, and that one can keep only the leading meson trajectories and the pomeron contribution.

Using the asymptotic expansion of the Legendre polynomials  $P_l$

$$P_l(-\cos(\theta_t)) \rightarrow \frac{\Gamma(2l+1)}{[\Gamma(l+1)]^2 2^l} \left( \frac{\nu}{m_p^2} \right)^l, \quad (8.6)$$

we obtain, by the residue theorem, from Eq. (7.28), the following contributions to the total cross section for simple, double, and triple poles:

$$\begin{aligned} A(j, 0) &= \frac{g}{j - \alpha} \\ &\rightarrow \sigma_{tot} = g \left( \frac{\nu}{m_p^2} \right)^\alpha \frac{(2\alpha + 1)\Gamma(2\alpha + 1)}{(\Gamma(\alpha + 1))^2 2^\alpha}, \end{aligned} \quad (8.7)$$

$$\begin{aligned} A(j, 0) &= \frac{g}{(j - \alpha)^2} \\ &\rightarrow \sigma_{tot} = g \left( \frac{\nu}{m_p^2} \right)^\alpha \log \left( \frac{\nu}{m_p^2} \right) \frac{(2\alpha + 1)\Gamma(2\alpha + 1)}{(\Gamma(\alpha + 1))^2 2^\alpha}, \end{aligned} \quad (8.8)$$

$$\begin{aligned} A(j, 0) &= \frac{g}{(j - \alpha)^3} \\ &\rightarrow \sigma_{tot} = g \left( \frac{\nu}{m_p^2} \right)^\alpha \log^2 \left( \frac{\nu}{m_p^2} \right) \frac{(2\alpha + 1)\Gamma(2\alpha + 1)}{(\Gamma(\alpha + 1))^2 2^{\alpha+1}}. \end{aligned} \quad (8.9)$$

In the photon case, things are a little different. Looking first at the  $\gamma p$  amplitude with off-shell photons, we have

$$|\cos(\theta_t)| = \frac{\nu}{m_p \sqrt{Q^2}}. \quad (8.10)$$

In the on-shell limit  $Q^2 \rightarrow 0$ , the Legendre polynomial of Eq. (7.28) becomes infinite, hence one must assume that the amplitude goes to zero in a way that will make the limit finite. One can take for instance

$$A^{\gamma p} = \tilde{A}^{\gamma p} \left( \frac{\sqrt{Q^2}}{q_\gamma(Q^2)} \right)^j \quad (8.11)$$

with  $q_\gamma(0)$  finite. Such a choice introduces a new scale that effectively replaces  $\sqrt{Q^2}$  with  $q_\gamma(Q^2)$  in  $\cos(\theta_t)$ , and  $T$  with  $\tilde{T}$ . In the  $\gamma\gamma$  case, with  $Q^2$  and  $P^2$  the off-shellnesses of the

two incoming photons, in order to keep the unitarity relations (7.10) for the amplitude  $\tilde{T}$  instead of  $T$ , one needs to assume that

$$A^{\gamma\gamma} = \tilde{A}^{\gamma\gamma} \left( \frac{\sqrt{Q^2 P^2}}{q_\gamma(Q^2) q_\gamma(P^2)} \right)^j \quad (8.12)$$

and the scales  $q_\gamma(Q^2)$  and  $q_\gamma(P^2)$  replace  $m_p$  in Eqs. (8.7-8.9).

## 8.2 Regge region

As we have seen in section 5.2.3, we use cuts on the natural Regge variables  $2\nu$  and  $\cos(\theta_t)$ . We find that data are well reproduced taking  $n = 7$  and  $x_{\max} = 0.3$ , *i.e.* in the region<sup>2</sup>

$$\cos(\theta_t) \geq \frac{49 \text{ GeV}^2}{2m_p^2}, \quad (8.13)$$

$$\sqrt{2\nu} \geq 7 \text{ GeV}, \quad (8.14)$$

$$x \leq 0.3. \quad (8.15)$$

Furthermore, all the residues are expected to be functions of  $Q^2$ . These form factors are unknown, and are expected to contain higher twists. In order to check factorisation, we do not want to be too dependent on these guesses. Hence we choose a modest region of

$$Q^2 \leq 150 \text{ GeV}^2, \quad (8.16)$$

where most of the  $\gamma^* \gamma^*$  points lie.

We shall consider in the next section possible extensions to a wider region.

## 8.3 Factorising $t$ CU relations

As explained above, the simple-pole singularities will factorise in the usual way. Note that there is no charge-odd singularity in the photon case, hence only the  $a/f$  lower trajectory will enter the relations. One then gets

$$Y_{pp} Y_{\gamma\gamma}(P^2, Q^2) = Y_{\gamma p}(P^2) Y_{\gamma p}(Q^2). \quad (8.17)$$

In the case of a soft-pomeron pole, one obtains similarly

$$X_{pp} X_{\gamma\gamma}(P^2, Q^2) = X_{\gamma p}(P^2) X_{\gamma p}(Q^2). \quad (8.18)$$

The case of multiple poles is given by Eqs. (7.56, 7.58), and can be made more transparent by using the forms (8.4, 8.5) which give factorisation-looking relations for the constants<sup>3</sup>:

$$f_{pp} f_{\gamma\gamma}(P^2, Q^2) = f_{\gamma p}(P^2) f_{\gamma p}(Q^2) \quad (8.19)$$

with  $f = D, C, t, d$  or  $c$ .

---

<sup>2</sup>Recall that, for the total cross-sections, only the cut on  $2\nu$  constraints the Regge region.

<sup>3</sup>This is not true for all the residues! See Eqs. (7.56) and (7.58)

## 8.4 Dataset

For the total cross sections, we have used the updated COMPETE dataset of [51], which is the same as that of [28] except for the inclusion of the latest ZEUS results on  $\gamma p$  cross section [81] and for the inclusion of cosmic-ray data. For  $\gamma p$  scattering, we have used the full set of available data [67–84, 86]. For the  $\gamma\gamma$  measurements of  $F_2^\gamma$ , we have used the data of [88, 89], whenever these included the joint  $x$  and  $Q^2$  (and  $P^2$ ) dependence. We have not included other data as they do not have points in the Regge region. Note that we have not taken the uncertainties in  $x$  into account, hence the  $\chi^2$  values are really upper bounds in the  $\gamma\gamma$  case.

## 8.5 Parametrisations

### 8.5.1 Previous parametrisations

We have first considered the results using previous studies (see [18] and chapter 6) of  $\gamma^{(*)}p$  and  $pp$  scattering. Making use of the  $t$ CU relations (7.56) and (7.58), we have obtained reasonably good predictions for  $\sigma_{\gamma\gamma}$  and  $F_2^\gamma$ . However, the formalism breaks down in the case of  $\gamma^*\gamma^*$  scattering, because the form factors that we used do not guarantee the positivity of the charge-even part of the cross sections. Re-fitting them enables one to get closer to the data, but the problem of negativity remains in some part of the physical region. Hence, at this point, the factorisation relations have one major consequence: the parametrisations of chapter 6 can only be approximate.

We have also considered the hard pomeron fit of [14] where the charge-parity +1 rising term contains two different simple poles: the soft and the hard pomeron. In this case, the soft pomeron residues factorise. The hard pomeron, with intercept  $\alpha_h$  not present in  $pp$  cross sections, then comes in as a double pole in  $\gamma\gamma$  cross sections, see Eq. (7.41), and produces a cross section proportional to  $\nu^{\alpha_h} \log \nu$ . Its residue will then depend on the value of  $\Delta(\alpha_h)$ , which is unknown. This means that factorisation does not say much about the hard pomeron contribution, which can always be arbitrarily re-scaled. It is possible to get good fits using these forms, but as they do not test factorisation, we shall not present these results here.

### 8.5.2 New parametrisation: triple pole

In the triple-pole case, the problem of negativity can be cured through the introduction of another functional form for the form factors. To convince ourselves that this is possible, we have fitted  $F_2$  in several  $Q^2$  bins to

$$F_2^p(Q^2) = a(\log \nu + b)^2 + c\nu^{-0.47}. \quad (8.20)$$

From the values of  $a$ ,  $b$  and  $c$ , and the  $t$ CU relations, one can then predict the symmetric  $F_2^\gamma(Q^2, Q^2)$ . The result of this exercise is shown in Fig. 8.1.

One clearly sees that there are two branches in the fit to HERA data: one with positive  $b$ , and another one with negative  $b$ . Both have comparable  $\chi^2$ , but one produces positive  $\gamma\gamma$

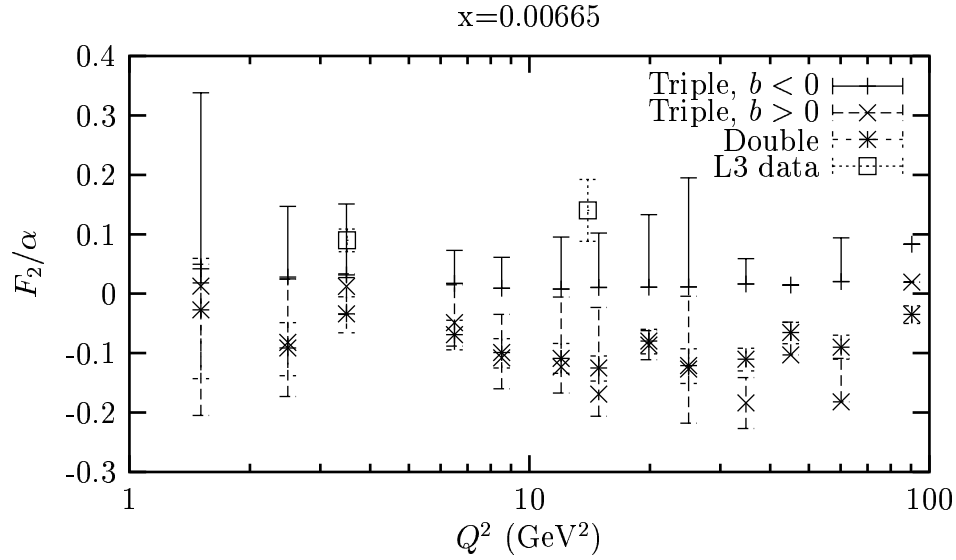


Figure 8.1: Prediction from  $t$ CU relations for the  $\gamma^*\gamma^*$  cross section, including the box diagram of Appendix C.

cross sections, whereas the other one does not. Armed with this information, we found that the resulting form factors could be well approximated by the following forms:

$$\begin{aligned}
 t_{\gamma p}(Q^2) &= t_1 \left( \frac{1}{1 + \frac{Q^2}{Q_t^2}} \right)^{\epsilon_t}, \\
 Y_{\gamma p}^+(Q^2) &= Y_1 \left( \frac{1}{1 + \frac{Q^2}{Q_y^2}} \right)^{\epsilon_y}, \\
 \log d_{\gamma p}(Q^2) &= d_1 \left( \frac{Q^2}{Q^2 + Q_d^2} \right)^{\epsilon_d}, \\
 \log c_{\gamma p}(Q^2) &= c_0 + c_1 \left( \frac{1}{1 + \frac{Q^2}{Q_c^2}} \right)^{\epsilon_c}.
 \end{aligned} \tag{8.21}$$

With the form factors obtained from our fit, we have then checked that the  $\gamma^*\gamma^*$  cross section remains positive everywhere.

### 8.5.3 New parametrisation: double pole

In the case of a double pole, Fig. 8.1 shows that the situation is more difficult, as one cannot guarantee positivity. We have tried several possibilities, among which a further splitting of leading trajectories along the lines of [52], but found that positivity is still not guaranteed.

However, it is possible to obtain a good fit, positive everywhere, if one assumes a slightly modified version of the double pole [53].

Instead of taking an  $\tilde{s}D \log \tilde{s}$  term in  $H_{ab}$  as in Eq. (8.4), one can consider

$$H_{ab} = \tilde{s}D_{ab} [L_{ab} + \log C_{ab}] \quad (8.22)$$

with

$$L_{ab}(\tilde{s}) = \Im m \left[ \frac{i}{2} \log(1 + \Lambda_{ab} \tilde{s}^\delta) + \frac{i}{2} \log(1 + \Lambda_{ab}(-\tilde{s})^\delta) \right]. \quad (8.23)$$

Asymptotically, this gives the same form as a double pole. Furthermore, one can rewrite  $\log(1 + \Lambda_{ab}(\tilde{s})^\delta) = \delta \log(\tilde{s}) + \log(\Lambda_{ab} + 1/(\tilde{s})^\delta)$ . The first term comes from a double pole at  $j = 1$ , whereas the Taylor expansion of the remaining term comes from a series of simple poles. Hence  $D_{ab}$  and  $\Lambda_{ab}$  factorise according to

$$\begin{aligned} D_{\gamma\gamma}(P^2, Q^2)D_{pp} &= D_{\gamma p}(P^2)D_{\gamma p}(Q^2), \\ \Lambda_{\gamma\gamma}(P^2, Q^2)\Lambda_{pp} &= \Lambda_{\gamma p}(P^2)\Lambda_{\gamma p}(Q^2). \end{aligned} \quad (8.24)$$

We found good fits using the following form factors:

$$\begin{aligned} D_{\gamma p} &= D_1 \left( \frac{1}{1 + \frac{Q^2}{Q_d^2}} \right)^{\epsilon_d}, \\ D_{\gamma p} \log C_{\gamma p} &= C_1 \left( \frac{1}{1 + \frac{Q^2}{Q_c^2}} \right)^{\epsilon_c}, \\ \Lambda_{\gamma p} &= \Lambda_1 \left( \frac{1}{1 + \frac{Q^2}{Q_\lambda^2}} \right)^{\epsilon_\lambda}. \end{aligned} \quad (8.25)$$

Quantity	Nb Data	double		triple	
		$\chi^2$	$\chi^2/pt$	$\chi^2$	$\chi^2/pt$
$F_2^p$	821	789.624	0.962	870.599	1.060
$F_2^\gamma$	65	57.686	0.887	59.963	0.923
$\sigma_{\gamma\gamma}$	32	19.325	0.604	15.568	0.487
$\sigma_{\gamma p}$	30	17.546	0.585	21.560	0.719
$\sigma_{pp}$	90	100.373	1.115	82.849	0.921
$\sigma_{p\bar{p}}$	49	55.240	1.127	58.900	1.202
$\rho_{pp}$	67	93.948	1.402	98.545	1.471
$\rho_{p\bar{p}}$	11	16.758	1.523	4.662	0.424
Total	1165	1150.500	0.988	1212.645	1.041

Table 8.1: Results of fits to a generalised double pole model and to a triple pole model, using the form factors of Eqs. (8.21) and (8.25).

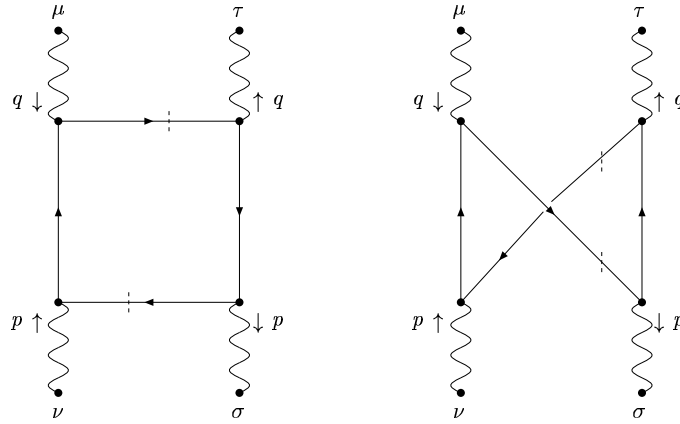


Figure 8.2: The box diagram contribution.

## 8.6 Box diagram

One new singularity must in fact be present in  $\gamma\gamma$  scattering: it is the box diagram, shown in Fig. 8.2, which couples directly two photons to quarks. As we have seen before, it is possible that this extra-singularity only appears at nonzero  $Q^2$  and, in fact, we get better fits if we include it only for off-shell photons.

We have re-calculated it and confirm the results of [54] (see Appendix C<sup>4</sup>). In the following, we shall fix the quark masses at

$$\begin{aligned}
 m_u = m_d &= 0.3 \text{ GeV}, \\
 m_s &= 0.5 \text{ GeV}, \\
 m_c &= 1.5 \text{ GeV}, \\
 m_b &= 4.5 \text{ GeV}.
 \end{aligned}
 \tag{8.26}$$

and the quarks are included only above threshold  $s = 2\nu - P^2 - Q^2 > 4m_q^2$ .

## 8.7 Results

As we want to be able to vary the minimum value of  $2\nu$ , and as the fits of [44] neither include the generalised dipole nor use  $2\nu$  as the energy variable, we have re-fitted the  $pp$  and  $\bar{p}p$  cross sections and  $\rho$  parameter together with those for  $\gamma^{(*)}p$  and  $\gamma^{(*)}\gamma^{(*)}$ , and imposed  $t$ CU relations for the residues.

We show in Table 8.1 the  $\chi^2/dof$  and number of points for each process. We see that one obtains a very good global  $\chi^2$  for both models. It is well known [44] that the partial  $\chi^2$  for  $\sigma_{p\bar{p}}$  and  $\rho_{pp}$  never reach low values, presumably because of the presence of contradictory data.

---

<sup>4</sup>We want to point out that one need to calculate  $\sigma_{LL}$ ,  $\sigma_{TL}$ ,  $\sigma_{LT}$  and  $\sigma_{TT}$  separately and sum them to obtain the off-shell cross section. A contraction of  $g_{\mu\nu}$  does not resum the helicities properly [55] which probably explains the discrepancies between [54] and [56].

triple		double	
Parameter	Value	Parameter	Value
$t_{pp}$	$0.6264 \pm 0.0055$	$\Lambda_{pp}$	$1.36 \pm 0.15$
$\log(d_{pp})$	$0.534 \pm 0.044$	$D_{pp}$	$40.3 \pm 1.4$
$t_{pp} \log c_{pp}$	$65.86 \pm 0.48$	$D_{pp} \log C_{pp}$	$-32.7 \pm 5.3$
$Y_{pp}^+$	$122.0 \pm 1.5$	$Y_{pp}^+$	$231.1 \pm 4.7$
$\alpha_+$	$0.6905 \pm 0.0023$	$\alpha_+$	$0.7263 \pm 0.0010$
$Y_{pp}^-$	$84.6 \pm 4.1$	$Y_{pp}^-$	$97.6 \pm 4.6$
$\alpha_-$	$0.4596 \pm 0.0010$	$\alpha_-$	$0.505 \pm 0.015$
$c_0$	$-613.93 \pm 0.91$	$\delta$	$0.3313 \pm 0.0092$
$c_1$	$740.8 \pm 1.2$	$C_1$	$-0.105 \pm 0.016$
$Q_c^2$	$0.1557 \pm 0.0030$	$Q_c^2$	$0.0219 \pm 0.0076$
$\epsilon_c$	$0.11619 \pm 0.00047$	$\epsilon_c$	$0.553 \pm 0.025$
$t_1$	$0.001667 \pm 0.000011$	$\Lambda_1$	$1.49 \pm 0.23$
$Q_t^2$	$0.964 \pm 0.016$	$Q_\lambda^2$	$0.111 \pm 0.032$
$\epsilon_t$	$0.8237 \pm 0.0034$	$\epsilon_\lambda$	$0.658 \pm 0.019$
$d_1$	$-8.067 \pm 0.033$	$D_1$	$0.1305 \pm 0.0062$
$Q_d^2$	$7.56 \pm 0.25$	$Q_d^2$	$0.379 \pm 0.061$
$\epsilon_d$	$0.3081 \pm 0.0059$	$\epsilon_d$	$0.434 \pm 0.021$
$Y_1$	$0.1961 \pm 0.0031$	$Y_1$	$0.515 \pm 0.017$
$Q_y^2$	$2.056 \pm 0.067$	$Q_y^2$	$0.158 \pm 0.016$
$\epsilon_y$	$0.5448 \pm 0.0049$	$\epsilon_y$	$0.709 \pm 0.016$

Table 8.2: Parameters (in natural units) of the global fits.

The values of the parameters are given in Table 8.2 for the triple-pole and the double-pole cases, and the form factors are plotted in Fig. 8.3. We show the corresponding curves in Fig. 8.4.

We see that the intercepts of the leading meson trajectories are close, in fact closer than those of [44]. This is due to the smaller region of  $s$ , and to the much larger influence of photon data on  $\alpha_+$ .

It may also be noted, in the double-pole case, that the parameter  $\delta$  is close to the hard pomeron intercept of [14]. At high  $Q^2$ , because the form factor  $\Lambda$  falls off, the logarithm starts looking like a power of  $2\nu$ , and somehow mimics a simple pole. It may thus be thought of as a unitarised version of the hard pomeron, which would in fact apply to hard and soft scatterings.

In the triple-pole case, this is accomplished by a different mechanism: the scale of the logarithm is a rapidly falling function of  $Q^2$ , and hence the  $\log^2$  term becomes relatively more important at high  $Q^2$ . Interestingly, when one writes the triple-pole parametrisation as a function of  $x$  and  $Q^2$ , one obtains only very small powers (of the order of 0.1) of  $Q^2$ , which do not contain any higher twists, contrarily to the soft pomeron of [14].

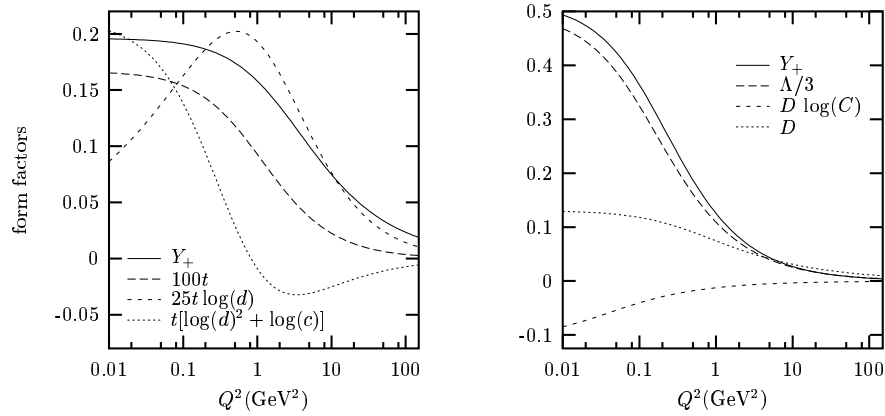


Figure 8.3: Form factors of the triple pole (left) and double pole (right) parametrisations.

### 8.7.1 Total $\gamma p$ and $\gamma\gamma$ cross sections

We see from Table 8.1 that one obtains an excellent  $\chi^2$  for  $\sqrt{2\nu} > 7$  GeV, for a total of 62 points. The curves are shown in Fig. 8.4. The fit can in fact be continued to  $\sqrt{2\nu} = 2$  GeV, with a  $\chi^2/\text{point}$  of 0.74 for 219 points. We have checked that adding the box diagram leads to a slight degradation of the fit, whether one fits the total cross sections alone or with all other data. As the contribution of the box is calculated perturbatively, one might object that one cannot use the result down to  $Q^2 = 0$ , and that only the  $\nu$  dependence should be kept. Hence we have also tried to add an extra term, proportional to  $\log \nu/\nu$  in the total cross section, but found that the fit prefers to set the proportionality constant to zero. Hence it seems that this singularity is not needed at  $P^2 = Q^2 = 0$ . However, because of large uncertainties in the data, it is not possible to rule it out altogether.

Similarly, we do not find the need to introduce any new rising contribution. However, it is clear in view of the large uncertainties that it is not possible to rule out completely such a possibility. In fact, our fit prefers the  $\gamma\gamma$  data unfolded with PHOJET [57], which rise more slowly than those unfolded with PYTHIA [58]. Interestingly, as we reproduce both HERA and LEP data, for  $Q^2$  nonzero, it is not true that an extrapolation of the nonzero- $Q^2$  data leads to a higher estimate of the  $\gamma p$  and  $\gamma\gamma$  cross sections. Our fit can be considered as an explicit example for which such an extrapolation leads to a cross section on the lower side of the experimental errors.

### 8.7.2 Fits to $F_2^p$

The fit to  $F_2$  has quite a good  $\chi^2$  as well. We have checked that one can easily extend it to  $Q^2 \approx 400$  GeV<sup>2</sup> for the triple pole, and to  $Q^2 \approx 800$  GeV<sup>2</sup> in the double-pole case. It is interesting that one cannot go as high as in chapter 6. This can be attributed either to too simple a choice for the form factors, or to the onset of perturbative evolution<sup>5</sup>.

<sup>5</sup>We shall see in chapter 10 that one can obtain the high- $Q^2$  behaviour of the triple-pole residues from pQCD.

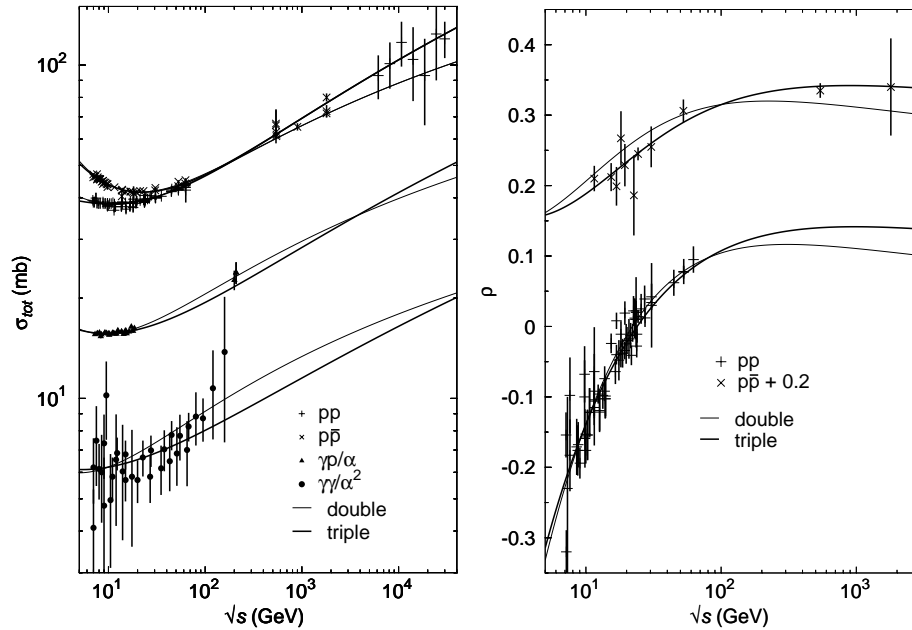


Figure 8.4: Fits to the total cross sections and to the  $\rho$  parameters.

Figs. 8.5 and 8.6 show the  $F_2^p$  fit for the most populated  $Q^2$  bins. As pointed out before, we see that our fits do reproduce the low- $Q^2$  region quite well, but predict total cross sections on the lower side of the error bands. Hence the extrapolation to  $Q^2 = 0$  of DIS data does not require a hard pomeron.

### 8.7.3 Fits to $F_2^\gamma$

As the number of data points is dominated by  $pp$  and  $\gamma p$  data, the fit to  $\gamma\gamma$  data is really a test of the  $t$ CU relations. As we explained above, the strongest constraint comes from the positivity of the  $\gamma^*\gamma^*$  cross section, which is not guaranteed by the  $t$ CU relations in the case of multiple poles. As Fig. 8.7, 8.8 and 8.9 show, one obtains a good description of the points within the Regge region.

Here, we have observed that the quality of the fit improves if we add the box diagram for nonzero  $Q^2$  and  $P^2$ . There is no need however to include other singularities, such as a hard pomeron or a perturbative one.

For  $Q^2 \neq 0$  and  $P^2 = 0$ , the box diagram makes little difference in the double-pole case, but does reduce the  $\chi^2$  appreciably in the triple-pole case. We have included it in both cases.

## 8.8 Conclusion

We have shown in this chapter that  $t$ -channel unitarity can be used to map the regions where new singularities, be they of perturbative or non-perturbative origin, can occur. Indeed, we

have seen that although hadronic singularities must be universal, this is certainly not the case for  $F_2^p$  and  $F_2^\gamma$ , as DIS involves off-shell particles.

We have shown however that up to<sup>6</sup>  $Q^2 = 150 \text{ GeV}^2$ , the data do not call for the existence of new singularities, except perhaps the box diagram.

For off-shell photons, our fits are rather surprising as the standard claim is that the perturbative evolution sets in quite early. This evolution is indeed allowed by  $t$ -channel unitarity constraints: it is possible to have extra singularities in off-shell photon cross sections, which are built on top of the non-perturbative singularities. But it seems that Regge parametrisations can be extended quite high in  $Q^2$  without the need for these new singularities.

Finally, the BFKL singularity is purely perturbative: the position of the singularity and the form factor come from pQCD. As such, it can manifest itself only in  $\gamma^*\gamma^*$ , but we have seen that there is no definite need for such a singularity in present data.

---

<sup>6</sup>The region we have considered excludes the highest- $Q^2$   $\gamma\gamma^*$  points from OPAL. For the point which falls in the Regge region, at  $P^2 = 0$ ,  $Q^2 = 780 \text{ GeV}^2$  and  $x = 0.275$ , the experimental value is  $0.93 \pm 0.16$ , the extrapolation of the double-pole fit predicts 0.71, while the triple pole prediction is 0.74.

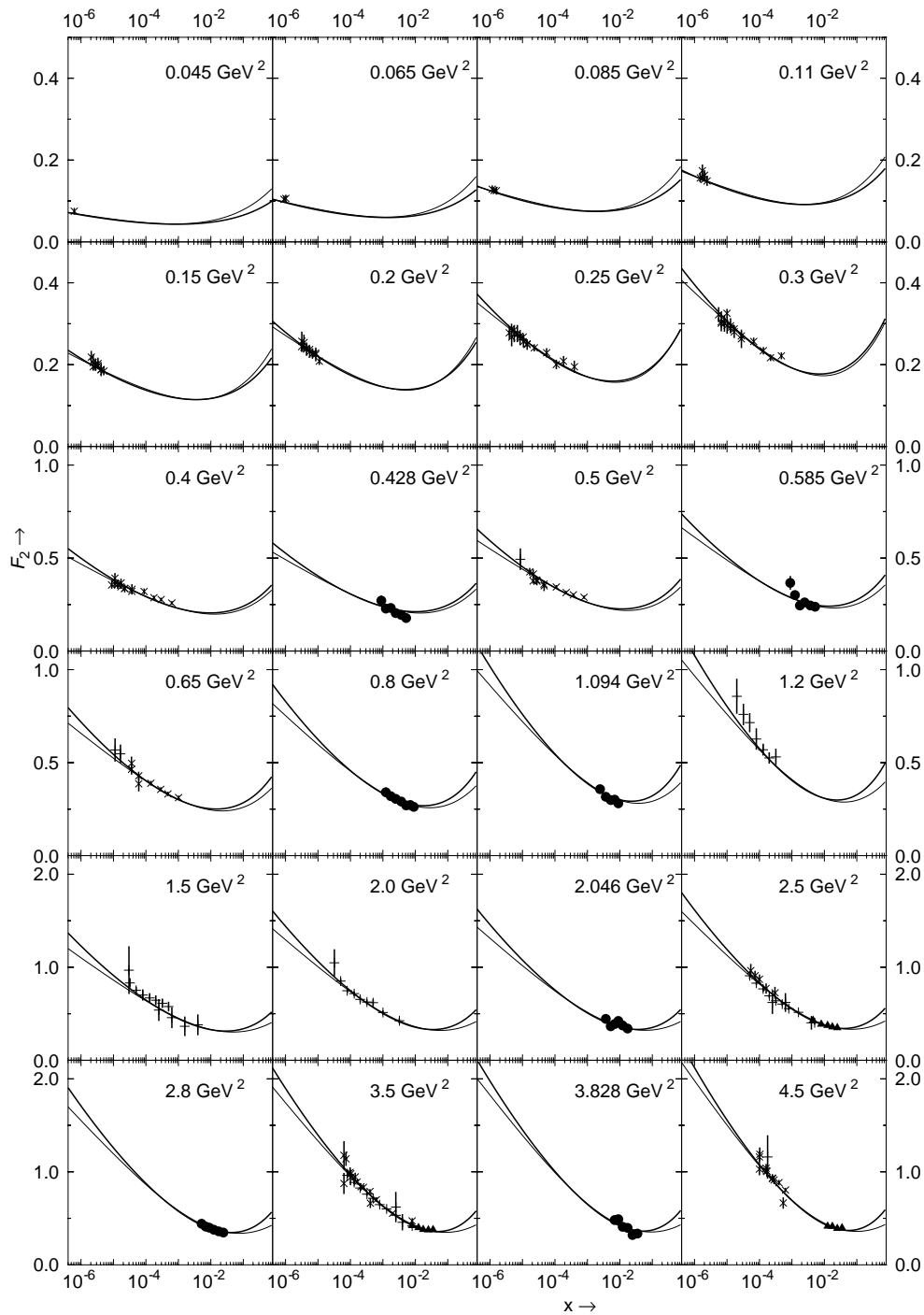


Figure 8.5: Fits to  $F_2^p$  in the low- $Q^2$  region. We show only graphs for which there are more than 6 experimental points, as well as the lowest  $Q^2$  ones. The curves and the data are as in Fig. 8.6.

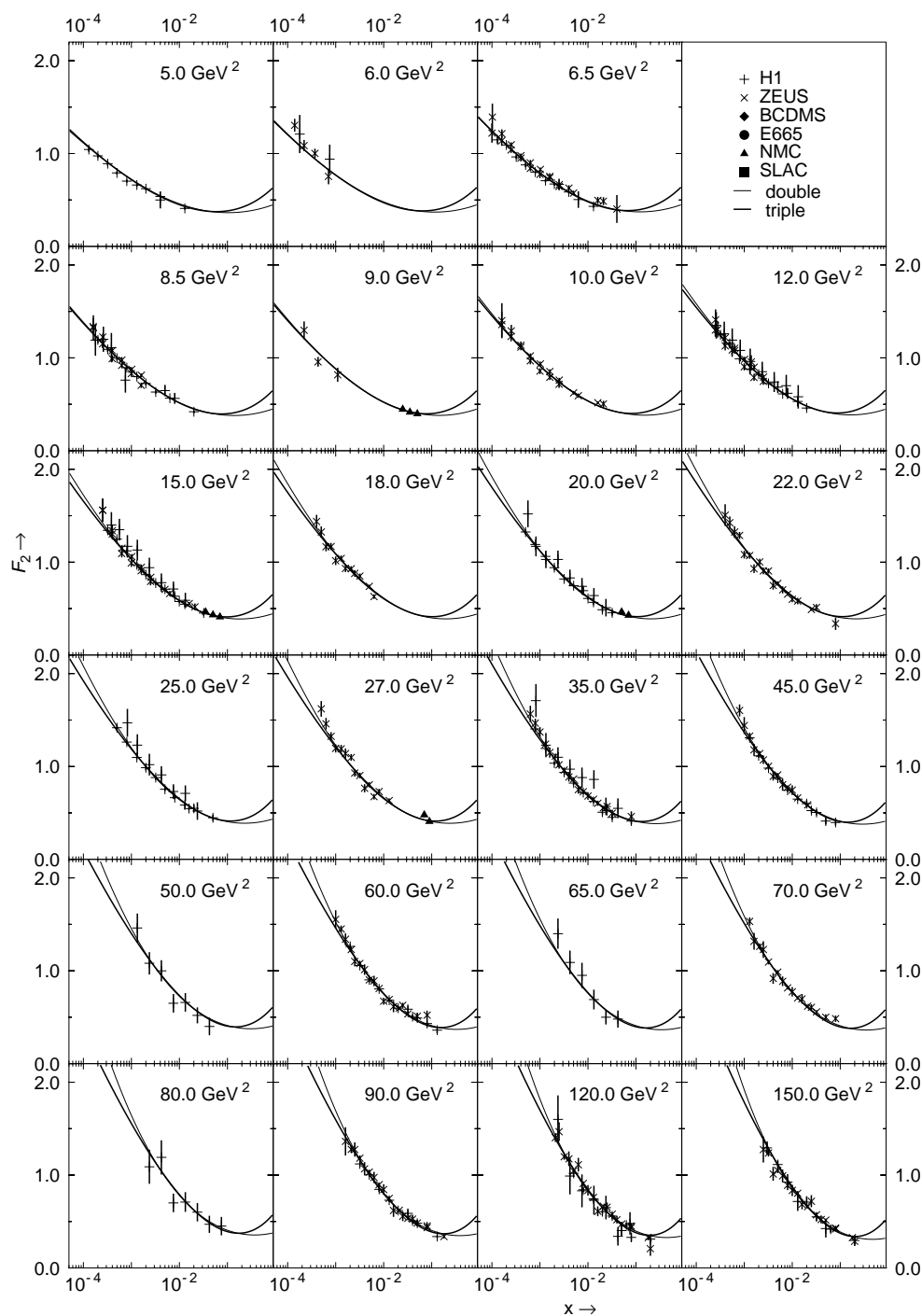


Figure 8.6: Fits to  $F_2^p$  in the high- $Q^2$  region. We show only graphs for which there are more than 6 experimental points.

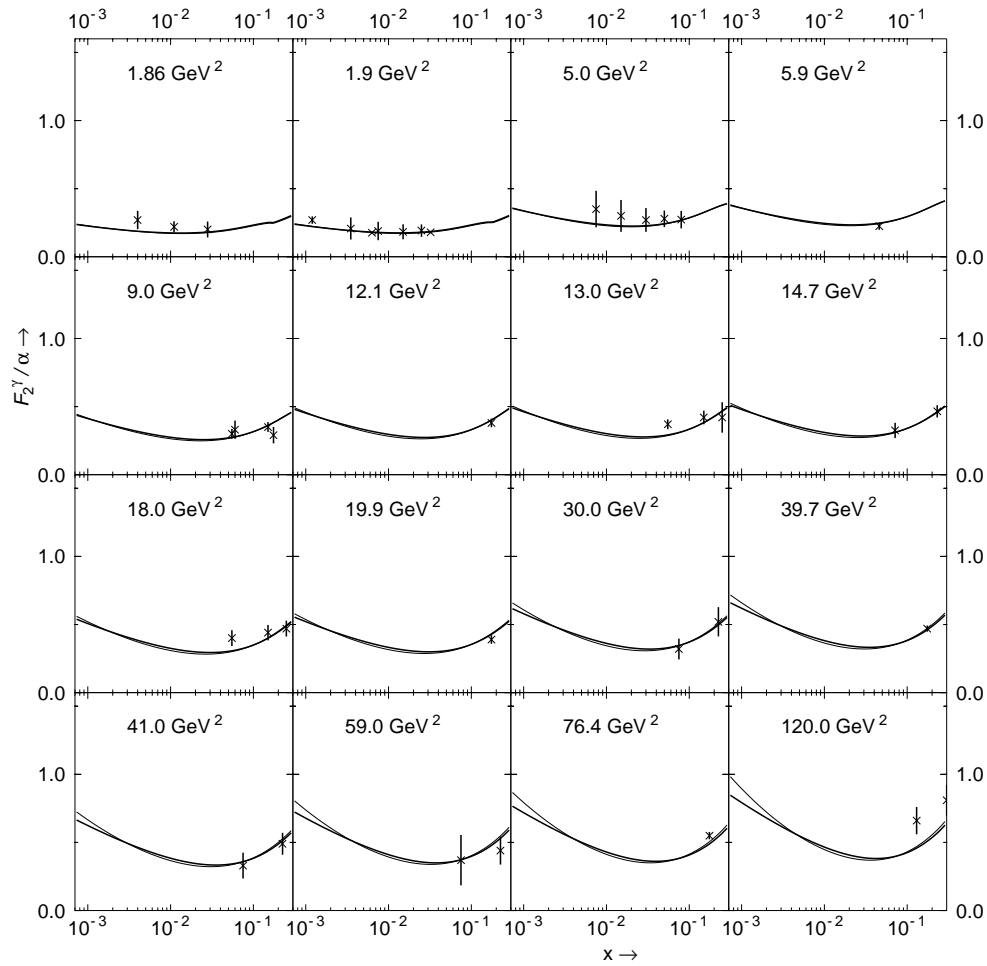


Figure 8.7: Fits to  $F_2^\gamma$ . The curves are as in Fig. 8.6. The data are from [88, 89].

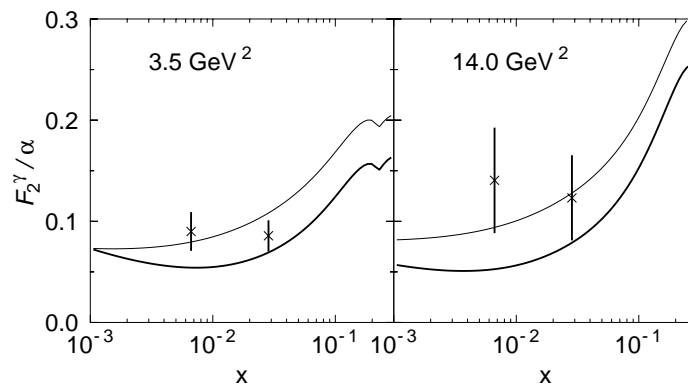


Figure 8.8: Fits to  $F_2^\gamma$  for  $P^2 = Q^2$ . The curves are as in Fig. 8.6. The data are from [88].

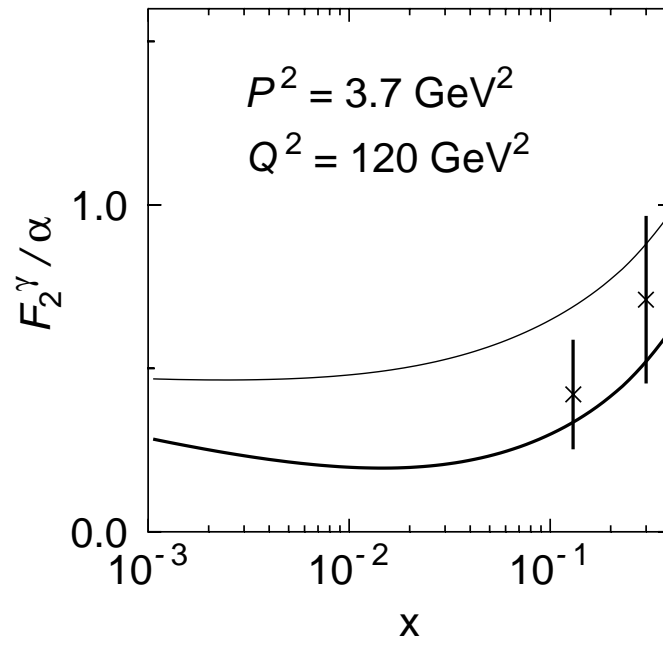


Figure 8.9: Fits to  $F_2^\gamma$  for nonzero asymmetric values of  $P^2$  and  $Q^2$ . The curves are as in Fig. 8.4. The data are from [88].



## Part III

# Linking DGLAP evolution with Regge theory



*Strangers passing in the street  
 By chance two separate glances meet  
 And I am you and what I see is me  
 And do I take you by the hand  
 And lead you through the land  
 And help me understand the best I can*  
 Pink Floyd - Echoes

## Chapter 9

# Constraints on initial distributions

We have shown previously that, using Regge theory, it is possible to fit the experimental data for  $F_2^p$  with a double- or triple-pole pomeron model in the region

$$\left\{ \begin{array}{l} 2\nu \geq 49 \text{ GeV}^2, \\ \cos(\theta_t) = \frac{\sqrt{Q^2}}{2xm_p} \geq \frac{49 \text{ GeV}^2}{2m_p^2}, \\ Q^2 \leq 150 \text{ GeV}^2, \\ x \leq 0.3. \end{array} \right. \quad (9.1)$$

We have also shown that one can extend the usual  $t$ -channel unitarity relations [29] to the case of multiple thresholds and multiple poles. This allowed us to predict  $F_2^\gamma$  from  $F_2^p$  and the  $pp$  total cross-section. In the latter case, we have shown that *all processes have the same singularity structure*.

However, in the usual parton distribution sets, each parton distribution presents its own singularities. As an example, in the MRST2002 parametrisation [20], we have

$$xq(x, Q_0^2) = A(1 + B\sqrt{x} + Cx)(1 - x)^{\eta_q} x^{\varepsilon_q},$$

with  $\varepsilon_{\text{sea}} = -0.12$ ,  $\varepsilon_g^{(1)} = -0.27$ ,  $\varepsilon_g^{(2)} = 0.00$ . In fact, these singularities do not correspond to any singularity present in hadronic cross sections and, conversely, cross section singularities are not present in parton distributions. There must therefore exist a mechanism explaining how the residues of these singularities in partonic distributions vanish when  $Q^2$  goes to zero, and how the residues of the singularities observed in the total cross-sections vanish for nonzero  $Q^2$ . Such a mechanism is unknown and seems forbidden in Regge theory. In this framework, describing both total cross-sections and partonic distributions with the same singularity structure is the most natural choice.

At that level, one may ask whether the Regge fits introduced previously are compatible with pQCD and whether it is possible to have the same singularities in all parton distributions. Actually, although Regge theory [10, 11] and DGLAP evolution [6] both provide well-known descriptions of the structure functions [13, 17, 18, 20–24], the connection between the two approaches is unclear. In the last part of this thesis, we shall confront the Regge parametrisations (double or triple pole) extended to parton distribution with pQCD.

The first step, developed in this chapter<sup>1</sup>, is to use Regge theory to fix the initial distribution at  $Q_0^2$  in order to reproduce the  $F_2^p$  values obtained from the previous Regge fit (see chapter 8) and to use the DGLAP equation to obtain distribution functions at higher scales. We shall see that we are able to produce a fit to experimental data which is compatible both with Regge theory and with the DGLAP equation. This comparison of two aspects of the theory will allow us to split the  $F_2$  structure function in smaller contributions and to predict the density of gluons, which is not accessible directly from Regge fits.

Varying the initial scale  $Q_0^2$ , we can predict where perturbative QCD breaks down. However, due to the application domain (9.1) of the global fit, the Regge constraints on the initial parton distributions are not valid at large  $x$ . In order to solve this problem, we use the GRV98 parton distributions [21] at large  $x$  ( $x > x_{\text{Regge}}$ ). We shall argue that the results do not significantly depend on the choice of the large- $x$  parametrisation. Since we shall use leading order (LO) DGLAP evolution, one can choose any of the usual LO PDF sets to extend our fits to large  $x$ . We shall extend our fit up to  $x = 1$  in chapter 11.

We shall show that, within a reasonable region of  $Q_0^2$  and  $x_{\text{Regge}}$ , the double-pole and the triple-pole pomeron models provide an initial condition for LO DGLAP evolution which reproduces the experimental data. The scale  $Q_0^2$  should be considered as the minimal scale where perturbative QCD can be applied. We end up with a model where Regge theory describes the small- $Q^2$  region and pQCD the high- $Q^2$  one.

Since a good precision on the gluon density is of primary importance for the LHC, it is also interesting to look at the prediction of this model for the density of gluons. We shall see that the densities we obtain are of the same order of magnitude as in the usual DGLAP fits.

One should mention that such an extension of a Regge fit by a DGLAP evolution has already been introduced in [60]. However, as we shall see, our approach here is different: our parametrisation is much more constrained, we are able to extract a gluon distribution and all the distributions have the same singularity structure. There are also some less important differences in the treatment of the large- $x$  domain.

## 9.1 Initial distributions

In our approach, the soft and hard singularities are both at  $j = 1$ , it is not possible to dissociate them, as was done in [14]. However, it is possible to assume that the perturbative essential singularity (at  $j = 1$ ) becomes a double or a triple pole at small  $Q^2$ . This may come from further resummation of pQCD [61]. We thus have two regimes: for  $Q^2 > Q_0^2$ , we have a perturbative DGLAP evolution with an essential singularity, while for  $Q^2 \leq Q_0^2$ , the Regge fit applies, and  $F_2$  behaves like a triple pole at small  $x$ .

Since we want to use the fit presented in chapter 8 to reproduce  $F_2$  at small  $Q^2$ , we want to have an initial distribution of the form ( $Q_0^2$  is the scale at which we start the DGLAP

---

<sup>1</sup>The model presented here is based on [59].

evolution)

$$F_2(x, Q_0^2) = a\Im m \left\{ \frac{i}{2} \log \left[ 1 + \Lambda \left( \frac{Q_0^2}{x} \right)^\delta \right] + \frac{i}{2} \log \left[ 1 + \Lambda \left( -\frac{Q_0^2}{x} \right)^\delta \right] \right\} + b + dx^\eta, \quad (9.2)$$

or

$$F_2(x, Q_0^2) = a \log^2(1/x) + b \log(1/x) + c + dx^\eta, \quad (9.3)$$

*i.e.* described by a generalised double-pole pomeron and an  $f, a_2$ -reggeon trajectory or by a triple-pole pomeron and an  $f, a_2$ -reggeon trajectory ( $\eta = 0.264$ ,  $\delta = 0.33$  for the double-pole model and  $\eta = 0.31$  for the triple-pole model, as obtained in chapter 8). Once we have that initial distribution, we can evolve it with DGLAP and compare it with experimental data.

However, the DGLAP equation (3.22) does not allow us to compute  $F_2$  directly. Performing linear combinations in (3.22), one can easily check that the minimal set of densities needed to obtain  $F_2$  from the DGLAP equation is given by a flavour-non-singlet quark density, the flavour-singlet quark density and the gluon density:

$$T = x [(u^+ + c^+ + t^+) - (d^+ + s^+ + b^+)], \quad (9.4)$$

$$\Sigma = x [(u^+ + c^+ + t^+) + (d^+ + s^+ + b^+)], \quad (9.5)$$

$$G = xg, \quad (9.6)$$

where  $q^+ = q + \bar{q}$  for  $q = u, d, s, c, t, b$ . The evolution equations for these distributions turn out to be

$$\begin{aligned} Q^2 \partial_{Q^2} T(x, Q^2) &= \frac{\alpha_s}{2\pi} \int_x^1 \frac{xd\xi}{\xi^2} P_{qq} \left( \frac{x}{\xi} \right) T(\xi, Q^2), \\ Q^2 \partial_{Q^2} \begin{pmatrix} \Sigma \\ G \end{pmatrix} &= \frac{\alpha_s}{2\pi} \int_x^1 \frac{xd\xi}{\xi^2} \begin{pmatrix} P_{qq} & 2n_f P_{qg} \\ P_{gq} & P_{gg} \end{pmatrix} \begin{pmatrix} \Sigma \\ G \end{pmatrix} \end{aligned} \quad (9.7)$$

and  $F_2$  is then given by

$$F_2 = \frac{5\Sigma + 3T}{18}.$$

This clearly shows that, if we want to use (9.2) or (9.3) as the initial condition for a DGLAP evolution, we need to split  $F_2$  into  $T$  and  $\Sigma$  contributions, but we also need to introduce a gluon density. In this way, using (9.2) or (9.3) as the initial condition for the evolution allows us to predict the gluon distribution.

### 9.1.1 The large- $x$ problem

As we have seen in section 5.2.3, Regge theory is expected to be valid for  $\cos(\theta_t) \gg 1$ . In the case of DIS,  $\cos(\theta_t) = \frac{\sqrt{Q^2}}{2x m_p}$ , where  $m_p$  is the mass of the proton. The Regge region is thus<sup>2</sup>

$$\frac{\sqrt{Q^2}}{2x m_p} \geq K, \quad (9.8)$$

---

<sup>2</sup>The cut on  $2\nu$  is only affecting the values of  $Q^2$  smaller than 1 GeV<sup>2</sup>. So we do not need to take it into account here.

with  $K$  a fixed number. We clearly see that the domain does not extend up to  $x = 1$ . However, in the DGLAP evolution equations (9.7), the small- $x$  domain is coupled to large- $x$  values and therefore we need a parametrisation for the parton distribution functions at large  $x$ . In principle, we could introduce powers of  $(1 - x)$ , or of any polynomial vanishing at  $x = 1$ , in our initial distributions. This would take into account daughter trajectories in Regge theory and ensure that parton distributions go to 0 as  $x \rightarrow 1$ . Unfortunately, this has two drawbacks:

1. it introduces a lot of additional parameters which are not directly related to the small- $x$  Regge behaviour,
2. a precise description of the parton distributions at large  $x$  requires more than simply fitting  $F_2^p$  and splitting it into flavour-singlet component, coupled to the gluons, and one additional non-singlet distribution. We need to introduce valence quark distributions and sea quark distributions. Fitting many kinds of experiments like  $F_2^p$ ,  $F_2^n$ ,  $F_2^d$ ,  $F_2^{\nu N}$  and  $xF_3^{\nu N}$  allows to constrain all these distributions separately. Again, introducing more parton distributions requires more parameters. Moreover, most of the experimental points except those from  $F_2^p$ , lies outside the region of interest (9.8). Also, note that all these experiments are not on the same theoretical footing (*e.g.* jet cross-sections).

In order to keep the parameters of our model as closely linked as possible to the Regge domain of the evolution, we shall first use an external distribution for the large- $x$  parton distributions and postpone the full study to chapter 11. For  $x \geq x_{\text{Regge}}$ , we shall use GRV98 [21]. It is worth mentioning that, in the DGLAP equation (3.22), the evolution for  $x > x_{\text{Regge}}$  does not depend on the distribution below  $x_{\text{Regge}}$ . This means that the evolution of the GRV98 distribution functions for  $x > x_{\text{Regge}}$  is not influenced by the parametrisation we shall impose for  $x \leq x_{\text{Regge}}$ .

It is also interesting to check whether our results depend on the choice of the large- $x$  parametrisation. Since the DGLAP evolution equation couples the small- $x$  distributions to the large- $x$  ones, at first sight, our results may depend on such a choice. However, looking at the studies of the PDF uncertainties, it can be seen that the large- $x$  behaviour of the  $T$  and  $\Sigma$  distributions hardly depends on the chosen fit down to  $x \approx 0.1$ . Moreover, in the large- $x$  limit, the splitting matrix can be written

$$\begin{pmatrix} P_{qq} & P_{qg} \\ P_{gq} & P_{gg} \end{pmatrix} \approx \frac{1}{(1-x)_+} \begin{pmatrix} 2C_F & \cdot \\ \cdot & 2C_A \end{pmatrix}.$$

Thus, in the large- $x$  region, the gluon distribution and the sea are not coupled. Since, in our method, both  $T$  and  $\Sigma$  are fixed, we study the influence of the gluon distribution on  $F_2$ . Due to the fact that these are not coupled at large  $x$ , we expect that our fit does not depend on the large- $x$  behaviour of the distributions. We have chosen here the GRV98 parton set as an example, and checked that our conclusions do not depend on this choice.

The parametrisations (9.2) and (9.3) will therefore be used for  $x \leq x_{\text{Regge}}$  and we shall ask that they match with the GRV distributions at  $x = x_{\text{Regge}}$ .

### 9.1.2 The triple-pole case

Since, below  $Q_0^2$ , we do not use singularities of order larger than 3, we expect this behaviour to be valid for the  $T$  and  $\Sigma$  distributions. The natural way of separating the initial  $F_2$  value given by (9.3) is thus to consider both  $T$  and  $\Sigma$  as a sum of a triple-pole pomeron and a reggeon. The gluon distribution, being coupled to  $\Sigma$ , should not contain any singularities either. Thus, we can write

$$T(x, Q_0^2) = a_T \log^2(1/x) + b_T \log(1/x) + c_T + d_T x^\eta, \quad (9.9)$$

$$\Sigma(x, Q_0^2) = a_\Sigma \log^2(1/x) + b_\Sigma \log(1/x) + c_\Sigma + d_\Sigma x^\eta, \quad (9.10)$$

$$G(x, Q_0^2) = a_G \log^2(1/x) + b_G \log(1/x) + c_G + d_G x^\eta, \quad (9.11)$$

Most of the 12 parameters in these expressions are constrained. First of all, since the triple-pole pomeron, describing the high-energy interactions, has vacuum quantum numbers, it will not be sensitive to the quark flavours. This means that, at high energy, one expects  $T \rightarrow 0$ . Therefore, we set  $a_T = b_T = c_T = 0$ . Then, since we connect our parametrisation with GRV's at  $x_{\text{Regge}}$ , we want the distribution functions to be continuous over the whole  $x$  range. Continuity of the  $T$  distribution fixes  $d_T$  and we finally have

$$T(x, Q_0^2) = T^{(GRV)}(x_{\text{Regge}}, Q_0^2) \left( \frac{x}{x_{\text{Regge}}} \right)^\eta.$$

Moreover, we want to fix  $F_2(Q_0^2)$  to be equal to  $F_2^{(R)}$  obtained from our previous global fit<sup>3</sup>. Since  $T$  is entirely known, this constraint fixes all the  $\Sigma$  parameters through the relation

$$\phi_\Sigma = \frac{18\phi^{(R)} - 3\phi_T}{5}, \quad \phi = a, b, c, d. \quad (9.12)$$

Therefore, since our fit keeps consistency with the Regge fit for  $Q^2 \leq Q_0^2$ , it can also be used to reproduce the  $\gamma^{(*)}\gamma^{(*)}$  experimental results for  $Q_1^2 \leq Q_2^2 \leq Q_0^2$ .

At this level, only the gluon distribution parameters are free. However, since the reggeon trajectory is expected to be mainly constituted of quarks, its contribution to the gluon density is expected to be small. Thus, we shall make the approximation  $d_G = 0$ . Finally, we used continuity of the gluon density with the GRV distribution at  $x_{\text{Regge}}$  to fix  $c_G$ . We are finally left with only 2 free parameters:  $a_G$  and  $b_G$ .

### 9.1.3 The generalised double-pole case

If we want to use (9.2) instead of (9.3) for  $Q^2 \leq Q_0^2$ , we can follow the same method as for the triple-pole pomeron case. The  $T$  distribution will only contain a reggeon term, fixed by continuity with  $x_{\text{Regge}}$ , the  $\Sigma$  distribution will entirely be imposed by the double-pole pomeron fit presented in chapter 8 and the gluon distribution will be described with only a

---

<sup>3</sup>Each quantity with a superscript  $^{(R)}$  refers to the corresponding quantity obtained from the Regge fit in chapter 8.

pomeron contribution where the constant term is fixed by continuity with GRV<sup>4</sup>:

$$\begin{aligned}
T(x, Q_0^2) &= d_T^* \cos\left(\frac{\eta\pi}{2}\right) x^\eta, \\
\Sigma(x, Q_0^2) &= a_\Sigma^* \Im m \left\{ \frac{i}{2} \log \left[ 1 + \Lambda_\Sigma^* \left( \frac{Q_0^2}{x} \right)^\delta \right] + \frac{i}{2} \log \left[ 1 + \Lambda_\Sigma^* \left( -\frac{Q_0^2}{x} \right)^\delta \right] \right\} + b_\Sigma^* + d_\Sigma^* x^\eta, \\
G(x, Q_0^2) &= a_G \Im m \left\{ \frac{i}{2} \log \left[ 1 + \Lambda_G \left( \frac{Q_0^2}{x} \right)^\delta \right] + \frac{i}{2} \log \left[ 1 + \Lambda_G \left( -\frac{Q_0^2}{x} \right)^\delta \right] \right\} + b_G^*. \quad (9.13)
\end{aligned}$$

Note that, due to the parameter  $\Lambda$ , the generalised double-pole pomeron has the same number of free parameters as the triple-pole pomeron. Moreover, the parameter  $\delta$  fixes the position of the series of simple poles<sup>5</sup> and therefore must have the same value in quark and gluon distributions. This value is directly taken from the fit obtained in chapter 8. Therefore, as in the triple-pole case, there only remains 2 free parameters:  $a_G$  and  $\Lambda_G$ .

### 9.1.4 Remark: influence of the GRV parametrisation

Before turning to the fits, one must stress that the GRV parametrisation at large  $x$  does not modify the triple-pole-singularity structure of the initial distributions. Actually, one may write the Mellin transform

$$\begin{aligned}
\int_0^1 dx x^{j-1} q(x) &= \int_0^{x_{\text{Regge}}} dx x^{j-1} q_{\text{regge}}(x) \\
&+ \int_{x_{\text{Regge}}}^1 dx x^{j-1} q_{\text{grv}}(x).
\end{aligned}$$

In this expression, the first term contains the triple-pole pomeron and the reggeon. The singularities of the second term come from the behaviour near  $x = 1$ . Since parton distributions behave like  $x^{\varepsilon-1}(1-x)^n$ , the GRV parton distributions give the following contribution

$$\sum_{k=0}^n (-)^k \binom{n}{k} \frac{1 - x_{\text{Regge}}^{j+\varepsilon+k-1}}{j + \varepsilon + k - 1}.$$

and the zeroes of the numerator cancel those from the denominator. Thus, using GRV at large  $x$  does not interfere with the singularity structure imposed from the low- $x$  parametrisation.

## 9.2 Fit

We shall fit the DIS data coming from H1 [67–73], ZEUS [74–81], BCDMS [82], E665 [83], NMC [84] and SLAC [86]. We shall only consider data for  $F_2^p$ .

<sup>4</sup>The constrained parameters are marked with a \*.

<sup>5</sup>We have  $\log(1 + \Lambda\nu^\delta) = \log(\Lambda\nu^\delta) + \sum_{n=1}^{\infty} \frac{(-)^{n+1}}{n} \Lambda^{-n} \nu^{-n\delta}$ , thus  $\delta$  gives the position of the simple poles in the series while  $\Lambda$  is related to their residues.

Since we want to test the domain common to Regge theory and to the DGLAP evolution, we only keep the experimental points verifying

$$\begin{cases} \cos(\theta_t) \leq \frac{49}{2m_p^2}, \\ Q_0^2 \leq Q^2 \leq 3000 \text{ GeV}^2, \\ x \leq x_{\text{Regge}}. \end{cases} \quad (9.14)$$

We have tried several values of the initial scale  $Q_0^2$  around 5 GeV<sup>2</sup>. Given an initial scale, the Regge limit on  $\cos(\theta_t)$  translates into a natural value for  $x_{\text{Regge}}$

$$x_{\text{Regge}}^{(0)} = \frac{m_p \sqrt{Q_0^2}}{49}. \quad (9.15)$$

A graph of that limit is presented in Fig. 9.1. However, as one can see from Fig. 9.2, if we

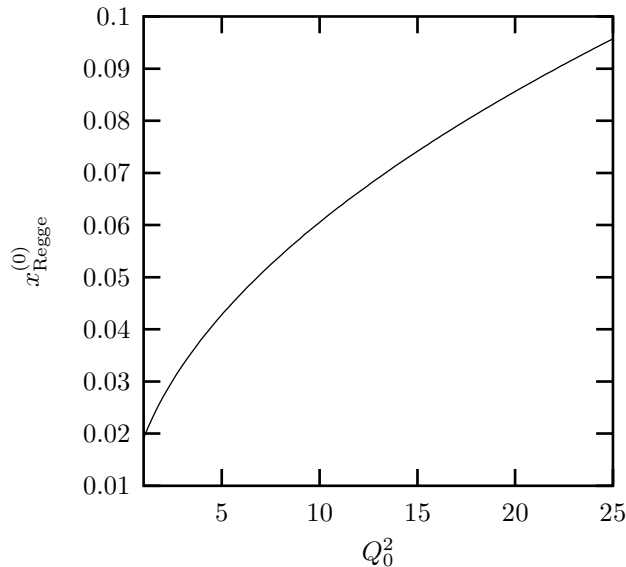


Figure 9.1: Natural value of  $x_{\text{Regge}}$  as a function of the scale.

take that limit on  $x$ , we cut most of the high- $Q^2$  experimental points which are at large  $x$ . It is therefore interesting to extrapolate the initial distributions to larger  $x$ , hence we have tried some higher values for  $x_{\text{Regge}}$ .

## 9.3 Results

The results of the fits are given in table 9.1 as a function of  $Q_0^2$  and  $x_{\text{Regge}}$ . We can see that this 2-parameter fit reproduces very well the experimental points in the intervals (9.14) for  $Q_0^2 \geq 3 \text{ GeV}^2$  and  $x_{\text{Regge}} \leq 0.1$ . The values of the fitted parameters, as well as the constrained parameters are given in table 9.2 and 9.3. We can see in these tables that when  $x_{\text{Regge}}$  goes from 0.1 to 0.15, the parameters remain stable.

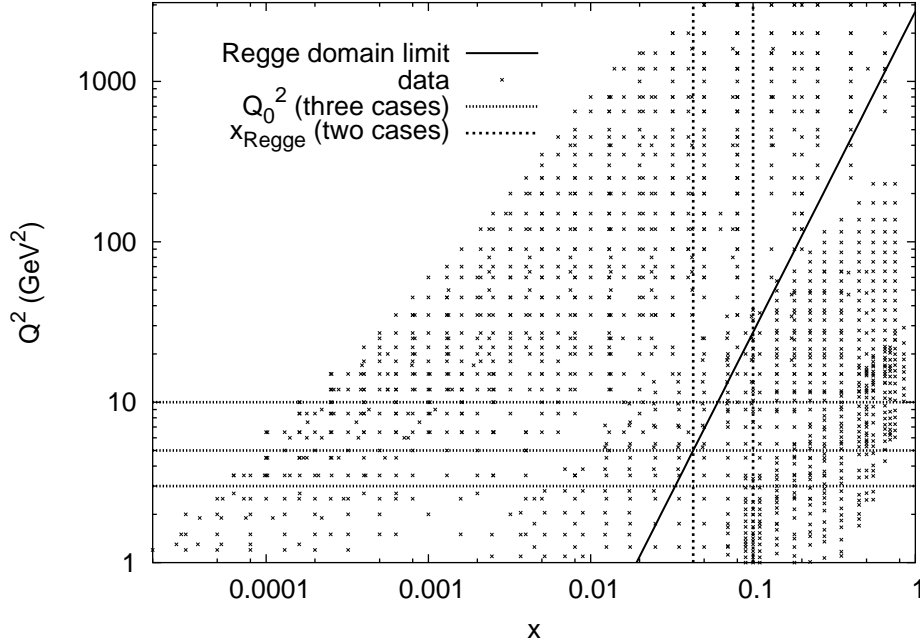


Figure 9.2: Experimental points, Regge domain limit and fit domain limits for  $Q_0^2 = 5 \text{ GeV}^2$  and  $x_{\text{Regge}} = x_{\text{Regge}}^{(0)}$  or 0.1. It clearly appears that, without extrapolation, we miss the high- $Q^2$  points.

We show the initial distributions and the  $F_2^p$  plot for  $Q_0^2 = 5 \text{ GeV}^2$  and  $x_{\text{Regge}} = 0.1$  in Fig. 9.3 and Figs. 9.5 and 9.6 respectively. We can see on these figures that there are very few differences between the double- and the triple-pole models.

In Fig. 9.4, we have compared the gluon distribution obtained from our fit with that of well-known DGLAP fits like GRV [21], CTEQ [22] and MRST [20]. One can see that our gluon distribution is of the same order of magnitude as that from other DGLAP fits and that it is impossible to distinguish between the double- and the triple-pole pomeron models.

Furthermore, one can easily check that the  $\chi^2$  per data point ( $\chi^2/nop$ ) of the fit remains of order 1 for  $0.04 \lesssim x_{\text{Regge}} \lesssim 0.15$  and grows when we take  $x_{\text{Regge}} \sim 0.01$  or smaller. At that point, parton distributions depend on the chosen parametrisation and the one we used, namely GRV98, does not take into account the latest HERA points. If we want to go to smaller values of  $x_{\text{Regge}}$ , we need a more recent parametrisation and thus a NLO study. Note that the interval on  $x_{\text{Regge}}$  for which we have an acceptable  $\chi^2$  hardly depends on  $Q_0^2$  for  $Q_0^2$  in  $[3, 15] \text{ GeV}^2$ , and that the  $\chi^2$  of the fit does not change very much in that domain.

Unfortunately, it is quite hard to determine a unique scale  $Q_0^2$  or  $x_{\text{Regge}}$  from the fit. From Table 9.1, it is clear that  $x_{\text{Regge}}$  can be taken to be around 0.1. It can be pushed up to 0.15 in the triple-pole pomeron case and even to higher values in the double-pole pomeron case. However, as we have argued, for the values of  $Q_0^2$  under consideration and such high  $x_{\text{Regge}}$ , we are outside the domain (9.1) and we may not ensure that Regge theory will still be valid at  $x \approx 0.1$  and  $Q^2 = Q_0^2$ . We can thus adopt two different points of view:

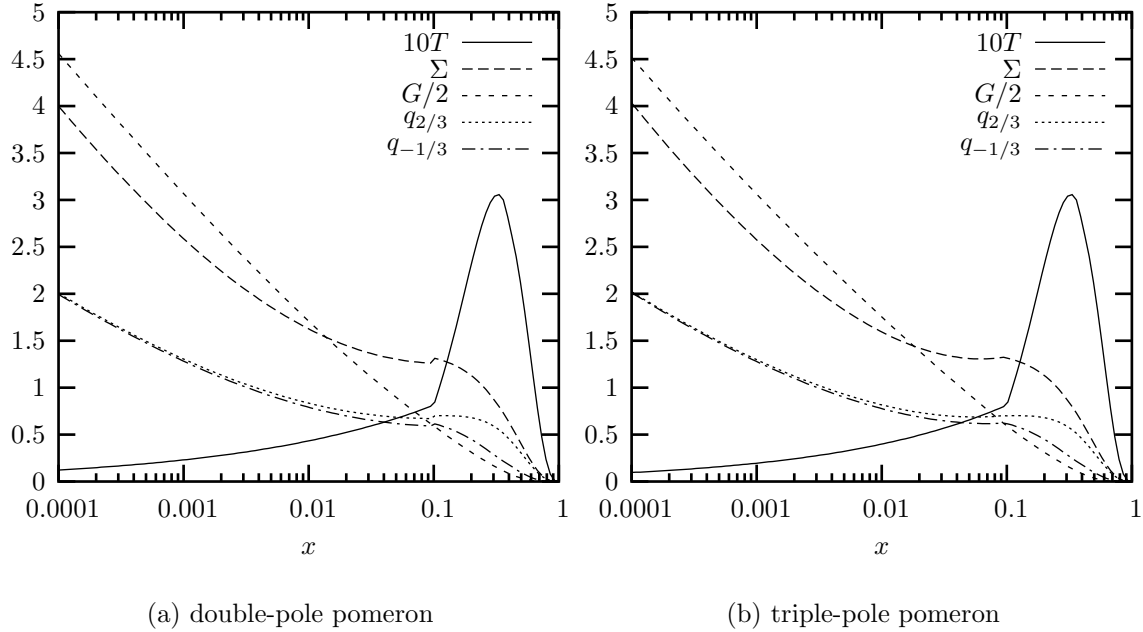


Figure 9.3: Initial distributions for  $Q_0^2 = 5 \text{ GeV}^2$  and  $x_{\text{Regge}} = 0.1$ .  $q_{2/3} = x(u^+ + c^+ + t^+)$  and  $q_{-1/3} = x(d^+ + s^+ + b^+)$ .

1. we stay in the domain (9.1). We have thus  $x_{\text{Regge}} = x_{\text{Regge}}^{(0)}$  and we can take  $Q_0^2$  down to  $3 \text{ GeV}^2$ . The problem is that as  $Q_0^2$  goes down,  $x_{\text{Regge}}$  goes down too. And, since high- $Q^2$  experimental points have large values of  $x$ , we do not test pQCD over a large range of  $Q^2$  values. This effect can be clearly seen in Fig. 9.2 where we have plotted the experimental points, the Regge domain limit and the fit domain for  $Q_0^2 = 5 \text{ GeV}^2$  and  $x_{\text{Regge}} = x_{\text{Regge}}^{(0)}$  or 0.1. It is therefore difficult to predict a “best value” for  $Q_0^2$ .
2. we extrapolate the Regge fit outside the domain (9.1). The number of points concerned by this interpolation can be seen in Fig. 9.2. In such a case, depending on our confidence in this extrapolation, we can consider that pQCD applies down to  $3 \text{ GeV}^2$  or  $5 \text{ GeV}^2$  and  $x_{\text{Regge}} \approx 0.1$ . This value is compatible with the Donnachie-Landshoff prediction [14]. Below  $2 \text{ GeV}^2$ , the  $\chi^2$  is larger than 1 whatever  $x_{\text{Regge}}$  is and values of the initial scale smaller than  $1.45 \text{ GeV}^2$  are ruled out at the 90% confidence level.

## 9.4 Conclusion

In this chapter, we have shown that it is possible to use a very simple analytic form, namely a double-pole or a triple-pole pomeron and a reggeon, as an initial condition for the DGLAP evolution. Applying the constraint from the global Regge fit obtained in chapter 8 as well as some expected properties of the parton distribution functions, we have shown that we can

$Q_0^2$	3.0			5.0			10.0		
	$n$	$\chi^2/n$		$n$	$\chi^2/n$		$n$	$\chi^2/n$	
$x_{\text{Regge}}$		double	triple		double	triple		double	triple
$x_{\text{Regge}}^{(0)}$	591	1.156	1.071	577	0.986	0.966	515	0.924	0.939
0.1	735	1.088	1.008	686	1.030	0.985	581	0.953	0.996
0.15	761	1.153	1.024	712	1.053	1.014	607	0.961	1.039
0.2	-	-	-	744	1.047	1.159	639	0.986	1.212

Table 9.1:  $\chi^2$  for various values of  $Q_0^2$  and  $x_{\text{Regge}}$ . ( $n$  is the number of experimental point satisfying (9.14)).

fit the DIS data in the domain  $Q_0^2 \geq 3 \text{ GeV}^2$ ,  $x \leq 0.15$  and  $\cos(\theta_t) \geq 49/(2m_p^2)$ . These fits have only 2 free parameters in the gluon distribution. Below  $Q_0^2$ ,  $F_2$  is described by Regge theory (see chapter 8).

Our fit is at the interface between Regge theory and pQCD. We have thus proven that Regge theory can be used to extend a pQCD evolution down to the non-perturbative domain. From the fit, we can also say that the scale down to which we can apply pQCD is of the order of 3-5  $\text{GeV}^2$ .

Moreover, we have seen that our approach can be used to split  $F_2$  in  $T$  and  $\Sigma$ -components with precise physical properties. In this way, it is of prime importance to point out that all the initial distributions have the same singularity structure, which is rarely the case for the usual parton sets. Since  $\Sigma$  is coupled to the gluon distribution, the latter can also be predicted. We have shown that the fitted gluon distribution is of the same order of magnitude as the gluon distributions obtained by the usual DGLAP fits to DIS data.

By requiring the same singularities in each distribution, we have seen that we are able to construct a full model both for DGLAP evolution and Regge theory in the case of a multiple-pole pomeron model. It should be interesting, in the future, to test if we can apply the same method to the case of the Donnachie-Landshoff two-pomeron model.

Finally, we shall see in chapter 11 that we can get rid of the external parametrisation at large  $x$  and extend this approach to  $x = 1$ . However, this requires a much more complete treatment, and the method developed in this chapter, concentrating in the small- $x$  domain, is interesting for its simplicity.

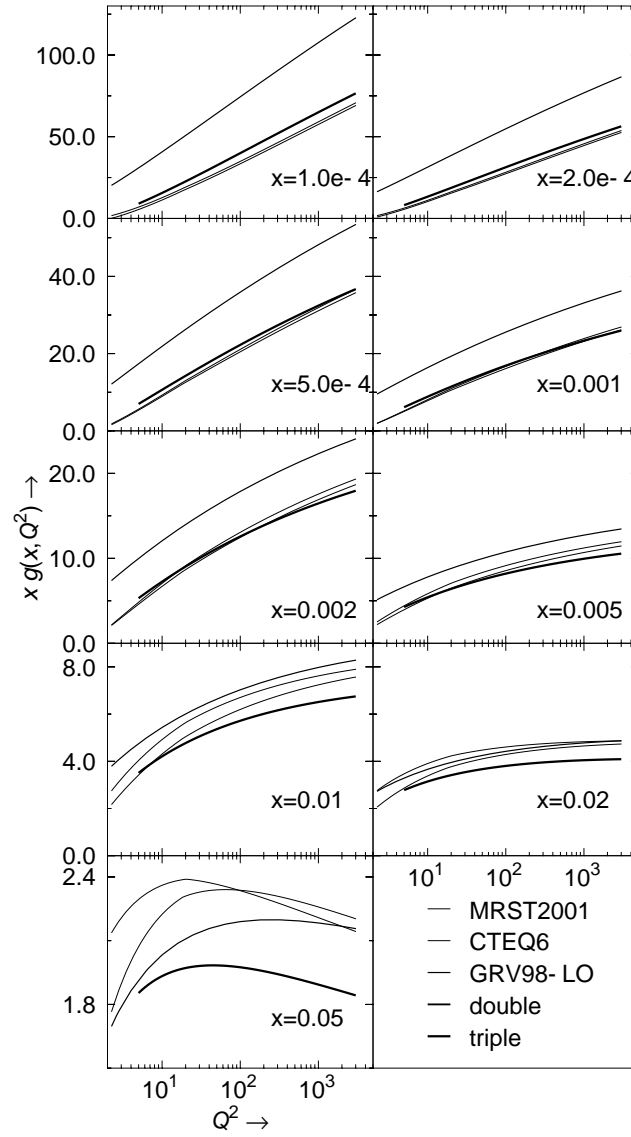


Figure 9.4: Fitted gluon distribution compared with some well-known parton distributions.

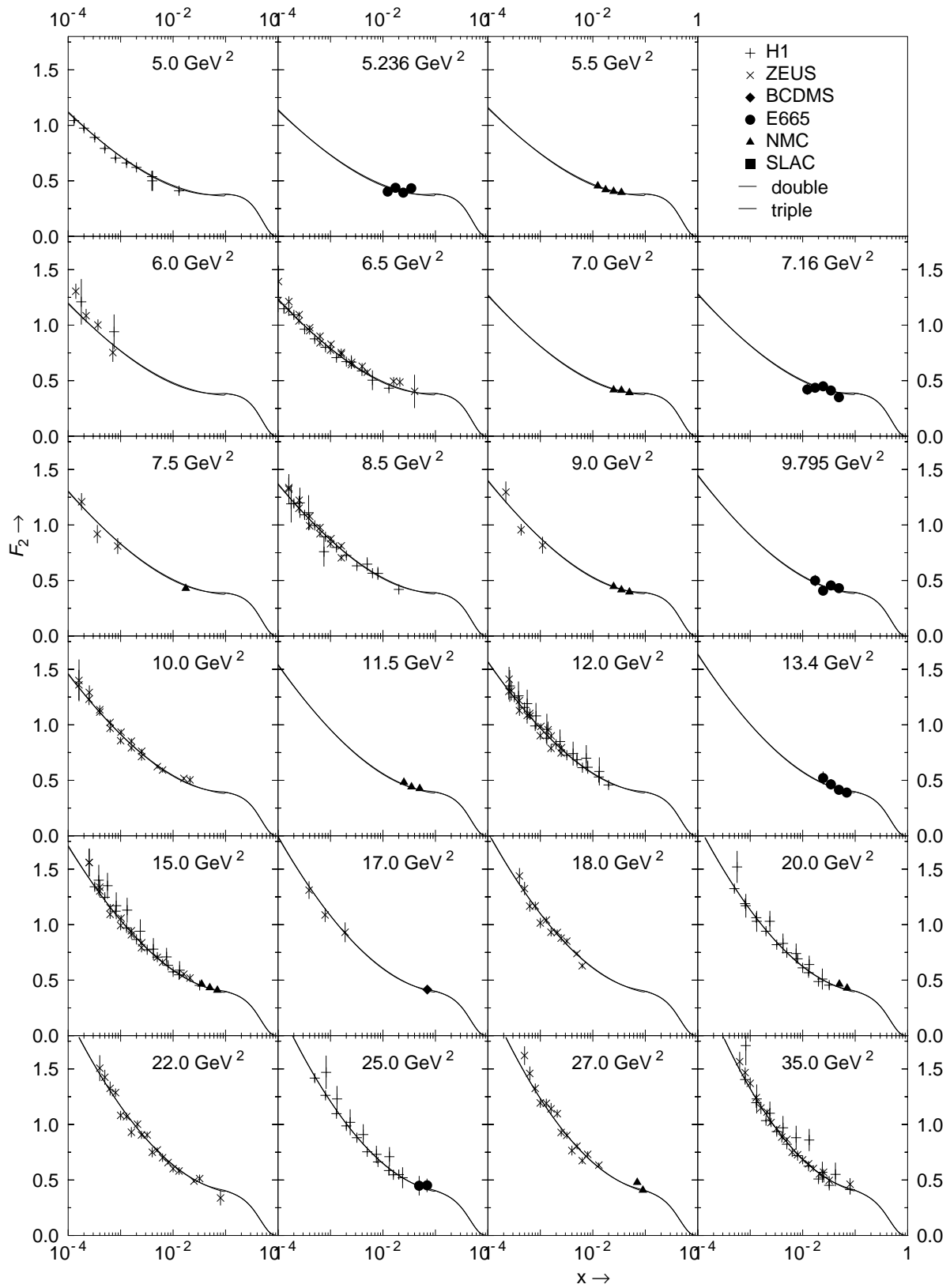


Figure 9.5:  $F_2^p$  fit for  $Q_0^2 = 5 \text{ GeV}^2$  and  $x_{\text{Regge}} = 0.1$  (low- $Q^2$  values).

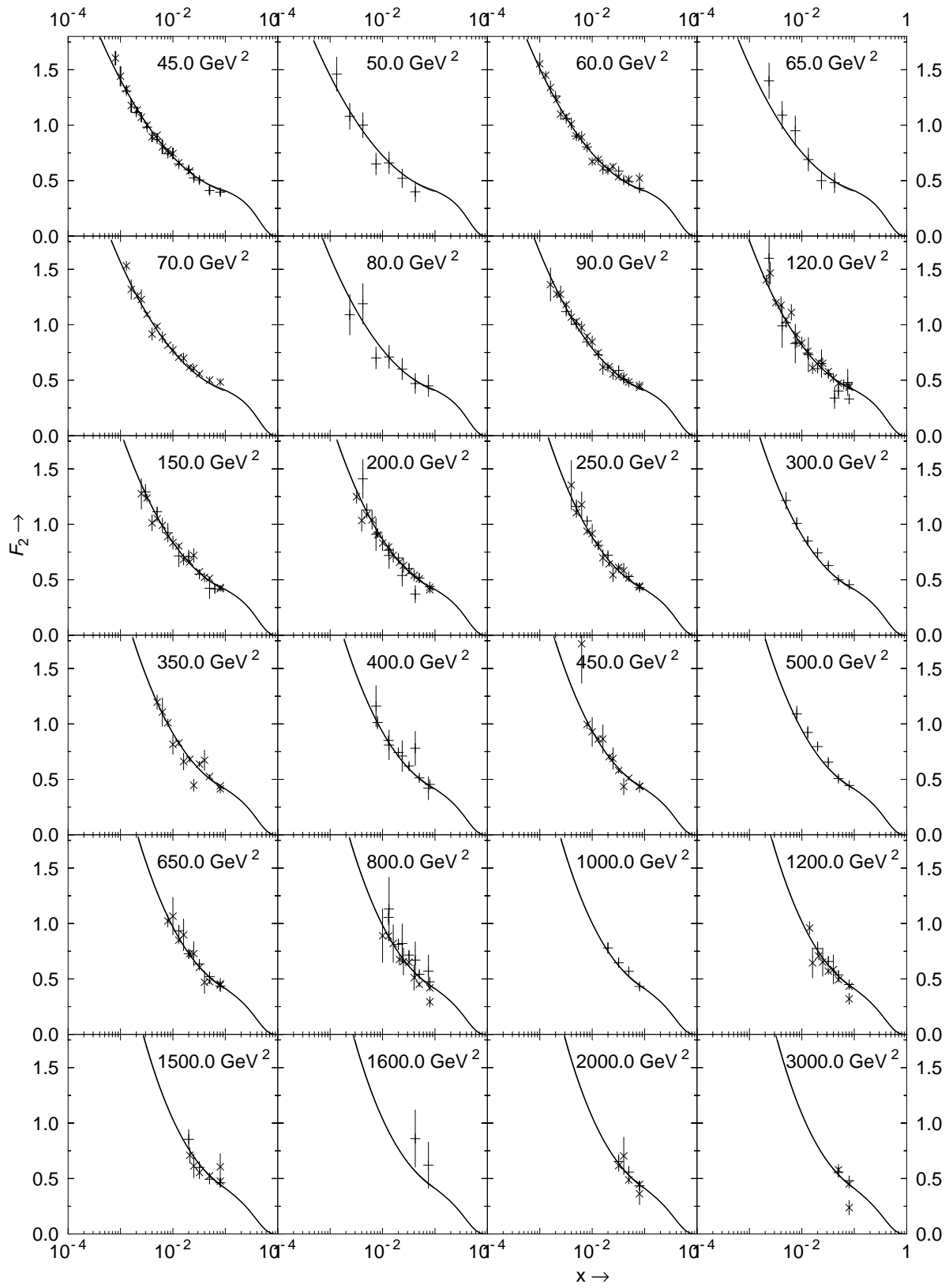


Figure 9.6:  $F_2^p$  fit for  $Q_0^2 = 5 \text{ GeV}^2$  and  $x_{\text{Regge}} = 0.1$  (high- $Q^2$  values).

$Q_0^2$	3.0		
$a_{\gamma p}$	0.00541		
$b_{\gamma p}$	0.0712		
$c_{\gamma p}$	0.00541		
$d_{\gamma p}$	0.890		
$x_{\text{Regge}}$	$x_{\text{Regge}}^{(0)} = 0.0332$	0.1	0.15
$d_T$	-0.0722	0.167	0.291
$a_G$	<b>0.147 ± 0.014</b>	<b>0.006 ± 0.051</b>	<b>0.0000 ± 0.0044</b>
$b_G$	<b>-0.85 ± 0.13</b>	<b>0.718 ± 0.086</b>	<b>0.7300 ± 0.0050</b>
$c_G$	3.45	-0.495	-0.524
$Q_0^2$	5.0		
$a_{\gamma p}$	0.00644		
$b_{\gamma p}$	0.0990		
$c_{\gamma p}$	0.0064		
$d_{\gamma p}$	1.06		
$x_{\text{Regge}}$	$x_{\text{Regge}}^{(0)} = 0.0428$	0.1	0.15
$d_T$	-0.0478	0.166	0.293
$a_G$	<b>0.091 ± 0.019</b>	<b>0.027 ± 0.010</b>	<b>0.0327 ± 0.0081</b>
$b_G$	<b>0.19 ± 0.16</b>	<b>0.822 ± 0.077</b>	<b>0.768 ± 0.055</b>
$c_G$	0.595	-0.851	-0.730
$Q_0^2$	10.0		
$a_{\gamma p}$	0.00780		
$b_{\gamma p}$	0.142		
$c_{\gamma p}$	0.00780		
$d_{\gamma p}$	1.27		
$x_{\text{Regge}}$	$x_{\text{Regge}}^{(0)} = 0.0605$	0.1	0.15
$d_T$	0.0101	0.165	0.0295
$a_G$	<b>0.158 ± 0.028</b>	<b>0.131 ± 0.019</b>	<b>0.137 ± 0.014</b>
$b_G$	<b>0.18 ± 0.22</b>	<b>0.42 ± 0.14</b>	<b>0.376 ± 0.093</b>
$c_G$	0.0299	-0.463	-0.378

Table 9.2: Values of the parameters for  $3 \leq Q_0^2 \leq 10 \text{ GeV}^2$  and  $x_{\text{Regge}} \leq 0.15$  for the triple-pole pomeron case. Only  $a_G$  and  $\Lambda_G$  are fitted, while the other parameters are constrained.

$Q_0^2$	3.0		
$a_{\gamma p}$	0.526		
$\Lambda_{\gamma p}$	0.166		
$b_{\gamma p}$	-0.0712		
$d_{\gamma p}$	0.434		
$x_{\text{Regge}}$	$x_{\text{Regge}}^{(0)} = 0.0332$	0.1	0.15
$d_T$	-0.646	0.145	0.272
$a_G$	<b><math>20.0 \pm 3.4</math></b>	<b><math>2.36 \pm 0.17</math></b>	<b><math>2.182 \pm 0.014</math></b>
$\Lambda_G$	<b><math>0.13953 \pm 0.00034</math></b>	<b><math>1.36 \pm 0.72</math></b>	<b><math>10.0 \pm 6.9</math></b>
$b_G$	1.33	-2.62	-6.38
$Q_0^2$	5.0		
$a_{\gamma p}$	0.716		
$\Lambda_{\gamma p}$	0.120		
$b_{\gamma p}$	-0.0896		
$d_{\gamma p}$	0.444		
$x_{\text{Regge}}$	$x_{\text{Regge}}^{(0)} = 0.0428$	0.1	0.15
$d_T$	-0.0470	0.144	0.276
$a_G$	<b><math>6.1 \pm 2.7</math></b>	<b><math>2.13 \pm 0.18</math></b>	<b><math>1.95 \pm 0.13</math></b>
$\Lambda_G$	<b><math>0.095 \pm 0.054</math></b>	<b><math>0.75 \pm 0.19</math></b>	<b><math>1.04 \pm 0.24</math></b>
$b_G$	0.0896	-2.18	-2.70
$Q_0^2$	10.0		
$a_{\gamma p}$	1.08		
$\Lambda_{\gamma p}$	0.0765		
$b_{\gamma p}$	-0.122		
$d_{\gamma p}$	0.456		
$x_{\text{Regge}}$	$x_{\text{Regge}}^{(0)} = 0.0605$	0.1	0.15
$d_T$	0.0116	0.153	0.278
$a_G$	<b><math>12.4 \pm 3.2</math></b>	<b><math>9.7 \pm 1.5</math></b>	<b><math>9.4 \pm 1.1</math></b>
$\Lambda_G$	<b><math>0.073 \pm 0.027</math></b>	<b><math>0.109 \pm 0.026</math></b>	<b><math>0.114 \pm 0.022</math></b>
$b_G$	-1.64	-2.14	-2.18

Table 9.3: Values of the parameters for  $3 \leq Q_0^2 \leq 10 \text{ GeV}^2$  and  $x_{\text{Regge}} \leq 0.15$  for the double-pole pomeron case. Only  $a_G$  and  $b_G$  are fitted, while the other parameters are constrained.



# Chapter 10

## DGLAP evolution of residues

### 10.1 Regge theory at large $Q^2$ and the DGLAP essential singularity

In the previous chapter, we have seen that we can use Regge theory to constrain the initial condition for a DGLAP evolution. In this approach, all parton distributions, described as the sum of a multiple-pole pomeron term and a reggeon term, have the same singularity structure. If  $Q_0^2$  is the scale where we start the DGLAP evolution,  $F_2^p$  is described by Regge theory at small values of  $Q^2$  ( $Q^2 \leq Q_0^2$ ) and by pQCD at larger scales ( $Q^2 \geq Q_0^2$ ). The matching point may therefore be considered as the scale where Regge theory breaks down, and as the point where DGLAP evolution breaks down. Nevertheless, although it is clear that we cannot extend DGLAP evolution down to  $Q^2 = 0$ , the fact that Regge theory may not be applied at large values of  $Q^2$  is unclear. Actually, as we have seen in chapter 6, it is possible to reproduce  $F_2^p$  up to  $Q^2 = 3000 \text{ GeV}^2$  using a triple-pole pomeron model. However, if this is the case, both Regge theory and DGLAP evolution describe the proton structure function at large scales, and therefore, one must be able to use the DGLAP evolution equation to obtain the residues of the triple-pole pomeron at large  $Q^2$ . The main obstacle in solving that problem lies in the fact that the DGLAP evolution generates an essential singularity which seems to be incompatible with Regge fits. To solve that problem, we need to remember that the DGLAP evolution is just an approximation and that only a full resummation of the perturbative series, including all-order corrections to the DGLAP equation as well as small- $x$  and higher-twist effects, should give the correct analytical behaviour. Due to the success of DGLAP fits, one expects corrections to be small and the DGLAP equation to be a good approximation. We shall therefore choose a Regge-compatible parametrisation at an initial scale  $Q_0^2$  and evolve it, using the DGLAP equation, without worrying about the presence of the essential singularity for  $Q^2 \neq Q_0^2$ . Adjusting the parameters of that initial distribution in order to reproduce  $F_2$  over the whole  $Q^2$  range will give us the Regge residues at the scale  $Q_0^2$ .

## 10.2 Mixing DGLAP evolution with Regge theory

We show<sup>1</sup> here that we can use this approach to obtain form factors which are compatible with DGLAP evolution. We present in this section the model used to extract these residues as functions of  $Q^2$ . Always considering that DGLAP evolution does not lead to a relevant singularity structure but only to an approximation of the parton distributions, we consider that the initial distribution fitted by starting the evolution at the scale  $Q_0^2$  gives the residues at  $Q_0^2$ . We just need to repeat this by varying  $Q_0^2$  to get the residues over the whole  $Q^2$  range. Note that since we want to *predict* the  $F_2$  residues, we do not constrain  $F_2$  with a soft QCD fit as was done in the previous chapter. However, it is known that the triple-pole pomeron model can be used to reproduce soft processes. Therefore, one knows that the residues found here can be extended down to  $Q^2 = 0$ . Since we only want to study the domain where both DGLAP and Regge theory are expected to apply, we shall firstly consider the overlapping region and come back to the small- $Q^2$  region later.

Once again, the Regge domain does not extend up to  $x = 1$ . As said in the previous chapter, we may solve that problem by introducing powers of  $(1 - x)$ , but this requires fitting other structure functions than  $F_2^p$  which are not in the domain of interest, and adds parameters unnecessary if we want to consider the Regge limit. Therefore, as was done in the previous chapter, we shall use the GRV98 parametrisation for  $x > x_{\text{Regge}}$ .

## 10.3 Initial distributions

Once again, if we only want to reproduce  $F_2^p$ , we do not need the full set of quarks and anti-quarks but only the  $T$  and  $\Sigma$  distributions. If  $Q_0^2$  is the scale at which we start the DGLAP evolution, we shall describe the distributions at that scale using a triple-pole-pomeron term and a reggeon term. With the same assumptions as in the previous chapter, we have

$$\begin{aligned} T(x, Q_0^2) &= d_T x^\eta, \\ \Sigma(x, Q_0^2) &= a_\Sigma \log^2(1/x) + b_\Sigma \log(1/x) + c_\Sigma + d_\Sigma x^\eta, \\ G(x, Q_0^2) &= a_G \log^2(1/x) + b_G \log(1/x) + c_G, \end{aligned}$$

where  $d_T$ ,  $c_\Sigma$  and  $c_G$  are fixed by requiring continuity with GRV98 at  $x = x_{\text{Regge}}$ . However, we have seen that we obtain much better results if we multiply each distribution by some power of  $(1 - x)$ . This new factor, effectively including daughter trajectories, is expected from Regge theory. As already pointed out, this factor is not directly connected to the small- $x$  domain. One can see that its main effect in the fit is to reproduce an inflexion point present around  $x \approx 0.01$  in the parton distributions, particularly at large  $Q^2$ . In order to minimise the number of parameters, we used only two different powers in all distributions.

---

<sup>1</sup>The model presented here is based on [62].

We thus end up with the following functions

$$\begin{aligned} T(x, Q_0^2) &= d_T^* x^\eta (1-x)^{b_2}, \\ \Sigma(x, Q_0^2) &= a_\Sigma \log^2(1/x) + b_\Sigma \log(1/x) + c_\Sigma^* (1-x)^{b_1} \\ &\quad + d_\Sigma x^\eta (1-x)^{b_2} \\ G(x, Q_0^2) &= a_G \log^2(1/x) + b_G \log(1/x) + c_G^* (1-x)^{b_1}. \end{aligned}$$

The parameters with a superscript \* are constrained by continuity with GRV parametrisation and 7 free parameters remain:  $a_\Sigma$ ,  $b_\Sigma$ ,  $d_\Sigma$ ,  $a_G$ ,  $b_G$ ,  $b_1$  and  $b_2$ .

These parameters must depend on  $Q_0^2$  and we shall see in the next section how we can find their  $Q^2$  dependence.

## 10.4 Fitting the form factors

It is well-known that DGLAP evolution generates an essential singularity at  $j = 1$ . From that point of view, finding the  $Q^2$  dependence of the residues of a triple-pole pomeron may seem impossible. However, DGLAP evolution always involves a finite-order calculation of the splitting functions and, moreover, it resums large- $Q^2$  corrections while resumming large- $s$  (small- $x$ ) contributions should be preferable for a comparison with Regge theory. Consequently, we argue that the singularity structure generated by DGLAP evolution is physically irrelevant and that only a full resummation of QCD should end up with a correct Regge behaviour.

One must note that if we consider a resummation *à la* BFKL, we have a stable square-root branch-point instead of an essential singularity. Furthermore, even in this case, we still need to unitarise the pomeron, which may lead to another singularity structure.

So, which singularity do we need to take? How can we use the DGLAP evolution to calculate residues in Regge theory? Our point of view is that, although it does not provide a correct Regge behaviour, DGLAP evolution can still be considered as a good numerical approximation. In such a case, we argue that Regge theory can be extended to high values of  $Q^2$ . The DGLAP evolution equation will therefore be considered as a numerical approximation to the triple-pole model. In this approach, if we want to use the DGLAP equation to find information about the residues at high  $Q^2$ , the only place where Regge theory can be used is for the initial distribution. If we want the residues at the scale  $Q_0^2$ , we end up with a Regge-compatible distribution at the initial scale  $Q_0^2$  and a DGLAP approximation everywhere else.

As we shall see, obtaining the Regge residues from this strategy is quite straightforward.

### 10.4.1 Scheme 1

As initial condition for DGLAP evolution, we shall use the distributions obtained in section 10.3 for  $x \leq x_{\text{Regge}}$  and the GRV98 distribution for larger  $x$  values. The parameters are considered as functions of  $Q^2$  and they can be found as follows:

1. choose an initial scale  $Q_0^2$ ,

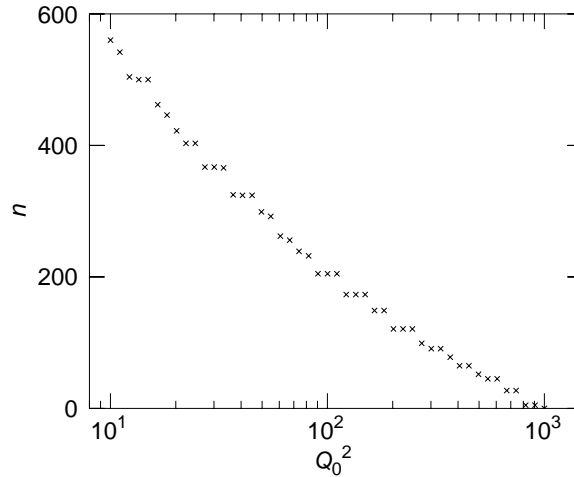


Figure 10.1: Number of points involved in the forward evolution.

2. choose a value for the parameters in the initial distribution,
3. compute the parton distributions at larger  $Q^2$  using DGLAP evolution equations,
4. repeat 2 and 3 until the best values of the parameters reproducing the experimental  $F_2$  data for  $Q^2 > Q_0^2$  and  $x \leq x_{\text{Regge}}$  is found.
5. This gives the residues at the scale  $Q_0^2$  and steps 1 to 4 are repeated in order to obtain the residues at all  $Q^2$  values.

This technique works quite well but has one drawback: calculation of the residues at the scale  $Q_0^2$  relies on the experimental points satisfying

$$Q_0^2 \leq Q^2 \leq Q_{\text{max}}^2.$$

Unfortunately, this domain depends on the initial scale and as we can see on Fig. 10.1 the number of points used for the fit decrease quite fast when  $Q_0^2$  rises.

### 10.4.2 Scheme 2

There is a way to keep the same set of points in each fit: adding backward evolution. The previous scheme thus becomes

1. choose an initial scale  $Q_0^2$ ,
2. choose a value for the parameters in the initial distribution,
3. compute the parton distributions for  $Q_0^2 \leq Q^2 \leq Q_{\text{max}}^2$  using forward DGLAP evolution and for  $Q_{\text{min}}^2 \leq Q^2 \leq Q_0^2$  using backward DGLAP evolution,

Exp	n	$\chi^2/nop$	CTEQ6 LO	CTEQ6 NLO	MRST2001 NLO
BCDMS [82]	5	4.185	6.043	1.505	2.210
E665 [83]	10	0.797	0.770	0.818	0.813
H1 [71–73]	240	0.913	1.433	0.935	0.920
NMC [84]	11	1.553	2.434	1.247	1.975
ZEUS [80, 81]	294	1.042	2.098	1.034	1.116
Total	560	1.020	1.831	0.996	1.053

Table 10.1: Experimental points in the domain (10.1) and results of the analytical triple-pole fit as well as some standard set predictions.

4. repeat 2 and 3 until the value of the parameters reproducing the  $F_2$  data for  $Q^2 > Q_{\min}^2$  and  $x \leq x_{\text{Regge}}$  is found.
5. This gives the residues at the scale  $Q_0^2$  and steps 1 to 4 are repeated in order to obtain the residues at all  $Q^2$  values.

This way, we take into account the experimental points with  $Q_{\min}^2 \leq Q^2 \leq Q_{\max}^2$  whatever the value of  $Q_0^2$  is.

## 10.5 Results

We have chosen to use the second scheme with both forward and backward evolution. We have fitted the data in the region

$$\begin{cases} 10 \leq Q^2 \leq 1000 \text{ GeV}^2, \\ x \leq x_{\text{Regge}} = 0.15, \\ \cos(\theta_t) = \frac{\sqrt{Q^2}}{xm_p} \geq \frac{49 \text{ GeV}^2}{2m_p^2}. \end{cases} \quad (10.1)$$

This method ensures that  $Q^2$  is large enough to apply DGLAP evolution, that  $\cos(\theta_t)$  is large enough to use Regge theory and that the large- $x$  domain is excluded from the fit. Once again, the limit on  $\cos(\theta_t)$  has been taken from the pure Regge fit presented in chapter 8. In this region, the experimental points are as shown in Table 10.1.

### 10.5.1 Form factors

When we apply the method explained in section 10.4.2 using the parametric distributions obtained in section 10.3, we obtain the form factors presented in Fig. 10.2 and calculated from 10 to 1000  $\text{GeV}^2$ . The  $\chi^2$  per data point obtained for each fit, shown in Fig. 10.3, is of order 1 and the form factors appear to be smooth functions of  $Q_0^2$ .

One must also notice that the  $\chi^2$  grows with  $Q_0^2$ . One possible explanation for this phenomenon is the following: as we see in figure 10.4, if we want to reproduce the data at  $x = x_{\min}$  and  $Q^2 = Q_{\min}^2$  we need to fix the initial condition at  $Q_0^2$  down to  $x = x_{\min}$ . This

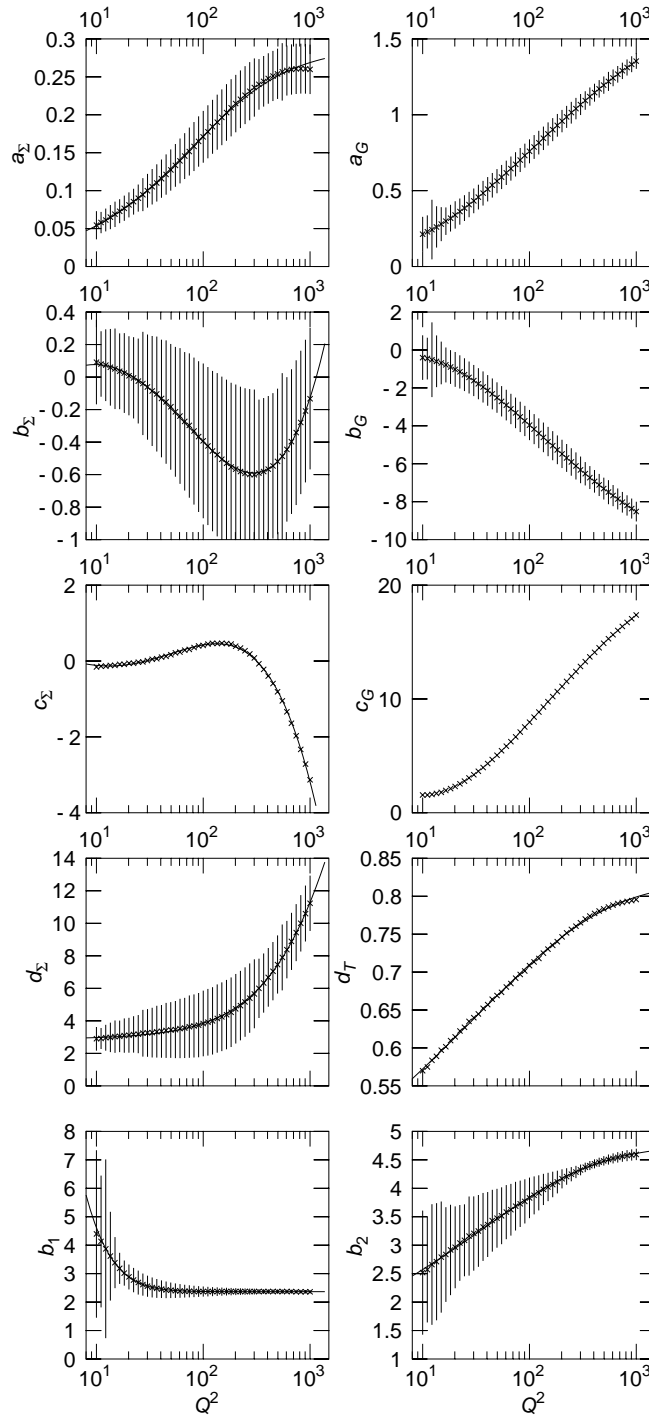


Figure 10.2: Form factors as functions of  $Q_0^2$ .

means that we reach values of  $W^2$  up to  $Q_0^2/x_{\min}$ . Therefore, when  $Q_0^2$  grows, we go higher and higher in  $W^2$  in order to describe the full experimental dataset. In other words, we go into the region where we can expect high-energy corrections. Another explanation can

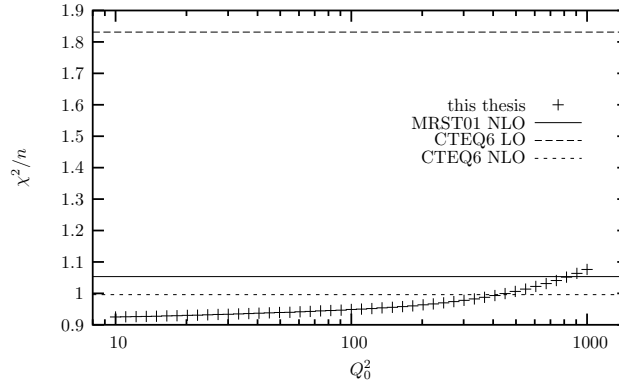


Figure 10.3:  $\chi^2/n_{op}$  per data point of the fit as a function of the initial scale for evolution.

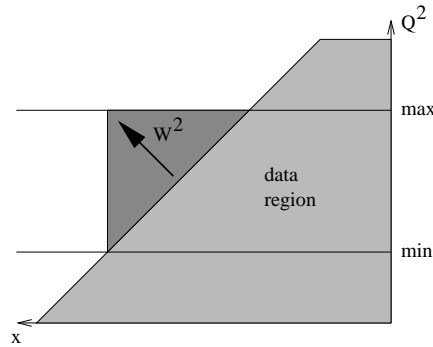


Figure 10.4: When  $Q_0^2$  grows up, the initial distribution moves to higher  $W^2$ .

be that the triple-pole model must be supplemented by new perturbative singularities at  $Q^2 \gtrsim 300 \text{ GeV}^2$ .

Finally, when choosing  $x_{\text{Regge}}$ , we do not want to take the high- $x$  experimental points for reasons explained previously, but we want to set  $x_{\text{Regge}}$  as high as possible to maximise the number of experimental points, particularly in the large- $Q^2$  domain where DGLAP evolution is expected to work better. We found that  $x_{\text{Regge}} = 0.15$  was a good compromise between those constraints.

## 10.5.2 Parton Distributions

Once we have fitted the form factors, it is interesting to see if the distributions we obtain at a scale  $Q_0^2$  are the same if we start evolution at  $Q_0^2$  or if we start at  $Q_1^2$  and evolve until  $Q_0^2$ . As we see in Fig. 10.5, for the sea-quark distribution, the difference is very small. This shows clearly that the DGLAP essential singularity can be considered as a numerical approximation to a triple-pole singularity, at least for quarks.

For the gluon case, presented in Fig. 10.6, things are different. One can see that backward evolution tends to produce lower gluon distribution at small  $x$ . These can even become negative if we evolve to lower  $Q^2$  values. However, the structure function only depends on the

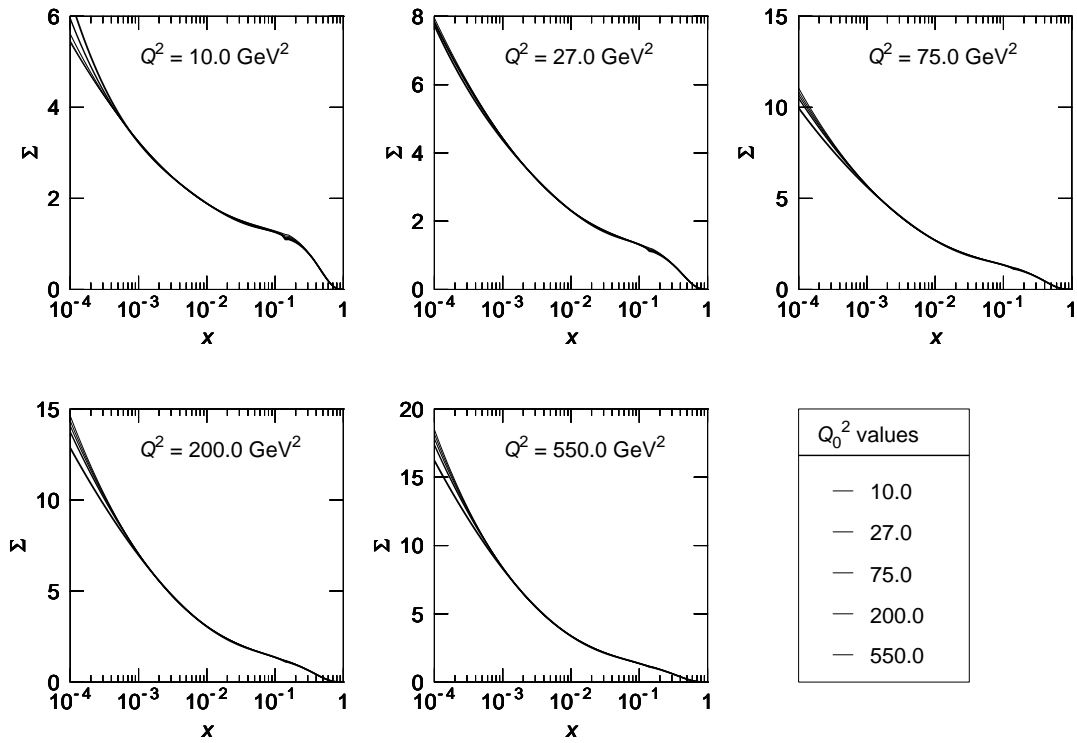


Figure 10.5:  $\Sigma$  distribution at various  $Q^2$ . Different curves correspond to different values of  $Q_0^2$ .

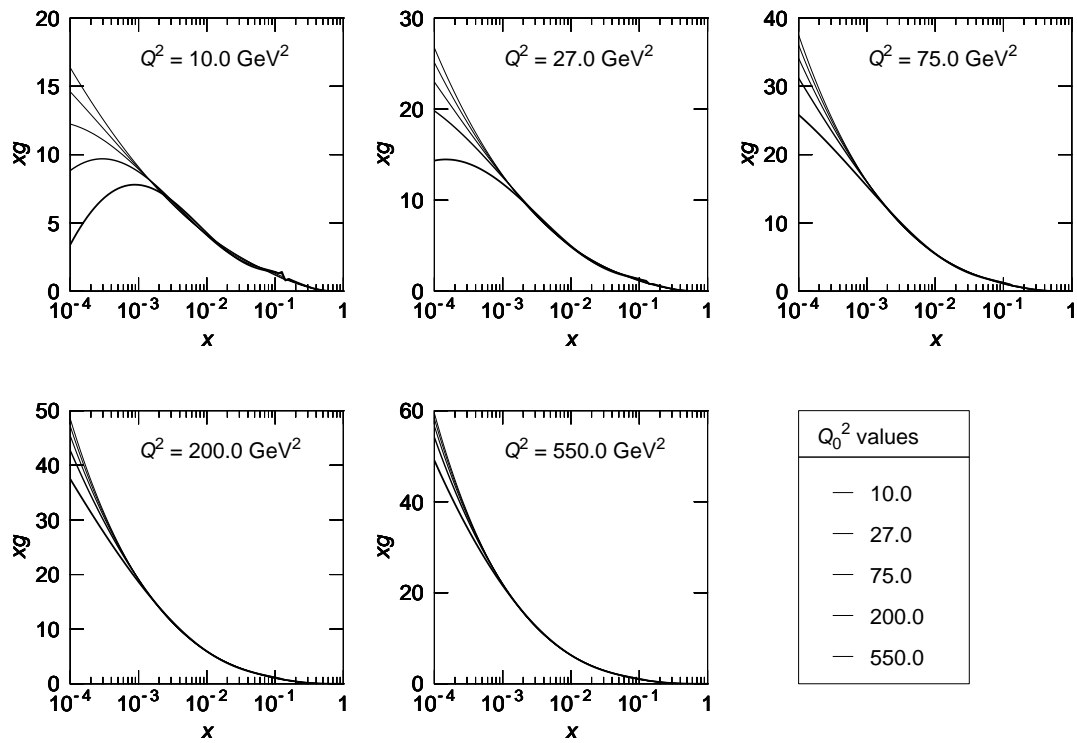


Figure 10.6: gluon distribution at various  $Q^2$ . Different curves correspond to different values of  $Q_0^2$ .

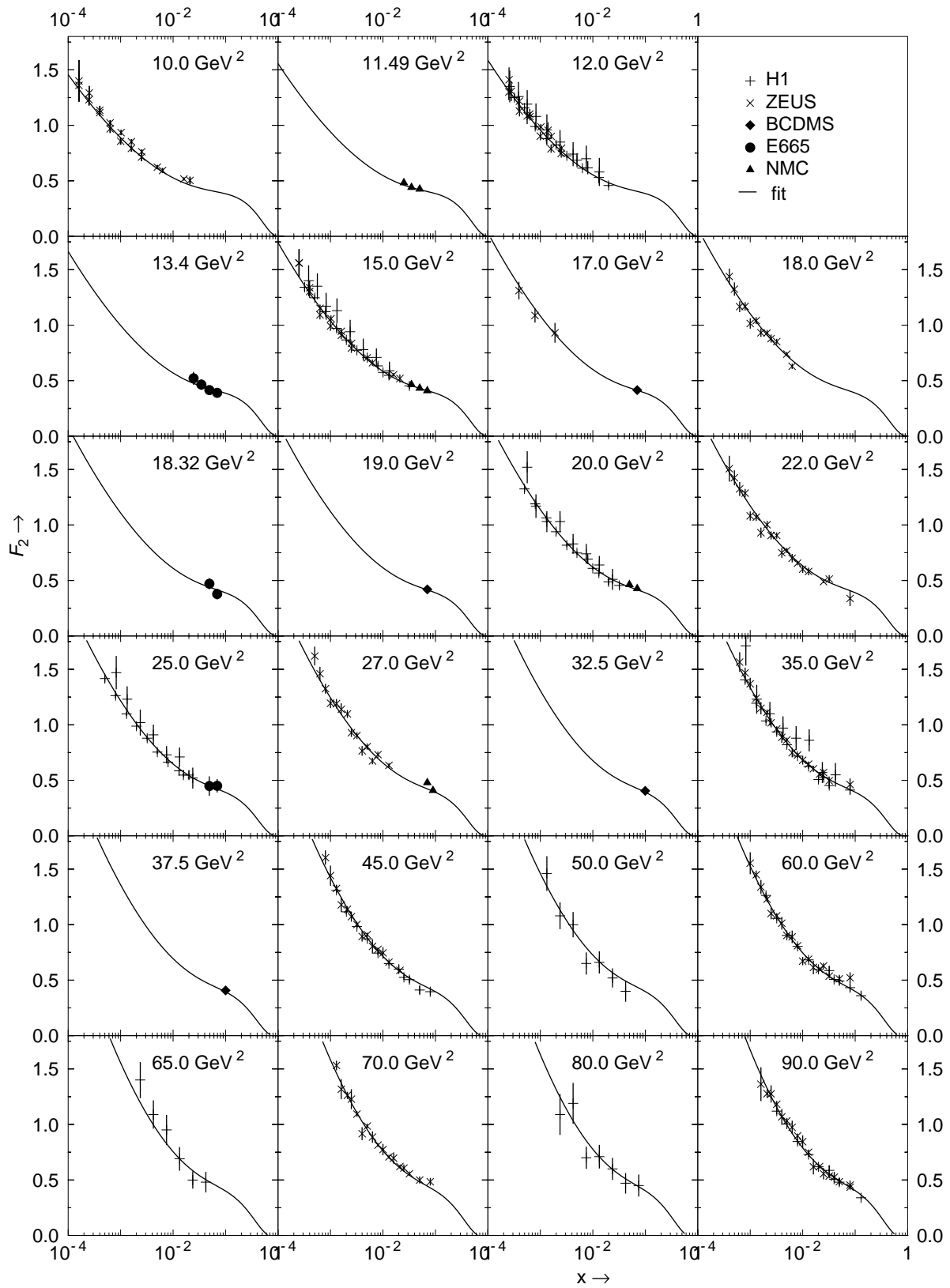


Figure 10.7:  $F_2$  fit using analytical approximation of the residues (low- $Q^2$  values).

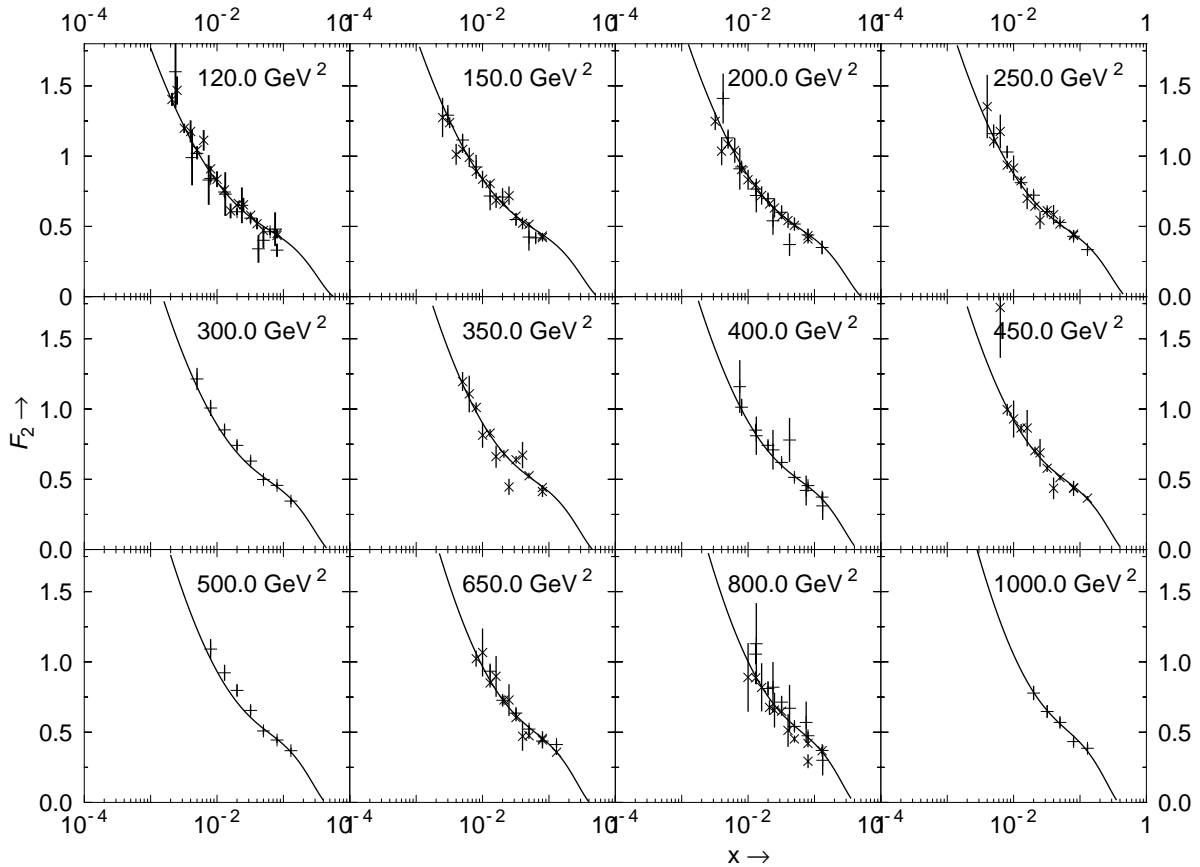


Figure 10.8:  $F_2$  fit using analytical approximation of the residues (high- $Q^2$  values).

quark distributions which are stable as shown in Fig. 10.5. Thus, from the phenomenological point of view, all these distributions provide a correct description of the data and are perfectly acceptable. The differences in the gluon distribution obtained for different values of  $Q_0^2$  must therefore be considered as uncertainties on the gluon distribution. One clearly sees from Fig. 10.6 that even at  $Q^2 = 10 \text{ GeV}^2$ , the uncertainties are very large. These large errors on the gluon distribution at small  $x$  and small  $Q^2$  can be of prime importance in the study of LHC physics. Note also that if we look at the gluon distribution at a scale  $Q_1^2$ , we obtain fewer gluons at small  $x$  when we start evolution at  $Q_1^2$  than when we evolve from  $Q_0^2 < Q_1^2$ . This effect comes from the fact that the DGLAP equation does not take gluon recombination into account.

### 10.5.3 Analytic form factors

As a final step, we have tried to find analytic expressions for the form factors produced by the fit. Actually, it is much easier to work with analytic expressions reproducing the results of Fig. 10.2 than to refit everything for each  $Q_0^2$  values. In the  $Q^2$ -range studied here, we have found that the following expressions, plotted in Fig. 10.2, reproduce very well the form

factors extracted from the DGLAP fit.

$$\begin{aligned}
a_\Sigma &= 0.29 \left( \frac{Q^2}{Q^2 + 123.3} \right)^{0.65} \\
b_\Sigma &= \left[ 0.0048 \log^2 \left( \frac{Q^2}{9.666} \right) - 0.114 \right] \log^2 \left( \frac{Q^2}{9.666} \right) - 0.077 \\
c_\Sigma &= \left[ 0.218 - 0.02 \log^2 \left( \frac{Q^2}{13.1} \right) \right] \log^2 \left( \frac{Q^2}{13.1} \right) - 0.13 \\
d_\Sigma &= 2.66 \log^2 \left( 2.83 + \frac{Q^2}{199.13} \right) \\
d_T &= 0.82 \left( \frac{Q^2}{Q^2 + 301.8} \right)^{0.105} \\
a_G &= 0.779 \exp \left[ 1 - \left( \frac{Q^2}{106.86} \right)^{-0.3625} \right] \\
b_G &= 4.577 \exp \left[ 1 - \left( \frac{Q^2}{133.2} \right)^{-0.4804} \right] \\
c_G &= 5.935 \log^{0.628} \left[ 1.0495 + \left( \frac{Q^2}{47.21} \right)^{1.825} \right] \\
b_1 &= 2.367 + \log^{3.38} \left( 1.0 + \frac{25.63}{Q^2} \right) \\
b_2 &= 4.78 \left( \frac{Q^2}{Q^2 + 181.8} \right)^{0.21}
\end{aligned}$$

Using these analytical expressions, one can compare their predictions with the experimental data. We obtain a  $\chi^2$  of 1.02 per data point, in very good agreement with experimental measurements. The results are presented in Table 10.1 and in Figs. 10.7 and 10.8.

In the above equations, we only wanted to find some analytical expression reproducing the form factors extracted numerically from the DGLAP fits. We have not taken care of their analytical properties in  $Q^2$ . To obtain better expressions, one should find an analytical equation for the form-factors  $Q^2$ -evolution. Since we have seen that the evolved distributions, containing an essential singularity, are numerically close to the triple-pole distributions, one may hope that subleading corrections to the DGLAP equations will stabilise a triple-pole distribution.

Finally, the form factors obtained here are compatible with those from chapter 6 for  $10 \leq Q^2 \lesssim 100 \text{ GeV}^2$ .

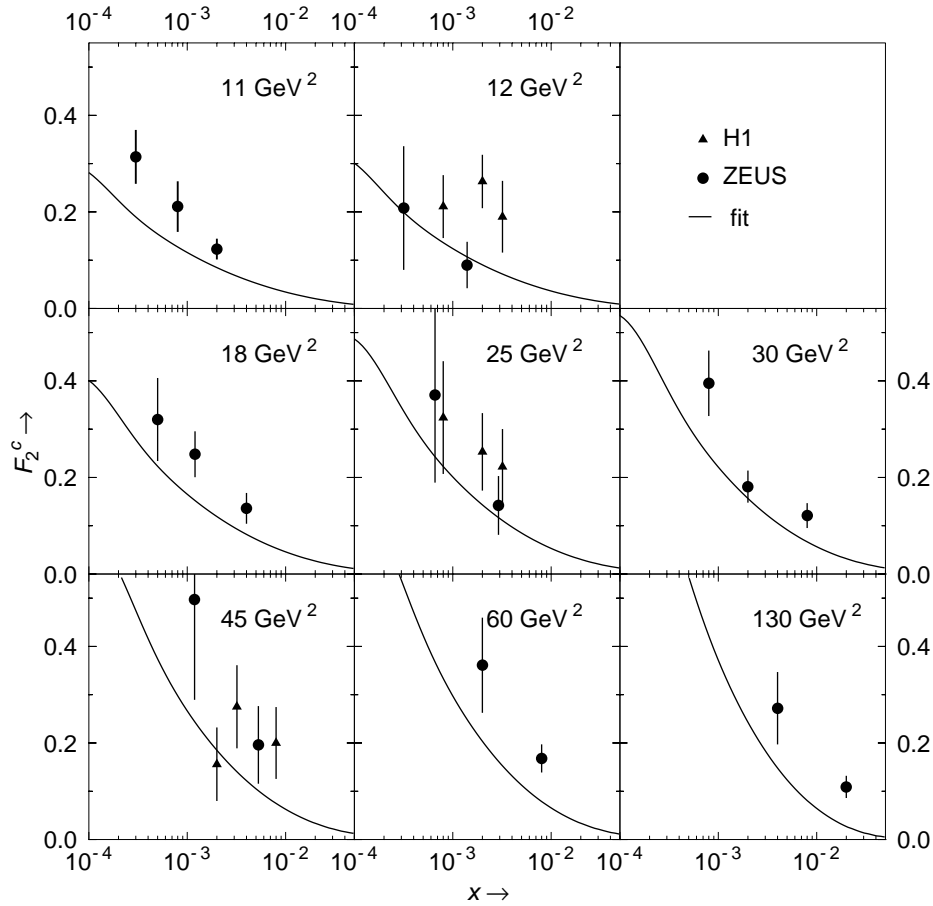


Figure 10.9: Predictions for the charm structure function using our gluon distributions.

#### 10.5.4 $F_2^c$ and $F_L$

Although only  $F_2^p$  is included in the fit, it is interesting to see if our predictions agree with the measurements of  $F_2^c$  [80,90,91] and  $F_L$  [73]. Actually, these quantities are directly sensitive to the gluon distribution and are therefore a good test of our predictions. The charm structure function is given by [63]

$$F_2^c(x, Q^2) = \frac{2e_c^2 \alpha_s(Q^2 + 4m_c^2)}{2\pi} \int_{ax}^1 d\xi g(\xi, Q^2 + 4m_c^2) f(x/\xi, Q^2),$$

<sup>2</sup>At larger  $Q^2$ , the discrepancy comes from the fact that the functional form used in chapter 6 is unable to reproduce the behaviour observed here.

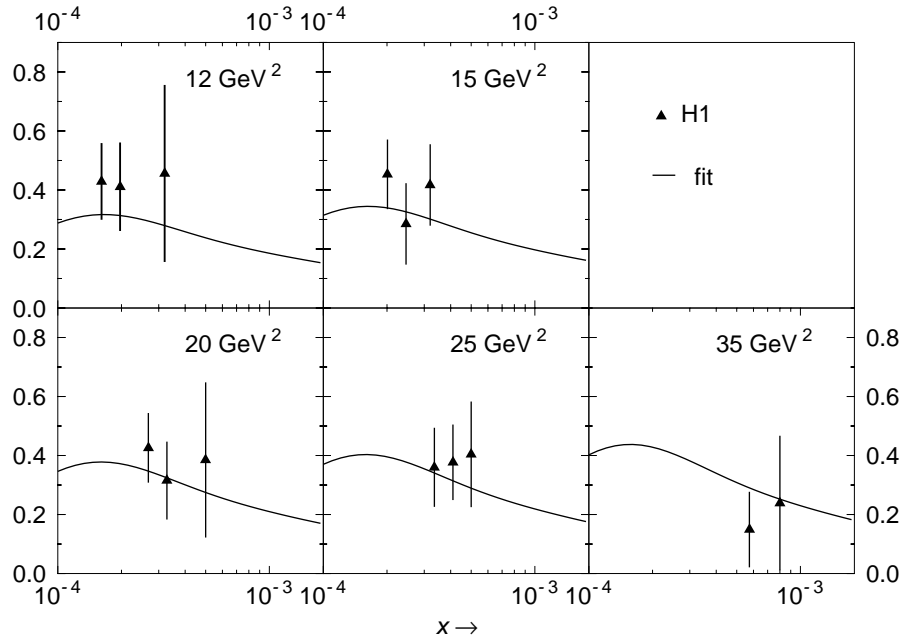


Figure 10.10: Predictions for the longitudinal structure function using our parton distributions.

with

$$\begin{aligned}
 f(x, Q^2) &= v \left[ (4 - \mu)x^2(1 - x) - \frac{x}{2} \right] \\
 &\quad + L \left[ \frac{x}{2} - x^2(1 - x) + \mu x^2(1 - 3x) - \mu^2 z^3 \right], \\
 \mu &= \frac{2m_c^2}{Q^2}, \\
 v &= \sqrt{1 - \frac{2x\mu}{1-x}}, \\
 L &= \log \left( \frac{1+v}{1-v} \right) \\
 a &= 1 + 2\mu.
 \end{aligned}$$

We have adopted a value of 1.3 GeV for the charm quark mass and the predictions for  $F_2^c$  obtained from our model are presented in Fig. 10.9. We see that the data are reasonably reproduced ( $\chi^2/nop = 2.92$ ). Hence, there might be a correction of about 20% to the gluon distribution.

For the case of the longitudinal structure function, we are sensitive both to quarks and gluons:

$$F_L = \sum_{q=u,d,s,c} G_q + \frac{4\alpha_s(Q^2)}{3\pi} \int_x^1 \frac{d\xi}{\xi} \left( \frac{x}{\xi} \right)^2 F_2(\xi, Q^2),$$

where

$$G_q = 2e_q^2 \frac{\alpha_s(Q^2 + 4m_q^2)}{\pi} \int_{ax}^1 d\xi \left(\frac{x}{\xi}\right)^2 g(\xi, Q^2 + 4m_c^2) \left[ \left(1 - \frac{x}{\xi}\right) v - \frac{\mu x}{\xi} L \right]$$

with  $m_u = m_d = m_s = 0$  and  $m_c = 1.3$  GeV. The results obtained from our parton distributions set are shown in Fig. 10.10 and show good agreement with the data ( $\chi^2/nop = 0.413$ ).

## 10.6 Extension to $Q^2 = 0$

Since the method explained in the beginning of this chapter gives us the Regge residues at large scales, one may ask if it is possible to extend the results down to  $Q^2 = 0$ . The main problem here is that, instead of using  $x$  and  $Q^2$ , we must use  $\nu$  and  $Q^2$  if we want to obtain a relevant expression for the total cross section. Of course, we shall only extend the  $F_2^p$  predictions instead of the parton distributions  $T$  and  $\Sigma$ .

As a starting point, we shall not consider the powers of  $(1-x)$  since, at low  $Q^2$ , there are no point inside the Regge domain over  $x = 0.01$ , which means that it is just a correction of a few percents. At low  $Q^2$ , we require that  $F_2$  has the same form as used in chapters 6 and 8

$$\begin{aligned} F_2(\nu, Q^2) &= \frac{Q^2}{4\pi^2\alpha_e} \left\{ A(Q^2) [\log(2\nu) - B(Q^2)]^2 + C(Q^2) + D(Q^2)(2\nu)^{-\eta} \right\} \\ &= \underbrace{\frac{Q^2}{4\pi^2\alpha_e} A(Q^2) \log^2(1/x)}_{a(Q^2)} + \underbrace{\frac{2Q^2}{4\pi^2\alpha_e} A(Q^2) [\log(Q^2) - B(Q^2)] \log(1/x)}_{b(Q^2)} \\ &+ \underbrace{\frac{Q^2}{4\pi^2\alpha_e} \left\{ A(Q^2) [\log(Q^2) - B(Q^2)]^2 + C(Q^2) \right\}}_{c(Q^2)} + \underbrace{\frac{Q^2}{4\pi^2\alpha_e} D(Q^2) (Q^2)^{-\eta} x^\eta}_{d(Q^2)}. \end{aligned} \quad (10.2)$$

The total  $\gamma p$  cross-section is then

$$\sigma_{\gamma p} = A(0) [\log(s) - B(0)]^2 + C(0) + D(0) s^{-\eta}.$$

The unknown functions  $A$ ,  $B$ ,  $C$  and  $D(Q^2)$  are parametrised in the same way as in chapter 6:

$$\begin{aligned} A(Q^2) &= A_a \left( \frac{Q_a^2}{Q^2 + Q_a^2} \right)^{\varepsilon_a}, \\ B(Q^2) &= A_b \left( \frac{Q^2}{Q^2 + Q_b^2} \right)^{\varepsilon_b} + A'_b, \\ C(Q^2) &= A_c \left( \frac{Q_c^2}{Q^2 + Q_c^2} \right)^{\varepsilon_c}, \\ D(Q^2) &= A_d \left( \frac{Q_d^2}{Q^2 + Q_d^2} \right)^{\varepsilon_d}. \end{aligned}$$

Parameter	value	error
$A_b$	69.151	0.055
$Q_a^2$	25.099	0.088
$Q_b^2$	4.943	0.086
$Q_c^2$	0.002468	0.000042
$Q_d^2$	0.01292	0.00074
$\varepsilon_a$	1.5745	0.0046
$\varepsilon_b$	0.08370	0.00052
$\varepsilon_c$	0.92266	0.00019
$\varepsilon_d$	0.3336	0.0029

Table 10.2: Values of the parameters for the low- $Q^2$  fit ( $0 \leq Q^2 \leq Q_{\min}^2$ ).

We shall ask that the form factors  $a$ ,  $b$ ,  $c$  and  $d$  of (10.2) match with the form factors extracted from DGLAP evolution at  $Q^2 = Q_0^2 = 10 \text{ GeV}^2$ . If we use the subscript  $_0$  to refer to the form factors obtained in the beginning of this chapter, this leads to the following relations

$$\begin{aligned}
A(Q_{\min}^2) &= \frac{4\pi^2\alpha_e}{Q_{\min}^2} a_0, \\
B(Q_{\min}^2) &= \log(Q_{\min}^2) - \frac{b_0}{2a_0}, \\
C(Q_{\min}^2) &= \frac{4\pi^2\alpha_e}{Q_{\min}^2} \left( c_0 - \frac{b_0^2}{4a_0} \right), \\
D(Q_{\min}^2) &= \frac{4\pi^2\alpha_e}{Q_{\min}^2} d_0 (Q_{\min}^2)^\eta.
\end{aligned}$$

If we use these relations to fix the parameters  $A_a$ ,  $A'_b$ ,  $A_c$  and  $A_d$ , we find the final form of the small- $Q^2$  form factors:

$$\begin{aligned}
A(Q^2) &= \frac{4\pi^2\alpha_e}{Q_{\min}^2} a_0 \left( \frac{Q_{\min}^2 + Q^2}{Q_a^2 + Q^2} \right)^{\varepsilon_a}, \\
B(Q^2) &= \log(Q_{\min}^2) - \frac{b_0}{2a_0} + A_b \left[ \left( \frac{Q^2}{Q_b^2 + Q^2} \right)^{\varepsilon_b} - \left( \frac{Q_{\min}^2}{Q_b^2 + Q_{\min}^2} \right)^{\varepsilon_b} \right], \\
C(Q^2) &= \frac{4\pi^2\alpha_e}{Q_{\min}^2} \left( c_0 - \frac{b_0^2}{4a_0} \right) \left( \frac{Q_{\min}^2 + Q^2}{Q_c^2 + Q^2} \right)^{\varepsilon_c}, \\
D(Q^2) &= \frac{4\pi^2\alpha_e}{Q_{\min}^2} d_0 (Q_{\min}^2)^\eta \left( \frac{Q_{\min}^2 + Q^2}{Q_d^2 + Q^2} \right)^{\varepsilon_d}.
\end{aligned}$$

If we now want to reinsert the large- $x$  corrections, we need to multiply  $c$  and  $d$  by some

Experiment	$n$	$\chi^2$	$\chi^2/n$
E665	69	59.811	0.867
H1	99	104.924	1.060
NMC	37	28.392	0.767
ZEUS	216	201.790	0.934
$F_2^p$	421	394.916	0.938
$\sigma_{\gamma p}$	30	17.171	0.572
Total	451	412.086	0.914

Table 10.3:  $\chi^2$  resulting from the small- $Q^2$  Regge fit. The results are given for all  $F_2^p$  experiments and for the total cross-section.

power of  $(1-x)$ . This gives

$$\begin{aligned}
\frac{4\pi^2\alpha_e}{Q^2}F_2(x, Q^2) &= A(Q^2) \log(1/x) \{ \log(1/x) + 2 [\log(Q^2) - B(Q^2)] \} \\
&+ \left\{ A(Q^2) [\log(Q^2) - B(Q^2)]^2 + C(Q^2) \right\} (1-x)^{b_1} \\
&+ D(Q^2) \left( \frac{Q^2}{x} \right)^{-\eta} (1-x)^{b_2}.
\end{aligned}$$

These large- $x$  corrections do not modify the expression of the total cross section since, when  $Q^2 \rightarrow 0$

$$1-x = 1 - \frac{2\nu}{Q^2} \rightarrow 1.$$

Moreover, since the large- $x$  corrections are only a few percents effects, we shall keep the exponents  $b_1$  and  $b_2$  constants and equal to their value at  $Q^2 = Q_0^2$ .

Now, we may adjust the parameters in the form factors by fitting  $F_2^p$  in the Regge domain at small values of  $Q^2$  ( $Q^2 \leq Q_{\min}^2$ ) and the total cross-section for  $\sqrt{s} \geq 7$  GeV. The resulting parameters are presented in table 10.2 and the form factor are plotted in Fig. 10.11. As we can see from table 10.3 and from figures 10.12 and 10.18, this gives a very good extension in the soft region (see table 10.3).

## 10.7 $F_2^\gamma$ predictions

One may naturally also ask if the form factors extracted from DGLAP evolution give good results for the  $\gamma\gamma$  interactions if we combine them with the  $t$ -channel-unitarity rules developed in chapter 7. Once again, we shall neglect the powers of  $(1-x)$  which are not a large correction in the Regge domain. Here we shall consider two types of structure functions:  $F_2^\gamma(Q_1^2, Q_2^2)$  where both  $Q_1^2$  and  $Q_2^2$  are greater than 10 GeV<sup>2</sup>, and  $F_2^\gamma(0, Q^2)$  with  $Q^2 \geq 10$  GeV<sup>2</sup>. For the latter case, we shall use the results for the total  $\gamma p$  and  $pp$  cross-sections obtained in chapter 8. In order to apply the  $t$ CU rules, we need again to express  $F_2$  in terms of  $\nu$

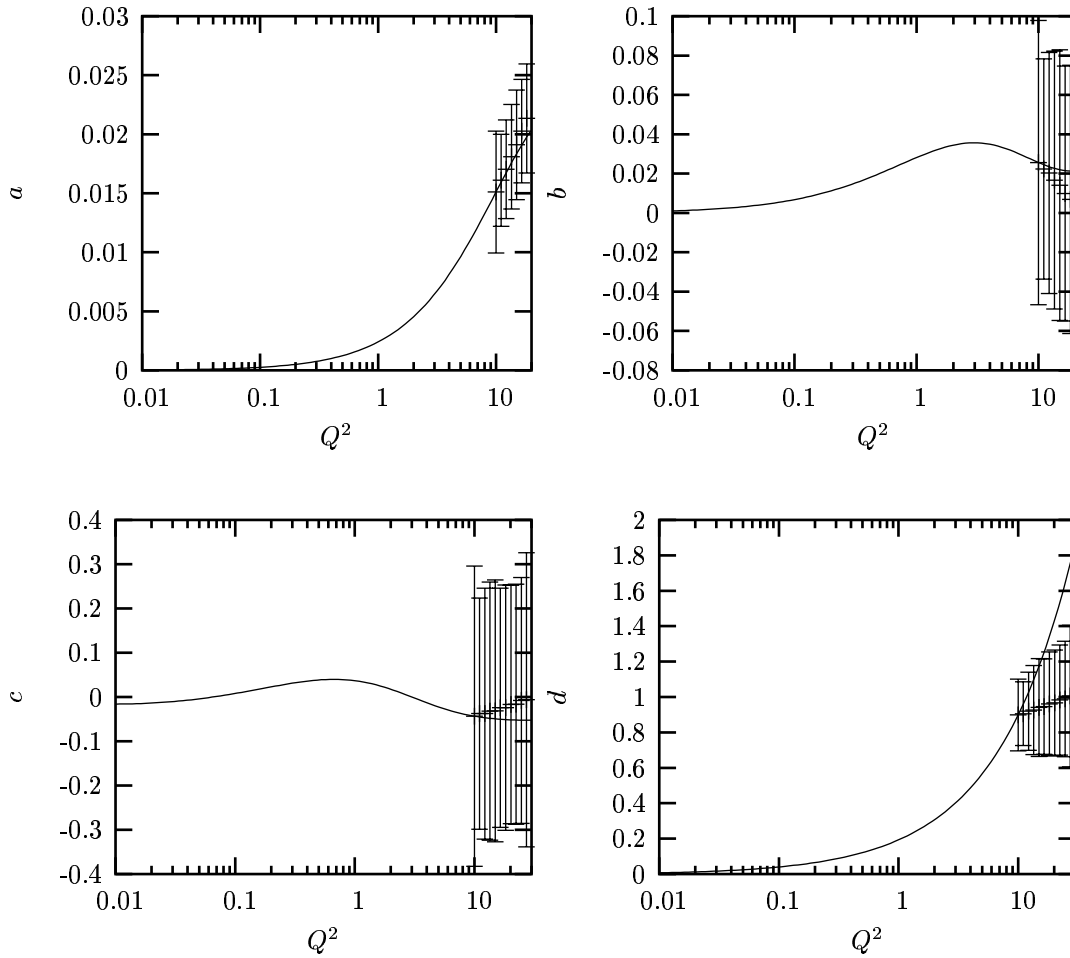
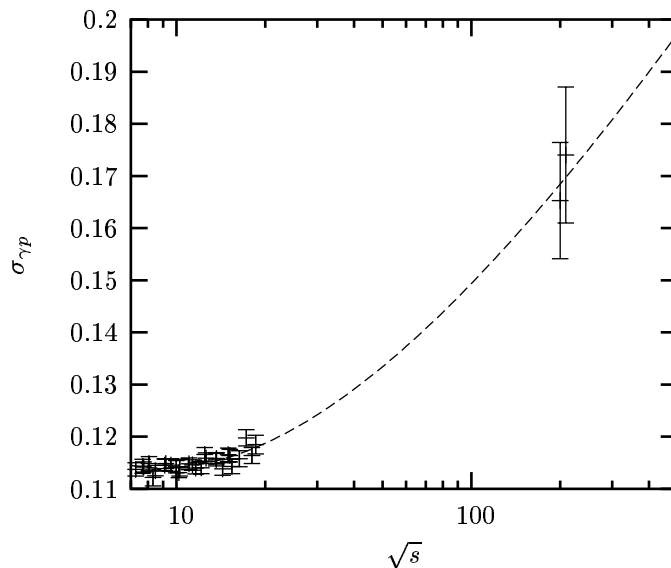


Figure 10.11: Regge theory predictions for the form factors at small values of  $Q^2$ . The lines show the analytical curve for  $0 \leq Q^2 \leq 10 \text{ GeV}^2$  and the points are the results obtained from DGLAP evolution.

and  $Q^2$ . Unfortunately, although we obtain some positive predictions not too far from the experimental data when  $Q_1^2 = 0$ , the predictions for  $Q_1^2 = Q_2^2$  give negative results for  $F_2^\gamma$  as shown in figure 10.13, even if we include the box-diagram contribution.

This problem is very similar to the one encountered in chapter 8 where the form factors obtained from a pure  $\gamma p$  fit needed to be replaced. Actually, the form factor  $B(Q^2)$ , related to the scale in the logarithm, has a positive value in the residues extracted from DGLAP evolution, while some negative value seems required in order to reproduce the  $\gamma\gamma$  interactions.

For this reason, we have re-run the fit and imposed a positive prediction for  $F_2^\gamma(Q_0^2, Q_0^2)$ . The  $\chi^2$  gets slightly degraded and still grows with  $Q^2$ . As shown in figures 10.14 and 10.15, we still obtain acceptable predictions for the photon structure function, when  $Q_1^2 = 0$ , but, although  $F_2^\gamma$  is positive, the result for  $Q_1^2 = Q_2^2$  is not very good.

Figure 10.12: Fit for the total  $\gamma p$  cross-section.

A possible solution to this problem is to include the  $F_2^\gamma$  data in the fit<sup>3</sup>. We have not done it in details but we can give some elements that may help future investigations.

If we want to include  $\gamma\gamma$  data in the DGLAP fit using the factorisation relations, we first need to check that the DGLAP evolution (see Figure 10.16 for a picture of the DGLAP evolution in the proton and photon cases) is compatible with the factorisation theorem. This means that, assuming that the factorisation theorem gives  $F_2^\gamma$  at the initial scale  $Q_0^2 \gg Q_1^2$

$$F_2^\gamma(j, Q_1^2, Q_0^2) = \frac{\mathcal{A}_{\gamma p}(j, Q_1^2)}{\mathcal{A}_{pp}(j)} F_2^p(j, Q_0^2),$$

we must check that we have

$$F_2^\gamma(j, Q_1^2, Q_2^2) = \frac{\mathcal{A}_{\gamma p}(j, Q_1^2)}{\mathcal{A}_{pp}(j)} F_2^p(j, Q_2^2)$$

where  $F_2^\gamma(j, Q_1^2, Q_2^2)$  and  $F_2^p(j, Q_2^2)$  are obtained by DGLAP evolution with  $Q_0^2$  as initial scale. As a first step, we must note that the factorisation theorem uses the Mellin transform with respect to  $\nu$  while the solution of the DGLAP equation is usually obtained using the Mellin transform with respect to  $x$ . For a parton distribution  $f$ , the DGLAP evolution equation gives<sup>4</sup>

$$\tilde{f}(j, Q^2) = \tilde{f}(j, Q_0^2) \exp[C\gamma(j)\tau]$$

with  $C = \frac{6}{33-2n_f}$  and  $\tau = \log\left[\frac{\alpha_s(Q_0^2)}{\alpha_s(Q^2)}\right]$ . Using the relation (B.2), we have

$$\hat{f}(j, Q^2) = \hat{f}(j, Q_0^2) \exp[C\gamma(j)\tau]$$

<sup>3</sup>Of course, the fact that our predictions are too low can also mean that we need additional singularities.

<sup>4</sup> $\tilde{f}$  (resp.  $\hat{f}$ ) refers to the Mellin transform of  $f$  with respect to  $x$  (resp.  $\nu$ ).

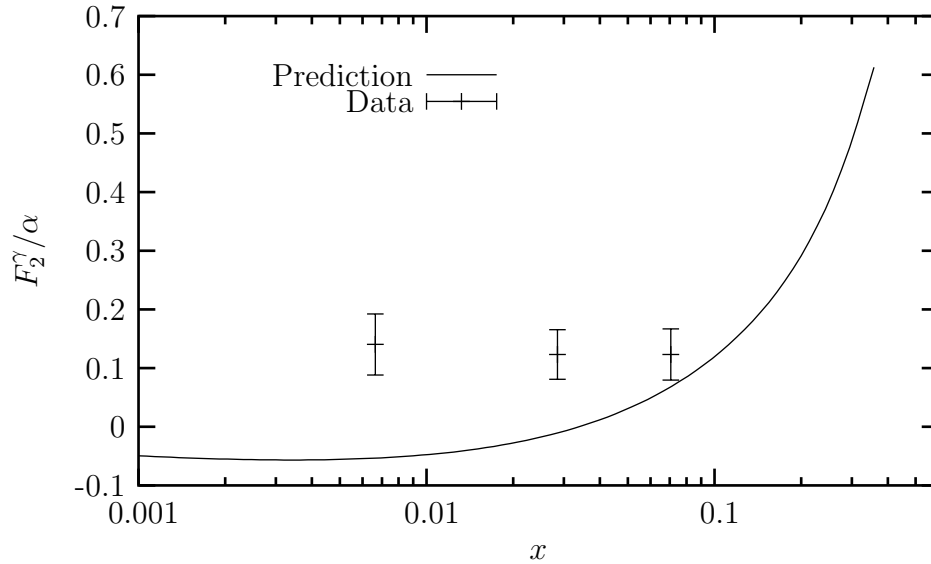


Figure 10.13: Predictions for  $F_2^\gamma$  with  $Q_1^2 = Q_2^2 = 14 \text{ GeV}^2$  using the form factors extracted from DGLAP evolution.

showing that the solution of the DGLAP evolution equation keeps the same form if we use the Mellin transform with respect to  $\nu$ . If we introduce<sup>5</sup>

$$\gamma(j) = \begin{pmatrix} \gamma_{qq}(j) & 2n_f \gamma_{qg}(j) \\ \gamma_{qg}(j) & 2n_f \gamma_{gg}(j) \end{pmatrix}, \quad \vec{q}^p(j, Q^2) = \begin{pmatrix} \Sigma(j, Q^2) \\ G(j, Q^2) \end{pmatrix} \quad \text{and} \quad \vec{q}^{\gamma(j, Q_1^2, Q^2)} = \begin{pmatrix} \Sigma(j, Q_1^2, Q^2) \\ G(j, Q_1^2, Q^2) \end{pmatrix}$$

the solution of the DGLAP equation for the flavour-singlet distribution can be written

$$\begin{aligned} \vec{q}^p(j) &= \exp[C\gamma(j)\tau] \vec{q}_0^p(j), \\ \vec{q}^{\gamma(j, Q_1^2)} &= \exp[C\gamma(j)\tau] \vec{q}_0^{\gamma(j, Q_1^2)}, \end{aligned} \quad (10.3)$$

where the index  $_0$  refers to the distribution taken at  $Q^2 = Q_0^2$  and with  $Q^2, Q_0^2 \gg Q_1^2$ . Since only the quark distribution appears in  $F_2$ , we extract its evolution from (10.3). If the matrix  $\mathbf{M}$  diagonalises  $\gamma$  (*i.e.*  $\mathbf{M}^{-1}\gamma\mathbf{M} = \text{diag}(\gamma_1, \gamma_2)$ ), (10.3) can be rewritten

$$q_i = M_{ik} e^{C\gamma_k \tau} (M^{-1})_{kl} q_{0,l},$$

for the proton and the photon. On the other hand, the flavour-non-singlet quark distribution evolves according to

$$T = e^{C\gamma_{NS}\tau} T_0,$$

with  $\gamma_{NS} = \gamma_{qq}$ . Using these notations, the photon structure function becomes

$$F_2^\gamma(j, Q_1^2, Q^2) = \frac{3}{18} e^{C\gamma_{NS}\tau} T_0^\gamma(j, Q_1^2) + \frac{5}{18} M_{ik} e^{C\gamma_k \tau} (M^{-1})_{kl} q_{0,l}^\gamma(j, Q_1^2),$$

<sup>5</sup>One may introduce the quark and gluon distributions inside the photon. These distributions are of course different of their equivalent inside the proton but evolve in  $Q^2$  with the same splitting matrix.

and we must compare this result with

$$F_2^\gamma(j, Q_1^2, Q^2) = \frac{\mathcal{A}_{\gamma p}(j, Q_1^2)}{\mathcal{A}_{pp}(j)} \left( \frac{3}{18} e^{C\gamma_{NS}\tau} T_0^p(j) + \frac{5}{18} M_{ik} e^{C\gamma_k\tau} (M^{-1})_{kl} q_{0,l}^p(j) \right)$$

in order to check that DGLAP evolution is consistent with the factorisation theorem. Since, in the Regge domain, we have  $T \ll \Sigma, G$ , we shall neglect the contribution from  $T$ . We must thus prove that

$$M_{ik} e^{C\gamma_k\tau} (M^{-1})_{kl} q_{0,l}^\gamma(j, Q_1^2) = \frac{\mathcal{A}_{\gamma p}(j, Q_1^2)}{\mathcal{A}_{pp}(j)} M_{ik} e^{C\gamma_k\tau} (M^{-1})_{kl} q_{0,l}^p(j),$$

which gives

$$M_{ik} e^{C\gamma_k\tau} (M^{-1})_{kl} \left[ q_{0,l}^\gamma(j, Q_1^2) - \frac{\mathcal{A}_{\gamma p}(j, Q_1^2)}{\mathcal{A}_{pp}(j)} q_{0,l}^p(j) \right] = 0$$

and

$$q_{0,l}^\gamma(j, Q_1^2) - \frac{\mathcal{A}_{\gamma p}(j, Q_1^2)}{\mathcal{A}_{pp}(j)} q_{0,l}^p(j) = 0.$$

This means that, under the assumption  $T = 0$ , the DGLAP evolution conserves the factorisation relations if and only if the factorisation theorem holds for the gluon distribution at  $Q^2 = Q_0^2$ .

Note also that, as we want to stay in the DGLAP regime, we have required  $Q^2 \gg Q_1^2$  for the  $\gamma^*\gamma^*$  interactions. Therefore, if we start the evolution at a scale  $Q_0^2$ , the only way to obtain  $F_2^\gamma(j, Q^2, Q^2)$  is to evolve the proton parton densities to the scale  $Q^2$  and to use the  $t$ CU relations. If we compute the photon densities at  $Q^2 = Q_0^2$  using the factorisation theorem, the DGLAP evolution cannot give  $F_2^\gamma(j, Q^2, Q^2)$  because we have not strong ordering between the top and the bottom of the parton ladder. If we use the factorisation theorem combined with DGLAP evolution to predict  $F_2^\gamma$  with  $Q_1^2 = Q_2^2$ , one includes contributions shown in Figure 10.17(a) and miss those from Figure 10.17(b) with no ordering. Adding these diagrams may lead to good predictions for the  $F_2^\gamma(Q_1^2 = Q_2^2)$  measurements. Finally, if  $Q_1^2 \ll Q_2^2$ , only diagrams from Figure 10.17(a) with  $Q_1^2 = \mu^2$  contribute and we expect good predictions as is indeed the case.

## 10.8 Conclusion

In summary, we have seen that, if we assume that Regge theory can be applied at large  $Q^2$ , DGLAP evolution can be used to extract the residues of the triple-pole pomeron if we adopt the following strategy: we choose triple-pole distributions both for quarks and gluons at an initial scale  $Q_0^2$  and we evolve them using the DGLAP equation. A comparison with the experimental data gives the residues of the triple-pole pomeron at the scale  $Q_0^2$ . In order to keep the same data points when  $Q_0^2$  varies, we evolve the initial distribution both forwards and backwards between  $Q_{\min}^2$  and  $Q_{\max}^2$ . We have repeated that fit for various values of  $Q_0^2$  resulting in smooth form factors for the triple-pole residues.

In this model, quarks and gluons have the same singularity structure, as suggested by Regge theory. The essential singularity generated by DGLAP evolution appears to be a good

numerical approximation to a triple pole for the  $F_2$  structure function. For the gluons, we found that there are quite large uncertainties in the gluon distribution at small  $x$  and small  $Q^2$ . These uncertainties should certainly be taken into account in LHC phenomenology.

We were also able to find analytic expressions for our form factors. A comparison of these expressions with experimental data gives a  $\chi^2$  per point of 1.02, which proves the very good agreement between pQCD and Regge theory. We have also checked that our gluon distribution was acceptable by comparing our predictions for  $F_2^c$  and  $F_L$  with the H1 and ZEUS measurements.

Fitting the parton distributions up to  $x = 1$  involves many complications, therefore we used the GRV98 parametrisation for the large- $x$  behaviour. As pointed out previously, this does not influence the small- $x$  distributions much. Extension of this model up to  $x = 1$  is left for future work.

Once we know the  $F_2$  form factors extracted from DGLAP evolution, we have seen that it is possible to extend them down to  $Q^2 = 0$  using parametrisations from Regge theory.

In section 10.7, we have seen that this method, combined with the  $t$ CU relations, can be used to predict  $F_2^\gamma$  with  $Q_1^2 = 0$  but fails when  $Q_1^2 = Q_2^2$ . This problem may come from the fact that we do not include  $\gamma\gamma$  in the analysis, from a problem of ladder resummation or from the details of the analytic form for the pomeron.

Finally, we used DGLAP evolution to *extract* the residues from the data. As we have seen, these are smooth functions of  $Q^2$  and give numerical predictions close to the DGLAP essential singularity. It should therefore be of prime interest to find an equation which stabilises the triple-pole singularity and keeps the correct large- $Q^2$  behaviour.

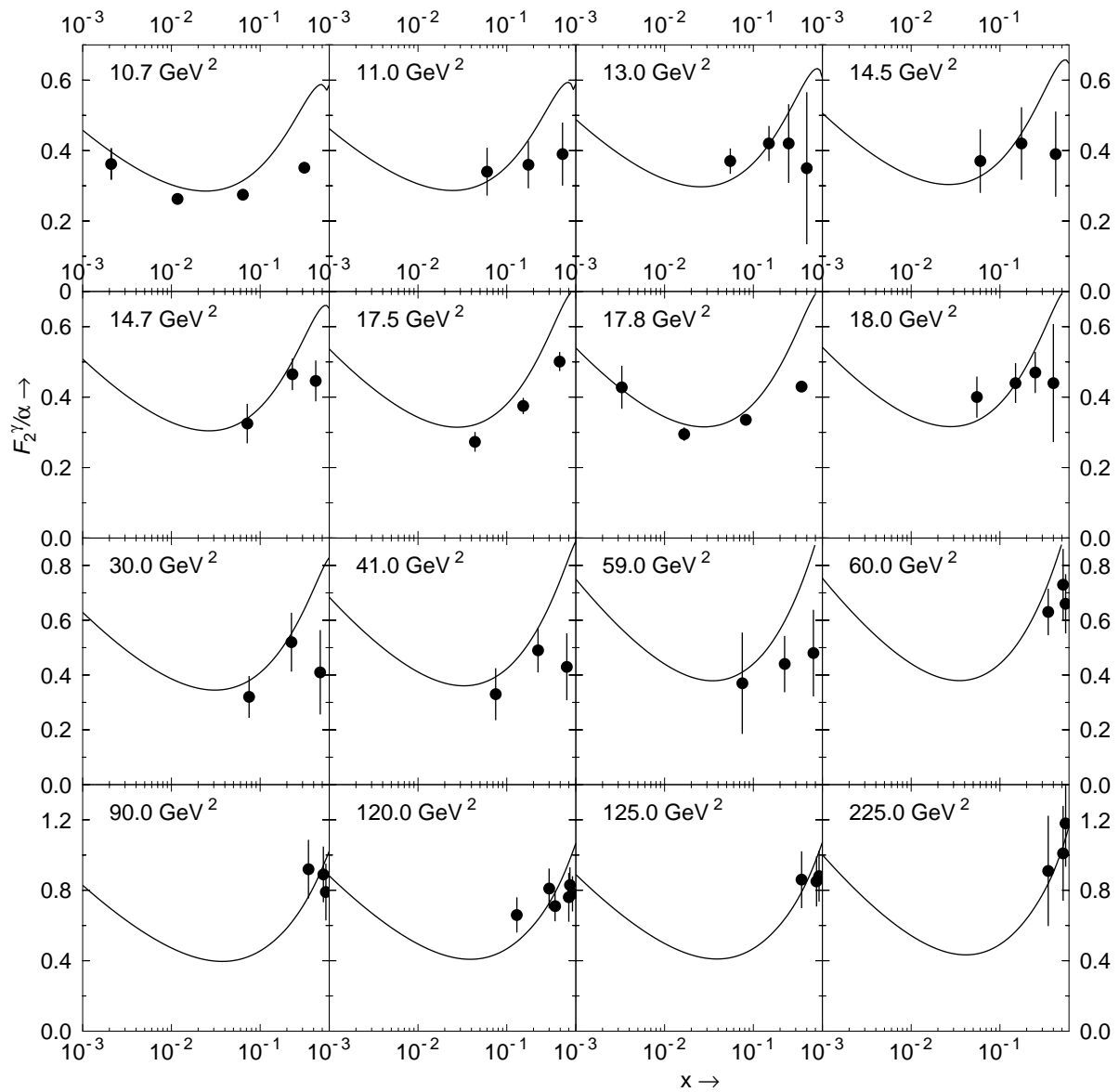


Figure 10.14: Predictions for the photon structure function  $F_2^\gamma(Q^2, 0)$ , obtained from  $t\text{CU}$  rules and including the box-diagram contribution.

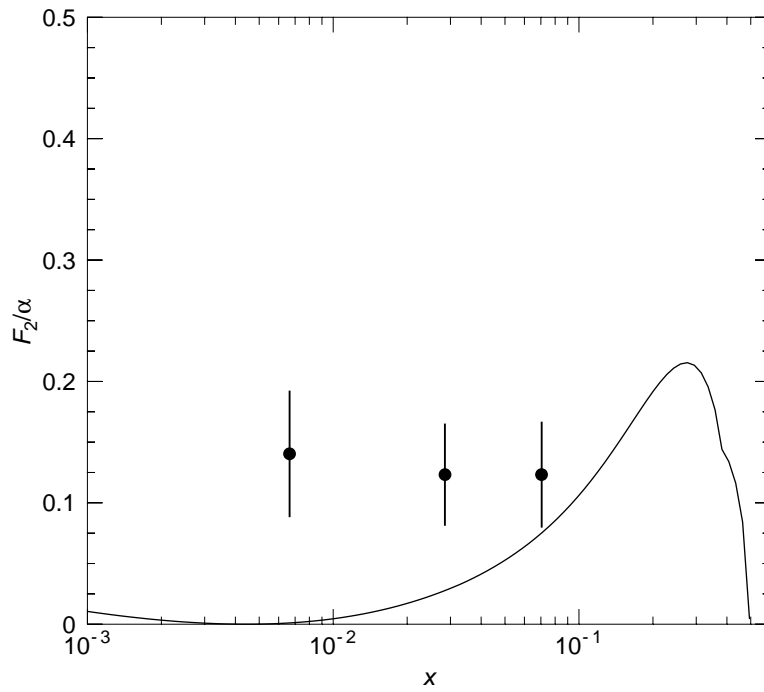


Figure 10.15: Predictions for the photon structure function  $F_2^\gamma(14, 14)$ , obtained from  $t$ CU rules and including the box-diagram contribution.

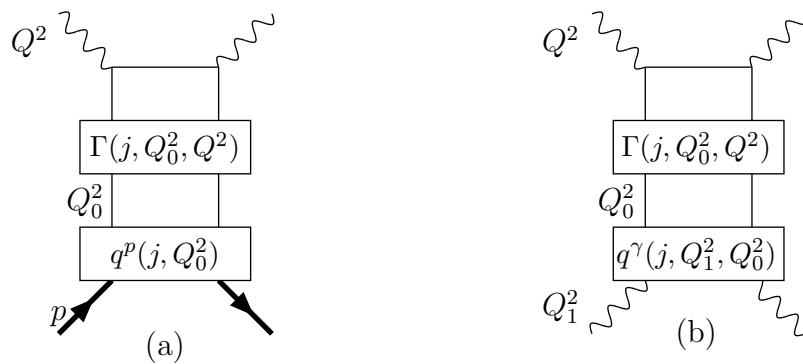


Figure 10.16: DGLAP evolution (a) for  $F_2^p(j, Q^2)$  with  $m_p^2 \ll Q_0^2 \ll Q^2$  and (b) for  $F_2^\gamma(j, Q_1^2, Q_2^2)$  with  $Q_1^2 \ll Q_0^2 \ll Q_2^2$ .

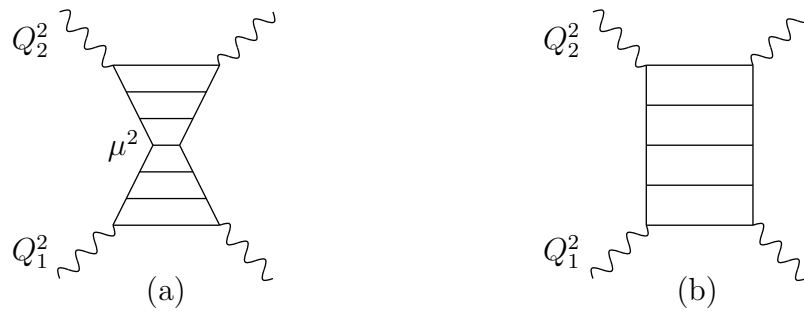


Figure 10.17: Diagram contributing to  $F_2^\gamma$ : (a) with  $k^2$ -ordering ( $\mu^2 \ll Q_1^2, Q_2^2$ ) and (b) without ordering. Note that the size of the rungs symbolises the scales.

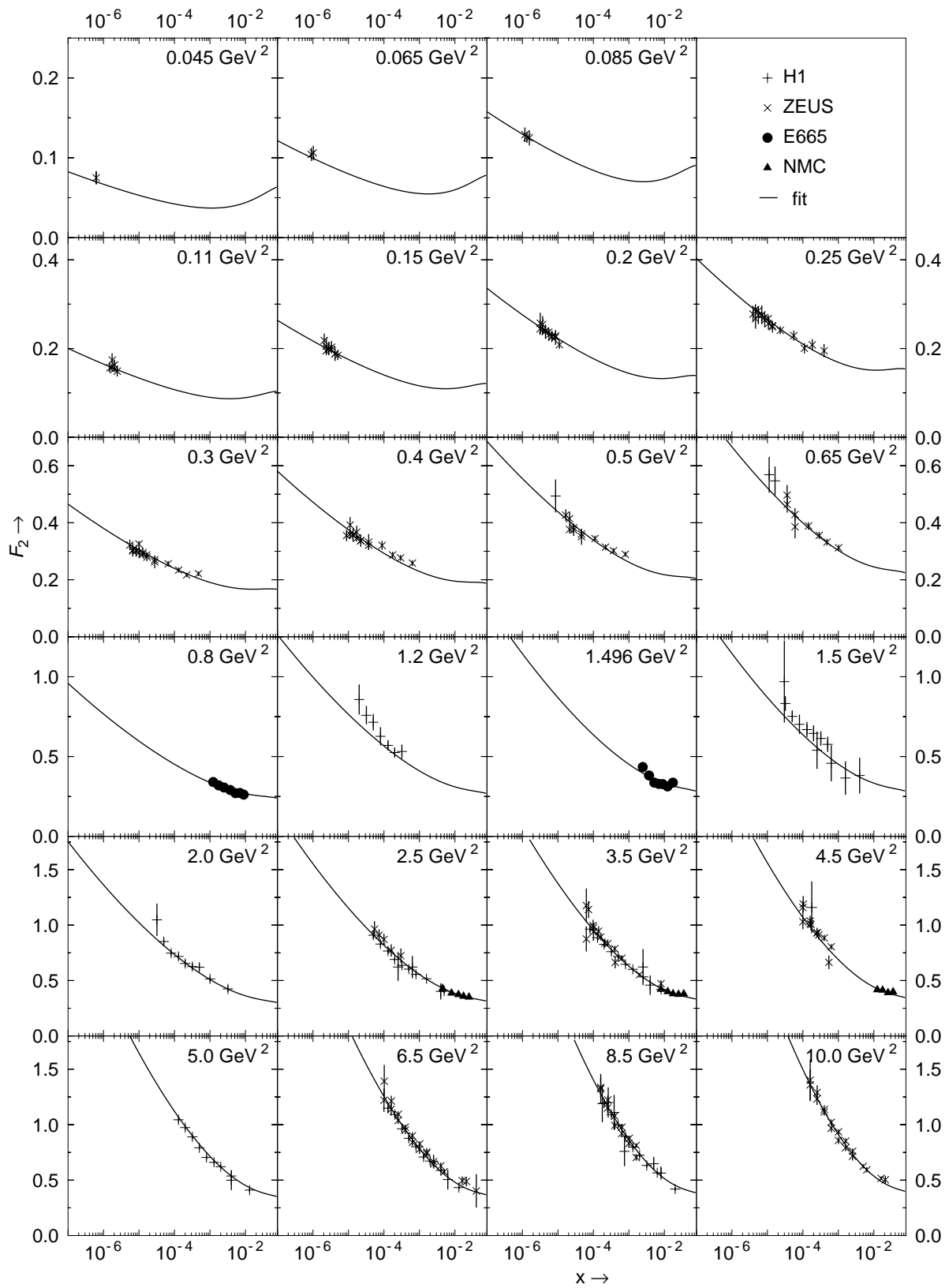


Figure 10.18:  $F_2^p$  fit obtained by extending the DGLAP predictions for residues to  $Q^2 \leq 10 \text{ GeV}^2$ .



# Chapter 11

## Global QCD fit

As pointed out at the end of chapter 9, it is to replace the GRV parton distributions at large  $x$  by some parametrisation such as for example a power of  $(1 - x)$ . If we do so, we must not only concentrate on the Regge domain but also on the large- $x$  experimental measurements, including other experiments like  $\gamma^*d$  scattering or the neutrino data. In this way, our approach is very close to the global fits. We shall fit all structure functions over the whole  $x$  range at all scales greater than  $Q_0^2$ . This will allow us to extract the parton distribution functions, which will be parametrised in such a way that they agree with Regge theory at small values of  $x$ .

### 11.1 Fitted and evolved quantities

If we want to extend the parametrisation introduced in chapter 9 up to  $x = 1$ , we cannot only restrict ourselves to  $F_2^p$ . In order to have a good determination of the valence quarks and of the sea asymmetry, we also need to include other structure functions, measured in the large- $x$  region. In this global fit, we thus include the following quantities:

- The proton structure function  $F_2^p$ : this is by far the most important type of experimental data. Moreover, it is nearly the only one to contribute to the fit in the small- $x$  or in the high- $Q^2$  region.
- The deuteron structure function  $F_2^d$ : as we shall see, these data allow the determination of the sea asymmetry. Many points are available in the large- and middle- $x$  regions, where the sea asymmetry is expected to be large.
- The neutrino structure functions  $F_2^{\nu N}$  and  $xF_3^{\nu N}$ : these data, in which most of the points are at large values of  $x$ , are important to fix the strange quark and the valence quark distributions. Note that the data considered here are averaged over neutrinos and anti-neutrinos.
- The  $F_2^n/F_2^p$  measurements: these data constrain the valence quark distributions and the sea asymmetry.

Once we know which experiments are fitted, we must find which quantities need to be evolved. Since the  $Q^2$  range under consideration in global fits extends up to 30000 GeV<sup>2</sup>, we need to consider 5 quark flavours:  $u$ ,  $d$ ,  $s$ ,  $c$  and  $b$ . As we have learned in chapter 3, it is easier to perform linear combinations of the quark distributions. Here, we shall use 6 flavour-non-singlet distributions

$$\begin{aligned}
xu_V &= x(u - \bar{u}), \\
xd_V &= x(d - \bar{d}), \\
T_3 &= x(u^+ - d^+), \\
T_8 &= x(u^+ + d^+ - 2s^+), \\
T_{15} &= x(u^+ + d^+ + s^+ - 3c^+), \\
T_{24} &= x(u^+ + d^+ + s^+ + c^+ - 4b^+),
\end{aligned} \tag{11.1}$$

where  $q^+ = q + \bar{q}$ . Note that since the proton does not contain strange, charm or bottom valence quarks, we have  $s = \bar{s}$ ,  $c = \bar{c}$  and  $b = \bar{b}$ . At leading order, the  $Q^2$  evolution of each of these distributions is given by the DGLAP equation<sup>1</sup> with the splitting  $xP_{qq}(x)$ . In addition to the non-singlet distributions, we still have the singlet quark distribution

$$\Sigma = x(u^+ + d^+ + s^+ + c^+ + b^+)$$

which evolves coupled to the gluon distribution  $G = xg$ , with the full splitting matrix

$$\begin{pmatrix} xP_{qq}(x) & 2n_f xP_{qg}(x) \\ xP_{gq}(x) & xP_{gg}(x) \end{pmatrix}.$$

It is also important to point out that for  $Q^2 \leq 4m_q^2$ , the quark  $q$  does not enter into the evolution equations.

If we invert the relations (11.1) and express the quark densities  $q^+$  in terms of the evolved quantities, we obtain

$$\begin{aligned}
xu^+ &= \frac{1}{60}(12\Sigma + 3T_{24} + 5T_{15} + 10T_8 + 30T_3), \\
xd^+ &= \frac{1}{60}(12\Sigma + 3T_{24} + 5T_{15} + 10T_8 - 30T_3), \\
xs^+ &= \frac{1}{60}(12\Sigma + 3T_{24} + 5T_{15} - 20T_8), \\
xc^+ &= \frac{1}{20}(4\Sigma + T_{24} - 5T_{15}), \\
xb^+ &= \frac{1}{5}(\Sigma - T_{24}).
\end{aligned}$$

Now, we can of course write the structure functions considered here in terms of the parton distributions or in terms of the flavour-singlet and flavour-non-singlet distributions<sup>2</sup>. If, for

<sup>1</sup>We use once again the LO DGLAP evolution.

<sup>2</sup>At leading order, the quark coefficient functions are proportional to  $\delta(1-x)$  and the gluon coefficient function vanishes.

the sake of clarity, we include other quantities like the neutron structure function, this gives

$$\begin{aligned}
F_2^p &= \frac{4x}{9}(u^+ + c^+) + \frac{x}{9}(d^+ + s^+ + b^+) \\
&= \frac{1}{90}(22\Sigma + 3T_{24} - 5T_{15} + 5T_8 + 15T_3), \\
F_2^n &= \frac{4x}{9}(d^+ + c^+) + \frac{x}{9}(u^+ + s^+ + b^+) \\
&= \frac{1}{90}(22\Sigma + 3T_{24} - 5T_{15} + 5T_8 - 15T_3), \\
F_2^d &= \frac{F_2^p + F_2^n}{2} \\
&= \frac{5x}{18}(u^+ + d^+) + \frac{4x}{9}c^+ + \frac{x}{9}(s^+ + b^+) \\
&= \frac{1}{90}(22\Sigma + 3T_{24} - 5T_{15} + 5T_8),
\end{aligned}$$

and for the neutrino structure functions

$$\begin{aligned}
F_2^{\nu p} &= 2x(d + s + b + \bar{u} + \bar{c}), \\
F_2^{\nu n} &= 2x(u + s + b + \bar{d} + \bar{c}), \\
F_2^{\bar{\nu} p} &= 2x(u + c + \bar{d} + \bar{s} + \bar{b}), \\
F_2^{\bar{\nu} n} &= 2x(d + c + \bar{u} + \bar{s} + \bar{b}), \\
xF_3^{\nu p} &= 2x(d + s + b - \bar{u} - \bar{c}), \\
xF_3^{\nu n} &= 2x(u + s + b - \bar{d} - \bar{c}), \\
xF_3^{\bar{\nu} p} &= 2x(u + c - \bar{d} - \bar{s} - \bar{b}), \\
xF_3^{\bar{\nu} n} &= 2x(d + c - \bar{u} - \bar{s} - \bar{b}),
\end{aligned}$$

If we average over proton and neutron targets, we obtain the neutrino-nucleon structure functions<sup>3</sup>

$$\begin{aligned}
F_2^{\nu N} = F_2^{\bar{\nu} N} &= x(u^+ + d^+ + s^+ + c^+ + b^+), \\
xF_3^{\nu N} &= x(u_V + d_V + s^+ - c^+ + b^+), \\
xF_3^{\bar{\nu} N} &= x(u_V + d_V - s^+ + c^+ - b^+).
\end{aligned}$$

We may finally average over neutrinos and anti-neutrinos, which leads to

$$\begin{aligned}
F_2^{(\bar{\nu})N} &= x(u^+ + d^+ + s^+ + c^+), \\
&= \Sigma, \\
xF_3^{(\bar{\nu})N} &= x(u_V + d_V).
\end{aligned}$$

---

<sup>3</sup>Neutrino experiments are often performed with heavy nuclei which means that the averaged structure function is measured.

## 11.2 Initial parametrisation

If we want to perform a DGLAP evolution, we need to fix the parton distribution functions at an initial scale  $Q_0^2$ . Following the same ideas as in chapter 9, we shall parametrise each quark distribution as the sum of a triple-pole pomeron term and an  $a_2/f$ -reggeon term. In addition, each distribution will be multiplied by a power of  $(1-x)$ , to ensure that the parametrisation extended to  $x=1$  goes to 0 when  $x \rightarrow 1$ . This leads to the following parametrisation

$$xq(x, Q_0^2) = [A_q \log^2(1/x) + B_q \log(1/x) + C_q + D_q x^\eta] (1-x)^{b_q},$$

with<sup>4</sup>  $q = u_V, d_V, u_s, d_s, s_s, c_s$  and  $g$ . Fortunately, we can restrict many of the 35 parameters introduced here:

- First of all, the charm (bottom) distribution will be set to zero for  $Q^2 \leq 4m_c^2$  ( $Q^2 \leq 4m_b^2$ ). We shall therefore take  $Q_0^2 \leq 4m_c^2$  so that we can set  $c(x, Q_0^2) = 0$  and  $b(x, Q_0^2) = 0$ . In other words, we have  $T_{15}(x, Q^2) = \Sigma(x, Q^2)$  for  $Q^2 \leq 4m_c^2$  and  $T_{24}(x, Q^2) = \Sigma(x, Q^2)$  for  $Q^2 \leq 4m_b^2$ .
- The pomeron does not distinguish between quarks and anti-quarks. This means that the valence distributions  $u_V$  and  $d_V$  do not contain a pomeron term.
- The pomeron, having vacuum quantum numbers, is insensitive to the quark flavour. Thus, the only parameter through which the quark flavour may influence the pomeron is its mass. In other words, the couplings  $A_q, B_q$  and  $C_q$  are functions of  $Q^2$  and  $m_q^2$  only. Consequently, the pomeron contributions to the  $u_s$  and  $d_s$  densities are the same. Assuming that the strange mass is very small compared to the virtualities  $Q^2$  under consideration, we shall also take the same pomeron contribution in  $s_s$ .

$$\begin{aligned} A_u &= A_d = A_s = A, \\ B_u &= B_d = B_s = B, \\ C_u &= C_d = C_s = C. \end{aligned}$$

- Once again, we shall assume that the reggeon, being mainly constituted of quarks, does not contribute to the gluon distribution. The parameter  $D_g$  will thus<sup>5</sup> be set to 0.
- We know from [64] that, at large  $x$ , the following behaviour is stable against DGLAP evolution

$$\begin{aligned} \Sigma &\sim (1-x)^b, \\ G &\sim \frac{(1-x)^{b+1}}{\log\left(\frac{1}{1-x}\right)}. \end{aligned}$$

---

<sup>4</sup>The sea distribution  $q_s$  is simply  $\frac{1}{2}q^+$ .

<sup>5</sup>If we do not impose  $D_g = 0$ , the parameter stays small in the fit.

The denominator  $\log(1-x)$  in the gluon distribution does not have a good behaviour at small  $x$  so we have not included it<sup>6</sup>. Nevertheless, we shall impose

$$\begin{aligned} b_u &= b_d = b_s = b, \\ b_g &= b + 1. \end{aligned}$$

- If we look at the large- $x$  data, we can see that if we only use  $Dx^\eta(1-x)^b$  for the valence quarks, the resulting distribution is too spread, or has a peak at too small a value of  $x$ . In order to solve that problem, we have multiplied the valence-quark distributions by a factor  $(1 + \gamma_q x)$ .
- Finally, we still need to impose sum-rules. The quark number conservation can be used to fix the valence-quark normalisation factors. If we write

$$A_{uV} = \frac{2}{N_u} \quad \text{and} \quad A_{dV} = \frac{1}{N_d},$$

we find

$$N_q = \frac{\Gamma(b_q + 1)\Gamma(\eta)}{\Gamma(\eta + b_q + 1)} \left( 1 + \frac{\gamma_q \eta}{\eta + b_q + 1} \right). \quad (11.2)$$

The momentum sum-rule is used to fix the constant term  $C_g$  in the gluon distribution. Although all functions involved are analytically integrable, the resulting expression for  $C_g$  is quite complicated and we give it in Appendix D.

Taking all these considerations into account, we obtain the following parametrisation for the initial distributions

$$xu_V = \frac{2}{N_u^*} x^\eta (1 + \gamma_u x) (1-x)^{b_u}, \quad (11.3)$$

$$xd_V = \frac{1}{N_d^*} x^\eta (1 + \gamma_d x) (1-x)^{b_d}, \quad (11.4)$$

$$xu_s = [A \log^2(1/x) + B \log(1/x) + C + D_u x^\eta] (1-x)^b, \quad (11.5)$$

$$xd_s = [A \log^2(1/x) + B \log(1/x) + C + D_d x^\eta] (1-x)^b, \quad (11.6)$$

$$xs_s = [A \log^2(1/x) + B \log(1/x) + C + D_s x^\eta] (1-x)^b, \quad (11.7)$$

$$xc_s = 0, \quad (11.8)$$

$$xb_s = 0, \quad (11.9)$$

$$xg = [A_g \log^2(1/x) + B_g \log(1/x) + C_g^*] (1-x)^{b+1}, \quad (11.10)$$

where the parameters marked with an asterisk are constrained by sum-rules.

---

<sup>6</sup>One solution is to multiply the gluon distribution by an overall factor  $x$ . This makes no change at large  $x$  and ensures a good behaviour at small  $x$  because, when  $x \rightarrow 0$ ,

$$\frac{x}{\log\left(\frac{1}{1-x}\right)} \rightarrow 1.$$

Numerically, including this factor into the gluon distribution only makes a small correction. Moreover, we cannot integrate  $xg$  analytically, which is annoying for requiring momentum conservation. Therefore, this factor is dropped out.

### 11.3 Fitted experiments

As said previously, we have fitted  $F_2^p$ ,  $F_2^d$ ,  $F_2^{\nu N}$ ,  $x F_3^{\nu N}$  and  $F_2^n/F_2^p$ . We shall now detail more precisely which experiments are included in the fit for all these quantities.

For the proton structure function, we have fitted the experiments from<sup>7</sup> H1 [67–73], ZEUS [74–81], BCDMS [82], E665 [83], NMC [84] and SLAC [86]. For the deuterium structure function measurements, we have included data from E665 [83] and NMC [84]. We have also taken into account the measurements of  $F_2^n/F_2^p$  from NMC [85]. Finally, the neutrino data used here come from CCFR [92–94].

Among all these experimental papers, some give, besides the statistical and the systematic errors, an additional normalisation uncertainty. For each of these subsets of the data, we have allowed an overall normalisation factor. Let  $R_i$  be the normalisation uncertainty for the subset  $i$ , and  $\rho_i$  the effective normalisation factor. We may easily minimise the  $\chi^2$  with respect to this parameter by requiring

$$\frac{\partial \chi^2}{\partial \rho_i} = \frac{\partial}{\partial \rho_i} \sum_j \frac{(\rho_i d_j - t_j)^2}{\varepsilon_j^2} = 0,$$

where  $j$  runs over the data in the subset  $i$ ,  $d_j$ ,  $\varepsilon_j$  and  $t_j$  are respectively the  $j$ th data, its uncertainty and the associated theoretical prediction. We easily find

$$\rho_i = \frac{\sum_j \frac{d_j t_j}{\varepsilon_j^2}}{\sum_j \frac{d_j^2}{\varepsilon_j^2}}.$$

Finally, we shall require that  $\rho_i$  does not lead to a normalisation bigger than the uncertainty  $R_i$ . This means that we shall constrain  $\rho_i$  to verify

$$1 - R_i \leq \rho_i \leq 1 + R_i.$$

Before going to the result, one must point out that we have used here the latest CCFR data<sup>8</sup> from 2001 [94]. These data from U.K. Yang's thesis are used by adding the errors in quadrature and, in order to solve a discrepancy with the other data, we have also allowed an overall normalisation factor of at most 3%.

---

<sup>7</sup>The dataset is coming from the DURHAM database (<http://durpdg.dur.ac.uk>) to which we have added the 2000 and 2001 data from HERA as well as the reanalysed CCFR 2001 data.

<sup>8</sup>They consist into a reanalysis of the 1997 data.

Parameter	Value	Error
$A$	0.00876	0.00043
$B$	0.0197	0.0035
$C$	0.000	0.017
$A_g$	0.258	0.032
$B_g$	-0.62	0.25
$D_u$	0.378	0.030
$D_d$	0.480	0.030
$D_s$	0.000	0.013
$\eta$	0.392	0.019
$\gamma_u$	7.46	0.91
$\gamma_d$	9.1	1.6
$b_u$	3.625	0.016
$b_d$	5.261	0.086
$b$	6.67	0.27
$N_u$	2.015	-
$N_d$	1.723	-
$C_g$	3.158	-

Table 11.1: Values of the fitted parameters in the parton distributions. The last three parameters are not fitted but are obtained from sum-rules.

Experiment information					This fit		CTEQ6 LO		CTEQ6 NLO		
Quant.	Colab.	Reference	Nb Pts	Norm.	$\chi^2$	$\chi^2/nop$	norm.	$\neg$ norm.	norm.	$\neg$ norm.	
$F_2^p$	BCDMS	PLB223(1989)485	167	-	154.607	0.926	5.303	5.303	2.652	2.652	
	E665	PRD54(1996)3006	30	1.80	40.368	1.346	1.177	1.233	1.251	1.383	
	H1	EPJC19(2001)269		126	-1.50	129.673	1.029	1.516	1.626	1.077	1.122
		EPJC21(2001)33		86	-	75.774	0.881	0.942	0.942	1.008	1.008
		EPJC13(2000)609		130	-1.50	117.682	0.905	1.612	1.962	0.882	1.032
		NPB470(1996)3		156	-	104.206	0.668	0.835	0.835	0.658	0.658
		NPB439(1995)471		90	-4.50	49.499	0.550	0.597	0.901	0.574	0.737
		NPB407(1993)515		21	-8.00	6.233	0.297	0.289	0.466	0.287	0.401
		NMC	NPB483(1997)3		79	2.10	101.927	1.290	1.728	1.260	1.138
	SLAC	PLB282(1992)475		52	-	97.861	1.882	2.123	2.123	1.355	1.355
	ZEUS	EPJC21(2001)443		214	-	207.294	0.969	2.454	2.454	0.875	0.875
		EPJC7(1999)609		12	-	11.297	0.941	0.744	0.744	1.259	1.259
		ZPC72(1996)399		172	-	238.882	1.389	1.299	1.299	1.429	1.429
		ZPC65(1995)379		56	2.00	27.477	0.491	0.495	0.415	0.453	0.470
		ZPC69(1995)607		9	-1.54	11.493	1.277	1.201	1.270	1.309	1.289
PLB316(1993)412			17	6.94	6.048	0.356	0.370	0.372	0.344	0.474	
Total			1417		1380.321	0.974	1.864	1.900	1.150	1.187	
$F_2^d$	BCDMS	PLB237(1989)592	154	-	127.941	0.831	1.546	1.546	0.903	0.903	
	E665	PRD54(1996)3006	30	-	33.563	1.119	0.913	0.913	1.132	1.132	
	NMC	NPB483(1997)3	79	1.00	90.330	1.143	1.438	1.131	0.969	1.071	
	SLAC	SLAC-357(1990)	50	-	98.376	1.968	2.515	2.515	1.278	1.278	
	Total			313		350.210	1.119	1.613	1.536	1.002	1.027
$F_2^{\nu N}$	CCFR	UK. Yang's thesis	65	3.00	165.512	2.546	3.118	4.570	3.523	6.135	
$xF_3^{\nu N}$	CCFR	PRL79(1997)	76	-	42.066	0.554	0.658	0.658	1.252	1.252	
$F_2^n/F_2^p$	NMC	NPB371(1995)3	91	-	116.720	1.283	1.315	1.315	1.285	1.285	
Total			1962		2054.830	<b>1.047</b>	1.794	1.855	1.215	1.333	

Table 11.2: Fit results detailed experiment by experiment. For comparison we have added the predictions for CTEQ6 at leading and next-to-leading order (the NLO predictions are taken in the DIS scheme). In the comparison with CTEQ, the results are given with and without taking into account our normalisation factors.

## 11.4 Results

We have adjusted the 14 parameters  $A, B, C, A_g, B_g, D_u, D_d, D_s, b, b_u, b_d, \gamma_u, \gamma_d$  and  $\eta$  to the experimental data in the region

$$\begin{aligned} Q^2 &\geq 4m_c^2 = 6.76 \text{ GeV}^2, \\ W^2 &\geq 12.5 \text{ GeV}^2. \end{aligned}$$

The second boundary is used to cut the region where higher-twists effects are expected to be large and we have adopted the same limit on  $W^2$  as MRST. The values of the fitted parameters are presented in Table 11.1 and the result, detailed experiment by experiment, in Table 11.2.

We can see from the parameter table that both the large- $x$  exponents and the reggeon intercept have acceptable values.

In the  $\chi^2$  table, we have also shown the CTEQ6 results<sup>9</sup> at LO and at NLO (in the DIS scheme<sup>10</sup>), with and without taking the normalisation factors into account. We see that the CCFR 2001 neutrino data probably need to be renormalised up and are still poorly reproduced. We can also see that, apart from the SLAC data, we obtain a very good description. This means that it would be a good idea to add a renormalisation factor of a few percents to the SLAC  $F_2^p$  and  $F_2^d$  data.

The correlation matrix for the parameters is presented in Table 11.3.

In Figure 11.1, we have shown some typical distributions and their  $Q^2$  evolution. The  $u_V$  and  $d_V$  valence quarks distributions both present a peek around  $x \approx 0.1 - 0.2$  and are, roughly speaking, within a factor 2. The sea asymmetry  $\bar{d} - \bar{u}$  can be written in the following form:

$$\begin{aligned} \bar{d} - \bar{u} &= \frac{u_V - d_V - T_3}{2} \\ &= (D_d - D_u)x^\eta(1-x)^b. \end{aligned}$$

This distribution has a maximum for

$$x = \frac{\eta}{b + \eta} \approx \begin{cases} 0.1 & \text{for } xu_V, \\ 0.07 & \text{for } xd_V, \\ 0.056 & \text{for } x(\bar{d} - \bar{u}) \end{cases}.$$

The evolution in  $Q^2$  of these three distribution shows the same behaviour: the peek is moved to smaller values of  $x$  and tamed while its width grows. We have also shown in Figure 11.1 the gluon distribution which grows quickly with  $Q^2$ .

The parton densities at various scales are plotted in Figure 11.2. First of all, when  $Q^2 = Q_0^2 = 4m_c^2$ , we have no charm or bottom quark and both quark and gluon distributions

---

<sup>9</sup>These results are obtained by using directly the CTEQ parton distribution and comparing it with our dataset without any refit.

<sup>10</sup>The DIS scheme is the renormalisation scheme where, at any order, the quark coefficient function is  $\delta(1-x)$  and the gluon coefficient function vanishes.

are described by Regge theory, more precisely by a triple-pole and a reggeon contribution. At higher virtualities, charm quarks are non-vanishing and, for  $Q^2 > 4m_b^2$ , we also have  $b$  quarks. For  $Q^2 > Q_0^2$ , the parton distributions have an essential singularity at  $j = 1$ .

Finally, we can estimate the uncertainty on the initial distributions in the following way: for the sea quarks or for the gluon, we have ( $D = 0$  for the gluon distribution)

$$xq = [A \log^2(1/x) + B \log(1/x) + C + Dx^\eta] (1-x)^b.$$

If we assume that the uncertainties on the parameters are uncorrelated, we obtain easily

$$\begin{aligned} (\delta xq)^2 &= \{ \log^4(1/x) \delta A^2 + \log^2(1/x) \delta B^2 + \delta C^2 + [\delta D^2 + \log^2(1/x) D^2 \delta \eta^2] x^{2\eta} \\ &+ [A \log^2(1/x) + B \log(1/x) + C + Dx^\eta] \log^2(1-x) \delta b^2 \} (1-x)^{2b}. \end{aligned}$$

For the valence quarks, the initial distribution has the form

$$xq_V = K x^\eta (1-x)^b (1+\gamma x)$$

with  $K$  fixed by quark number conservation, and we find that the uncertainty is

$$(\delta xq)^2 = K^2 x^{2\eta} (1-x)^{2b} \{ [\log^4(1/x) \delta \eta^2 + \log^2(1-x) \delta b^2] (1+\gamma x)^2 + x^2 \delta \gamma^2 \}.$$

The resulting uncertainties on the initial distributions are shown in Figure 11.16. We see that this “traditional” way of estimating errors leads to much smaller uncertainties than the joint consideration of forward and backward evolution given in chapter 10.

## 11.5 Conclusions and perspectives

We have seen in this chapter that we can use Regge theory to constrain the initial parton densities at  $Q^2 = Q_0^2$  and obtain the distributions at higher virtualities with the DGLAP evolution equation.

We thus have extended the approach of chapter 9 to  $x = 1$  using only forward evolution. We have not applied the techniques developed in chapter 10 and extracted the  $Q^2$  behaviour of the fitted parameters by combining forward and backward evolution. The reason is that, even with a few parameters, there often exist multiple minima and it is quite hard to obtain a continuous result for all parameters. This situation is expected to be even worse with the parametrisation used in this chapter due to the larger number of parameters.

However, we may improve the model presented in many ways:

- Study the effects of the cuts on the fitted region. The effects of the  $W^2$  cut can be studied by simply varying its value and refitting. It can probably give interesting information on the domain where higher-twists become important. The analysis of the  $Q^2$ -cut effects is slightly more complicated. We know that in order to have a consistent fit, the  $\chi^2/dof$  should not depend on the cuts. Therefore, looking for the region of stability when the scale  $Q_0^2$  varies, should give us the region where the DGLAP

evolution equation is valid<sup>11</sup>. However, the parametrisation introduced here can only be used for  $Q_0^2 \leq 4m_c^2$ . For higher values of  $Q_0^2$ , we need to put  $c$  quarks in the initial distributions. This can, for example be done in the following way

$$c = \bar{c} = \eta_c [A \log^2(1/x) + B \log(1/x) + C + D_c x^\eta] (1-x)^b$$

which introduces 2 new parameters in the fit.

- A complete study of the parton-distribution uncertainties, and particularly of the gluon-distribution uncertainties, can, of course be very useful.
- A more precise treatment of the correlated systematic errors can be done.
- We can try to apply the same methods as in chapter 10 *i.e.* let  $Q_0^2$  vary, use forward and backward evolution and get the evolution of the parameters in the initial distribution as a function of  $Q_0^2$ .
- Finally, a NLO analysis will be performed in the near future. This gives a much more reliable description of the data, allows a more complete comparison with other parametrisations and gives a description of the  $F_c$  and  $F_L$  structure functions.

---

<sup>11</sup>This type of study have been performed recently by MRST and they obtained a breakdown of the DGLAP evolution around 10 GeV<sup>2</sup>.

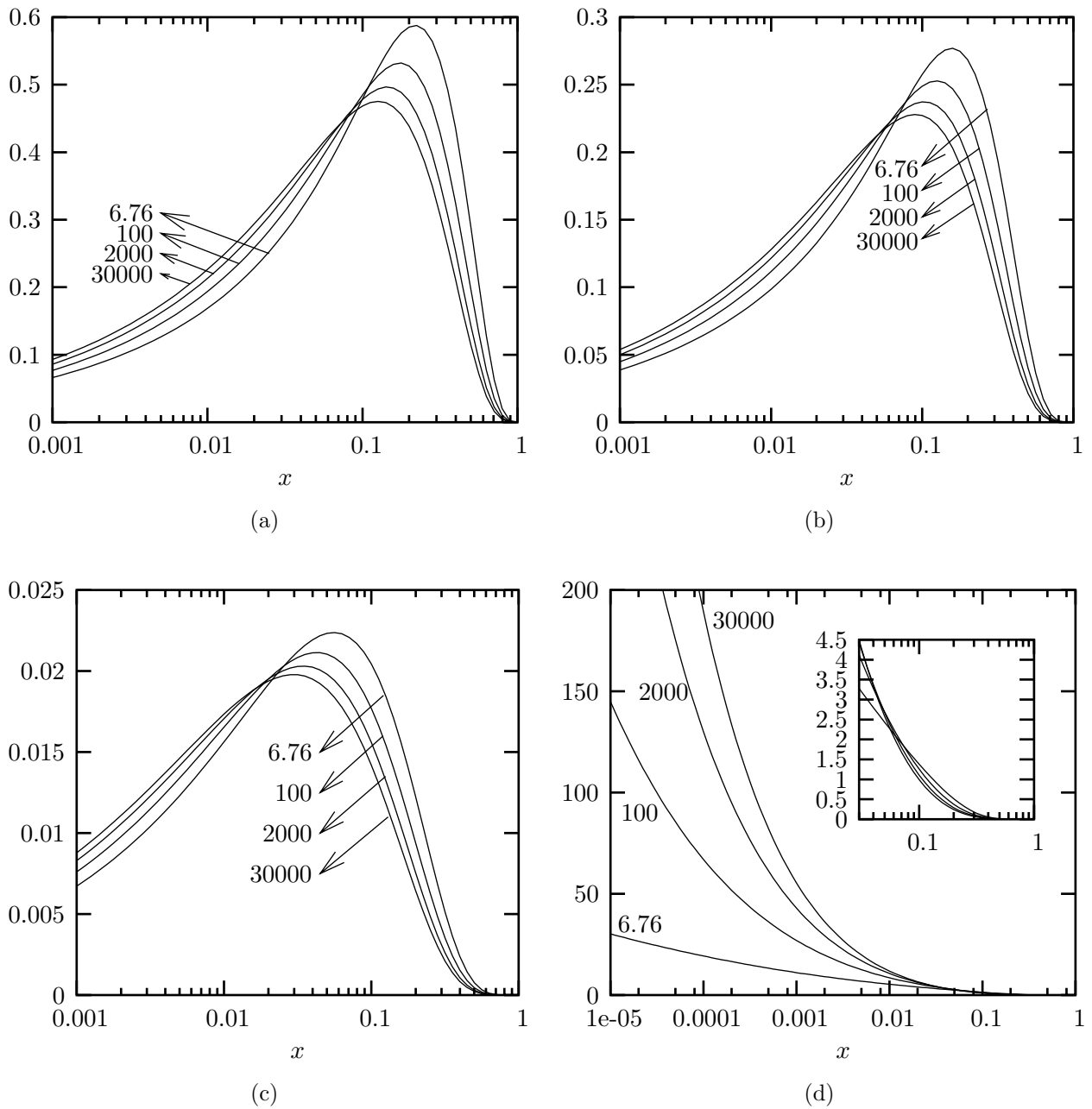


Figure 11.1: Typical momentum distributions inside the proton at various  $Q^2$ : (a)  $u$  valence quarks, (b)  $d$  valence quarks, (c) sea asymmetry  $\bar{d} - \bar{u}$  and (d) gluon distribution.

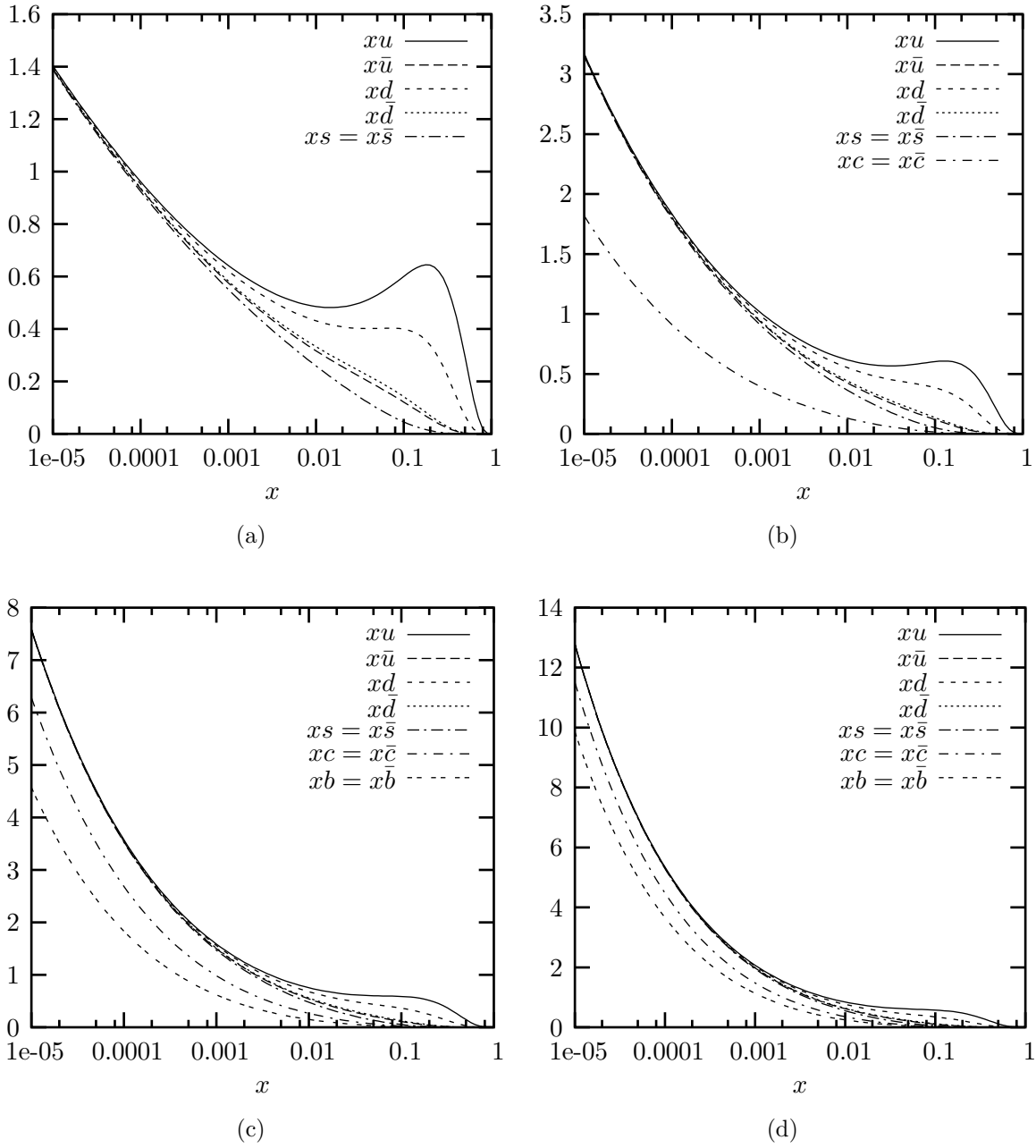


Figure 11.2: Quark distributions inside the proton at various  $Q^2$ : (a)  $Q^2 = Q_0^2 = 4m_c^2$ , (b)  $Q^2 = 4m_b^2$ , (c)  $Q^2 = 2000 \text{ GeV}^2$  and (d)  $Q^2 = 30000 \text{ GeV}^2$ .

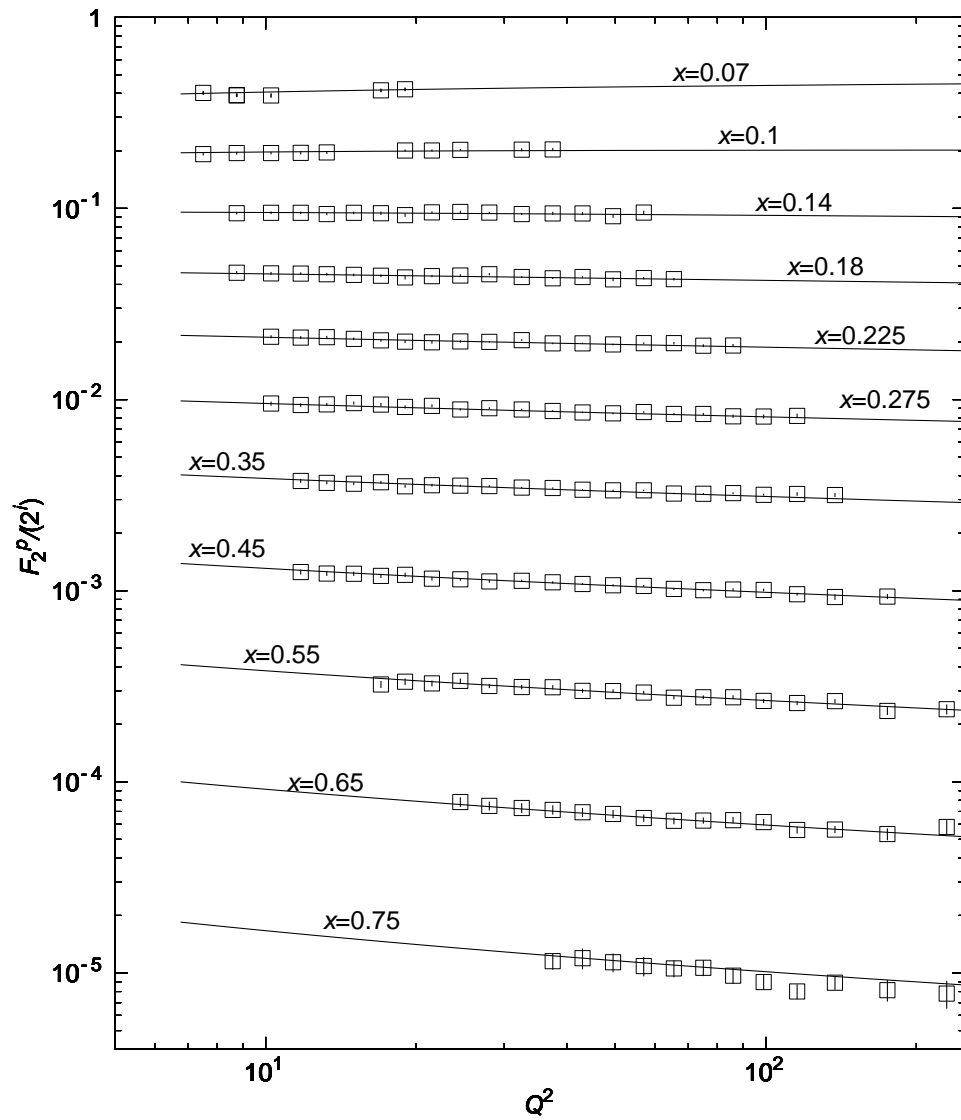
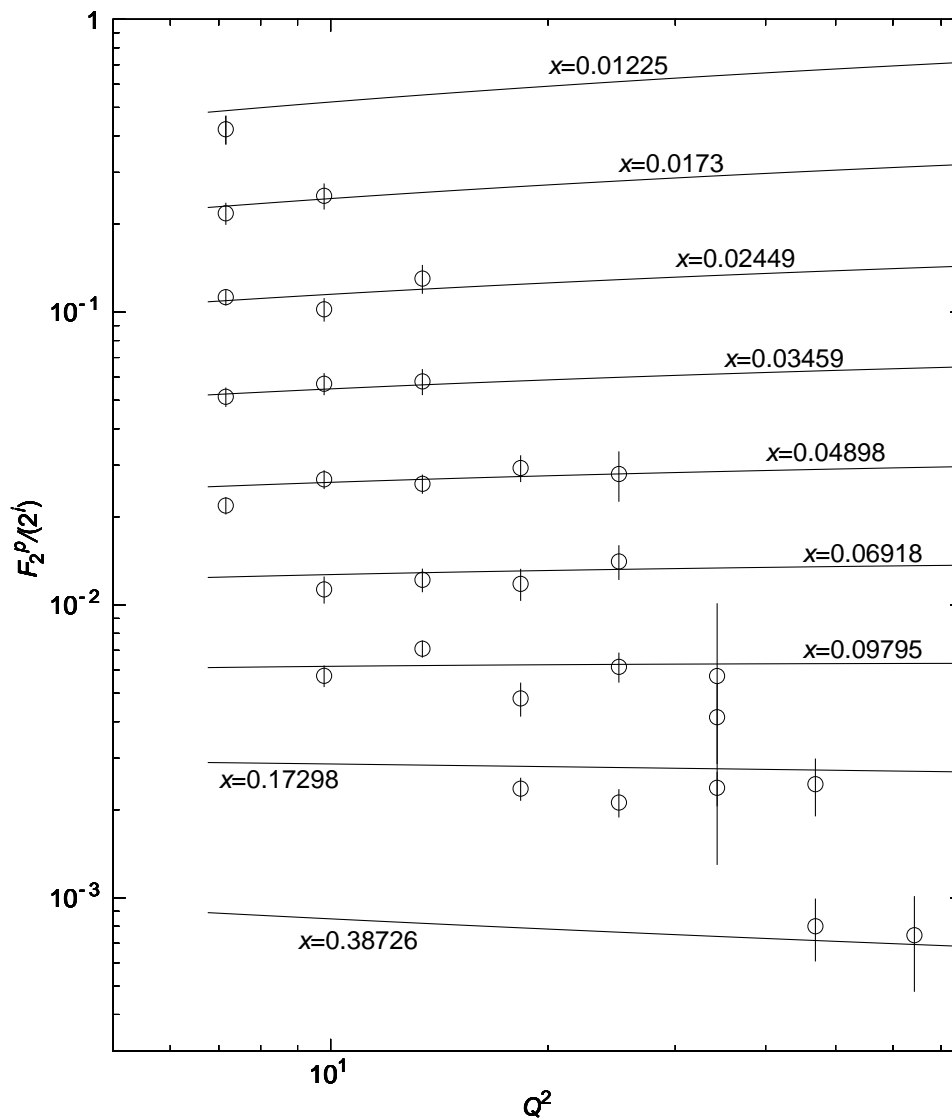


Figure 11.3: DGLAP evolution results for BCDMS  $F_2^p$  data.

Figure 11.4: DGLAP evolution results for E665  $F_2^p$  data.

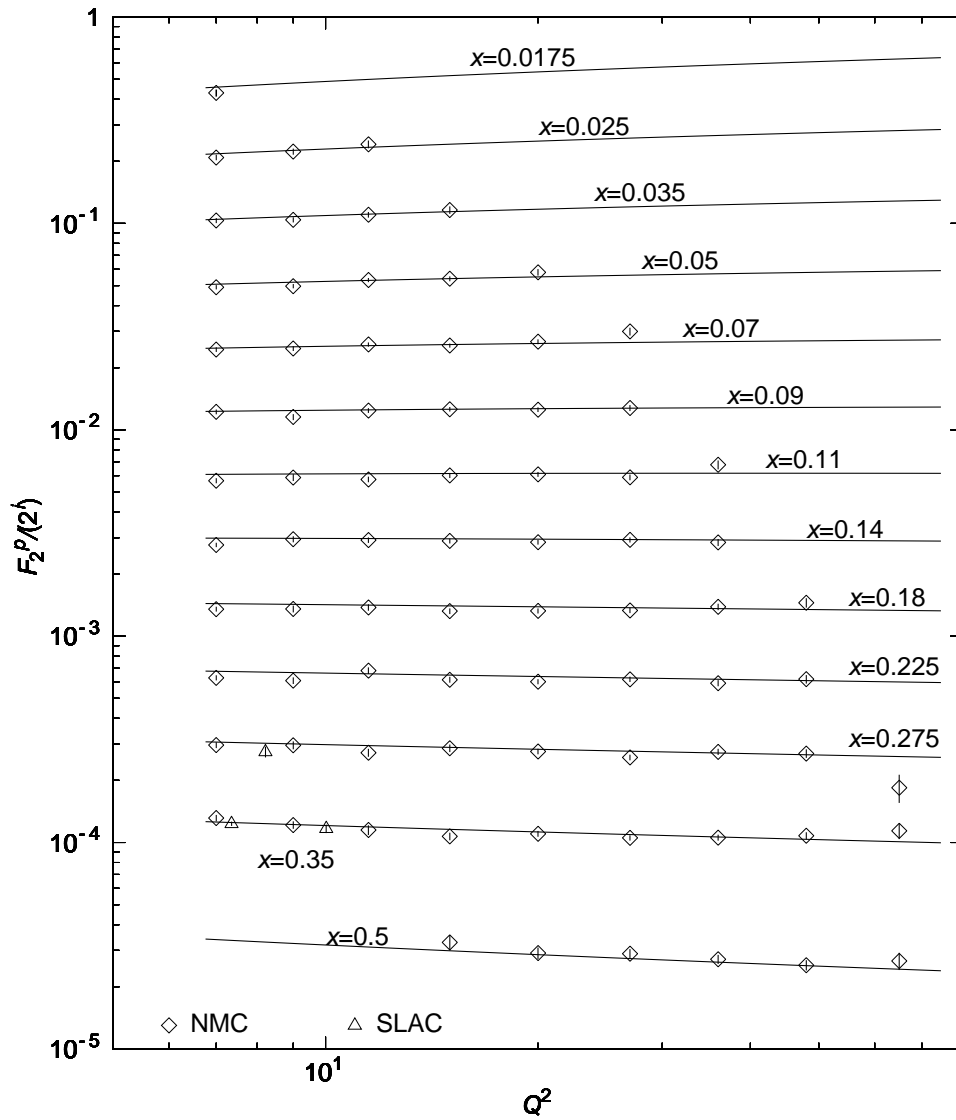


Figure 11.5: DGLAP evolution results for NMC  $F_2^p$  data (the SLAC data appearing in the NMC  $Q^2$  bins have been added to the plot).

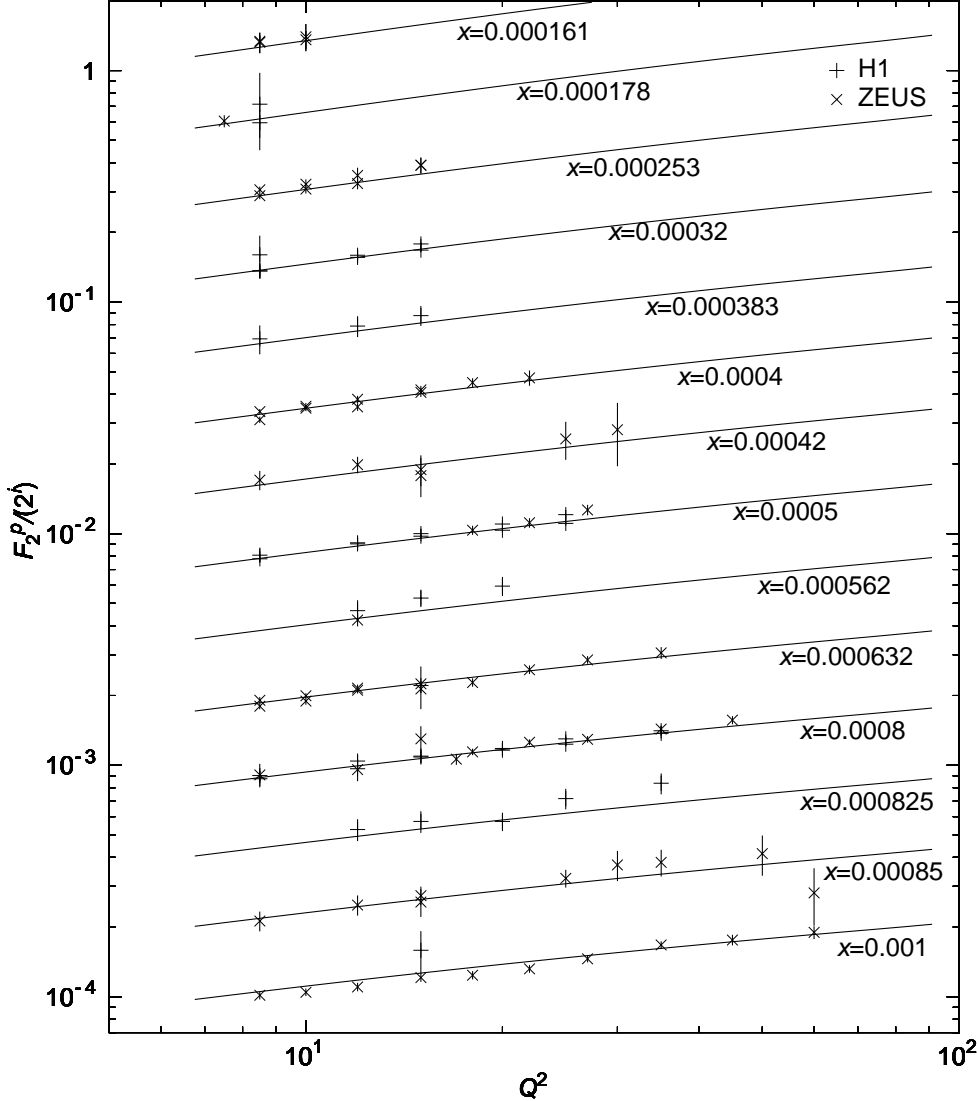


Figure 11.6: DGLAP evolution results for HERA  $F_2^p$  data ( $x \leq 0.001$ ).

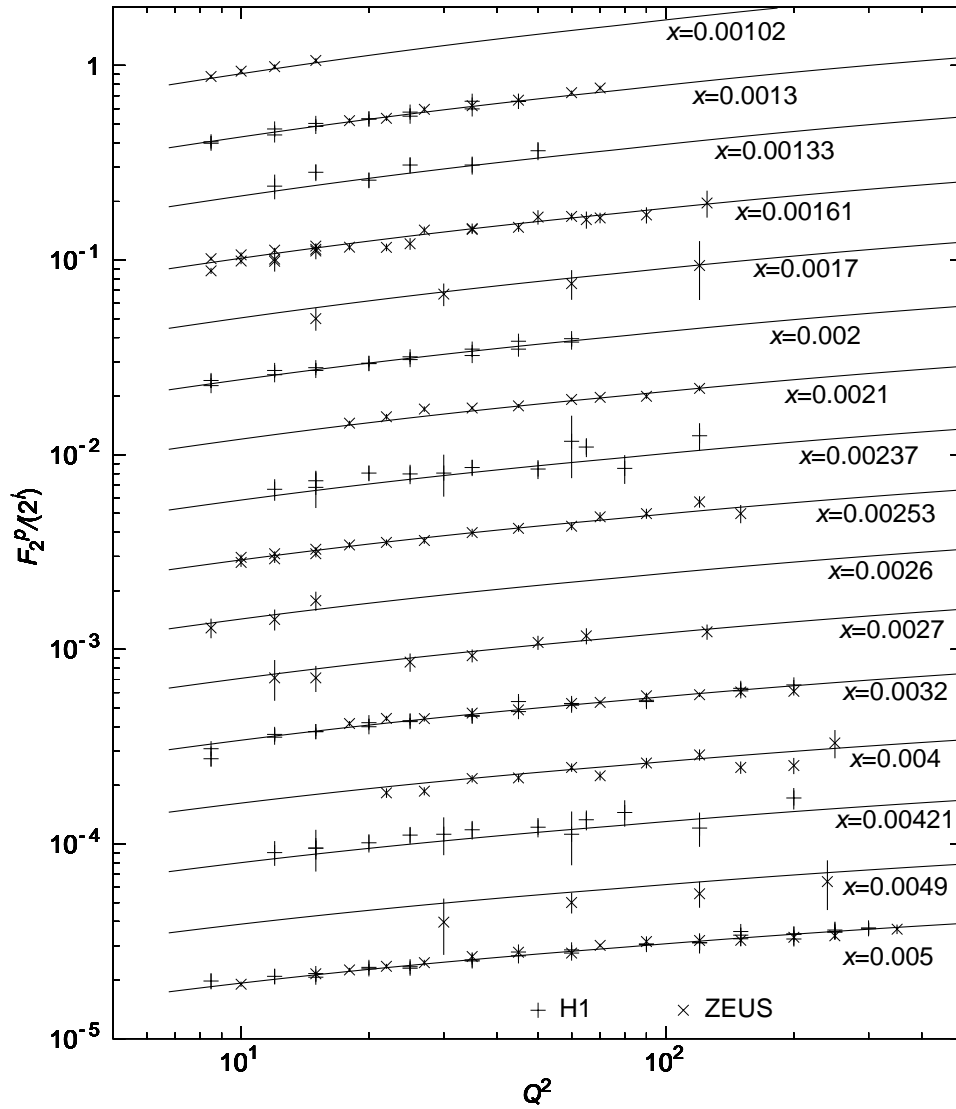


Figure 11.7: DGLAP evolution results for HERA  $F_2^p$  data ( $0.001 < x \leq 0.005$ ).

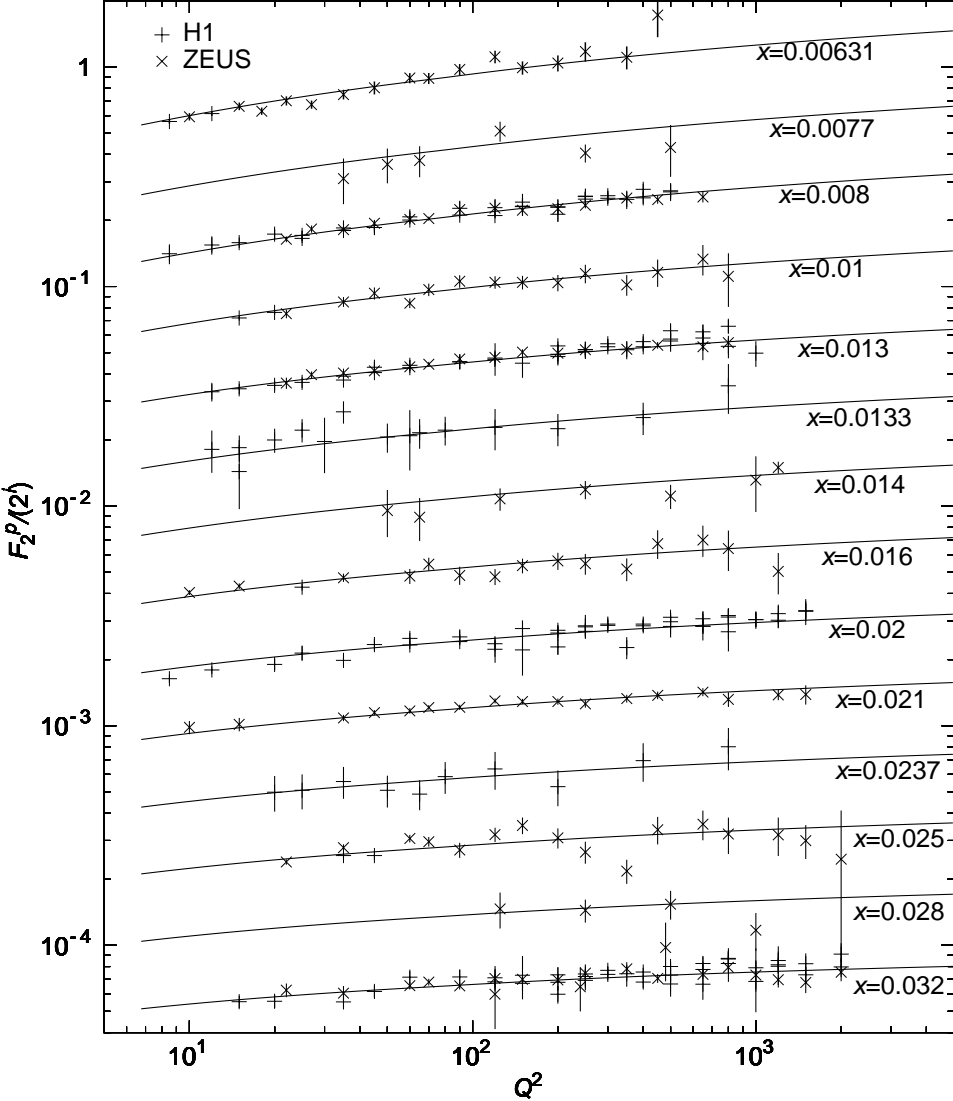


Figure 11.8: DGLAP evolution results for HERA  $F_2^p$  data ( $0.005 < x \leq 0.04$ ).

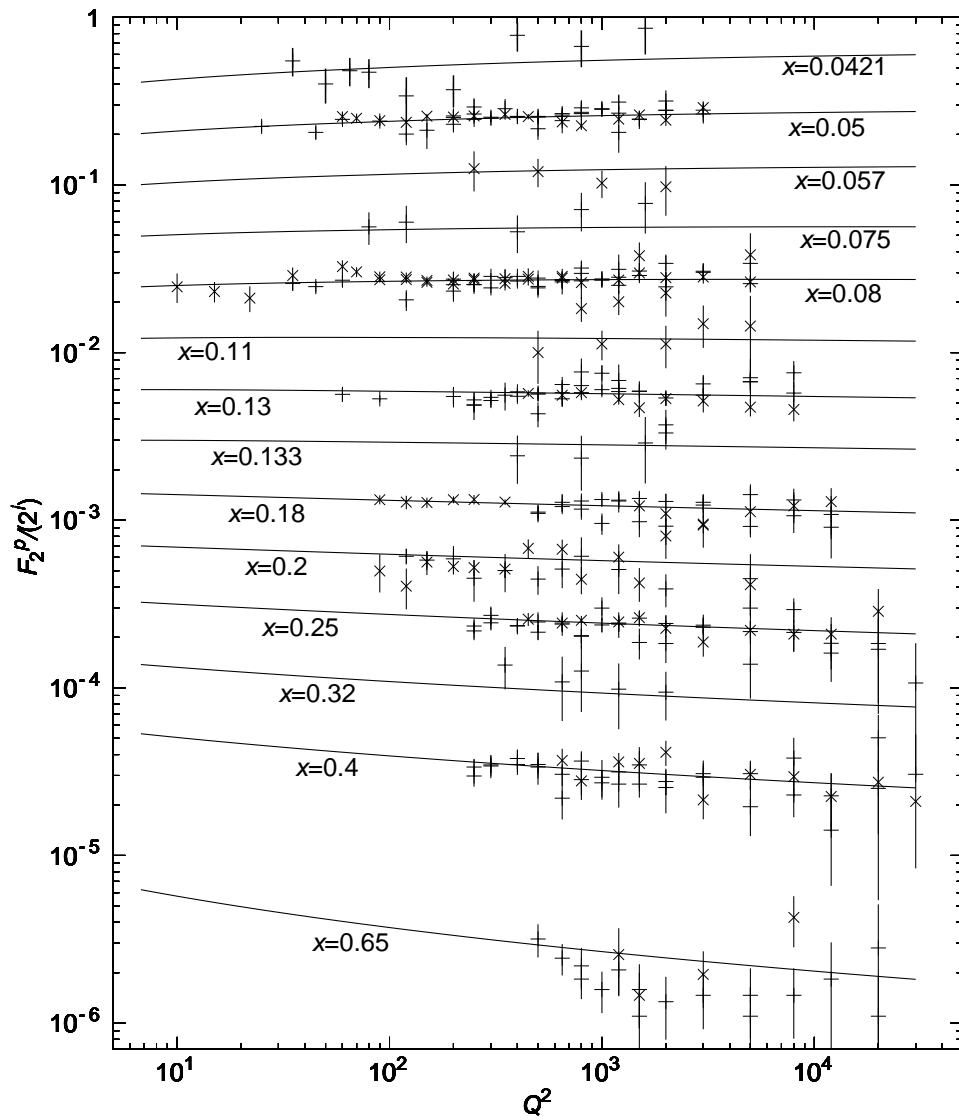


Figure 11.9: DGLAP evolution results for HERA  $F_2^p$  data ( $0.04 < x$ ).

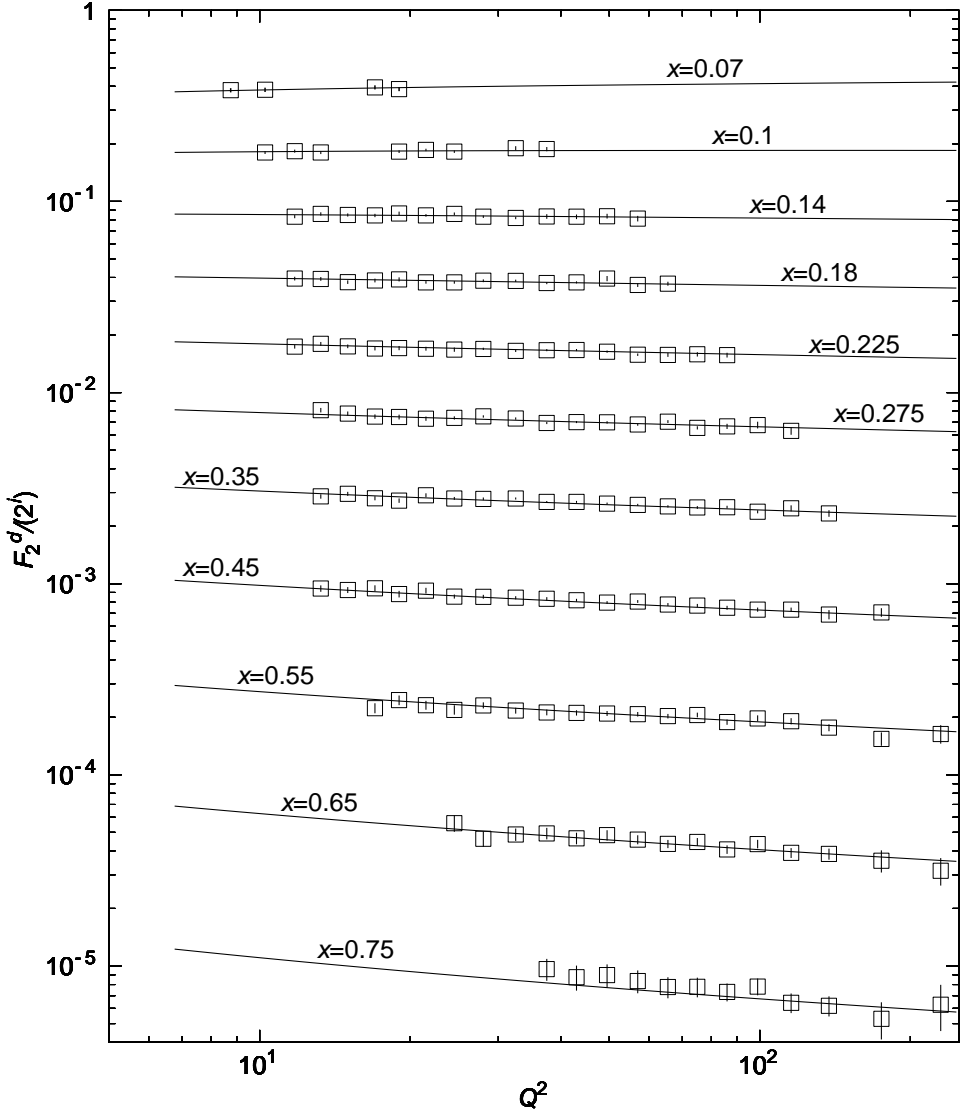


Figure 11.10: DGLAP evolution results for BCDMS  $F_2^d$  data.

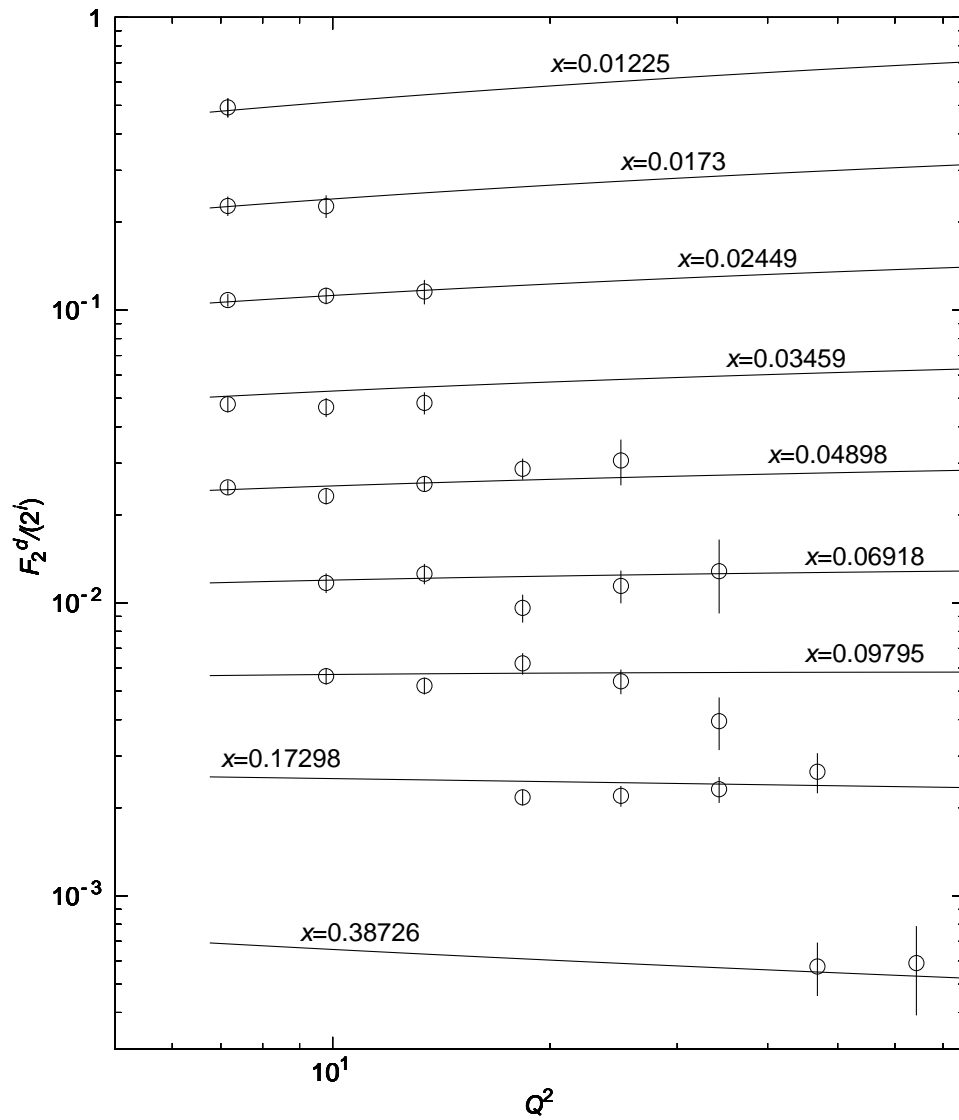


Figure 11.11: DGLAP evolution results for E665  $F_2^d$  data.

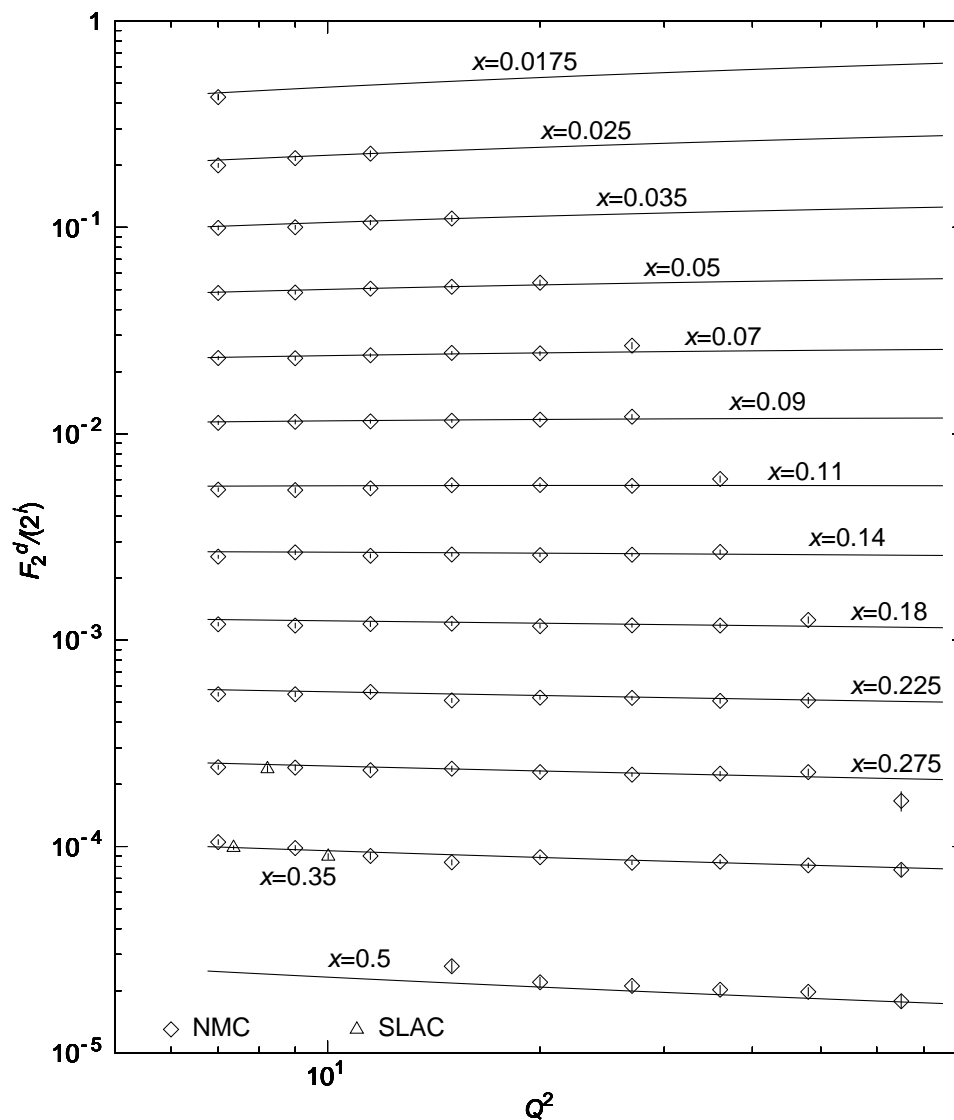


Figure 11.12: DGLAP evolution results for NMC  $F_2^d$  data (the SLAC data appearing in the NMC  $Q^2$  bins have been added to the plot).

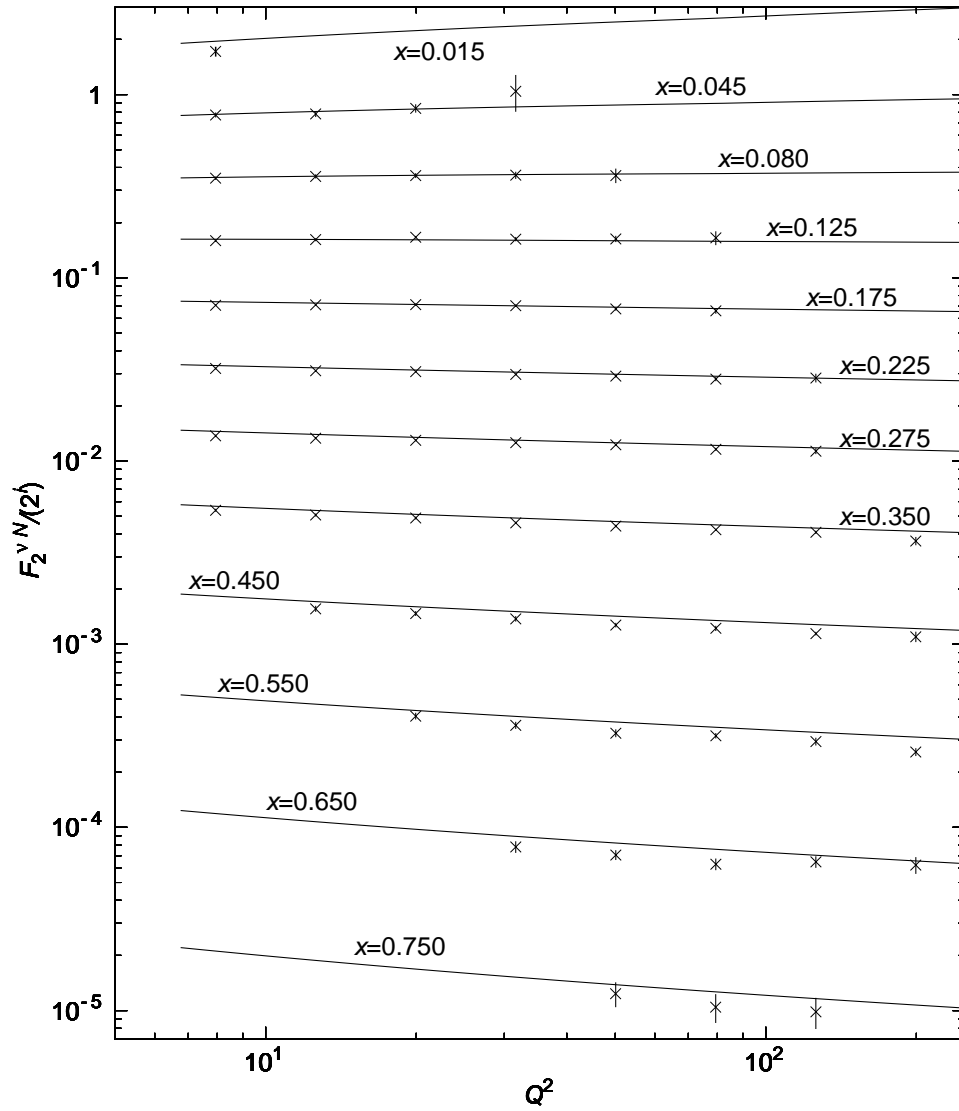


Figure 11.13: DGLAP evolution results for CCFR  $F_2^{\nu N}$  data.

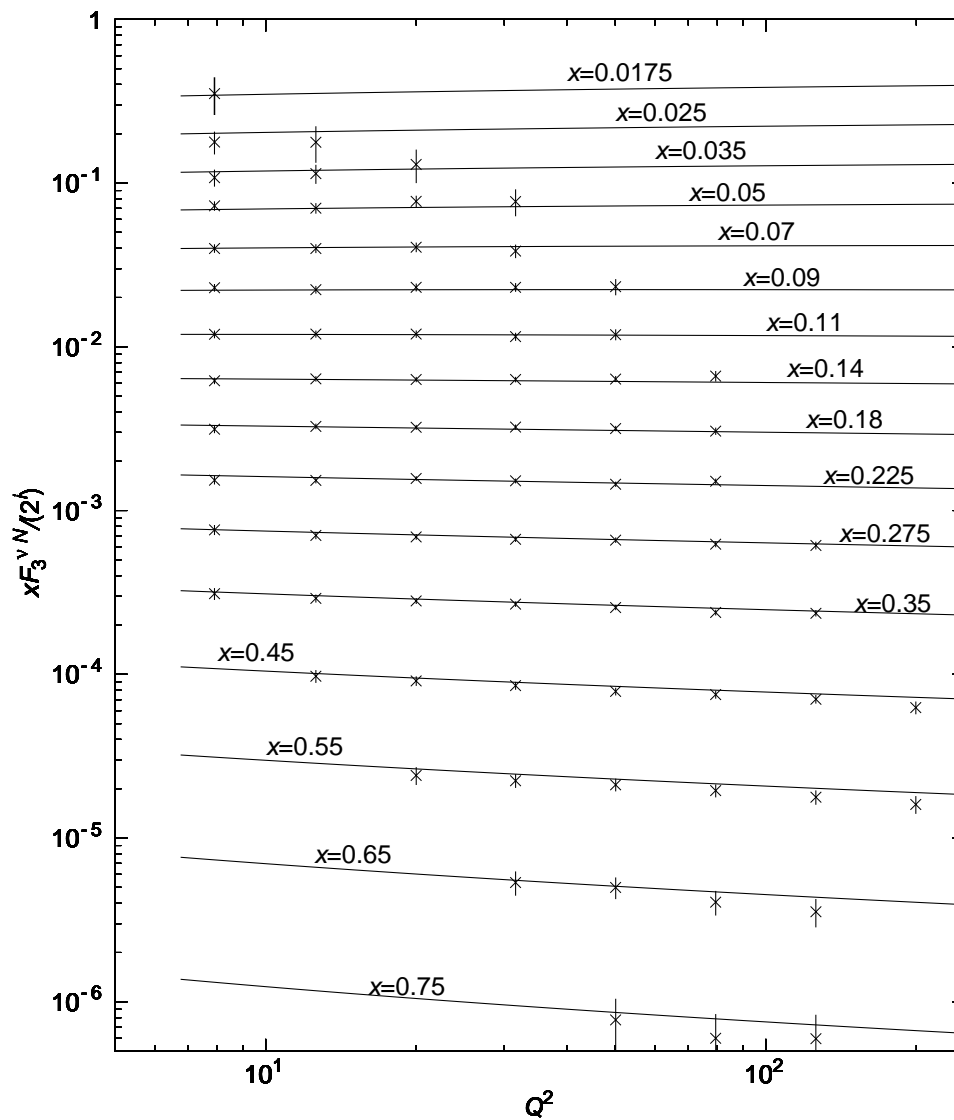


Figure 11.14: DGLAP evolution results for CCFR  $xF_3^{\nu N}$  data.

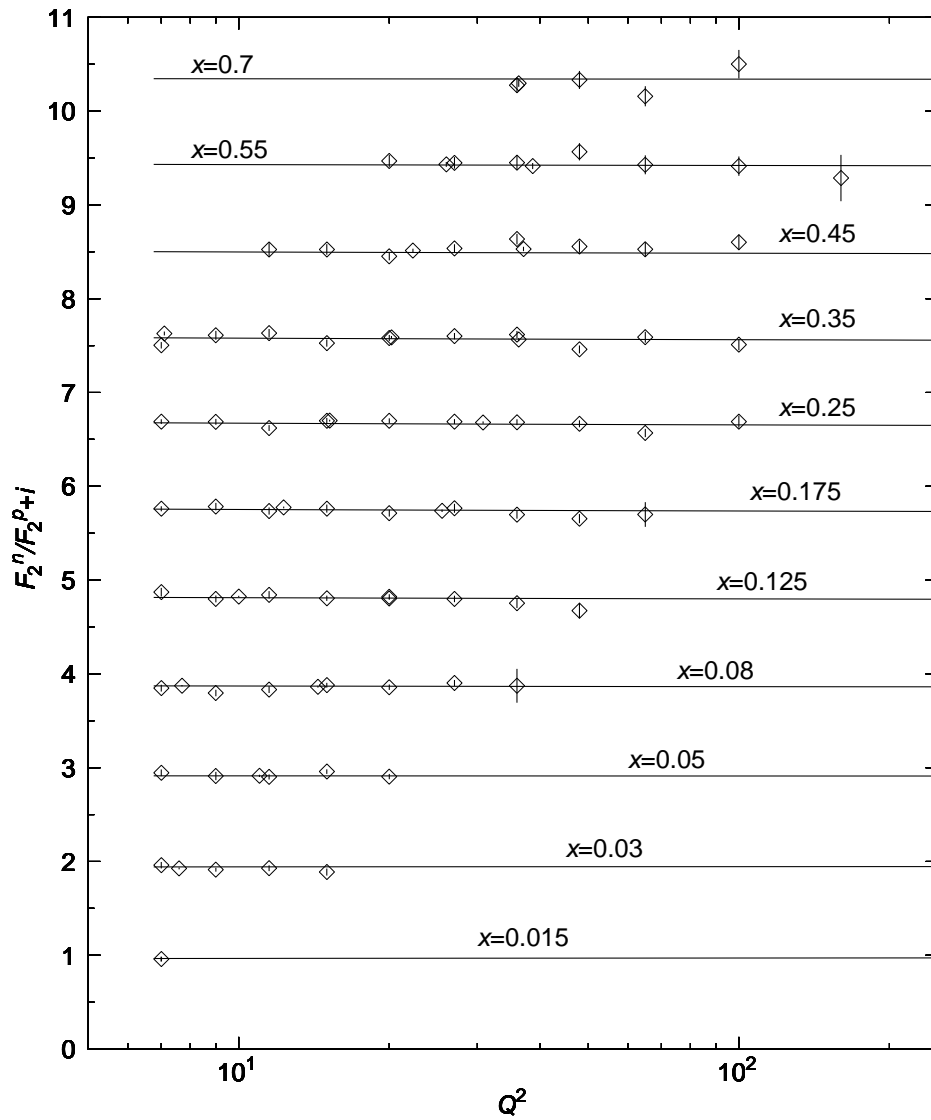


Figure 11.15: DGLAP evolution results for NMC  $F_2^n/F_2^p$  data.

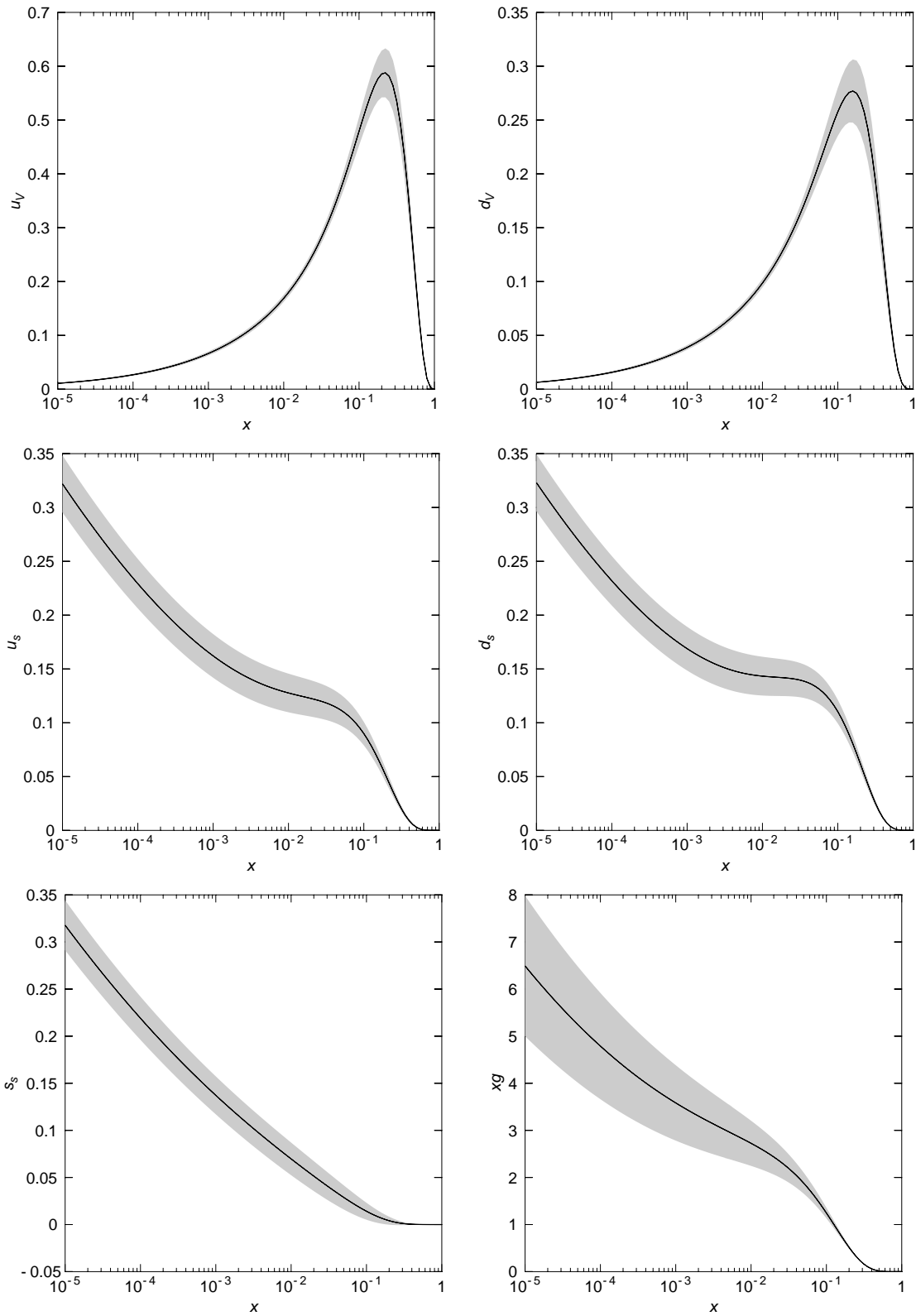


Figure 11.16: Initial distributions with their uncertainties.

Param.	global	$A$	$B$	$C$	$D_u$	$D_d$	$D_s$	$A_g$	$B_g$	$\gamma_u$	$\gamma_d$	$b_u$	$b_d$	$b$	$\eta$
$A$	0.99650	1.000	-0.895	-0.015	0.733	0.631	0.007	-0.363	0.268	0.365	0.304	0.018	-0.022	0.442	-0.368
$B$	0.99824	-0.895	1.000	0.025	-0.864	-0.668	-0.006	0.229	-0.148	-0.567	-0.494	-0.081	-0.042	-0.589	0.562
$C$	0.28980	-0.015	0.025	1.000	0.005	0.005	0.000	0.001	-0.002	0.001	0.001	0.001	0.000	0.000	0.002
$D_u$	0.99222	0.733	-0.864	0.005	1.000	0.822	0.006	0.086	-0.177	0.524	0.521	0.267	0.085	0.876	-0.460
$D_d$	0.98233	0.631	-0.668	0.005	0.822	1.000	0.005	-0.071	-0.009	0.110	0.040	0.397	-0.243	0.762	-0.009
$D_s$	0.02647	0.007	-0.006	0.000	0.006	0.005	1.000	0.001	-0.002	0.005	0.005	0.004	0.000	0.008	-0.004
$A_g$	0.99616	-0.363	0.229	0.001	0.086	-0.071	0.001	1.000	-0.980	0.346	0.380	0.253	0.199	0.356	-0.291
$B_g$	0.99649	0.268	-0.148	-0.002	-0.177	-0.009	-0.002	-0.980	1.000	-0.403	-0.443	-0.317	-0.228	-0.464	0.332
$\gamma_u$	0.99956	0.365	-0.567	0.001	0.524	0.110	0.005	0.346	-0.403	1.000	0.900	0.253	0.318	0.518	-0.980
$\gamma_d$	0.99665	0.304	-0.494	0.001	0.521	0.040	0.005	0.380	-0.443	0.900	1.000	0.081	0.648	0.552	-0.893
$b_u$	0.97469	0.018	-0.081	0.000	0.267	0.397	0.004	0.253	-0.317	0.253	0.081	1.000	-0.232	0.537	-0.073
$b_d$	0.97329	-0.022	-0.042	0.000	0.085	-0.243	0.000	0.199	-0.228	0.318	0.648	-0.232	1.000	0.174	-0.332
$b$	0.99685	0.442	-0.589	0.002	0.876	0.762	0.008	0.356	-0.464	0.518	0.552	0.537	0.174	1.000	-0.389
$\eta$	0.99965	-0.368	0.562	-0.001	-0.460	-0.009	-0.004	-0.291	0.332	-0.980	-0.893	-0.073	-0.332	-0.389	1.000

Table 11.3: Fitted parameters correlation coefficients.

*Down and out, it can't be helped but there's a lot of it about.  
With, without, and who'll deny it's what the fighting's all about ?  
Out of the way, it's a busy day, I've got things on my mind  
For the want of the price of tea and a slice, the old man died.*  
Pink Floyd - Us and Them

## Chapter 12

# Conclusions

It is now time to summarise our results and to conclude this thesis. Throughout this document, I have proposed several approaches, all of them leading to different fits to the experimental data. Therefore it is of prime importance to compare all of them. Since the advantages and drawbacks of each individual approach have been explained at the end of the corresponding chapters, I shall only briefly summarise the various methods introduced and concentrate on their comparison.

In the first part, I have introduced the DGLAP evolution equation which introduces the partonic densities and predicts their evolution at large  $Q^2$  from pQCD by resumming the large- $Q^2$  collinear singularities. Although this is considered as one of the most important tests of QCD, this approach is not free of problems: the DGLAP equation is an evolution equation and pQCD does not say anything about the initial distributions. Moreover, the evolution generates an essential singularity at  $j = 1$  which seems to be theoretically unacceptable and which is usually associated with the fact that the DGLAP equation does not resum properly the small- $x$  corrections.

Then, I have introduced another approach to DIS:  $S$ -matrix and Regge theory. It is an axiomatic theory which studies the analytical properties of the  $S$  matrix. This is very useful to constrain the high-energy behaviour of amplitudes, particularly in the framework of Regge theory where the asymptotic behaviour of amplitudes when  $s \rightarrow \infty$  is related to singularities in the complex-angular-momentum space. I have shown that it is possible to reproduce the proton structure function up to  $Q^2 = 3000 \text{ GeV}^2$  together with the  $\gamma p$  total cross-section using a triple-pole pomeron at  $j = 1$  (model 1). Still in the framework of  $S$ -matrix theory, we have proven that the factorisation theorem extends to multiple thresholds and to multiple poles in the hadronic case which means that all hadronic amplitudes must have the same  $j$ -plane singularity structure. Unfortunately, this argument cannot be directly extended to the case of photons. Even if an  $S$  matrix can be defined for QED, one still may add new singularities to the  $\gamma^* p$  and  $\gamma^* \gamma^*$  amplitudes. Nevertheless, I have shown in chapter 8 that, using a generalised double-pole or a triple-pole pomeron at  $j = 1$ , one can fit the  $\gamma \gamma$  cross-section using the factorisation theorem and the photon structure function adding only the box diagram as a new singularity (model 2).

In the last part, I have combined Regge theory with DGLAP evolution. This approach is motivated by the idea that all hadronic amplitudes may have the same singularity struc-

ture, so that one should be able to describe parton distributions with the same singularity structure. In this case, Regge theory constrains the  $x$  dependence of the parton densities and the DGLAP equation gives their  $Q^2$  evolution. In these models combining Regge theory and DGLAP evolution, I obtain the quark and gluon distributions which are not given by models based only on Regge theory.

As a first step, I have limited the analysis to the Regge domain, which imposes a limit on  $x$  ( $x \leq x_{\text{Regge}} \approx 0.15$ ), and used a standard PDF set at larger  $x$ . Within these limits, I have shown that one can use the fit obtained in chapter 8 (*i.e.* model 2) for  $Q^2 \leq Q_0^2 \approx 5 \text{ GeV}^2$  and extend it to larger  $Q^2$  using the DGLAP equation. This works both for the generalised double-pole and the triple-pole pomeron models (model 3). In this approach, Regge theory describes small- $Q^2$  data and pQCD is used in the large- $Q^2$  domain. I have therefore looked at the possible extension of Regge theory to higher  $Q^2$  values. I have shown that, using forward and backward DGLAP evolution, it is possible to obtain the residues of the triple-pole pomeron at high  $Q^2$ . These high- $Q^2$  residues can be phenomenologically extended to  $Q^2 = 0$  and give a good description of the charm and longitudinal structure functions  $F_2^c$  and  $F_L$  (model 4). The compatibility of this approach with the  $t$ CU rules is not complete. Although we can reproduce  $F_2^\gamma$  when  $Q_1^2 = 0$ , there remain problems when both  $Q_1^2$  and  $Q_2^2$  are nonzero. These problems may come from the fit itself, from the applicability of the  $t$ CU rules together with the DGLAP equation, from the fact that we may add perturbative singularities to the predictions of the factorisation theorem, or from the choice of a soft pomeron model.

Finally, I have shown that, using powers of  $(1-x)$  at large  $x$ , one can extend the analysis of chapter 9 (*i.e.* model 3) to  $x = 1$ , thus removing the dependence on an external PDF set. This approach requires to include other experiments constraining the fit at large  $x$  and thus to introduce more than one flavour-non-singlet quark distribution. Here, the parton densities still behave like triple poles at small  $x$  at the initial scale  $Q_0^2 = 4m_c^2 = 6.76 \text{ GeV}^2$  and are obtained by DGLAP evolution at larger  $Q^2$  (model 5).

A way to compare our models is to look at the gluon distributions<sup>1</sup>. One clearly sees in figure 12.1 that although all the models reproduce  $F_2^p$ , the gluon distributions are different<sup>2</sup>. Since all these distributions produce a correct fit to  $F_2^p$ , this should be considered as an uncertainty on the gluon distribution.

In this thesis, I have shown that one can obtain a description of the proton structure function consistent with Regge theory and DGLAP evolution. This new approach to DIS<sup>3</sup> nevertheless replaces the problem of the essential singularity generated by DGLAP evolution by the question of  $\gamma\gamma$  predictions using the factorisation theorem. I have shown that we can consider the DGLAP predictions as a numerical approximation to a Regge-compatible model. This is however not the case for the factorisation theorem. We have seen that different singularity structures lead to completely different  $t$ CU rules. Two models reproducing the

---

<sup>1</sup>This is only possible for models 3, 4 and 5.

<sup>2</sup>The DGLAP evolution with variable flavour number has only been implemented in model 5. One can expect that applying it to models 3 and 4 shall rise a little bit the gluon distribution. This should not modify the large uncertainties for the different curves of model 4.

<sup>3</sup>I would like to recall that DIS analysis using both Regge theory and DGLAP evolution have also been investigated by Csernai and collaborators [60] and by Donnachie and Landshoff [14].

$pp$  and  $\gamma^{(*)}p$  measurements can predict completely different results, even negative ones, for the  $\gamma^*\gamma^*$  interactions. It may be worth noting here that a small numerical correction in  $F_2^p$  can lead to huge modifications in  $F_2^\gamma$ . For example, if one add  $\frac{10^{-10}}{j-\alpha}$  to  $F_2^p$  and  $\frac{10^{-20}}{j-\alpha}$  to  $\sigma_{pp}$ , it predicts corrections to  $F_2^\gamma$  of order  $\frac{1}{j-\alpha}$  which change completely the description of  $\gamma\gamma$  interactions.

To conclude, I shall list some perspectives coming from the models presented here. Of course, all these models can be improved but they also open doors to new types of analyses. First of all, there are trivial (but useful) enhancements that can be added. As an example, one can produce a standard set using NLO QCD<sup>4</sup>. We can also try to extend the method used in model 4 to<sup>5</sup>  $x = 1$ , or extend the model 5 to small values of  $Q^2$ . One may also study the effect of the cuts on  $Q^2$  and  $W^2$  in model 5, which should give information about the domain of applicability of the DGLAP equation. Then, one can study models 4 and 5 using a generalised double-pole pomeron model and models 3, 4 and 5 using the Donnachie-Landshoff two-pomerons approach. This last point can be directly compared with the results obtained by Donnachie and Landshoff after a modification of the DGLAP evolution equation [14]. However, all these improvements should not give much more information about the singularity structure of amplitudes.

It is certainly more interesting to look at the following question. The fact that we can use the DGLAP evolution equation to extract the residues of a triple-pole pomeron begs some theoretical questions. One can probably modify the DGLAP equation and introduce saturation effects in order to obtain a Regge-compatible solution. These modifications can be of different types, *e.g.* subleading corrections or higher-twists effects. If we want to obtain a good description at large  $Q^2$  and small  $x$ , we probably need to take into account unitarity effects and gluon recombination as shown in Figure 12.2. Note that non-linear corrections should take into account diagrams which contain more than one parton going out of the proton and which are expected to behave as higher-twist effects. However, it is unclear how a resummation of higher-twist effects could remove the essential singularity which is a leading-twist effect. Consider for example the following very simple non-linear correction to the DGLAP equation:

$$Q^2 \partial_{Q^2} g(j, Q^2) = \frac{2C_A \alpha_s}{2\pi} \left( \frac{1}{j-1} g(j, Q^2) - \Psi(j, Q^2) g^2(j, Q^2) \right),$$

where we have kept only the leading part of the gluon splitting function. If we assume  $\Psi = \psi(Q^2)(j-1)^{n-1}$ , one can adjust  $\psi(Q^2)$  in order to obtain solutions of the form

---

<sup>4</sup>Such a standard set should allow for a direct comparison with CTEQ, MRST and other usual parton sets.

<sup>5</sup>Since the number of parameters in the fit will increase, one will certainly have problems with local minima. It is possible that, for example, one branch corresponding to a local minimum gives the best results at small  $Q^2$  and another at large  $Q^2$ . This shall lead to non-continuous form factors. One possible solution to this problem is the following: since distributions such as  $A(Q^2)(1-x)^{b(Q^2)}$  are stable against DGLAP evolution, one may fix the  $Q^2$  dependence of the high- $x$  behaviour using DGLAP evolution. In this case, we can fix the high- $x$  behaviour once for all, for every  $Q^2$ . This is nevertheless not easy to implement because we must fit at all values of  $Q^2$  at the same time instead of browsing the values of  $Q^2$  one by one.

$g(j, Q^2) = \frac{A(Q^2)}{(j-1)^n} + \frac{B(Q^2)}{(j-1)^{n-1}}$ . One easily obtains

$$xg(x, Q^2) = \left[ \frac{\log(Q^2/\Lambda^2)}{\log(\mu^2/\Lambda^2)} \right]^{\frac{12C_A}{33-2n_f} \frac{B_0}{A_0}} \frac{\log^{n-2}(1/x)}{(n-1)!} [A_0 \log(1/x) - (n-1)B_0],$$

$$\psi(Q^2) = \frac{1}{A_0} \left[ \frac{\log(Q^2/\Lambda^2)}{\log(\mu^2/\Lambda^2)} \right]^{-\frac{12C_A}{33-2n_f} \frac{B_0}{A_0}}.$$

The problem in this expression is that the non-linear correction “kernel”  $\psi(Q^2)$  decreases like a power of  $\log(Q^2)$  and not like a power of  $Q^2$ . But, this shows that it is possible to modify the DGLAP equation in order to stabilise a multiple-pole pomeron in the small- $x$  limit. It is worth noting that these theoretical questions are important for LHC physics. For example, if we look at the  $D$ -meson production through the  $gg \rightarrow c\bar{c}$  fusion process with ALICE, we have (see [65])

$$x_1 = \frac{m_{c\bar{c}}}{\sqrt{s}} \exp(y_{c\bar{c}}) \quad \text{and} \quad x_2 = \frac{m_{c\bar{c}}}{\sqrt{s}} \exp(-y_{c\bar{c}}).$$

This means that, for central rapidities, we have  $x_1 \approx x_2 \approx 2 \cdot 10^{-4}$ , while, in the forward rapidity region ( $y \approx 4$ ), one can access  $x$  values down to  $10^{-6}$  *i.e.* two orders of magnitude smaller than the corresponding HERA regime. Therefore, the LHC will reach very small values of  $x$  which will be very useful to constrain theoretical models for the gluon distribution.

Fit	Domain	Regge theory	pQCD (DGLAP)	facto. thm.	$j$ -plane singularities	$F_2^p$	$\sigma_{\text{tot}}$	$\gamma^{(*)}\gamma^{(*)}$	$\frac{F_2^c}{F_L}$	$\frac{F_2^{d,n}}{F^\nu}$	PDF
1. Regge fit	$\cos(\theta) \geq 100$ $Q^2 \leq 3000 \text{ GeV}^2$	✓	×	×	triple-pole at $j = 1$ (or 2 simple poles, or 1 double-pole at $j = 1$ )	✓	✓	×	×	×	×
2. $t$ CU tests	$\cos(\theta) \geq \frac{49 \text{ GeV}^2}{2m_p^2}$ $Q^2 \leq 150 \text{ GeV}^2$ $x \leq 0.3$	✓	×	✓	generalised double-pole or triple-pole at $j = 1$	✓	✓	✓	×	×	×
3. DGLAP extension of Regge fit	$\cos(\theta) \geq \frac{49 \text{ GeV}^2}{2m_p^2}$ $Q^2 \geq Q_0^2 \approx 5 \text{ GeV}^2$ $x \leq x_{\text{Regge}} \approx 0.15$	✓	✓	from 2 for $Q^2 \leq Q_0^2$	generalised double-pole or triple-pole at $j = 1$ for $Q^2 \leq Q_0^2$ , DGLAP ess. sing. for $Q^2 > Q_0^2$	✓	from 2	from 2 for $Q^2 \leq Q_0^2$	×	×	✓
4. Regge residues from DGLAP	$\cos(\theta) \geq \frac{49 \text{ GeV}^2}{2m_p^2}$ $10 \leq Q^2 \leq 10^3 \text{ GeV}^2$ $x \leq x_{\text{Regge}} \approx 0.15$	✓	✓	?	triple-pole at $j = 1$ at all $Q^2$	✓	possible extension	?	✓	×	✓
5. Global Fit	$Q^2 \geq Q_0^2 = 4m_c^2$ $W^2 \geq 12.5 \text{ GeV}^2$	✓	✓	×	generalised double-pole or triple-pole at $j = 1$ for $Q^2 = Q_0^2$ , DGLAP ess. sing. for $Q^2 > Q_0^2$ (extension to $Q^2 = 0$ ?)	✓	?	×	×	✓	✓

Table 12.1: Summary of all models studied in this thesis with their properties (✓ =done, × =not done).

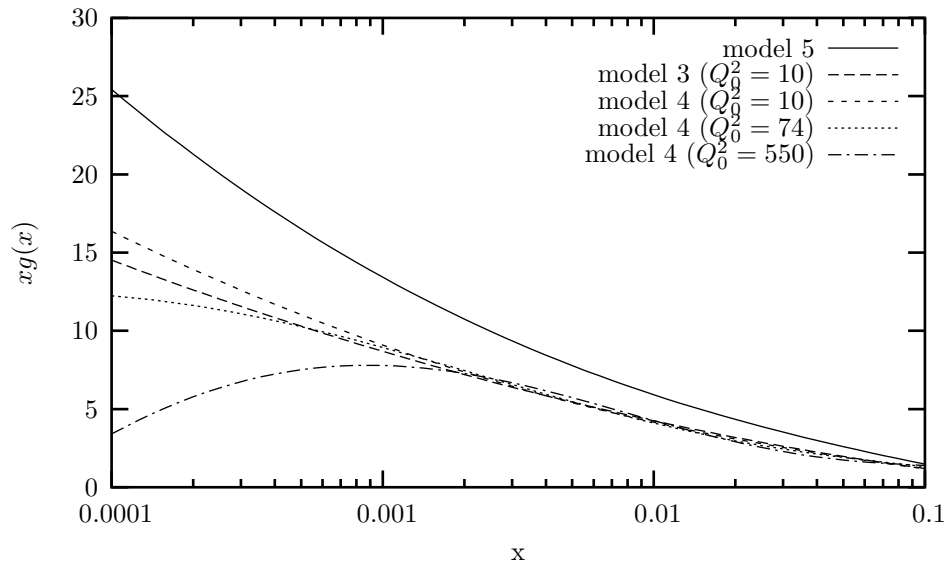


Figure 12.1: Gluon distribution at  $Q^2 = 10 \text{ GeV}^2$  obtained from models 3, 4 and 5. Scales are given in  $\text{GeV}^2$ .

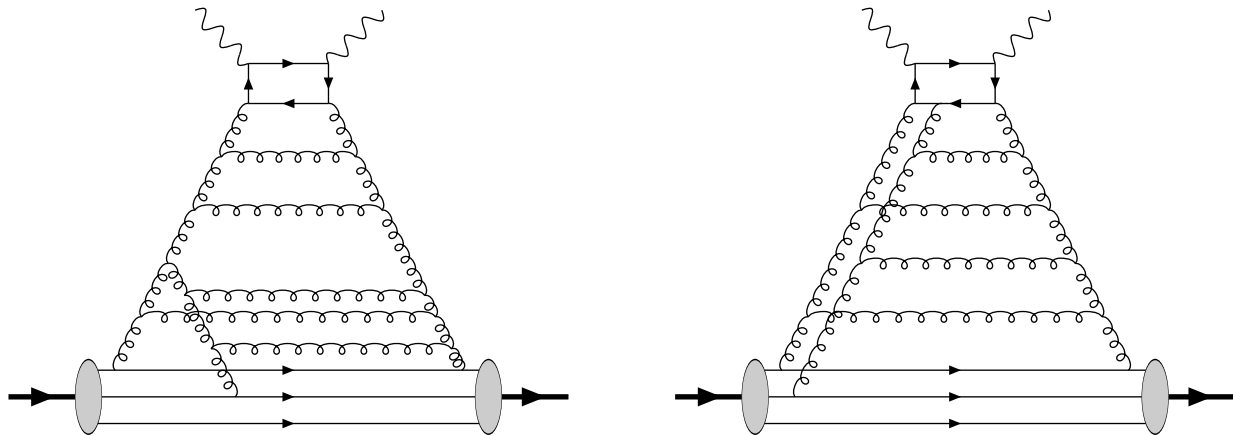
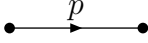
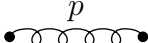
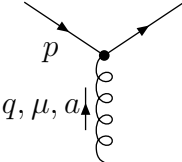
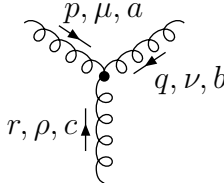
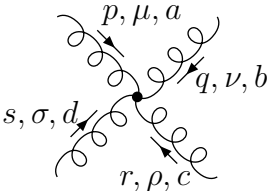


Figure 12.2: Corrections to the DGLAP evolution equation : gluon recombination and unitarity effects.

# Appendix A

## Feynman rules in QCD

Although we do not use Feynman rules extensively in this thesis, we need them as soon as we do a practical calculation in pQCD. We therefore summarise here Feynman rules for propagators and vertices in QCD. Since we always use the light-cone gauge, they are given in this case<sup>1</sup>.

	$d(p) = \frac{i}{\not{p} - m}$
	$d_{\mu\nu}(p) = \frac{i}{p^2} \left( -g_{\mu\nu} + \frac{p_\mu n_\nu + n_\mu p_\nu}{p \cdot n} \right)$
	$V_a^\mu(p, q) = -ig\tau_a\gamma^\mu$
	$V_{abc}^{\mu\nu\rho}(p, q, r) = -gf_{abc}[(q-r)^\mu g^{\nu\rho} + (r-p)^\nu g^{\rho\mu} + (p-q)^\rho g^{\mu\nu}]$
	$V_{abcd}^{\mu\nu\rho\sigma}(p, q, r, s) = -ig^2 [f_{abc}f^{cde} (g^{\mu\rho}g^{\nu\sigma} - g^{\mu\sigma}g^{\nu\rho}) + f_{ace}f^{bde} (g^{\mu\nu}g^{\rho\sigma} - g^{\mu\sigma}g^{\nu\rho}) + f_{ade}f^{bce} (g^{\mu\nu}g^{\rho\sigma} - g^{\mu\rho}g^{\nu\sigma})]$

---

<sup>1</sup>Note that we do not need ghosts in the axial gauge.



# Appendix B

## Useful Mellin transforms

Throughout this thesis, we have widely used the Mellin transform to relate the  $x$ -dependence of parton distributions and structure functions to the complex- $j$  plane where Regge theory applies. We shall gather in this appendix the properties of Mellin transform used in the thesis.

Let us start by the definition, allowing to go from  $x$  space to  $j$  space:

$$\tilde{f}(j) = \int_0^1 dx x^{j-1} f(x). \quad (\text{B.1})$$

It is possible to invert this relation, yielding the inverse Mellin transform:

$$f(x) = \frac{1}{2i\pi} \int_{c-i\infty}^{c+i\infty} dj x^{-j} \tilde{f}(j),$$

where  $c$  is chosen in such a way that the integration axis is to the right of all singularities of  $\tilde{f}$ .

A very useful property of the Mellin transform is that it transform convolutions in  $x$  space into simple products in  $j$  space:

$$\pi(x) = \int_x^1 \frac{d\xi}{\xi} f\left(\frac{x}{\xi}\right) g(\xi) \longrightarrow \tilde{\pi}(j) = \tilde{f}(j) \tilde{g}(j)$$

Here is a table containing the Mellin transforms used in this thesis<sup>1</sup>

$f(x)$	$\tilde{f}(j)$
$xf(x)$	$\tilde{f}(j+1)$
$\partial_x f(x)$	$f(1) - (j-1)\tilde{f}(j-1)$
$x^\alpha$	$\frac{1}{j-\alpha}$
$\log^n(1/x)x^\alpha$	$\frac{(n-1)!}{(j-\alpha)^n}$

---

<sup>1</sup>A complete table of Mellin transform is given in [66].

Finally, note that the Mellin transform is used in DIS when  $F_2$  is written in terms of  $x$  and  $Q^2$ . If we want to go down to  $Q^2 = 0$ , the variable  $x$  must be replaced by  $\nu$  and the Mellin transform becomes

$$\hat{f}(j) = \int_{\kappa^2}^{\infty} d\left(\frac{\nu}{\kappa^2}\right) \left(\frac{\nu}{\kappa^2}\right)^{-j-1} f(\nu),$$

where  $\kappa$  is a small scale. One easily checks that, for  $Q^2 \geq 2\kappa^2$ , when  $f(x \geq 1) = 0$ , we have

$$\hat{f} = \left(\frac{Q^2}{2\kappa^2}\right)^{-j} \tilde{f}(j). \quad (\text{B.2})$$

This relation shows that  $\tilde{f}$  and  $\hat{f}$  have the same singularities.

# Appendix C

## The box diagram

We have re-calculated the contribution of the box diagram of Fig. (8.6), and confirm the results of [54]. Our results can be recast in the following form, which may be more transparent in the present context:

We use  $x_1 = P^2/(2\nu)$  and  $x_2 = Q^2/(2\nu)$ , with  $\nu = p.q$ , which give

$$P^2 = \frac{x_1 w^2}{1 - x_1 - x_2}, \quad (\text{C.1})$$

$$Q^2 = \frac{x_2 w^2}{1 - x_1 - x_2} \quad (\text{C.2})$$

with  $w^2 = s$ . We set

$$\mu = \frac{m^2}{\nu} = \frac{2m^2(1 - x_1 - x_2)}{w^2}, \quad (\text{C.3})$$

$$\tau = 1 - 4x_1x_2, \quad (\text{C.4})$$

$$\delta = -x_1 - x_2 + 1, \quad (\text{C.5})$$

$$\delta_\mu = \delta - 2\mu. \quad (\text{C.6})$$

The cross sections then take the form

$$\sigma_i = \frac{12\alpha^2\pi\delta}{w^2} \left[ \frac{\sqrt{\delta_\mu}}{\sqrt{\delta\tau}(2\delta x_1x_2 + \tau\mu)\tau^2} \Sigma_i + \frac{\Lambda_i}{\tau^3} \log(\rho) \right] \quad (\text{C.7})$$

where  $i = LL, LT, TL, TT$ , which gives

$$\rho = \frac{\sqrt{\delta\delta_\mu\tau} - \delta_\mu\tau}{\sqrt{\delta\delta_\mu\tau} + \delta_\mu\tau}. \quad (\text{C.8})$$

The cross sections then are built from:

$$\begin{aligned}
\Sigma_{TT} &= 4\delta x_1 x_2 [2x_1 x_2 (x_1^2 + x_2^2 - 1 + 2x_1 + 2x_2) \\
&\quad - 12x_1^2 x_2^2 - 2(x_1^2 + x_2^2) + 2(x_2 + x_1) - 1] \\
&\quad - \tau\mu(2x_1 - 1)^2(2x_2 - 1)^2 - 2\delta\mu^2\tau^2, \\
\Lambda_{TT} &= 2\delta\mu\tau - 2\mu^2\tau^2 \\
&\quad + [8x_1^2 x_2^2 (x_1^2 + x_2^2) + 16x_1^3 x_2^3 - 16x_1^2 x_2^2 (x_1 + x_2) \\
&\quad - 4x_1 x_2 (x_1^2 + x_2^2) + 16x_1^2 x_2^2 - 2(x_1 + x_2) + 2(x_1^2 + x_2^2) + 1], \\
\Sigma_{TL} &= \mu\tau\delta x_2 [(6x_1^2 + 1 + 2x_2 x_1 - 6x_1) \\
&\quad + 2\delta x_1 ((2x_1^2 + 1)x_2 + (2x_2^2 + 1)x_1 - 6x_1 x_2)], \\
\Lambda_{TL} &= -x_2 [2\delta x_1 (2x_2 - 1 - 2x_1^2 x_2 - 2x_1 x_2^2 - 2x_1 x_2 + 2x_1) \\
&\quad + \mu\tau(2x_1^2 + 1 - 2x_2 x_1 + x_1)], \\
\Sigma_{LT} &= \Sigma_{TL}(x_1 \leftrightarrow x_2), \\
\Lambda_{LT} &= \Lambda_{TL}(x_1 \leftrightarrow x_2), \\
\Sigma_{LL} &= -2\delta^2 x_1 x_2 (3\delta x_1 x_2 + \mu\tau), \\
\Lambda_{LL} &= -\delta^2 x_1 x_2 (2x_1 x_2 + 1).
\end{aligned}$$

# Appendix D

## Momentum sum rule and gluon distribution

In this appendix, we shall give the expression of the constant in the gluon distribution introduced in chapter 11, constrained by the momentum sum rule. Recall that we have, at  $Q^2 = Q_0^2$ ,

$$\begin{aligned}xu_V(x) &= \frac{2}{N_u} x^\eta (1 + \gamma_u x) (1 - x)^{b_u}, \\xd_V(x) &= \frac{1}{N_d} x^\eta (1 + \gamma_d x) (1 - x)^{b_d}, \\x\bar{q}_i(x) &= [A \log^2(1/x) + B \log(1/x) + C + D_i x^\eta] (1 - x)^b, \\xg(x) &= [A_g \log^2(1/x) + B_g \log(1/x) + C_g] (1 - x)^{b+1},\end{aligned}\tag{D.1}$$

where  $N_q$  is given by equation (11.2). We shall use momentum conservation (3.26) to constrain the constant term  $C_g$  in the gluon distribution. Let us first introduce the special functions that we need. The Euler Gamma function is defined by

$$\Gamma(x) = \int_0^\infty dt t^{x-1} e^{-t}.$$

We can then introduce the Beta function  $B(x, y)$ , the digamma function  $\Psi(x)$  and the polygamma function  $\Psi^{(m)}(x)$  related to the gamma functions by the following formulae

$$\begin{aligned}B(x, y) &= \frac{\Gamma(x)\Gamma(y)}{\Gamma(x+y)}, \\ \Psi(x) &= \frac{\partial_x \Gamma(x)}{\Gamma(x)}, \\ \Psi^{(m)}(x) &= \partial_x^m \Psi(x).\end{aligned}$$

With these definitions, the momenta carried by the distributions (D.1) are given by the following expressions:

$$\begin{aligned}
p_{u_V} &= \frac{2\eta}{b_u + \eta + 1} \left( 1 + \gamma_u \frac{\eta + 1}{b_u + \eta + 2} \right) \left( 1 + \gamma_u \frac{\eta}{b_u + \eta + 1} \right)^{-1}, \\
p_{d_V} &= \frac{\eta}{b_d + \eta + 1} \left( 1 + \gamma_d \frac{\eta + 1}{b_d + \eta + 2} \right) \left( 1 + \gamma_d \frac{\eta}{b_d + \eta + 1} \right)^{-1}, \\
p_{\bar{q}_i} &= \frac{1}{b+1} \left( A \left\{ [\gamma_E + \Psi(b+2)]^2 - \Psi^{(1)}(b+2) + \frac{\pi^2}{6} \right\} + B [\gamma_E + \Psi(b+2)] + C \right) \\
&\quad + D_i B(b+1, \eta+1), \\
p_g &= \frac{1}{b_g + 1} \left( A_g \left\{ [\gamma_E + \Psi(b_g+2)]^2 - \Psi^{(1)}(b_g+2) + \frac{\pi^2}{6} \right\} + B_g [\gamma_E + \Psi(b_g+2)] + C_g \right).
\end{aligned}$$

From the proton momentum conservation

$$p_g + p_{u_V} + p_{d_V} + 2(p_{\bar{u}} + p_{\bar{d}} + p_{\bar{s}}) = 1,$$

we finally obtain

$$\begin{aligned}
c_G &= A_g \left\{ [\gamma_E + \Psi(b_g+2)]^2 - \Psi^{(1)}(b_g+2) + \frac{\pi^2}{6} \right\} + B_g [\gamma_E + \Psi(b_g+2)] \\
&\quad + (b_g + 1) [1 - p_{u_V} - p_{d_V} - 2(p_{\bar{u}} + p_{\bar{d}} + p_{\bar{s}})].
\end{aligned}$$

# Bibliography

- [1] N. N. Bogolyubov, B. V. Struminsky, and A. N. Tavkhelidze, preprint JINR-D-1968 (Dubna 1965).
- [2] S. Weinberg, Phys. Rev. Lett. **31** (1973) 494.
- [3] D.J. Gross, F. Wilczek, Phys. Rev. **D8** (1973) 3633.
- [4] H. Fritzsche, M. Gell-Mann and H. Leutwyler, Phys. Lett. B **47** (1973) 365.
- [5] J. D. Bjorken, Phys. Rev. **179** (1969) 1547.
- [6] V.N. Gribov and L.N. Lipatov, Sov. J. Nucl. Phys. **15** (1972) 438. G. Altarelli and G. Parisi, Nucl. Phys. **B126** (1977) 298. Yu.L. Dokshitzer, Sov. Phys. JETP **46** (1977) 641.
- [7] V. S. Fadin, E. A. Kuraev and L. N. Lipatov, Phys. Lett. B **60** (1975) 50. L. N. Lipatov, Sov. J. Nucl. Phys. **23** (1976) 338 [Yad. Fiz. **23** (1976) 642]. I. I. Balitsky and L. N. Lipatov, Sov. J. Nucl. Phys. **28** (1978) 822 [Yad. Fiz. **28** (1978) 1597].
- [8] V. S. Fadin and L. N. Lipatov, JETP Lett. **49** (1989) 352 [Yad. Fiz. **50** (1989 SJNCA,50,712.1989) 1141].
- [9] The reader who wants a modern overview of  $S$ -matrix and Regge theory and diffraction can read the books S. Donnachie, G. Dosch, P. Landshoff and O. Nachtmann, *Pomeron Physics and QCD* (Cambridge University Press, Cambridge, 2002), and V. Barone and E. Predazzi, *High-Energy Particle Diffraction* (Springer, Berlin Heidelberg, 2002).
- [10] T. Regge, Nuovo Cim. **14** (1959) 951.
- [11] T. Regge, Nuovo Cim. **18** (1960) 947.
- [12] A. Donnachie and P. V. Landshoff, Phys. Lett. B **437** (1998) 408 [arXiv:hep-ph/9806344].
- [13] A. Donnachie and P. V. Landshoff, Phys. Lett. B **518** (2001) 63 [arXiv:hep-ph/0105088].
- [14] A. Donnachie and P. V. Landshoff, Phys. Lett. B **533** (2002) 277 [arXiv:hep-ph/0111427].

- [15] L. L. Jenkovszky, F. Paccanoni and E. Predazzi, Nucl. Phys. Proc. Suppl. **25B** (1992) 80.
- [16] P. Desgrolard, M. Giffon, L. L. Enkovsky, A. I. Lengyel and E. Predazzi, Phys. Lett. B **309** (1993) 191.
- [17] J. R. Cudell and G. Soyez, Phys. Lett. B **516** (2001) 77 [arXiv:hep-ph/0106307].
- [18] P. Desgrolard and E. Martynov, Eur. Phys. J. C **22** (2001) 479 [arXiv:hep-ph/0105277].
- [19] G. Curci, W. Furmanski and R. Petronzio, Nucl. Phys. B **175** (1980) 27.
- [20] A. D. Martin, R. G. Roberts, W. J. Stirling and R. S. Thorne, Eur. Phys. J. C **23** (2002) 73 [arXiv:hep-ph/0110215].
- [21] M. Gluck, E. Reya and A. Vogt, Eur. Phys. J. C **5** (1998) 461 [arXiv:hep-ph/9806404].
- [22] J. Pumplin, D. R. Stump, J. Huston, H. L. Lai, P. Nadolsky and W. K. Tung, JHEP **0207** (2002) 012 [arXiv:hep-ph/0201195].
- [23] A. M. Cooper-Sarkar, J. Phys. G **28**, 2669 (2002) [arXiv:hep-ph/0205153].
- [24] S. I. Alekhin, Phys. Rev. D **63**, 094022 (2001) [arXiv:hep-ph/0011002].
- [25] R. E. Cutkosky, J. Math. Phys. **1** (1960) 429.
- [26] M. Froissart, Phys. Rev. **123** (1961) 1053.
- [27] A. Martin, Phys. Rev. **129** (1963) 1432.
- [28] K. Hagiwara et al., *Review of Particle Physics*, Phys. Rev. D**66** (2002) 010001. The data on total cross-sections can be obtained from <http://pdg.lbl.gov>.
- [29] V. N. Gribov and I. Y. Pomeranchuk, Sov. Phys. JETP **15** (1962) 788L [Zh. Eksp. Teor. Fiz. **42** (1962 PRLTA,8,343.1962) 1141].
- [30] P. P. Kulish and L. D. Faddeev, Theor. Math. Phys. **4** (1970) 745 [Teor. Mat. Fiz. **4** (1970) 153].
- [31] G. Zweig, preprint CERN-TH-412
- [32] M. Gell-Mann, Phys. Lett. **8** (1964) 214.
- [33] T. Kinoshita, J. Math. Phys. **3** (1962) 650.
- [34] K. G. Wilson, Phys. Rev. **179** (1969) 1499.
- [35] R. A. Brandt and G. Preparata, Nucl. Phys. B **27** (1972) 541.
- [36] N. H. Christ, B. Hasslacher and A. H. Mueller, Phys. Rev. D **6** (1972) 3543.

- [37] K. Symanzik, Commun. Math. Phys. **23** (1971) 49; **34** (1973) 7.
- [38] A. H. Mueller, Phys. Rev. D **9** (1974) 963.
- [39] R. K. Ellis, H. Georgi, M. Machacek, H. D. Politzer and G. G. Ross, Nucl. Phys. B **152** (1979) 285.
- [40] A. De Rujula, S. L. Glashow, H. D. Politzer, S. B. Treiman, F. Wilczek and A. Zee, Phys. Rev. D **10** (1974) 1649.
- [41] R.J. Eden, P.V. Landshoff, D.I. Olive and J.C. Polkinghorne, *The Analytic S-Matrix*, (Cambridge University Press, Cambridge, 1966).
- [42] L. Lukaszuk and A. Martin, Nuovo Cimento **52A** (1967) 122.
- [43] A. Donnachie and P. V. Landshoff, Phys. Lett. B **296** (1992) 227 [arXiv:hep-ph/9209205].
- [44] J. R. Cudell *et al.*, Phys. Rev. D **65** (2002) 074024 [arXiv:hep-ph/0107219].
- [45] S. J. Brodsky, V. S. Fadin, V. T. Kim, L. N. Lipatov and G. B. Pivovarov, JETP Lett. **76** (2002) 249 [Pisma Zh. Eksp. Teor. Fiz. **76** (2002) 306] [arXiv:hep-ph/0207297].
- [46] [ALEPH, L3 and OPAL Collaborations], Eur. Phys. J. C **23** (2002) 201.
- [47] J. Charap and E.J. Squires, Phys. Rev. **127** (1962) 1387.
- [48] J. R. Cudell, E. Martynov and G. Soyez, arXiv:hep-ph/0207196.
- [49] F. Bloch and A. Nordsiek, Phys. Rev. **52** (1937) 54; D. R. Yennie, S. C. Frautschi and H. Suura, Annals Phys. **13** (1961) 379.
- [50] J. R. Cudell, K. Kang and S. K. Kim, Phys. Lett. B **395** (1997) 311 [arXiv:hep-ph/9601336].
- [51] J. R. Cudell *et al.* [COMPETE Collaboration], Phys. Rev. Lett. **89** (2002) 201801 [arXiv:hep-ph/0206172].
- [52] P. Desgrolard, M. Giffon, E. Martynov and E. Predazzi, Eur. Phys. J. C **18** (2001) 555 [arXiv:hep-ph/0006244].
- [53] P. Desgrolard, A. Lengyel and E. Martynov, JHEP **0202** (2002) 029 [arXiv:hep-ph/0110149].
- [54] V. M. Budnev, I. F. Ginzburg, G. V. Meledin and V. G. Serbo, Phys. Rept. **15** (1974) 181.
- [55] M. E. Peskin and D. V. Schroeder, *An Introduction To Quantum Field Theory*, (Reading, USA: Addison-Wesley, 1995, 842 p).

- [56] A. Donnachie, H. G. Dosch and M. Rueter, Phys. Rev. D **59** (1999) 074011 [arXiv:hep-ph/9810206].
- [57] R. Engel and J. Ranft, Phys. Rev. D **54** (1996) 4244 [arXiv:hep-ph/9509373]. See also <http://lepton.bartol.udel.edu/~eng/phojet.html>.
- [58] T. Sjostrand, L. Lonnblad and S. Mrenna, arXiv:hep-ph/0108264. See also <http://www.thep.lu.se/~torbjorn/Pythia.html>.
- [59] G. Soyez, arXiv:hep-ph/0211361.
- [60] L. Csernai, L. Jenkovszky, K. Kontros, A. Lengyel, V. Magas and F. Paccanoni, Eur. Phys. J. C **24** (2002) 205 [arXiv:hep-ph/0112265].
- [61] E. Iancu, A. Leonidov and L. McLerran, Lectures given at the NATO Advanced Study Institute “QCD perspectives on hot and dense matter”, August 6–18, 2001, in Cargèse, Corsica, France.
- [62] G. Soyez, arXiv:hep-ph/0306113.
- [63] R.G. Roberts, *The Structure of the Proton*, (Cambridge University Press, Cambridge, 1990)
- [64] C. Lopez and F. J. Yndurain, Nucl. Phys. B **171** (1980) 231.
- [65] N. Carrer and A. Dainese, arXiv:hep-ph/0311225.
- [66] F. Oberhettinger, *Tables of Mellin Transforms* (Springer-Verlag, Berlin Heidelberg New-York, 1974)
- [67] I. Abt *et al.* [H1 Collaboration], Nucl. Phys. B **407** (1993) 515.
- [68] T. Ahmed *et al.* [H1 Collaboration], Nucl. Phys. B **439** (1995) 471 [arXiv:hep-ex/9503001].
- [69] S. Aid *et al.* [H1 Collaboration], Nucl. Phys. B **470** (1996) 3 [arXiv:hep-ex/9603004].
- [70] C. Adloff *et al.* [H1 Collaboration], Nucl. Phys. B **497** (1997) 3 [arXiv:hep-ex/9703012].
- [71] C. Adloff *et al.* [H1 Collaboration], Eur. Phys. J. C **13** (2000) 609 [arXiv:hep-ex/9908059].
- [72] C. Adloff *et al.* [H1 Collaboration], Eur. Phys. J. C **19** (2001) 269 [arXiv:hep-ex/0012052].
- [73] C. Adloff *et al.* [H1 Collaboration], Eur. Phys. J. C **21** (2001) 33 [arXiv:hep-ex/0012053].
- [74] M. Derrick *et al.* [ZEUS Collaboration], Phys. Lett. B **316** (1993) 412.
- [75] M. Derrick *et al.* [ZEUS Collaboration], Z. Phys. C **65** (1995) 379.

- [76] M. Derrick *et al.* [ZEUS Collaboration], Z. Phys. C **69** (1996) 607 [arXiv:hep-ex/9510009].
- [77] M. Derrick *et al.* [ZEUS Collaboration], Z. Phys. C **72** (1996) 399 [arXiv:hep-ex/9607002].
- [78] J. Breitweg *et al.* [ZEUS Collaboration], Phys. Lett. B **407** (1997) 432 [arXiv:hep-ex/9707025].
- [79] J. Breitweg *et al.* [ZEUS Collaboration], Eur. Phys. J. C **7** (1999) 609 [arXiv:hep-ex/9809005].
- [80] J. Breitweg *et al.* [ZEUS Collaboration], Eur. Phys. J. C **12** (2000) 35 [arXiv:hep-ex/9908012].
- [81] S. Chekanov *et al.* [ZEUS Collaboration], Eur. Phys. J. C **21** (2001) 443 [arXiv:hep-ex/0105090].
- [82] A. C. Benvenuti *et al.* [BCDMS Collaboration], Phys. Lett. B **223** (1989) 485.
- [83] M. R. Adams *et al.* [E665 Collaboration], Phys. Rev. D **54** (1996) 3006.
- [84] M. Arneodo *et al.* [New Muon Collaboration], Nucl. Phys. B **483** (1997) 3 [arXiv:hep-ph/9610231].
- [85] P. Amaudruz *et al.* [New Muon Collaboration], Nucl. Phys. B **371** (1992) 3.
- [86] L. W. Whitlow, E. M. Riordan, S. Dasu, S. Rock and A. Bodek, Phys. Lett. B **282** (1992) 475.
- [87] The data on the total  $\gamma p$  cross-section prior to HERA are extracted from <http://pdg.lbl.gov>. The HERA data come from: H1 collaboration, S. Aid *et al.*, Zeit. Phys. C **69** (1995) 27; ZEUS Collaboration; S. Chekanov *et al.*, Nucl. Phys. B **627**, (2002).
- [88] M. Acciarri *et al.* [L3 Collaboration], Phys. Lett. B **408** (1997) 450; Phys. Lett. B **436** (1998) 403; Phys. Lett. B **447** (1999) 147; Phys. Lett. B **453** (1999) 333; Phys. Lett. B **483** (2000) 373 [arXiv:hep-ex/0004005]; Phys. Lett. B **519** (2001) 33 [arXiv:hep-ex/0102025].
- [89] R. Akers *et al.* [OPAL Collaboration], Z. Phys. C **61** (1994) 199; K. Ackerstaff *et al.* [OPAL Collaboration], Phys. Lett. B **411** (1997) 387 [arXiv:hep-ex/9708019]; Phys. Lett. B **412** (1997) 225 [arXiv:hep-ex/9708028]; Z. Phys. C **74** (1997) 33; G. Abbiendi *et al.* [OPAL Collaboration], Eur. Phys. J. C **14** (2000) 199 [arXiv:hep-ex/9906039]; Eur. Phys. J. C **18** (2000) 15 [arXiv:hep-ex/0007018]; Eur. Phys. J. C **24** (2002) 17 [arXiv:hep-ex/0110006]; Phys. Lett. B **533** (2002) 207 [arXiv:hep-ex/0202035].
- [90] C. Adloff *et al.* [H1 Collaboration], Z. Phys. C **72** (1996) 593 [arXiv:hep-ex/9607012].

- [91] J. Breitweg *et al.* [ZEUS Collaboration], Phys. Lett. B **407** (1997) 402 [arXiv:hep-ex/9706009].
- [92] E. Oltman *et al.*, Z. Phys. C **53** (1992) 51.
- [93] W. G. Seligman *et al.*, Phys. Rev. Lett. **79** (1997) 1213.
- [94] B. T. Fleming *et al.* [CCFR Collaboration], Phys. Rev. Lett. **86** (2001) 5430 [arXiv:hep-ex/0011094].